DYNAMIC RESPONSE OF AGEING CONCRETE GRAVITY DAMS WITH UNBOUNDED RESERVOIR

A thesis
Submitted in partial fulfilment of the requirements for the award of the degree of

DOCTOR OF PHILOSOPHY

By

Indrani Gogoi

CIVIL ENGINEERING DEPARTMENT

INDIAN INSTITUTE OF TECHNOLOGY GUWAHATI

FEBRUARY, 2006

CERTIFICATE

It is certified that the work contained in the thesis entitled "**Dynamic Response of Ageing Concrete Gravity Dams with Unbounded Reservoir**", by Indrani Gogoi, Roll Number 004402, a student in the Department of Civil Engineering, Indian Institute of Technology, Guwahati for the award of the degree of Doctor of Philosophy has been carried out under my supervision and that this work has not been submitted elsewhere for a degree.

28/02/06

Date:28-02-06

Dr. Damodar Maity
Associate Professor
Department of Civil Engineering
Indian Institute of Technology
Guwahati, Assam
India

Dedicated

To

my children

Prerana and Mrinank

PREFACE

The modelling and analysis of a concrete gravity dam exposed to an unbounded reservoir require special attention for its safe design. This problem comes under the purview of fluid-structure-soil interaction system, where behavior of each medium affects the other and in turn is a coupled phenomenon. As in most of the practical cases, dam is founded on a hard stratum, where the effect of soil-structure interaction is not significant compared to that of dam-reservoir interaction. Consideration of dam-reservoir interaction effects may alter the seismic response of dam significantly. During the lifetime of a dam the original safety margin will be reduced due to deterioration of its structural strength. Damage in a dam may be caused due to degradation of the concrete with age. With the ageing of a dam-reservoir system, the hydrodynamic response of the reservoir changes as the reservoir bottom becomes absorptive due to accumulation of sediment. It is therefore important to carry out a realistic seismic analysis not only for new dams but in the context of the safety evaluation of existing aged dams. Such an analysis procedure should appropriately account for the ageing effect so that an accurate seismic behavior of a dam-reservoir system can be predicted at any age.

Since analytical treatment of such coupled problems is extremely difficult, a large number of works in this area are directed towards the adaptation of various numerical techniques. This has gained further impetus with the advent of faster generations of computers.

The present work is an attempt to gain an understanding of the response of an ageing concrete gravity dam adjacent to an infinite reservoir. Computer codes are developed for the analysis of coupled dam-reservoir interaction problems using finite element technique. A post processor module is also developed to present the analysis data in graphical forms.

ACKNOWLEDGEMENT

I wish to express my profound gratitude to **Dr. Damodar Maity** for giving me the opportunity to work under his excellent supervision. I am grateful for his endless patience, constant encouragement, willingness to discuss and readiness to help. Without his help, motivation and commitment, this research would not have been possible.

I am grateful to the Department of Education, Government of Assam, the Director of Technical Education, Assam, the Principal and the Head of the Department of Civil Engineering, Assam Engineering Institute, Guwahati for giving me an official permission to carry out my Ph.D. work as a part time research student of IIT Guwahati. I thank **Prof. D. N. Buragohain, Dr. S. Talukdar, Dr. V. Chandramouli, Dr. D. Chakraborty** and **Dr. S. Dutta** for their comments and valuable suggestions. I thank **Prof. S.S. Saini** for initiating me into the problem of dam-reservoir interaction during my post graduation at IIT Roorkee.

Special thanks to **Dr. S. N. Bora,** Department of Mathematics and **Dr. P.K. Bora**, Department of Electronics and Communications for their useful insights into various aspects of mathematics and signal processing respectively. I thank **Dr. K. Barua**, Department of Humanities, for her valuable suggestions in writing skills. I thank all the **Faculty members** of the Civil Engineering Department, IIT Guwahati for their encouragement

I thank the **reviewers** of my publications for their valuable suggestions.

I am grateful to my fellow research scholars **T. Nayak, S. K. Pandit, S. C. Martha, Dr. J. A. Ahmed, Er. K. Nallasivam, Er. Girija T.R., Er. D. Devi, Er. A. Dutta** and **Er. A. Burman** for their help and support. I also wish to thank the M.Tech. and B. Tech. students of the Civil Engineering Department – **S. C. Ghadei. Sreenivasulu C., B.V. Reddy, R. A. Gujare, V. P. Singh, P. K. Lanka** and **V. Sharma** who assisted me in various aspects of my research work.

I am grateful to my mother **Jayasree Gogoi** and father **Kshirod Chandra Gogoi**, who are no more. Their inspiring and encouraging words in my memory were source of my strength and determination in pursuing this research. I express my sincere gratitude to my brothers and in-laws for their constant love and encouragement.

Above all, the one and only person to whom I will always be indebted to is my husband, **Er. Kevya K. Gogoi** for making the possibility of this research a reality. During the difficult times of finishing this dissertation, his support and patience was unfailing. My heartfelt thanks to my daughter **Prerana** and son **Mrinank** for all the sacrifices and compromises they made so that I could complete my work.

28/02/06

(Indrani Gogoi)

CURRICULUM VITAE

Indrani Gogoi

Office: Department of Civil Engineering,
Assam Engineering Institute, Chandmari, Guwahati,
Assam, India – 781 003

DATE OF BIRTH: 25th December, 1967

QUALIFICATION:

M.E. in Structural Engineering, Department of Civil Engineering, University of Roorkee, India, 2000
Thesis: *Dynamic Behavior of Concrete Gravity Dam*
Advisor: Dr. S.S. Saini

B.E. in Civil Engineering, Jorhat Engineering College, Jorhat, Assam, India, 1989
Concentrations: *Seismic Resistant Multi-Storey Building Design*

PROFESSIONAL EXPERIENCE:

Lecturer in Civil Engineering, 1996-present
Assam Engineering Institute, Chandmari, Guwahati.

Design Engineer, 1995 to 1996
Designers' Guild, Guwahati, Assam

Faculty, 1992 to 1995.
Aptech Computer Education Centre, Guwahati, Assam.

Graduate Engineer Trainee, 1990 to 1991
Water and Power Consultancy Services (WAPCOS, India) Ltd., A Government of India Undertaking.

AWARDS AND GRANTS RECEIVED:

Ministry of Water Resources – Subject Award (Institution of Engineers, India). An award for the paper "Seismic Performance of Aged Concrete Gravity Dams, Institution of Engineers, Journal of Civil Engineering Division, Feb 2005", December 2005.

National Programme on Earthquake Engineering Education **(NPEEE)** A fellowship for International Training in Earthquake Engineering by the Ministry of Human Resource and Development, Government of India.

PROFESSIONAL MEMBERSHIPS:

- Life Member of Indian Society of Technical Education, India.
- Life Member of the Institution of Engineers, India.
- Associate Member of Association of Consulting Civil Engineers, India.
- Member of Indian Institution of Bridge Engineers, India.
- Member of Indian Geotechnical Society.

ABSTRACT

The assessment of response of an aged concrete dam is important for the prediction of its behavior during earthquakes, so that remedial measures can be taken at the right time to withstand future earthquakes. The assessment is necessary, as the analyses procedures may become obsolete and the state of the art may change since the time of construction and the structural material may deteriorate due to harsh environmental conditions. At the same time, the sediment will be accumulated at the reservoir bottom on the upstream side of the dam. The decision of retrofitting or strengthening the aged dam necessitates accurate analysis of the same in the presence of accumulated sediment. In the present work, an approach to include the time dependent degradation of concrete owing to environmental factors and mechanical loading in terms of isotropic degradation index is developed. The absorption of pressure waves at the bottom of the reservoir due to the presence of sediments has been incorporated in the hydrodynamic pressure equation. Both the aged dam and the infinite reservoir with sediments are modeled and analyzed by finite element technique. A novel far-boundary condition is developed which can be truncated at a relatively closer distance away from the dam face for the finite element analysis of infinite reservoir. Both the aged dam and absorptive reservoir are analyzed separately with the interaction effects at the dam-reservoir interface enforced by an iterative scheme, in which both the pressure in the reservoir and displacement in the dam are converged simultaneously. The dynamic response of an aged concrete dam in the presence of sediment layers in the reservoir is studied. The encouraging outcome of the present investigation reveals the advantages of the proposed truncation boundary condition for the infinite reservoir domain and the iterative scheme for the solution of the coupled aged dam-reservoir system.

KEYWORDS:

Concrete Gravity Dam, Degradation, Truncation boundary condition, Dam-reservoir interaction, Infinite reservoir, Hydrodynamic pressure, Reservoir bottom absorption, Finite element method, Iterative scheme

CONTENTS

LIST OF FIGURES

LIST OF CHARTS

LIST OF TABLES

LIST OF SYMBOLS

a	Acceleration of dam-reservoir interface in the normal direction
a_g	Ground acceleration
a_s	Maximum allowable degradation due to mechanically induced porosity
a'	Acceleration of reservoir-reservoir bed interface in the normal direction
A, B	Variables derived from N sets of experimental data
$[A]$	Coefficient matrix of $\{\dot{p}\}$
$B_{\omega l}$	Complex frequency dependent reflection coefficient
$\{B\}$	Vector representing boundary conditions of fluid domain
$[B_0]$	Matrix correlating strain and displacement
$[B_1]$	Derivative of the shape function $[N_d]$ with respect to x
$[B_2]$	Derivative of the shape function $[N_d]$ with respect to y
$[B_l]$	Linear part of the strain-displacement matrix
$[B_{nl}]$	Nonlinear part of the strain-displacement matrix
c	Acoustic wave speed in water
c_s	Compressional wave velocity in sediment layer
$[C]$	Damping matrix of dam
d_g	Isotropic degradation index
d_m	Scalar degradation parameter
d_{gi}	Orthotropic degradation index, where i = 1,2 corresponds with the Cartesian axes x, y
d_{s1}, d_{s2}	Depth of sediment layers
$\{d\}$	Nodal displacement vector of the structural element
$\{d_e\}$	Elemental displacement vector

$\{\dot{d}\}$	Nodal velocity vector of the structural element
$\{\ddot{d}\}$	Nodal acceleration vector of the structural element
$[D]$	Constitutive matrices of the un-degraded dam
$[D_d]$	Constitutive matrices of the degraded dam
e_k	Measured numerical error
E_0	Elastic modulus of concrete considering strength gain at an age, t_a
E_1, E_2	Elastic modulus of sediment and rock
E_d	Elastic modulus of concrete in dam
E_m	Degraded elastic modulus due to porosity of concrete at an age, t_a
E_s	Elastic modulus of the foundation medium
$E_\infty(f)$	Maximum error
$E_1(f)$	Average error
$E_2(f)$	Root mean square error
$[H], [\overline{H}]$	Coefficient matrix of $\{\ddot{p}\}$
$[G], [\overline{G}]$	Coefficient matrix of $\{p\}$
f_i	Body forces in fluid
f_n	Sampling frequency of earthquake excitation
f_t	Static tensile strength
$f(x_k)$	Function of experimental data
$f(t)$	Compressive strength of concrete at age, t
$\{F\}$	Body forces vector
$\{F_c\}$	Elemental concentrated load vector
$\{F_d\}$	External load vector
g	Gravitational acceleration

H_f	Depth of the reservoir
j	Number of iterations
$[J]$	Jacobian matrix
k_1, k_2	Wave numbers in sediment and rock
k_d	Material damping parameter
$[K]$	Stiffness matrix of dam
L	Distance between the dam and the truncation boundary of reservoir
$[M]$	Mass matrix of dam
n	Direction normal to the surface
n_f	Excitation frequency in Hz
n_c	Number of concentrated loads on an element
N	Number of time steps
N_{ri}	Elemental shape function for reservoir
N_{di}	Elemental shape function for dam
N'	Number of sets of sampling data
N_i'	Bilinear shape function
p	Hydrodynamic pressure in reservoir
$\dot{p}$	Derivative of pressure with respect to time
$\ddot{p}$	Double derivative of pressure with respect to time
P_n	Normalized discrete-time Fourier transform
q	Coefficient dependent on reflection coefficient of reservoir bed
$[Q]$	Dam-reservoir coupling matrix
$[R_f]$	Matrix for the free surface boundary of the fluid domain
$[R_{fs}]$	Matrix at the dam-reservoir interface
$[R_r]$	Matrix for reservoir bed boundary

$[R_t]$	Matrix at the truncation surface
$S(\tau)$	Earthquake signal in time domain
$S_t(\omega)$	Windowed earthquake signal in frequency domain
t	Time
t_a	Age at which degradation index is determined
$[T]$	Transformation matrix for generalized acceleration at the dam-reservoir interface
U	Displacement of fluid particle in reservoir
u_i	Displacement at the i^{th} node in x direction
u_f	Displacement in the foundation
u_{f0}	Amplitude of peak displacement in foundation
$\{\overline{u}\}$	Nodal displacement vector in x
$\{\overline{v}\}$	Nodal displacement vector in y
v_i	Displacement at the i^{th} node in y direction
V_i	Velocity of fluid particle
$\dot{V}_i$	Acceleration of fluid particle
$\mathbf{x}$	Earthquake signal in time domain
x_i	Cartesian coordinate of the i^{th} node in x direction
x_k, y_k	Set of experimental data for concrete strength gain
y_i	Cartesian coordinate of the i^{th} node in y direction
y_{ls}	Least squares line
α	Reflection coefficient of reservoir bed
α_1, α_2	Reflection coefficient of sediment layers
α_c, β_c	Material parameters of concrete
α'	Stiffness proportional damping constant

β_1	First root of the wave equation
β'	Mass proportional damping constant
$\{\delta u\}$, $\{\delta \dot{u}\}$	Vector for small arbitrary displacements
$\{\delta\varepsilon\}$	Vector for small arbitrary strains
Δt	Time step
Δt_{cr}	Critical time step
ε'	Preassigned value for solution of geometrical nonlinearity
ε''	Preassigned value for solution of coupled dam-reservoir system
$\{\varepsilon\}$	Strain vector
$\varepsilon_x, \varepsilon_y$	Normal strain in x and y direction respectively
ϕ	Total porosity
ϕ_0	Initial porosity
ϕ_c	Porosity due to concrete matrix dissolution
ϕ_m	Apparent mechanical porosity
ϕ'	Angle of reservoir bed inclination
$\{\Phi\}$	Prescribed surface traction vector
$\gamma_{xy}, \gamma_{zx}, \gamma_{xz}$	Shearing strains in x-y, y-z and z-x plane respectively
Γ	Boundary under consideration
Γ_f	Free surface boundary of reservoir
Γ_r	Boundary at reservoir bottom of reservoir
Γ_t	Boundary at the truncation surface
Γ_{fs}	Boundary at the dam-reservoir interface
ϑ, γ	Newmark's integration constant
η_y	Elevation relative to the mean surface

$\ddot{\eta}_y$	Double derivative of η_y with respect to time
κ^0	Initial threshold degradation
κ	Internal variable defining the current damage threshold
λ_m	Eigenvalues of the reservoir
Λ_1	$(1-d_{g1})$
Λ_2	$(1-d_{g2})$
ν	Kinematic viscosity
θ	Inclination of dam-reservoir interface
ρ_d	Mass density concrete
ρ_f	Mass density of fluid
ρ_s	Mass density of sediment
σ_{p1}	Maximum tensile and minimum compressive principal stress
σ_{p2}	Maximum compressive and minimum tensile principal stress
$\{\sigma\}$	Stress vector
$\{\sigma_e\}$	Elemental stress vector
τ_a	Characteristic age for which the structure is designed
ς	Normalized process extent
$\dot{\varsigma}$	Time derivative of ς
ω	Excitation frequency
ω_d	Natural frequency of the dam
ω_i	Instantaneous excitation frequency of a signal
Ω	Region under consideration
Ω_e	Volume of an element
Ω_f	Reservoir domain

Ω_i	Tributary area of the dam surface in direction i
Ω_i^d	Area affected by degradation
Ω_d	Structural domain
ξ,η	Natural Coordinates
ξ_γ	Reaction extent corresponding to characteristic time, τ_r
ξ'	Critical damping ratio
ζ	Damping parameter at the truncation surface of reservoir
ζ_m	Complex coefficient at the truncation surface of reservoir

LIST OF ABBREVIATION

FFT	Fast Fourier Transform
HM	Hygro-Mechanical
HCM	Hygro-Chemo-Mechanical
NRBC	Non-Reflecting Boundary Condition
ORS	Over Rigid Stratum
OFS	Over Flexible Stratum
STFT	Short Time Fourier Transform
TBC	Truncation Boundary Condition

UNITS USED

m	: Meter
kg	: Kilogram
N	: Newton
kN	: Kilo-Newton
Pa	: Pascal
MPa	: Mega-Pascal
sec	: Second

CHAPTER 1

INTRODUCTION

A concrete gravity dam is a submerged structure with a complicated geometry and complex behavior under seismic condition. It is constructed mainly to harness the potential energy of rivers for generation of hydroelectricity and at times for irrigation. These dams are expected to retain the water impounded in the reservoir and to resist the unpredictable earthquakes with acceptable damages in seismic prone areas. With an increasing demand for power, large numbers of concrete dams are being built or in use all over the world, out of which many of them had been constructed decades ago. The failure of a concrete gravity dam can lead to catastrophic consequences of sudden release of the reservoir, devastating habitations in the vicinity. Failure may occur due to floods exceeding the designed full reservoir level. At a time, when reservoir level dangerously fluctuates, and an earthquake occurs, the stresses in the dam may exceed the calculated values leading to its failure. For the safety of the habitants living on its downstream side, it is important to ensure that these dams are not susceptible to failure due to severe earthquakes.

The issues of seismic safety of dams have been looked at with increased attention in various parts of the world in recent years. It has become a major factor in the planning and designing of new dams proposed to be built in seismic regions and for safety evaluation of existing dams in these regions. To prevent the failure of a dam, it is important to assess its behavior at any age during its lifetime, so that remedial measures can be undertaken to strengthen or perhaps decommission the dam at the right time. For the design of an earthquake-resistant dam and the evaluation of the safety of an existing dam, it is important to use a rational and reliable dynamic analysis procedure. The dynamic response of a linearly elastic dam can be determined by standard techniques if the reservoir is empty. But the problem becomes complicated, when the interaction effects of the unbounded reservoir and the elastic foundation has to be adequately accounted for. This problem requires special attention, as the overall system is a combination of three different systems and is much larger than the dam itself. The analysis procedure should be capable of evaluating the dynamic deformations and

stresses in a dam subjected to a given ground motion. The deformations and stresses so obtained will be more realistic if (i) the deterioration of concrete strength during its lifetime can be effectively incorporated in the numerical model, (ii) the interaction effect of the unbounded reservoir is determined appropriately, (iii) the boundaries of the infinite reservoir are modelled aptly and (iv) the dam-foundation interaction is considered when the geological site conditions necessitates.

To predict the safety of a dam at any age, generally stresses due to static and dynamic loading are evaluated. The elastic modulus of the concrete dam adopted at the time of analysis is same as considered at the time of design of the dam. Concrete develops strength with continued hydration. At an early age the rate of strength gain is faster but the rate gets reduced with age. It is customary to assume the 28 days strength as the full strength of concrete, but experimental evidences (Washa et al.1989) show that concrete develops strength beyond 28 days.

Though various non-linear analysis procedures have been developed to determine the effect of damage on the responses of the dam due to seismic excitation, primary mechanisms or factors that can produce premature deterioration of concrete dams need to be identified. Many researchers (El-Aidi & Hall 1989, Cervera et al. 1995 and Ghaemian & Ghobarah 1999) had considered the dam-reservoir-interaction problem with an isotropic damage while developing a non-linear damage model. The damage index used in the above procedures is mainly evaluated based on relation between the strain energy of the damaged material and elastic energy of the undamaged material.

Researchers have treated the evolution of damage index by different approaches (Ghrib & Tinawi, 1995a & 1995b, Hubert et al., 2001 and Mazzotti et al., 2001). The durability of concrete in dam is considerably affected by the accumulation of damage induced by the time variant external loading in conjunction with environmental loading processes such as moisture and heat transport, freeze-thaw action, dissolution processes such as calcium leaching, chemical expansive reactions (alkali-silica reaction) due to presence of silt deposited on the upstream face. Although considerable progress has been achieved in carrying out dynamic analysis by modelling concrete gravity dam considering the non-linear behavior of concrete including cracks, environmental effects are still accounted for by more or less heuristic evaluations of the degradation process

and its influence on the residual structural safety. Since the dam face is in constant touch with water, concrete degradation due to hygro-mechanical loading is inevitable and should be considered in the analysis procedure.

For simplification of the analytical procedures, the bottom of the reservoir is generally considered to be rigid, which does not represent the actual behavior of the system. The sedimentary material in the reservoir bottom absorbs or radiates energy at the bottom that will affect the hydrodynamic pressure developed at the upstream face of the dam. The fundamental parameter characterizing the effect of absorption of hydrodynamic pressure waves at the reservoir bottom due to sediment is the reflection coefficient. The wave reflection coefficient is determined from parameters based on sediment layer thickness, its material properties and excitation frequency. An analytical or a closed-form solution cannot account for the arbitrary geometry of the dam or the reservoir (Fig.1.1). This problem can be efficiently tackled with finite element technique. The need for an accurate truncation boundary is felt to reduce the computational domain of the unbounded reservoir system. The ageing of a concrete gravity dam further presents a new challenge for the development of a methodology that can adequately predict the stability of the dam under seismic excitations and identify those structures where remedial measures are to be taken.

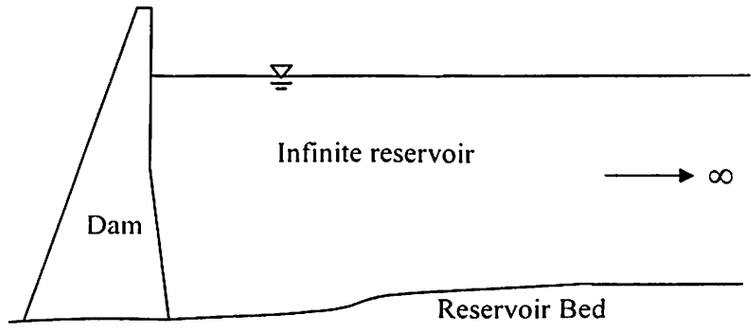

Fig.1.1 Geometry of a dam-reservoir system

The purpose of the present investigation is to develop a numerical scheme in time domain for evaluating the stresses inside the body of the submerged ageing dam interacting with the unbounded reservoir having sediment layers at its bottom. The response obtained by this novel procedure can be effective in earthquake vulnerability assessment of concrete gravity dam.

The existing literature indicates a wide range of research work for predicting the behavior of a dam-reservoir coupled systems. Westergaard (1933) was the first to study

the hydrodynamic pressure distribution in the vertical face of the rigid dam subjected to horizontal ground motion. The pressure at the dam-reservoir interface was evaluated by analytical methods. The investigations led to the added mass approach according to which the interaction forces were found to be proportional to the acceleration of the earthquake ground motion such that they may be approximated by a mass density distributed parabolically over the height of the dam. This approach was based on the argument that the dominant energy content of the spectral components of the earthquake ground motion is significantly smaller than the first eigen-frequency of the reservoir. But this approach is no longer valid as because the spectra of registered earthquake ground motions show significant amplitudes over a wide range of frequencies. The hydrodynamic pressure evaluated by the added mass approach does not consider any radiation damping. Therefore, the energy dissipation is only due to structural damping. Among the numerous publications devoted to dam-reservoir systems, Chopra (1967) emphasized the significance of compressibility effects on the dam-reservoir interaction forces. It was found that neglecting the compressibility of water led to significant errors, as the wave propagation speed is infinite in incompressible medium. Moreover, the effect of considering the flexibility of the dam was found to alter the natural frequencies of the dam-reservoir coupled system (Chopra 1968). Chwang (1978) proposed an analytical solution to determine the hydrodynamic pressure distribution on the rigid dam having inclined upstream face of constant slope considering the water to be incompressible. Further research led to the modification of the analytical solution considering vertical upstream face to incorporate the effect of reservoir bottom absorption that necessitates the determination of eigen-frequencies with the use of advanced programming techniques or specialized finite element program like Earthquake Analysis of Concrete Gravity Dams, EAGD (Fenves and Chopra, 1984). Alternative closed-form method (Bouaanani et al. 2003) was proposed to determine these eigen-frequencies, which significantly reduced the efforts required to determine the eigen-frequencies with negligible error. But all these analytical or closed-form methods are suitable only for rigid dam and the regular geometry of the upstream face (i.e., vertical face or inclined face with constant slope) of the dam or for regular geometry of reservoir. In most of the practical cases, the dam-reservoir interface is irregular in nature and the reservoir bed is not horizontal. Hence, it is difficult to obtain a closed form analytical solution for such problems. As a result, many researches have been directed towards the development of different numerical techniques. Several numerical techniques such as finite difference method, control volume method, panel

method, finite element method, boundary element method etc. have been used extensively to predict the behavior of coupled systems having arbitrary geometry. While different techniques have their own merits and limitations, it has been experienced by the researchers that the finite element method has certain distinct advantages over other methods.

The versatility of the finite element method has motivated researchers to apply the technique in the analysis of dam-reservoir systems. The significant advantage of finite element method is that it enables a single program to treat almost any configuration and to represent complex structures reliably for an accurate stress analysis. The literature (Yang et al. 1993) indicates that the boundary element technique which is often believed to be adequate for modelling of semi-infinite or infinite domains appears unable to show its efficiency in time domain analysis of fluid-structure systems.

While using finite element technique in the analysis of a dam-reservoir system, difficulty arises in effectively modelling the large extent of the reservoir that is practically unbounded. The unbounded reservoir has important consequence in the analysis of the dam-reservoir system, as waves travelling to infinity are not reflected back towards the dam. This leads to the development of an energy dissipation mechanism called radiation damping. The accurate modelling of radiation damping is of extreme importance as it effects the hydrodynamic pressure generated in the reservoir and hence the response of the dam. For efficient numerical solution of the system, the unbounded reservoir is truncated at a certain distance away from the dam. Accuracy in the results may be obtained by truncating the reservoir at a larger distance away from the dam. However, this results in an increased cost of computation. If the effect of dam-reservoir interaction is included in the analysis, the cost of computation will further increase to be prohibitive. Therefore, it is necessary to impose an efficient boundary condition at the truncated surface of the reservoir that can account for radiation damping. The boundary conditions imposed at the truncated surface are also termed as non-reflecting, silent, transmitting, radiation or absorbing boundaries. These truncation boundaries are mainly of two types: local or non-local. Local boundary conditions are formulated using differential operators with respect to space and time. Local boundaries are hence sensitive to location of the truncation surface from the dam. On the other hand non-local

boundaries are not dependent on the distance of the truncation surface away from the dam.

The most commonly used boundary condition along the truncation surface for the analysis of dam-reservoir system is the well-known Sommerfeld radiation condition, which is of local type. This boundary condition is inappropriate for excitation frequencies lower than the first natural frequency of the reservoir. Investigations made by Sharan (1985a) reveal that for excitation frequencies greater than the fundamental frequency of the reservoir, the results obtained by the use of Sommerfeld radiation condition oscillates about the exact result as the length of the reservoir is increased. The research conducted by Sharan (1987b, 1992) has led to the development of the boundary condition that can be used effectively in the analysis of dam-reservoir system, although it is also an inaccurate one (Maity & Bhattacharyya 1999). Although efficient, the boundary condition proposed by Maity & Bhattacharyya (1999) does not exist for excitation frequency equal to or greater than the resonant frequency. Also, this truncation boundary condition (TBC) can not include the absorption effect of the reservoir bed. To overcome these shortcomings many a non-local boundary conditions may be adopted. The analytical solution used to derive non-local conditions depends on the discretization process, which is carried out along its boundary. As a consequence, in order to obtain reliable results, the boundary discretisations are to be sufficiently refined.

The dynamic interaction between an elastic dam and its adjacent reservoir has been the subject of intensive investigations in recent years. Some simplified approaches are available in which the dam-reservoir system is studied in a decoupled manner. In this type of analysis, the reservoir response is first obtained assuming the dam as rigid and the resulting pressure field is imposed on the dam to obtain its response. The added mass approach is another simplified approach considering water to be incompressible. These approaches lead to conservative design of the dam. However if resonance between the dam and the energy dissipating mechanism in the reservoir occurs, it can lead to an unsound design. This approach is suitable for a case when fluid oscillation frequencies are sufficiently away from the structure's predominant frequencies. Thus, there is a need to study the dam-reservoir interaction problem in a coupled manner. The dam-reservoir interaction problem can be solved by coupling both the systems directly or indirectly. It

is important to predict the hydrodynamic response of the reservoir accurately in the presence of a dam and their interactions thereof for the safe design of the dam.

The most common approach being adopted is that both the systems are coupled and solved as single system (Zienkiewicz and Bettess 1978, Olson & Bathe 1985a Fenves & Vargas-Loli 1988 and Chen & Taylor 1990). Formulations based on displacement variables are generally chosen for the structure while the fluid is described by different variables such as displacement, pressure, velocity potential etc. for such coupled problems. A number of researchers (Zienkiewicz and Bettess 1978 and Yang et al. 1996) used hydrodynamic pressure as the unknown variable in finite element discretisation of the fluid domain. But the resulting equations in this case lead to unsymmetrical matrices and require a special purpose computer program (Sandberg 1995). Zienkiewicz et al. (1983) represented the equations of fluid domain in terms of a displacement potential. The coupled equations of motion in this case become unsymmetrical, but irrotationality condition on fluid motion is automatically satisfied. Many researchers (Bermúdez et al. 1995) formulated the governing equations of fluid in terms of displacements. The advantage of the displacement-based formulation is that the fluid elements can easily be coupled to the structural elements using standard finite element assembly procedures. But the degrees of freedom for the fluid domain increase significantly (especially for 3D problems). Moreover, the fluid displacements must satisfy the irrotationality condition, otherwise zero frequency spurious modes may occur. The variables such as velocity and pressure have also been used for representing the governing equations for fluid by Fenves & Vargas-Loli (1988). However, requirement of computational time becomes higher as number of unknown parameters increase in the fluid domain. Thus the need of a large computer storage and expense of vast computer time usually make the analysis impractical. The solution of the coupled system may be accomplished by solving the two systems separately with the interaction effects enforced by iteration (Singh et al. 1991). The major advantage of this method is that the coupled field problems may be tackled in a sequential manner. The analysis is carried out for each field and updating the variables of the fields in the respective coupling terms enforces the interaction effect.

The dynamic analysis of a dam-reservoir system can be performed either in time domain or frequency domain. A frequency domain analysis can be adopted when the

behavior of the coupled dam-reservoir system is considered to be linear. Semi-analytical solutions may be used considering the reservoir to be semi-infinite with constant depth (Chopra & Chakrabarti 1981) or a combination of finite elements and semi-analytical solution may be used for semi-infinite and irregularly shaped reservoirs (Hall & Chopra 1982 and Lotfi 1986). Wepf et al. (1988) derived a hydrodynamic stiffness matrix in frequency domain for a reservoir with arbitrary shape of the upstream dam face and reservoir bed using the boundary element method. To transform the hydrodynamic stiffness matrix from frequency domain to time domain, the singular part consisting of its asymptotic value of $\omega \rightarrow \infty$ is split off. It consist of an imaginary linear term provides damping to the system. This formulation leads to convolution integrals in time. A simplified model using an approximate one-dimensional wave propagation model (Chandrashaker & Humar 1993) have been exclusively developed for the analysis of dam-reservoir system in the frequency domain.

While the frequency domain models have been improved continuously, a very few time domain models which rigorously consider the radiation damping and reservoir bottom absorption effect have been developed so far. The interaction effects in time domain using a two-dimensional dam-reservoir model were computed by evaluation of convolution integrals (Feltrin et al. 1990, Tsai et al. 1990 and Guan et al. 1994) that require considerable computational effort. Darbre (1993) and Chavez & Fenves (1995) used the hybrid frequency time domain procedure to evaluate the dam-reservoir interaction forces, where the response of the system is computed in frequency domain. The radiation damping in the unbounded reservoir was represented by standard viscous dampers (Ahmadi & Khoshrang 1992, Daniell et al. 1995 and Küçükarslan 2003) that need large extent of the reservoir to be considered to obtain an adequate accuracy. Most of the analysis procedures in time domain are too rigorous and complicated; and simplified techniques may not give accurate results. This necessitates an analysis procedure in time domain that can be easily implemented.

The objectives of the present investigation are firstly, to develop a numerical scheme to predict the concrete degradation in an ageing dam due to adverse environmental factors; secondly, to develop an appropriate numerical model of the infinite reservoir that is effective for seismic analysis in time domain considering the reservoir bottom absorption effect and thirdly, to develop an efficient, robust and stable

numerical algorithm for the analysis of ageing concrete gravity dams in the vicinity of infinite reservoir considering fluid-structure interaction.

In the present investigation, a finite element iterative scheme is developed to study the dam-reservoir interaction problem. Assuming the water in the reservoir to be inviscid and irrotational, the pressure is considered as the unknown variable parameter in the reservoir. The elastic dam is analyzed by two-dimensional plane strain formulation considering geometrical nonlinearity as well. A degradation model is proposed for the ageing concrete gravity dam that considers strength gain with age and material degradation due to adverse environmental conditions. An appropriate non-reflecting boundary condition in time domain is proposed at the truncation surface to model the unbounded reservoir having an absorptive reservoir bed, into a finite one for the finite element analysis. An iterative scheme is developed that enables evaluation of divergent free displacement and pressure in the dam and the reservoir respectively at any instant of time. Since the two systems are dealt with separately, the resulting matrix becomes symmetric. The response of the coupled system is obtained by solving the two systems separately with the interaction effects enforced by iteration. The results are presented in both tabular and graphical forms.

The thesis is presented in five chapters. In Chapter 2 an overview of the relevant literature and the scope of the present investigation are addressed. The theoretical formulations are presented in Chapter 3 in three parts. Part A contains the formulation of the dam along with its geometrical non-linearity and the evaluation of degradation index. The FE formulation of the unbounded reservoir considering reservoir bottom absorption effect is presented in Part B. The solution scheme for the coupled dam-reservoir system is described in Part C. The numerical results and discussions are presented broadly in three parts in Chapter 4. In Part-I, the response of the concrete dam in the absence of the adjacent reservoir water with the effect of the geometrical nonlinearity is studied and presented considering material degradation. In Part-II, the hydrodynamic pressures in the reservoir is evaluated considering the absorptive reservoir bottom using the developed far-boundary condition. The response of the coupled dam-reservoir system is presented in Part-III considering dam-reservoir interaction effects. Chapter 5 comprises of the conclusions and the scope for further research.

CHAPTER 2

REVIEW OF LITERATURE

The response of any structural system comprising of more than one component is always interdependent. A concrete gravity dam consists of the structure itself, the reservoir beside it and the foundation below it (Fig. 2.1). Due to repeated earthquakes occurring in many of the earthquake-prone areas, causing severe damage to mankind, it has become very important to study the effect of earthquakes on dams. Many analysis procedures have been formulated - some simplified that may give conservative results; while others more complicated have the ability to estimate the dam response with better accuracy. The present computing scenario has led to the development of numerical analysis techniques to represent the physical problem of the dynamic behavior of concrete gravity dam accurately. Analysis procedures in the past had been carried out considering a rigid base and water in the reservoir as an added mass. Since this did not reflect the actual behavior of the dam-foundation-reservoir system, analysis procedures considering the interactions among them have been devised. The dynamic characteristics of the system and the characteristics of the ground motion affect the fluid-structure-soil interaction effect on the seismic response of the dam. Available results show that the response of the system is reduced due to damping effect of soil. The additional damping due to foundation-structure interaction is attributed to radiation damping of the unbounded soil. The accuracy of the analysis procedure used for design or safety assessment of the dams depends on how well the idealized interaction mechanisms and selected parameters represent the actual field condition.

The dynamic behavior of a submerged concrete gravity dam may change with age, as the porosity in concrete may lead to material degradation and increased permeability. The long-term degradation of concrete structures under aqueous environmental conditions is mainly controlled by interacting chemical and mechanical processes leading to the destruction of the microstructure of the concrete. During the entire lifetime of a dam, harsh environmental conditions and various types of loading induced by earthquakes, impacts due to blasts, freezing and thawing may affect material degradation. Ultimately, the collapse of such concrete structures may be caused by the

superposition of any of the deterioration mechanisms. For a more realistic estimation of the dynamic behavior of an existing or a new dam at any age, it is important to estimate the material degradation with ageing, so that the stiffness of the dam can be accurately determined. Although, a lot of research have been conducted to predict the behavior of a dams estimating the stiffness of the dam considering formation of cracks, adequate numerical methods do not exists that can bridge the gap between material degradation and loss of structural stiffness.

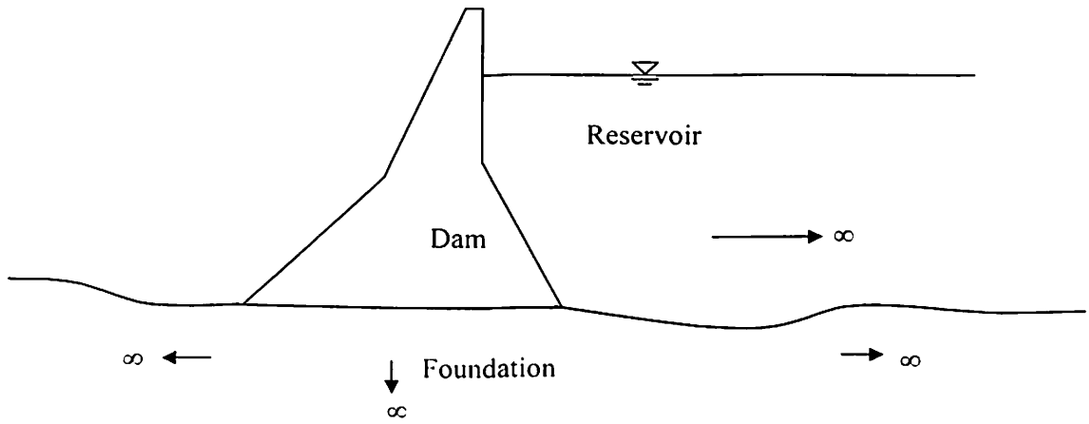

Fig. 2.1 A Typical Dam-Reservoir-Foundation System

This chapter is organized to trace the development of analysis procedures used for concrete gravity dams. A brief review on traditional design of concrete gravity dams is presented. In the following sections, a survey of various techniques of idealizing and modelling each element of the system: the dam, the reservoir and the foundation are discussed. A review of techniques adopted to model the fluid in the reservoir, structure, fluid-structure system, fluid-soil (reservoir bottom) interaction, and relevance of soil-structure interaction is outlined. The suitability of different methods and sensitivity to various parameters are discussed and summarized at the end of this chapter.

2.1 DETAILED REVIEW

2.1.1 Traditional Static Analysis and Design

The design methods, as specified by U.S. Bureau of Reclamation in Design Standards No.2 (1965, 66) and Design manual (1976), the dynamic behavior of the elastic dam, reservoir water and foundation rock system was not recognized. The Indian

Standards Code (IS: 1893-1984) specifies the determination of hydrodynamic pressures with an expression that was established by Zangar (1952) using an electric analog:

$$p = C_s \alpha_h \rho_f H_f \qquad (2.1)$$

where C_s is a coefficient that is determined experimentally and varies with shape and depth, α_h is the seismic coefficient, ρ_f is the density of water and H_f is the depth of water in the reservoir. The above expression could be used for determination of pressure against the inclined upstream face of rigid dams due to horizontal earthquakes. The forces associated with the inertia of dam were expressed as the product of seismic coefficient taken to be constant over the surface of the dam, with values ranging between 0.05 and 0.1; the weight of the dam per unit surface area expressed as a function of location. This analytical expression has been found to be useful for minor works or for preliminary design of major works, giving the hydrodynamic pressure distribution in the upstream face of the dam to calculate total horizontal force and the overturning moment above any elevation of the dam.

The standard static design procedure does not account for the random earthquake motions. The inertia forces induced by the earthquake are statically applied at the centre of gravity of the dam. The limitations of this method are that it disregards the elasticity of the dam, the time varying excitation force and the damping capacity of the dam. Despite these disadvantages, the method is still employed owing to its simplicity. It was shown that if the dynamic character of earthquake forces is ignored, the dynamic analysis does not indicate the actual principal tensile stresses, the region of stress concentration and areas where cracks are likely to occur (Chopra 1975). A large discrepancy exists between the stress distribution obtained by use of the equivalent static method and that resulting by use of proper dynamic methods (US Army Corps of Engineers 1977). Another drawback is the assumption of a height-wise uniform seismic coefficient which shows stresses to be greatest at the base of the dam. This has led to the concept of decreasing the concrete strength with increase in elevation. Fenves & Chopra (1987) proposed a simplified response spectrum analysis to determine the structural response, in the fundamental mode of vibration due to the horizontal component of ground motion. This procedure was developed as a hand calculated alternative to the more general analytical procedures that can be used to evaluate the compressive and tensile stresses at locations above the base of the dam. But dynamic analysis results show that the largest

stresses actually occur at the upstream and downstream faces in the upper part of gravity dams (Chandrashaker & Humar 1993) in the case of Koyna dam. However, the largest stresses may also occur at the base of the dam depending on dynamic characteristics and geometry.

2.1.2 Modelling of Dam

To evaluate the dynamic behavior of the concrete gravity dam most of the researchers assume the dam to be infinitely long which simplifies the problem to a two-dimensional system. This modelling would be appropriate if the length of the dam is large as compared to its height. Methods of analysis based on this assumption cannot be used reliably for dams having relatively small length to height ratios. This conclusion is supported by results of a vibration experiment performed by Selby and Severn (1972) on a model wall retaining a body of water. The monoliths of a gravity dam with plane vertical joints tend to vibrate independently; hence, a two-dimensional plane stress model of the individual monoliths is usually appropriate for evaluating the response due to intense or moderate earthquake motions. A plane-strain model may be adopted for roller compacted dams built in a broad valley, without any vertical joints. For dams having length to height ratio too small, it is necessary to perform a three dimensional analysis. Moreover, if the gravity dam has effective keyed contraction joint, or is located in a narrow canyon, it may not be appropriate to assume independent response of the blocks. Consideration of a three-dimensional model of the dam makes the problem computationally large.

Earlier, the effects of earthquakes on dams were represented considering dam to be a rigid system supported on a rigid foundation. But most of the recent work has incorporated the elastic properties of the dam materials into the mathematical model, which influences the vibration properties of the dam and influences the earthquake response behavior. When flexibility of dam is considered, the hydrodynamic responses show high peaks at the natural frequencies of the system (Saini et al. 1978). Considering the dam as rigid and water to be incompressible, the authors showed that the hydrodynamic forces and dynamic amplification factor remained independent of excitation frequency in a frequency domain analysis. However, when flexibility of dam was considered, the responses were dependent on the excitation frequency. They used the

discretized equation of motion in finite element form for the dam subjected to ground motion which is expressed as:

$$[M]\{\ddot{d}\}+[C]\{\dot{d}\}+[K]\{d\}=-[M]a_g(t)+[L]\{p\} \tag{2.2}$$

where,

$[M]$ = the mass matrix of the structure

$[C]$ = the damping matrix of the structure = $\alpha'[M]+\beta'[K]$

$[K]$ = the structural stiffness matrix

$\{d\}$ = the vector of nodal point displacements relative to ground

$[L]$ = the matrix which determines the hydrodynamic forces from pressures.

$\{p\}$= pressure at dam-reservoir interface

a_g = ground acceleration

α' = mass proportional damping constant

β' = stiffness proportional damping constant

In the above expression, dots define differentiation with respect to time, t. Damping is expressed as linear combination of the mass and stiffness of the system, where α' and β' can suitably be chosen to obtain the desired damping in the system. This type of damping is normally referred to as Rayleigh damping. However, when cracks are included in the analysis the mass proportional term may be omitted because it would provide artificial stability to the portion of the dam above the crack (El-Aidi & Hall 1989). The Rayleigh damping matrix is equivalent to using a modal analysis in which damping is expressed as a fraction of critical damping given by

$$\zeta_r=\frac{1}{2}\left[\left(\alpha'/\omega_r\right)+\beta'\omega_r\right] \tag{2.3}$$

where, ζ_r is the fraction of critical damping and ω_r is the natural frequency of vibration in the r^{th} mode of vibration. Rayleigh damping does not occur naturally, but is used only for numerical convenience.

2.1.2.1 Three Dimensional Modelling of Dam

The results (Rashed and Iwan 1984) obtained from the analytical expressions derived from the 3D modelling of the reservoir for short length gravity dams clearly show that hydrodynamic pressures generated in the reservoir depend on length to height ratio of the dam, the cross stream and vertical components of ground motion. When longitudinal

ground motions are applied to the flexible boundaries along the canyon profile of the reservoir, the pressures are found to vary along dam length unlike the 2D case. The vertical distribution of pressure due to vertical ground motion approaches those of 2D case at mid-length of the dam as width to height ratio of dam becomes large. Neglecting the flexibility of reservoir boundaries makes the pressure independent of the position along dam length and identical to 2D case. The effect of transverse ground motion can be accounted for only in 3D analysis and found to be maximum at the reservoir sides and decreases to zero at mid span of the dam.

Fok et al. (1986) developed the EACD-3D computer program implementing an analytical procedure for the three-dimensional analysis of earthquake response of concrete dams including the effects of dam-water interaction, water compressibility, and reservoir boundary absorption due to alluvium and sediments at the bottom.

A numerical correlation study was carried out along with an extensive dynamic testing on Outardes 3 gravity dam in northeastern Quebec, Canada (Proulx and Paultre 1997) to evaluate the performance of 2D and 3D models. It was concluded that for earthquake analysis of gravity dams with un-keyed construction joints, a 2D model is reasonable if sliding of vertical blocks is expected. However, for important projects and critical safety evaluation, a 3D analysis was recommended.

In a three-dimensional analysis of concrete gravity dam, Azmi and Paultre (2002) developed a nonlinear joint element to represent the dynamic behavior of vertical contraction joints in concrete dams. This element could account for partial joint opening and closing governed by normal stress criteria; and tangential displacement is governed by the Mohr-Coulomb friction criterion. However the dynamic analysis indicated that the joint opening was not significant. Further research is required to find out its significance and whether this non-linearity must be a parameter in the analysis of such dams.

Another 3D model as proposed by Fahjan et al. (2003) can account for the canyon profile and gives accurate response of the structure. But the computational effort required for a 3D analysis is so high that it is not found to be very beneficial unless the dam is located in a narrow canyon; for which it gives higher peak acceleration values than those

calculated by 2D idealization. This is due to excitation through lateral abutments and larger contribution of the higher modes of vibration.

A three-dimensional model can thus be used when the dam or loading is such that plane strain conditions may not be assumed, when the geometry is such that the stability of the dam depends upon stress distribution parallel to its axis, as is the case of a gravity-arch dam which is curved in plan, or when a dam is in a narrow valley. Three-dimensional analysis allows the rigorous determination of what forces will be applied to the foundation, and where. If 3D behavior is to be considered, features that enable horizontal force transfer such as shear keys or curvature in plane must be present.

2.1.2.2 Nonlinear Analysis

The response of a concrete gravity dam due to expected earthquake could be obtained by a linear dynamic analysis. But a severe earthquake may cause significant damages to concrete dams, which may be associated with changes in the structural stiffness. Consequently, if damage occurs, the actual performance can be predicted only by a nonlinear analysis that takes into account stiffness changes. In a nonlinear response analysis procedure, the seismic performance of the concrete dam is evaluated based on the behavior of the material and the components of the system, which is characterized by nonlinear force-displacement relationship. A study of the literature on non-linear analysis of concrete gravity dams due to cracking of concrete reveals that depending on the intensity of ground motion, tensile cracking can substantially alter the earthquake response of a dam and its ability to impound water. Before a gravity dam fails by overturning, other failure modes may occur due to crushing of toe material, cracking of upstream material with an increase in uplift pressure and reduction in shear resistance that may result in sliding instability (Copen et al. 1977).

A survey of the literature on finite element modelling of cracks and joints shows that two main approaches are used by researchers for dynamic analysis of dams: the *smeared crack* (Pal 1974, Zienkiewicz et al. 1981, Kuo 1982, Mlakar 1987 and El-Aidi & Hall 1989) and *discrete crack* (Skrikerud and Bachmann 1986) approach. The non-linear tensile and compressive behavior of concrete, including strain rate effects, was represented by modifying an equivalent uniaxial stress-strain relationship (Pal 1974) or by appropriately modifying the material properties at the integration points of regular

finite elements (Zienkiewicz et al. 1981). The limitation of the smeared crack model is that the response may not be accurate when coarse finite element mesh is used in the analysis. The discrete cracks are simulated by originally adjacent finite elements that can trace crack formation propagation i.e., initiation, extension, closure and reopening. The disadvantage is that to obtain accurate responses a very fine finite element mesh is required. Discrete or smeared crack models have only a limited ability to model sharp discontinuities, for which the use of joint elements is more appropriate. It is observed from the various nonlinear analyses (Mlakar 1987, El-Aidi & Hall 1989, Feltrin et al. 1992, Galli et al. 1992, 1994, Cervera et al. 1995 and Guanglun et al. 2000), that a large percentage of the energy is dissipated through the cracks formed in the dam. The fundamental period of the dam was found to increase as the dam became more flexible due to the formation of cracks. The formation of tensile cracks dissipates energy in the system that leads to reduction of dynamic water pressure.

The crack band theory (Vargas-Loli & Fenves 1989) has also been used to model tensile cracking to evaluate the nonlinear seismic response of a dam-reservoir system. The use of this theory allows use of large size finite elements. The continuum model proposed by Lemaître & Chaboche (1989) and Krajcinovic (1989) was found to be advantageous over the discrete approach, as it does not require re-meshing. A boundary element (BE) technique was formulated by Pekau et al. (1991) and Batta & Pekau (1996), which was found to be efficient for the analysis of seismic crack propagation due to simplification of the non-linear dynamic problem as it is based on linear elastic fracture mechanics. The various approaches that have been used by researchers, in the context of cracks (Ghrib and Tinawi 1995a) are briefly presented in Chart. 2.1.

Procedures to verify the seismic stability of concrete dams due to overturning and sliding were proposed by Léger & Katsouli (1989) and Chavez & Fenves (1995). Léger & Katsouli (1989) used gap-friction elements having nonlinear constitutive relation to model possible vertical separation and sliding of dam interface. The sliding of the dam was found to dissipate very little energy as compared to energy dissipation due to formation of cracks. The seismic fragility assessment using a probabilistic model (Tekie & Ellingwood 2003) indicated that sliding along the dam-foundation interface is likely if the dam is subjected to an earthquake with a magnitude of the maximum credible earthquake (MCE) as specified by the U.S. Army Corps of Engineers.

Chart 2.1 Strategies Available for Stress and Crack Response of Concrete Dams (Ghrib and Tinawi 1995a)

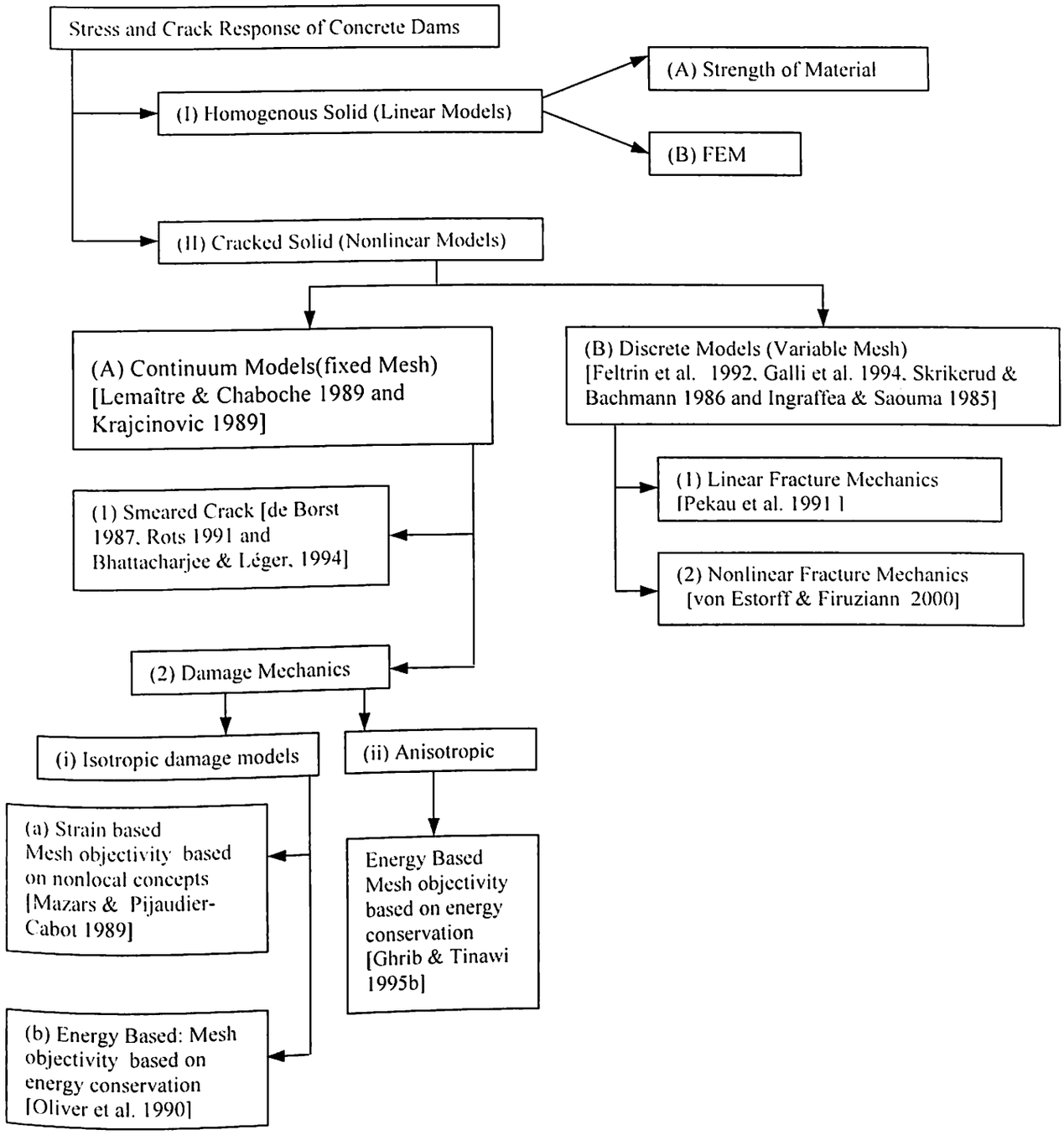

A dynamic nonlinear analysis may be adopted if cracks are present in the dam body, if the soil at the site where the dam is constructed is soft, heterogeneous having cracks, faults and fissures; and if possibilities of strong earthquakes occurring at the site are high. The choice of nonlinear analysis procedure to adopt will mainly depend on the geometry, material and dynamic characteristics of the dam-reservoir-foundation system.

2.1.2.3 Concrete Degradation

Concrete dams are in a constant state of submergence. Concrete is porous and characterized by a very large internal surface that strongly interacts with water. In the larger pores in concrete, due to capillary surface tension, capillary forces are induced along the solid-fluid interfaces. These water induced stresses although of different origin are related to the degree of saturation. As a result of saturation of the pores in concrete its material strength is reduced. At the macro-level, this effect is observed as a decrease of the elastic stiffness. In addition to these processes, structural deformations may occur due to inhomogeinities of the material and the non-uniform moisture distribution associated with the geometry of the structure. Restrained shrinkage deformations on the micro-level may lead to large stresses that induce micro-cracks as the local strength is exceeded. A state of damage may be induced already in the unloaded structure, which affects not only the apparent macroscopic material strength but also the permeability of the material. Hence, it is important to estimate material degradation with ageing. Moreover, during the entire lifetime, the dams may be subjected to harsh environmental conditions and various types of loading induced by earthquakes, impacts due to blasts, freezing and thawing that may affect material degradation. Since the scope of the present work is to predict the dynamic behavior of an ageing dam, a number of relevant literatures are reviewed and presented in brief.

Hydration of cement being a highly exothermic chemical reaction, after pouring the concrete during the construction of massive structures like concrete gravity dams the temperature may rise up to 50° - 60°C. As the rate of hydration slows down, the temperature decreases resulting in thermal shrinkage that leads to thermal stresses. Hydration is at the base of the ageing phenomena, which at a macro level appears to be a change in mechanical properties of concrete with time (Byfors 1980).

Experimental evidence (Tu & Niu 1988) shows that during construction autogeneous strain stabilizes after 70 days (Fig. 2.2). Autogeneous shrinkage occurs in a conservative system where no moisture movement is permitted to or from the paste and the temperature remains constant. Such deformations are important for the case of mass concrete in the interior of a concrete dam (Shetty 1998).

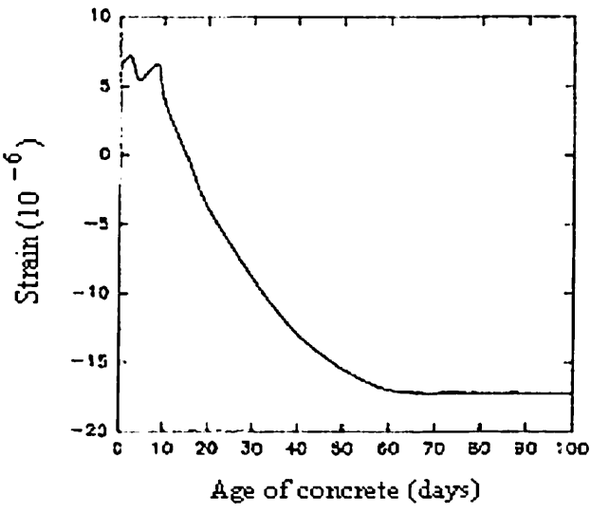

Fig. 2.2 Experimental data of autogenous deformation (Tu & Niu 1988)

Bazant's (1994) study of hydration of concrete at micro-level reveals that it is a change in concentration of non-ageing constituents like hardened cement gel constituting of tri and bicalcium silicate hydrates. Ulm and Coussy (1995) explored the theory of reactive porous media for modelling of concrete at early ages. The model accounts explicitly for hydration of cement by considering the thermodynamic imbalance between the chemical constituents. The intrinsic relation between heat generation, ageing and autogeneous shrinkage is derived.

Niu et al. (1995) developed a finite element modelling procedure for describing the thermo-mechanical damage of early-age concrete in the construction of large dam. The stress deformation analysis procedure includes temperature-induced, creep-induced and autogeneous deformations. A failure criterion for each failure mode was developed along with constitutive relationships for pre-failure and post-failure states during loading and unloading conditions.

Bazant et al. (1997) proposed a new physical theory and constitutive model considering effects of long term ageing and drying on concrete creep. This theory is an improvement over the solidification theory in which ageing is modelled by volume growth. Bazant & Xiang (1997) proposed a solution procedure to predict the design lifetime of concrete considering crack growth and long time loading. The results obtained by measuring the time rate of crack mouth opening in notched concrete specimens

subjected to constant load of almost one month are described by a previously proposed time-dependent generalization of the R-curve model. In the R-curve model the rate of crack growth is a function of the ratio of the stress intensity factor to the R-curve. The linear ageing viscoelastic creep in the bulk of the specimen is treated according to the operator method. The time curves of crack opening terminate with an infinite slope, indicating the lifetime. The finiteness of the lifetime is not caused by creep, but by time-dependent crack growth, which dominates the final stage of crack opening. The initial stage of crack opening, on the other hand, is dominated by creep. For the stronger concrete, the lifetimes are found to be longer.

Cervera et al. (1999, 2000a, b) proposed a thermo-chemical model to simulate the hydration and ageing process of concrete considering creep and damage in a roller compacted concrete dam. The evolution of temperature, elastic moduli, compressive and tensile stress distribution inside the dam can be predicted in terms of ageing degree at any time during the construction process and also during the first years following the completion of the dam. This procedure can be applied to understand the effect of some major variables such as the placing temperature, the starting date and the placing speed on the construction process. In the long term, ageing of concrete is affected by the concentration of various constituents in the concrete matrix, chemical reactions such as calcium leaching or alkali-silica reaction, moisture transport and loading due to submergence in water. According to Cervera et al. (2000b), the consideration of creep is significant if the stress analysis includes simulation of construction process. This is because rheological effects are most evident for early age concrete.

Lindvall (2001) determined the service life of concrete structures mathematically that was dependent on material properties, construction process and environmental effect. The prediction of deterioration of concrete was based on theories of transport in porous materials and empirical models, which were based on observations from structures. Prediction of service life was further made based on performance based design methodology and probabilistic methods. Probabilistic methods require extensive statistical quantifications of the parameters in the mathematical models. These statistical quantifications further require an understanding of the parameters that influence the deterioration of concrete such as concrete composition, environmental actions at the surface of the structure and the response from the concrete.

A coupled hygro-mechanical model for finite-element analyses of structures made of partially saturated porous media consisting of cementitious materials such as concrete was formulated by Meschke and Grasberger (2003). The multi-surface elastoplastic damage model, formulated in the space of plastic effective stresses, is employed to describe the nonlinear material behavior of concrete, considering stiffness degradation and the growth of inelastic strains as a consequence of the opening of microcracks. The effect of cracking on the isothermal liquid permeability was considered and was found to have strong influence on moisture transport. Bangert et al. (2003) evaluated the long-term material degradation in concrete structures due to a chemically induced degradation processes and calcium leaching.

Steffens et al. (2003) introduced an ageing approach to determine the degradation of concrete structures considering water effect on Alkali-Silica Reaction (ASR). A comprehensive mechanical model was proposed for the material swelling with a hydro-chemo-mechanical approach, to study structural effects of ASR. The model adopts a two-stage mechanism for the swelling kinetics, consisting of (i) the formation of an amorphous gel for which a characteristic time of reaction is identified and (ii) the quantity of water interacting with the gel. The ageing effect on the material degradation and structural response is validated with experimental results.

Sain & Chandra Kishen (2003) proposed a fatigue crack propagation law for concrete that considers the effect of overloads and loading frequencies. Based on this fatigue law and creep phenomenon, the residual life of concrete members is predicted. Static fracture theory was applied to obtain the crack propagation nature in a concrete member under constant load, whereas creep was considered by its effect on decreasing the elastic modulus. The authors concluded that creep dominates the initial stage of structural performance but the final failure occurs due to time dependent crack growth.

It is apparent from the literature referred above that the effect of thermal stresses is important for massive concrete structures at an early age. In the long term, ageing of concrete is mainly affected by environmental conditions. Creep in concrete affects only initial stage of structural performance. Hence, it is important to consider the ageing of the dam due to material degradation or its exposure to harsh environmental factors while

performing rigorous linear and nonlinear dynamic analysis of the existing dam-reservoir system.

2.1.3 Modelling of Reservoir

For an accurate dynamic analysis of dam, the interaction between the fluid and the structure had to be accounted for, thereby, modelling of the reservoir water to evaluate the hydrodynamic pressure generated, became essential.

The vibrating movements of an earthquake induce a concrete gravity dam to be in a state of forced vibration, where the acceleration of the dam-reservoir interface subsequently induces pressure waves in the reservoir. This undulatory system, which develops temporarily in the reservoir, entails pressure wave propagation that can be expressed mathematically by the wave equation as

$$\frac{\partial^2 p}{\partial x^2} + \frac{\partial^2 p}{\partial y^2} = \frac{1}{c^2}\frac{\partial^2 p}{\partial t^2} \tag{2.4}$$

where p is the hydrodynamic pressure at any point (x,y) in the reservoir and c is the acoustic velocity in water. Different methods of solution of eq. (2.4) allow an estimation of hydrodynamic pressure considering the dam to be a rigid structure. In a simplified seismic analysis of dams, the effect of the reservoir systems is incorporated by imposing the hydrodynamic force at the dam-reservoir interface.

Westergaard (1933) determined the hydrodynamic pressure in the reservoir considering that the dam and the foundation are rigid, the dam is rectilinear and of infinite length, the upstream face of the dam is vertical, the excitation force is harmonic and develop horizontally in a direction normal to the crest length, the reservoir is of infinite length and the water in the reservoir is compressible. The analytical expression prescribed to determine hydrodynamic pressure at a depth y from the bottom of the reservoir can be given as:

$$p = \frac{8\alpha_h \rho_f H_f}{\pi^2} \sum_{n=1,3,5..}^{\infty} \frac{1}{n^2 c_n} \sin\left(\frac{n\pi y}{2H_f}\right) \tag{2.5}$$

where,

$$c_n = \sqrt{1 - \frac{16\rho_f H_f^2}{n^2 g k T^2}} \qquad (2.6)$$

In the above expressions, α_h is the ratio measuring the intensity of earthquake *i.e.*, the maximum horizontal component of acceleration of the dam-reservoir interface in the normal direction divided by gravitational acceleration g, n is the wave number ($n = 2\pi/\lambda$) where λ denotes the wavelength of the pressure oscillations, k is the bulk modulus of water ($k = c^2/\rho_f$) and T is the period of horizontal ground vibrations. The author proposed the added mass approach to determine the hydrodynamic pressure exerted on the vertical upstream face of the rigid dam during earthquake. The dynamic action of the reservoir on the dam was visualized as an added mass, as if a certain body of water moved with the dam while the remainder of the reservoir remained inactive. The added mass effect was found to be neither too large nor negligible. The author suggested a series solution of the wave equation. Simple expressions were also suggested with relevant approximations for satisfactory performance of some practical problems. The distribution of hydrodynamic pressure along the reservoir depth may be either parabolic (Westergaard 1933) or elliptic (von Kármán 1933 and Werner & Sundquist 1949).

Kotsubo (1960) presented a theoretical solution for evaluation of dynamic water pressure caused by irregular earthquakes, unlike Westergaard's (1933) assumption of earthquake to be a simple harmonic motion and the earthquake period to be longer than that of the water body. Considering the earthquake period to be close to that of the reservoir, the pressures obtained were found to be larger than that of Westergaard (1933). Expressions were presented for earthquake forces vibrating in the direction of river course and in the direction at right angle to the river.

Zienkiewicz (1964) surveyed the various studies on the behavior of dams, water retaining and submerged structures that had been made until then. The experimental investigations carried out by Okamoto & Takahashi (1960) on Kamishiiba and Tonoyama dams in Japan had been referred. The natural frequencies of the dams were found to reduce when the reservoirs were full, which agreed with the predictions based on incompressible solutions. The author concluded that the compressibility effects were not significant for slower types of oscillation.

Bustamante and Flores (1966) proposed a simple computational method for estimating the transient hydrodynamic pressure to overcome the difficulties faced in computing using 1966 generation of computers. The validity of modal analysis to determine the hydrodynamic pressures caused by earthquakes was established.

Chopra (1967) considered the water as linearly compressible for the calculation of hydrodynamic pressure developed in the reservoir due to vibration of dam. Hydrodynamic forces were calculated assuming the dam as rigid. It was established that the hydrodynamic forces could not be represented by added mass effect, when compressibility effect of water is considered. Differences were found to be quite large in the incompressible solution near the natural frequencies of the system. Since the mathematical model proposed did not allow any energy dissipation, the response due to vertical ground motion were found to be very large. According to Chopra (1968) "*The compressibility of water could be ignored, with little loss of accuracy, if the dam is flexible enough compared to the reservoir. The relative rigidity of the reservoir and the dam system, given by the frequency ratio, is the basic parameter which governs the importance of compressibility of water*".

Nath (1969) investigated the effects of compressibility of water for vertical ground motion adopting finite element technique considering various lengths of the reservoir. The most significant fact, emerged from the analysis was that, for a given frequency of vertical ground motion, the pressure coefficients at the face of the dam were considerably higher than that due to horizontal ground motion.

Adopting von Kármán's (1933) momentum balance method, Chwang & Housner (1978) determined the hydrodynamic pressure distribution along inclined upstream face of rigid dam having constant slope. An explicit analytical formula was used to evaluate the total horizontal, vertical and normal loads. The normal force coefficient was found to remain constant at around 0.5 for all slopes. Chwang (1978) further proposed an integral solution based on the exact two-dimensional potential flow theory for the same problem. The Schwarz-Christoffel theory was implemented to map the reservoir boundaries including the sloped dam-reservoir interface. The fluid in the reservoir was considered to be incompressible and inviscid; hence the Laplace's equation could be used to determine the pressure p as

$$\nabla^2 p = 0 \qquad (2.7)$$

The hydrodynamic pressure obtained by the two methods was found to be in reasonable agreement. Many researchers (Saini et al. 1978 and Chopra & Chakrabarti 1981) have shown that the effects of incompressible water are independent of the excitation frequency. The hydrodynamic forces evaluated are large enough as compared to the values obtained by considering the reservoir water to be compressible. Using the finite element technique in a frequency domain analysis Saini et al. (1978) determined the hydrodynamic responses that are highly resonant at the fundamental natural frequency of the system, but reduce significantly at higher natural frequencies. Although, the compressibility effects were shown to be significant for evaluation of hydrodynamic pressure, analytical solutions were difficult to solve for complicated dam-reservoir systems having partially or fully inclined upstream faces. To simplify the problem, compressibility of the reservoir is often neglected to develop an acceptable analytical technique to determine the hydrodynamic pressure.

To overcome the difficulties faced in determining the hydrodynamic pressures due to irregular geometries of the reservoir, a number of numerical techniques such as boundary element method (Hanna & Humar 1982), finite difference method (Hung & Wang 1987), finite element method (Saini et al. 1978, Olson & Bathe 1985a, 1985b and Sharan 1987a, 1992) have been employed for the solution of problems with irregular geometry.

Hanna and Humar (1982) had developed a boundary element method for the calculation of hydrodynamic pressure in a reservoir with a rigid gravity dam subjected to harmonic ground motion. An integral equation was derived from the familiar Helmholtz wave equation (eq. 2.4) to represent the reservoir boundary extending to infinity with a series of boundary elements. This technique could also be used to evaluate the hydrodynamic pressure for dams having different inclinations.

Hung and Wang (1987) had employed a finite difference scheme to calculate non-linear hydrodynamic pressures on vertical and inclined faces of dams. This method suffers from two severe drawbacks. The finite difference scheme is disadvantageous as it is inefficient for calculation of hydrodynamic pressure on dam having irregular upstream

face; and a large number of grid points are required to model the infinite or semi-infinite fluid domain into a finite one.

The boundary integral equation for the scalar wave equation developed by Tsai and Lee (1989) can be used to obtain the hydrodynamic pressure distributions on dams when the dam-reservoir system is subjected to ground motions. Though the effect of water compressibility is included in the formulation, the solution procedure is independent of excitation frequency.

Due to complex topographical condition of the dam-reservoir system, the finite element method is recognised as one of the powerful numerical tools in most of the practical problems to obtain the hydrodynamic pressure distribution in the fluid domain. However, the degrees of freedom increase significantly when a large length of the reservoir is considered in the analysis to simulate its unbounded effect. To enhance the effectiveness of a finite element procedure, it becomes important to truncate the infinite reservoir at a short distance away from the upstream face of the dam and impose an appropriate far-field boundary condition to account for the radiation of waves to infinity.

2.1.3.1 Modelling of Far-Field Boundary

The study of waves in bounded and unbounded media appears naturally in many areas of engineering. Although common to many fields such as geophysics, meteorology, electromagnetic, etc., the subject has perhaps been driven most obviously over the last two decades by those seeking to predict acoustic radiation and scattering by submerged objects. The main difficulty in solving exterior radiation and scattering problems arises from the unboundedness of the domain that must be discretized. Evidently an exterior domain cannot be completely discretized with standard finite elements based on polynomial shape functions. Various remedies for this problem have been developed. Most prominent among these are *Absorbing Boundary Conditions* (*ABC*), *boundary element methods*, *infinite elements*, *Non-Reflecting Boundary Conditions* (*NRBC*), *DtN* (Dirichlet to Neumann) *conditions*, and the *Perfectly Matched Layer* (*PML*). The development of efficient schemes on *finite* domains is also an important topic due to the numerical difficulties that arise in the solution of wave problems particularly at high frequencies when the wavelength is small compared to the dimensions of the finite domain.

In a dam-reservoir system, interaction with surrounding media leads to important effects that have to be included in a numerical model. For an analysis with effort that is practically reasonable only the near-field consisting of the structure and a small portion of the surrounding media is modelled directly while the rest i.e., the far-field is captured by appropriate boundary conditions. For reservoir having simple boundary, classical solution treating reservoir as continuum may be used effectively. However, if the reservoir boundary is not regular, numerical methods such as finite element and boundary element method may be used. Due to varied geometric forms of dam and irregular geometry of the reservoir, the finite element method (FEM) is recognized to be one of the most powerful numerical tools for solving such problems. However, the use of FEM for discretization of reservoir, a computational difficulty exists if the length of the reservoir becomes infinite/semi-infinite. In such practical situations, the infinite reservoir is truncated by imposing an artificial boundary at a certain distance away from the structure. For a dynamic analysis, waves generated in the near field propagate to the far-field. Hence, a suitable boundary condition must be imposed at truncation surface to evaluate the effect of radiation damping, so that no spurious wave reflection occurs from the boundary.

When a structure or its near field behaves nonlinearly and the far-field remains linear, a solution is sought in a time domain procedure. This necessitates boundaries that are effective in time domain. Attempts to formulate artificial boundaries in time domain in the past have resulted in simple, frequency independent dashpot like local boundary conditions that are not equivalent to the far-field and hence called local, non-consistent boundaries.

The first local absorbing boundary condition was proposed by Lysmer and Kuhlemeyer (1969) for numerical solution of soil-structure interaction problems in civil engineering. The viscous boundary was developed for an elastic half-space and even today, after 36 years it is frequently used as absorbing boundary in numerical engineering mechanics and general purpose finite element programs like ADINA, ANSYS etc. It is popular as it has a simple physical interpretation in the form of a dashpot so that it is easy to implement in a finite element environment.

Several years later, a new set of higher order absorbing boundary conditions was proposed by Engquist and Majda (1977, 1979). These boundary conditions were

complicated as they were derived for acoustic and elastic waves described with respect to rectangular as well as cylindrical coordinates. Although, this technique was based on the rational approximation of pseudo-differential operators and was considerably different from Lysmer & Kuhlemeyer (1969) boundary condition, the simplest boundary condition for acoustic waves is equivalent to the viscous boundary condition of Lysmer & Kuhlemeyer. The general form of (Engquist & Majda 1977) N^{th} order boundary condition can be expressed as:

$$\left(\frac{\partial}{\partial x}+\frac{1}{c}\frac{\partial}{\partial t}\right)^{N} u = 0 \tag{2.8}$$

where the terms within the bracket is the differential operator that is multiplied N times. These local, non-consistent boundaries though accurate are not suitable for dam-reservoir problem as a large near field is required that will result in large computational effort.

Saini et al. (1978) applied the finite element method for simulating the hydrodynamic effects in a dam-reservoir system. Two different approaches were considered to account for the large extent of the reservoir. In the first approach, a non-reflective radiation boundary condition was applied at the far-field boundary of the reservoir. The non-reflective radiation boundary condition was derived from the wave equation (Zienkiewicz and Newton 1969)

$$p = F_1(n-ct)+F_2(n+ct) \tag{2.9}$$

which represents the wave propagation in a direction n perpendicular to the boundary. In the above equation F_1 stands for a wave advancing with a velocity c towards the boundary and F_2 for returning wave. Ensuring that no waves are reflected back ($F_2 = 0$) the radiation condition was given as

$$\frac{\partial p}{\partial n} = -\frac{1}{c}\frac{\partial p}{\partial t} \tag{2.10}$$

In the second approach, the unbounded reservoir was modelled using specially developed infinite elements (Bettess 1977, Zienkiewicz & Bettess 1978) coupled with standard finite elements. The frequency dependent shape function for the j^{th} node of the infinite element used at the truncated boundary of reservoir is mapped in the ξ-η natural coordinate system and is given by

$$L_j(\xi) = e^{\frac{(\xi_j-\xi)}{\lambda}} e^{(-ik\xi)} \prod_{\substack{q=1 \\ q\neq j}}^{m-1}\left(\frac{\xi^q-\xi}{\xi^q-\xi_j}\right) \tag{2.11}$$

In the above expression, λ is a decay parameter, which can be any large number, $i = \sqrt{-1}$ and k is the wave number dependent on the excitation frequency ω and wave speed c (as $k = \omega/c$). The shape function for the last node at infinity, L_m can be obtained as

$$L_m = 1 - \sum_{q=1}^{m-1} L_q \tag{2.12}$$

The use of infinite elements coupled with finite elements was found to be more effective than using non-reflective radiation boundary at the truncated boundary of the reservoir. For adequately representing the hydrodynamic effects on the dam, a length of reservoir equal to three times its depth had to be used while modelling the reservoir with finite and infinite elements.

Hall & Chopra (1982) represented the infinite reservoir with a combination of finite elements up to a length beyond which the reservoir was maintained at a constant depth and considered to be a continuum. The authors had mentioned that for compressible water and infinite fluid domain, time domain procedures require very long finite element meshes so that pressure waves reflecting from the truncated boundary do not return to the dam during the time domain of interest. However, the authors had developed a satisfactory treatment for infinite fluid in frequency domain.

Sharan (1985a) had developed a finite element technique to model the effects of radiation damping in the analysis of hydrodynamic pressure on dams subjected to a harmonic horizontal ground motion treating water as compressible. The author had proposed a truncation boundary condition, which is effective compared to the Sommerfeld radiation boundary for a wide range of excitation frequency. The radiation condition along the truncation surface, which is located at a distance L away from the dam, was given by

$$\frac{\partial p}{\partial x}(L, y, t) = -\frac{\alpha''}{c}\frac{\partial p}{\partial t} + \frac{\beta''\omega}{c} p \tag{2.13}$$

where the exciting frequency of the dam is ω and c is the acoustic speed of the fluid. The values α'' and β'' depend on the location of the truncation boundary and excitation frequency. These are expressed as

$$\alpha'' = 0 \text{ and } \beta'' = \sqrt{\left(\frac{\pi}{2\Omega}\right)^2 - 1} \text{ for } \Omega < \frac{\pi}{2} \tag{2.14}$$

and

$$\alpha'' = \sqrt{1 - \left(\frac{\pi}{2\Omega}\right)^2} \text{ and } \beta'' = 0 \text{ for } \frac{\pi}{2} < \Omega < \frac{3\pi}{2} \tag{2.15}$$

in which $\Omega = \omega H_f / c$, H_f being the depth of the reservoir. Analysis of the system was made in the frequency domain considering the dam to be rigid. Sharan (1985b) further proposed a far-boundary condition at the surface where the unbounded reservoir is truncated specifying a condition that is dependent on the height of the fluid domain, which can be expressed as

$$\frac{\partial p}{\partial n} = -\frac{\pi p}{2H_f} \tag{2.16}$$

This truncation boundary may be located at a closer distance away from the structure compared to Sommerfeld radiation boundary. Here the fluid domain was unbounded only in the direction of structural motion, whereas, a similar technique of two-dimensional added mass of structures surrounded by an unbounded extent of incompressible fluid in all directions was proposed by Sharan (1986). The boundary condition proposed for the truncation surface to represent the radiation damping in terms of directional derivative of pressure p, at any point (x,y) in the direction of n was given by

$$\frac{\partial p}{\partial n} = \Psi p \tag{2.17}$$

where

$$\Psi = \frac{2xy\sin\varphi - \left(y^2 - x^2\right)\cos\varphi}{x\left(x^2 + y^2\right)} \tag{2.18}$$

In the above equation φ is the angle between x and outwardly-directed normal to the elemental surface along the boundary. For the case of a circular truncation boundary the condition could be simplified as

$$\frac{\partial p}{\partial n} = \frac{\partial p}{\partial r} = -\frac{1}{r} p \tag{2.19}$$

r being the radial distance between the structure and the truncation boundary. The author (Sharan 1987a) proposed a damper for time domain analysis of compressible fluid, which is unbounded along the direction of structural vibration. The radiation condition may be expresses as

$$\frac{\partial p}{\partial n} = -\frac{\pi p}{2H_f} - \frac{1}{c}\dot{p} \qquad (2.20)$$

The effectiveness of the radiation damper is dependent on the period of excitation T (= $2\pi/\omega$). The errors resulting from the use of the proposed damper was found to be greater than those produced by the Sommerfeld damper for a relatively high frequency of excitation. The author had mentioned that all the other available techniques of modelling an unbounded fluid domain, such as the use of boundary elements, infinite elements, continuum solutions and mapping finite elements depend on the frequency of vibration and are therefore, unsuitable for a time domain analysis.

In a two-dimensional analysis of a fluid-structure system carried out in the frequency domain, Sharan (1987b) derived a non-reflecting boundary condition neglecting the effect of surface waves. The boundary condition derived was dependent on the frequency of vibration, fluid compressibility and the depth of unbounded fluid domain beyond the truncation surface and the condition was expressed as

$$\frac{\partial p}{\partial n} = -\zeta p \qquad (2.21)$$

in which

$$\zeta = \frac{1}{H_f}\sqrt{\left(\frac{\pi}{2}\right)^2 - \left(\frac{\omega H_f}{c}\right)^2} \qquad (2.22)$$

The terms in the above expression have their usual meaning. The value of ζ becomes imaginary for $\omega H_f/c > \pi/2$, i.e., for $\omega > \omega_1$ in which $\omega_1 = \pi c/2H_f$ is the first cut-off frequency of the constant depth fluid sub-domain. The author further recommended that the Sommerfeld boundary condition could be used when the dam is vibrated at a range of high frequency that is for $\omega > 3\omega_1$. Under such conditions, eq. (2.22) was replaced by

$$\zeta = \frac{i\omega}{c} \qquad (2.23)$$

Sharan (1992) proposed a frequency dependent truncation boundary condition for the unbounded reservoir considering reservoir bottom absorption that could be implemented with ease using a finite element technique. The boundary condition adopted at the reservoir bed was $\partial p/\partial y = i\omega q p$, ω being the circular frequency of vibration. The drawback of the solution procedure is that it is nonlocal in space and consisted of only

the first term of the infinite series, which defines the boundary condition. The accuracy of the solution could be improved by including several terms of the series without further spatial discretization of the finite element mesh (Li et al. 1996).

Yang et al. (1993, 1996) proposed an explicit time-domain transmitting boundary for the analysis of dam-reservoir interactions. This transmitting boundary is derived from a semi-analytical solution of the governing wave equation of the far field of the reservoir. The radiation damping and water compressibility effects can be incorporated in the time-domain analysis of dam-reservoir systems. The finite element method was used to analyze a dam-reservoir system including the semi-infinite reservoir. Results also show that the proposed explicit transmitting boundary is more efficient computationally than the implicit transmitting boundary presented by Tsai and Lee (1989).

Weber (1994) emphasizes the need of developing an algorithm in time domain that can account for decaying and wave propagation to infinity. The author proposed an algorithm that transforms the approximating system to a symmetric second order form of finite element matrices. The far-field is implemented by appending the second-order matrices of the far-field to the mass, damping and stiffness matrices of the near field. Although, this technique gives accurate results, the complicated procedure may result in large computational effort.

A space-time finite element method for solution of the exterior structural acoustics problem involving the interaction of vibrating elastic structures submerged in an infinite acoustic fluid was formulated by Thompson & Pinsky (1996a). The formulation employs a finite computational fluid domain surrounding the structure and incorporates time-dependent non-reflecting boundary conditions on the fluid truncation boundary. The authors emphasize that if accurate non-reflecting boundary conditions are used, fewer fluid elements are needed and considerable cost savings will result. Thompson & Pinsky (1996b) further obtained the time dependent boundary conditions using an inverse Fourier transform procedure. Although the space-time finite element approach using spherical coordinates advocated in the work of Thompson & Pinsky (1996a, b) provides a powerful framework for unified and simultaneous spatial and temporal adaptivity of the discretization, the technique is too complicated to be implemented in the practical analysis of a dam-reservoir system.

Darbre (1998) proposed a two-parameter phenomenological model, where an incompressible body of water is attached to the dam through distributed dampers. These dampers were modelled to simulate the radiation damping effect. At low excitation frequencies the dampers did not deform and the pressure originated from the water's inertia forces only. At high excitation frequencies, the water mass remained still and the pressure initiated from the dampers' deformation. The two-parameter model is a valid approximation when both the frequency content of the excitation and the significant natural frequencies of the dam extend over several resonant frequencies of the reservoir. It was observed from the results that the two-parameter model did not give very good results when the frequency content of excitation or the natural frequencies of the dam remained below the fundamental resonant frequency of the reservoir.

Maity & Bhattacharyya (1999) proposed a simple and effective far-boundary condition that could model the effects of radiation damping in the finite element analysis of hydrodynamic pressure of compressible water on dams subjected to harmonic ground motion in a time domain analysis. The proposed truncation boundary condition could be located at a relatively small distance away from the structure, resulting in great computational advantages by incorporating a truncation boundary in the finite element program which can be expressed as

$$\frac{\partial p}{\partial n} = \frac{\partial p}{\partial x} = -\frac{p}{H_f}\zeta \tag{2.24}$$

where,

$$\zeta = -\frac{\sum_{m=1}^{\infty}\left[\frac{(-1)^{m+1}}{(2m-1)}\right] e^{\left(-f_m \frac{x}{H_f}\right)} \cos\left(\lambda_m \frac{y}{H_f}\right)}{\sum_{m=}^{\infty}\left[\frac{(-1)^{m+1}}{(2m-1)f_m}\right] e^{\left(-f_m \frac{x}{H_f}\right)} \cos\left(\lambda_m \frac{y}{H_f}\right)} \tag{2.25}$$

In the above expressions,

$$\lambda_m = \frac{(2m-1)}{2}, \quad f_m = \sqrt{\lambda_m^2 - \Omega^2} \text{ and } \Omega = \frac{\omega H_f}{c} \tag{2.26}$$

The authors showed that the infinite fluid domain can be truncated using the proposed boundary condition at a relatively smaller distance away from the structure. This boundary condition is advantageous as it is quite simple and the additional computational effort required to include the proposed truncation boundary condition is insignificant.

The limitations of the above boundary condition are that it cannot account effectively for excitation frequencies higher than the fundamental frequency of the reservoir as f_m tends to become complex. Further, the analytical formulation of determining hydrodynamic pressure in the reservoir that is used in deriving the truncation boundary condition does not account for the effects due to surface waves and absorptive effect at the reservoir bottom. It may further be noted that this boundary condition is frequency dependent and hence may not be efficient for determining the seismic response in time domain.

Cetin & Mengi (2003) proposed a transmitting boundary condition using a continuum approach and based on the spectral properties of radiating waves, which is suitable for both boundary element and finite element analyses, for radiation of waves propagating in horizontal direction along a compressible inviscid fluid layer. The formulation is presented in Fourier space and incorporates the effects due to surface waves and radiation of waves due to viscoelastic foundation. The study indicates that this transmitting boundary condition is efficient when used in conjunction with boundary element analysis.

A boundary condition similar to that of Maity and Bhattacharyya (1999) was proposed by Küçükarslan (2005) for incompressible and inviscid fluid. The derived boundary condition is implemented in the finite element code and results are compared with by using Sommerfeld's and Sharan's boundary conditions.

It is evident from the review on NRBC (Givoli 2004) that in the last 50 years Non-Reflecting Boundary Conditions (NRBC) has been developed from zero-order Sommerfeld (1949) boundary condition to high order local boundaries. However, it is important that the NRBC is practically implementable and computationally efficient for a complex problem such as a dam-reservoir system considering the effect of reservoir bottom absorption.

2.1.3.2 Reservoir Bottom Absorption Effects

The hydrodynamic forces evaluated considering a rigid reservoir bottom are altered when the reservoir bottom is considered flexible and energy is dissipated in the unbounded domain in the vertical direction. In most of the investigations carried out, the earthquake response of concrete gravity dams were determined assuming the reservoir bottom to be rigid, causing complete reflection of the hydrodynamic pressure waves.

Lotfi (1986) analyzed the earthquake response of dams considering the water-sediment-foundation interaction rigorously. A hyper-element was used in the finite element model which included the effect of sediment layer that was assumed to be viscoelastic and almost incompressible.

Many researchers (Sharan 1992, Chandrashaker & Humar 1993, Tan & Chopra 1995, Li et al. 1996 and Hatami 1997) have incorporated a damping boundary condition, arising from partial absorption of hydrodynamic pressure waves at the reservoir bottom. Interaction between the impounded water and the foundation medium is represented by a boundary condition, which permits partial absorption of hydrodynamic pressure waves at the reservoir bottom. Interaction between the impounded water and the foundation medium is represented by a boundary condition, which permits partial absorption of hydrodynamic pressure waves at the reservoir bottom. The wave absorption along the reservoir bottom was accounted by an approximate one dimensional wave propagation model. The wave reflection coefficient α (Sharan 1992) which is the ratio of the amplitude of the reflected hydrodynamic pressure wave to the amplitude of a vertically propagating pressure wave incident on the reservoir bottom, is related to the damping coefficient q by

$$\alpha = \frac{1 - qc}{1 + qc} \tag{2.27}$$

where $q = \rho_f / \rho_r c_r$ and $c_r = \sqrt{E_r / \rho_r}$, E_r is the Young's modulus and ρ_r is the density of the foundation medium. ρ_f is the density of water and c is the velocity of pressure waves in water. For a rigid foundation medium, $c_r = \infty$ and thus $q = 0$, resulting in $\alpha = 1$. For a very low density or very soft foundation medium c_r approaches zero and $q = \infty$, resulting in $\alpha = -1$. It is believed that α value varies from 1 to 0 would cover the wide range of materials encountered at the bottom of actual reservoirs. This method of determining the reflection coefficient of the reservoir bottom is independent of the excitation frequency.

Bougacha & Tassoulas (1991a, 1991b, 1991c) determined the transient response of a concrete gravity dam to harmonic ground motion and to a selected earthquake record for evaluating the significance of the sedimentary material accumulating on the bottom of the reservoir. The sediment was modelled as a two-phase medium i.e., fluid-filled and

poroelastic solid. The analysis was carried out accounting for all interactions between the dam, water, sediment and foundation. The results indicated that the effects of fully saturated sediment are limited to a slight decrease in the maximum acceleration of the dam and the maximum hydrodynamic force. However, if the sediment is only partially saturated, there is a significant decrease in the fundamental frequency along with a substantial reduction of the peak acceleration under horizontal ground motion. These findings were based on the assumed sediment properties. The authors suggested that these parameters be measured in actual dam sites before any definitive conclusion is reached regarding the importance of sediment effects.

Domínguez et al. (1993) developed a boundary element approach for the dynamic analysis of continuous systems that may consist of water, viscoelastic and fluid-filled poroelastic zones of arbitrary shapes. This technique was applied in the seismic analysis of concrete gravity dam considering interaction effects of the reservoir, foundation and sediment at the reservoir bottom. The study revealed that the compressibility of sediment has important effect on the dam response; the effects of fully saturated sediment are not significant and the influence of sediment layer is important for the prediction of dynamic behavior of the dam.

The absorption effects of the reservoir bottom in the earthquake analysis of dams is modelled by Hatami 1997 and Chuhan et al. 2001 utilizing the wave reflection coefficient approach based on the solution of the wave equation in a sediment layer of visco-elastic material with a constant thickness overlying an elastic, semi-infinite foundation. This model results in a frequency dependent reflection coefficient. For a sediment layer overlying the foundation rock, frequency dependent equivalent relative impedance (Hatami 1997) is given by

$$\beta_h(\omega) = \frac{1+\alpha_h(\omega)}{1-\alpha_h(\omega)} \tag{2.28}$$

where $\alpha_h(\omega)$ is the overall reflection coefficient of the reservoir bottom which can be directly obtained from the impedance of the reservoir bottom defined as the ratio of the acting pressure to the particle velocity. The complex frequency dependent reflection coefficient was obtained from the solution of one-dimensional wave equation. The overall reflection coefficient $\alpha_h(\omega)$ was found to increase with the increase in elastic

modulii of elasticity of the sediment material and the foundation rock. A comparison of crest acceleration of a gravity dam (Hatami 1997) due to vertical ground motion considering sediment layer overlying a rigid and a flexible foundation show that modelling the reservoir foundation as flexible and allowing the refracted waves to be radiated in the unbounded soil domain plays a more important role than absorption of wave energy within the sediment layer (Fig.2.3). In the figure, d_s/H is the ratio of sediment depth to the reservoir depth. It is apparent that effect of the thickness of the sediment layer is to reduce the dynamic response of the dam. The effect of sediment layer may be considered in the system only if foundation is considered flexible and energy radiation concept is incorporated. The use of reflection coefficient as derived from eq. (2.27) would be appropriate if the sediment layer is thin, but if the sediment layer is thick the reflection coefficient should be evaluated taking into consideration the effect of thickness. However, these techniques would mainly depend on determining the characteristics of the sediment.

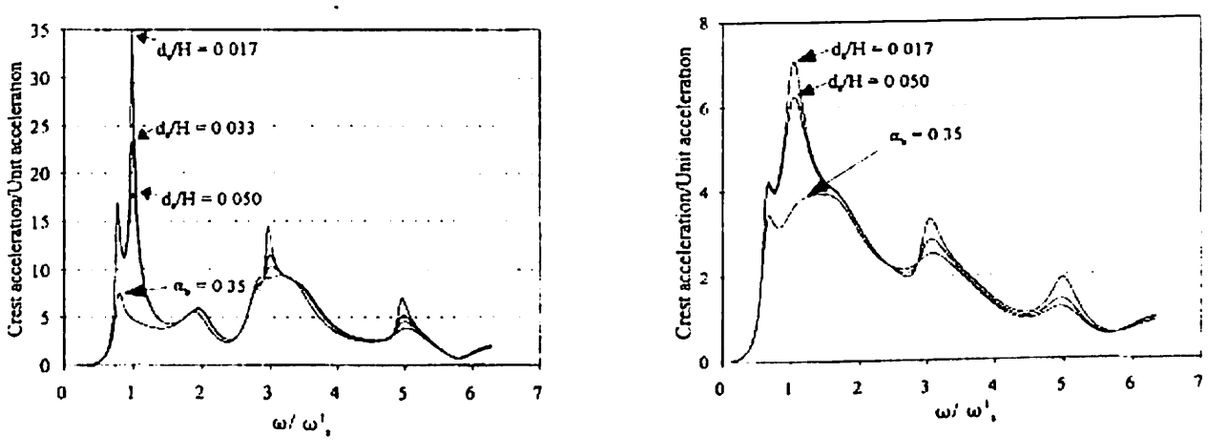

(a) (b)

Fig. 2.3 Effect of layer thickness on dam subject to vertical excitation on (a) rigid foundation and (b) flexible foundation (Hatami 1997)

A novel procedure for measuring the overall or average reflection coefficient of the reservoir boundaries in the immediate vicinity of the dam was developed based on acoustic reverberation technique by Ghanaat et al. 2000. Computer analyses using EACD-3D (Fok et al. 1986) and GDAP (Ghanaat 1993) that characterizes the sensitivity of the dam response to various modelling assumptions were carried out and compared with the results obtained from the experimental study of dam-water-foundation interaction of an arch dam. The GDAP model employs incompressible water while the EACD-3D considers water compressibility and reservoir bottom absorption effect. It was

found that both the incompressible and compressible fluid models produced frequencies of the dam-reservoir-foundation rock system that differed less than 10% from the measured values. The results showed that the effects of reservoir geometry and wave reflection coefficient on the response to harmonic motions are significant. The results indicate that both the GDAP and EACD-3D frequencies agree reasonably well with the measured values. The experimental and numerical investigations carried out by Proulx and Paultre (1997) further emphasizes the inclusion of water compressibility and wave absorption effect at the reservoir bottom in the numerical solution to reproduce the observed behavior.

2.1.3.3 Cavitation Effect

During severe ground motion, water at the reservoir may be separated partially from the dam itself. If the absolute pressure of water in the reservoir goes above the vapour pressure, micro-bubbles occur in the fluid domain. Cavitation is the formation of these micro-bubbles or void in a liquid, where the bubble is generally filled with vapour. Analytical and experimental studies of behavior of dam reservoir system performed during seismic safety evaluations have shown that the dynamically varying pressures may exceed the combined hydrostatic plus atmospheric pressure at the interface, thus producing cavitation.

Paul et al. (1981) stated that the response with and without cavitation is identical just before the onset of cavitation but significantly modifies thereafter. The total hydrodynamic force on the dam reduces but a slight increase in the crest displacement and the normal heel stresses are noted. Clough and Chang (1981) found that the effect on the response of the gravity dams to be small, though the consideration of cavitation led to reductions of response. Fenves & Vargas Loli (1988) had also shown that water cavitation had a very small effect on maximum displacements and stresses of the dam due to earthquake. Oskouei & Dumanoglu (2001) carried out a nonlinear analysis in Lagrangian formulation considering the nodal unknowns in fluid domain to be displacement. The cavitation effect was found to be prominent at the upper region of the dam, where the dam surface is exposed to high local stresses that causes pitting and erosion of the surface.

The study of the present literature reveals that during cavitation, the compressibility and the bulk modulus of water are reduced towards zero. Cavitation is not dangerous for a structure, but if it occurs close to flow boundaries, cavitation damage may occur and the structure will be seriously damaged. The surface damage begins at the downstream end; an elongated hole is formed in the boundary surface. This hole gets larger with time, the surrounding area may break away and aggregates may be swept off.

2.1.4 Fluid Structure Interaction Effects

Though the seismic response analysis of a concrete gravity dam is similar to any other structural dynamic analysis, the concrete dam analysis is greatly complicated because the structure interacts with the water retained in the reservoir and the deformable rock foundation that supports it. The dynamic interaction between an elastic structure and a compressible fluid has been the subject of intensive investigations in recent years. Some simplified approaches are available in which fluid-structure interaction is studied in a decoupled manner. In this type of analysis, the fluid response is first obtained assuming the structure as rigid and the resulting pressure field is imposed on the structure to obtain the structural response. But such type of analysis does not always lead to a conservative design of the structure. If resonance between the structure and the energy release mechanism in the fluid occurs, it can lead to the development of unsound design. Moreover, if coupled modes are excited, this approach gives non-conservative results. Thus, it is necessary to study the fluid-structure interaction problems in a coupled manner considering the flexibility effect of the structure. A study of the available literature shows that the fluid – structure interaction mechanism can be developed by either direct or indirect coupling techniques.

2.1.4.1 Direct Coupling

The most common approach being adopted at present is that both the systems are coupled and solved as one system. The most commonly used finite element approach is based on Lagrangian-Eulerian formulations, where displacement variables are generally chosen for the structure and the fluid is described by pressure. In other approaches for such coupled problems the fluid may be described by different variables such as displacement or velocity potential.

Zienkiewicz and Newton (1969) had presented a finite element technique to analyse a structure submerged in a compressible fluid. The infinite fluid domain was modelled into a finite one considering the Sommerfeld radiation boundary conditions. The authors represented the fluid motion in terms of pressure and the elastic structure in terms of displacement. Linearised free surface condition was adopted in the analysis. Discretizing the dam-reservoir system as an assemblage of finite elements, assuming pressure and displacements to be the nodal unknowns for the fluid and the structural domain respectively, the unsymmetrical coupled equations representing fluid structure interaction is given as

$$\begin{bmatrix} M & 0 \\ Q & G \end{bmatrix} \begin{Bmatrix} \ddot{u} \\ \ddot{p} \end{Bmatrix} + \begin{bmatrix} C & 0 \\ 0 & L \end{bmatrix} \begin{Bmatrix} \dot{u} \\ \dot{p} \end{Bmatrix} + \begin{bmatrix} K & -Q^T \\ 0 & H \end{bmatrix} \begin{Bmatrix} u \\ p \end{Bmatrix} = \begin{Bmatrix} -Ma_g \\ -Qa_g \end{Bmatrix} \tag{2.29}$$

In the above equation, M, C and K are the mass damping and the stiffness matrices of the dam, while G, L, H are assembled matrices representing the reservoir and Q is the interaction matrix. The unknown vector consists of nodal displacements u and nodal pressures p and a_g denotes the ground acceleration.

The solution scheme of coupled dam-reservoir system presented by Saini et al. (1978) was in frequency domain. An assemblage of finite elements and infinite elements to represent the dam-reservoir system, the coupled equation of motion for periodic excitation was given by

$$\left([K] - \omega^2 [\overline{M}] + [C] i\omega\right)\{d_0\} = -[\overline{M}]\{a_g\} \tag{2.30}$$

where

$$[\overline{M}] = [M] + \frac{\rho_f}{g}[L]\left([H] - \omega^2 [Q]\right)^{-1}[L]^T \tag{2.31}$$

In the above expressions, [K], [M], [C] and [L] has same meaning as stated in eq. (2.2), $\{d_0\}$ is the vector of nodal point displacements of the dam relative to the ground, ρ_f is the mass density of the reservoir water, g is the gravitational acceleration, [H] and [Q] are matrices having complex coefficients due to introduction of infinite elements in the system. The second term on the right hand side of eq. (2.31) is in general complex and represents frequency dependent added mass and added damping due to the unbounded reservoir.

Müller (1981) carried out a simple finite element analysis of coupled fluid-structure interaction problem by neglecting the viscous and nonlinear convective term of the fluid-motion. While the fluid is considered to be incompressible, the problem reduces to a structural problem with an added mass due to fluid. For compressible fluid, an additional term was included in the previously calculated mass matrix, which the author described as the mass matrix. The unsymmetrical matrix was converted to a symmetrical one.

Zienkiewicz et al. (1983) used displacement potential as the unknown variable in finite element discretization of the fluid domain, which led to unsymmetrical coupled equations of motion and requires a special purpose computer program. A partitioned algorithm dealing successively with the structural equation and the fluid system had been adopted for time-stepping solution. In each partitioned system, the Newmark algorithm was used in iterative form.

Olson & Bathe (1983) had investigated the scope of displacement based fluid elements used for fluid-structure interaction problems. The authors had shown that the displacement based formulation for fluid-elements cannot be used successfully to fluid-structure interaction problem, in which natural frequency of the structure is involved. Later, a symmetric finite element method was presented by Olson & Bathe (1985a) to solve the coupled system. Velocity potential and hydrostatic pressure were considered as unknown parameters in the fluid domain whereas displacement was considered as unknown parameter in the structural domain. The authors found that the displacement based elements including the rotational penalty require a large number of elements to obtain accurate solution compared to the formulation proposed by the authors using velocity potential and hydrostatic pressure in the fluid elements.

Sharan & Gladwell (1985) made all the matrices in eq. (2.29) symmetrical and banded. To reduce the computation time and core storage requirement, certain approximations such as *added equivalent mass matrix* for the structure, *diagonalised mass* and *damping* matrices for the fluid were adopted. The coupled equation of motion was then solved by direct integration scheme based on constant average acceleration method. Sharan (1987b) used nodal pressure as the unknown variable in the finite element formulation of the fluid domain as

$$[M_f]\{\ddot{p}\}+([K_f]+\zeta[D_f])\{p\}=-\rho[S_{fs}]^T(\{a_g\}+\{\ddot{d}\}) \quad (2.32)$$

in which $[M_f]$, $[K_f]$ and $[D_f]$ are the matrices of the fluid domain. The value of ζ at the truncated boundary of the reservoir is as given in eq.(2.22), $[S_{fs}]$ is the coupling matrix of the fluid structure system and $\{\ddot{d}\}$ is the vector of nodal acceleration of fluid-solid interface with respect to ground acceleration $\{a_g\}$. The discretized equation of motion of the structure was given by

$$[M_s]\{\ddot{d}\}+[C_s]\{\dot{d}\}+[K_s]\{d\}=\{F\}+[S_{fs}]\{p\} \quad (2.33)$$

In the above equation $[M_s]$, $[C_s]$ and $[K_s]$ are the mass, damping and stiffness matrices of the structural domain respectively and $\{F\}$ is the vector of consistent nodal forces excluding those due to the hydrodynamic pressure.

Tsai & Lee (1987) formulated a numerical procedure employing finite element method for arch dam and boundary element method for the fluid domain for the analysis of the three-dimensional dam-reservoir system with arbitrary ground motions and geometry. The added mass matrix calculated from the fluid domain was made symmetrical and lumped to retain the banded and symmetrical characteristic in the finite element method. In the boundary element formulation, the mirror image method was used. Hydrodynamic pressure distribution on the upstream face of the dam was calculated and the authors studied the natural frequencies of the dam-reservoir system with various reservoir depths.

A numerical scheme for computing the dynamic response of coupled fluid-structure system was developed by Fenves & Vargas Loli (1988) to evaluate the effects of non-linear behavior of the fluid-structure system. The authors discretized the equation of fluid motion in terms of displacement and pressure and included the cavitation of the fluid, which was modeled as bilinear compressible material. Fluid was considered as inviscid and with small amplitude, irrotational motion. A penalty constraint was incorporated in the fluid motion to satisfy the irrotationality condition. The fluid pressures were solved at the element level and thus displacements were the only variable at global level. This allowed assembly of the fluid elements with displacements for the structure and lead to symmetric equation of motion for the coupled system. The coupled system was solved by a fully implicit time integration method.

A symmetric finite element formulation for coupled acoustic vibration between fluid and structures was proposed by Sandberg & Göransson (1988). The fluid equation was expressed by pressure and a displacement potential and the structure by displacement. The mass matrix had zero entries on the diagonal in the pressure degrees of freedom for the proposed symmetric finite element scheme. Under this consideration the system became positive semi-definite, which caused problems for the solution of the equations. Later, the author (Sandberg 1995) proposed a scheme for treating unsymmetrical coupled fluid-structure systems. The discretization is performed by means of the finite element method, using displacement formulation in the structure and either pressure or displacement potential in the fluid. Based on the eigenvalues of each sub-domain, a standard eigenvalue problem was derived. The author concluded that the unsymmetrical matrices have real eigenvalues.

Chen & Taylor (1990) presented a displacement based finite element solution for the interaction between an inviscid fluid and a solid. The stiffness matrix contributed by the fluid was calculated by using reduced integration to suppress circulation modes with non-zero frequency. In addition a projected mass matrix was used in order to remove spurious modes, which resulted from the use of reduced integration. Owing to the use of displacement formulation, no special consideration was required for the interface of the coupled systems. The authors demonstrated that the spurious modes were suppressed by adopting projected mass and under-integrated stiffness matrices.

von Estorff and Antes (1991) developed a finite element – boundary element coupling procedure, where the linear elastic structure was modelled by finite elements and the fluid domain was represented by boundary elements. The fluid was considered as linearly compressible, inviscid and of small amplitude of motion. The two different media, i.e., the fluid and the solid region, were coupled through the compatibility and equilibrium conditions along the common interface. The main advantage of this technique is that FE could model the in-homogeneous elastic dam and the homogenous and infinite fluid domain could be represented by boundary elements.

Lotfi (2004a) proposed a pseudo-symmetric technique for the seismic analysis of concrete dams in time domain, where the non-symmetric system of equation is avoided. The methodology introduced could be implemented in general-purpose finite element

programs by modifying the fluid-structure interaction modules. The advantage of using the direct method in time domain is that it is possible to efficiently transform the direct integration algorithm to enable working with symmetric matrices (Zienkiewicz & Taylor 2000 and Lotfi 2004a). However, in a modal analysis, the symmetrization of the mass and stiffness matrices requires introduction of additional variables in eigen-solution routines that creates complications in computer programming.

2.1.4.2 Indirect Coupling

To overcome the problems in the analysis of fluid-structure interaction problems in a coupled manner, the solution of the coupled system may be accomplished by solving the two systems separately with the interaction effects enforced by iteration.

Au-Yang & Galford (1982) reviewed the phenomenon of fluid-structure interaction and discussed the difference between the strongly and weakly coupled fluid-structure systems. A strongly coupled fluid-structure system is one in which the flow field induced by structural motion and the original flow field cannot be linearly superimposed on each other. This is usually caused by large structural displacement, resulting in large induced fluid velocity. A weakly coupled system is one in which flow field induced by the structural motion can be regarded as a small perturbation and therefore can be linearly superimposed onto the original field. According to the authors, the assumption of incompressibility of fluid seemed justified when the time for acoustic wave to traverse a characteristic length of the fluid-structure system is much smaller than the dominant model period of vibration of the structure.

Hall & Chopra (1982) had used finite element models of two-dimensional irregular fluid domains adopting the substructure method for analysing the linear dynamic response of dams including hydrodynamic effects. Both the dam and the fluid domain were treated as substructures and modelled with finite element. The response of the dam due to arbitrary ground acceleration was obtained using Fast Fourier Transform algorithm as the analysis was carried out in frequency domain. This procedure was further extended for arch dams with realistic fluid domains with complicated geometry (Hall & Chopra 1983). The reservoir consisting of a finite region of arbitrary geometry connected to an infinite region of uniform cross section was modelled with three-dimensional finite elements.

Singh et al. (1991) analysed three-dimensional fluid-structure interaction problems through a partitioning scheme. The interaction effect was studied by transferring the shell normal acceleration to the three-dimensional fluid domain and the fluid pressure to the shell surface at the shell-fluid interface for each time step in an iterative manner. The analysis was carried out for each field and interaction effect was accounted for by updating the field variables of both the fields in the respective coupling terms. Two methods for time integration, namely implicit and explicit for transient analysis of the system were discussed critically. The authors mentioned "*Implicit methods are unconditionally stable and larger time steps can be used based on the order of accuracy required. ..... On the other hand, explicit methods are conditionally stable, thus time step size is limited by the minimum period of the mesh.*" The authors considered an explicit integration scheme for the fluid domain, which is normally of larger size and an implicit scheme for the shell structure.

Antoniadis & Kancharos (1998) had developed a method for decoupling the acoustic fluid-structure interaction problem in the frequency domain. For decoupling procedure, a linear model transformation of the added matrices for the coupled system was incorporated. While calculating eigen-values, the authors considered pressure as the unknown variables for the 2-D fluid domain and modelled the structure by beam element for the coupled system. The authors studied the eigenvalue problem for different cases classifying the fluid and structure as (i) incompressible fluid, (ii) hyper compressible fluid, (iii) hyper light structures and (iv) hyper flexible structures.

Bouaanani et al. (2002) coupled the dam-reservoir system indirectly using the substructure technique while comparing the analytical predictions of ice covered dam-reservoir-foundation system with results obtained during a series of extensive dynamic tests on Outardes 3 gravity dam in Canada. The dam is discretized using finite elements and the hydrodynamic force is determined by analytical solution considering the effect of ice layer and imposed on the dam.

Maity & Bhattacharyya (2003) developed an iterative scheme to solve the coupled problem of dam-reservoir system. The major advantage of this method is that the coupled field problems may be tackled in a sequential manner. The analysis is carried out

for each field and updating the variables of the fields in the respective coupling terms accommodates interaction effect.

Lotfi (2004b) proposed a decoupled modal approach for dynamic analysis of dam-reservoir systems in frequency domain. The technique relies on mode shapes extracted by considering the symmetric parts of total mass and stiffness matrices. This technique employs eigen-vectors of the decoupled system and proved to be an effective analysis procedure in frequency domain.

2.1.5 Soil-Structure Interaction Effects

The effect of soil structure interaction significantly alters the dynamic characteristics of stiff and massive structures resting on relatively soft ground. Consideration of actual support flexibility reduces the overall stiffness of the structure and elongates the time period of the system. The assumption of a rigid boundary at the soil structure interface may result in serious distortion of foundation interaction effects because the energy loss or damping associated with radiation of vibration waves beyond the assumed foundation block is not properly represented. These effects may show reduced seismic stresses in the structure. However, dams are constructed generally on a hard rock stratum where the impedance ratio (E_f/E_d) may vary from 2.0 to ∞, where E_f and E_d are the elastic modulus of the foundation and the dam respectively.

The problem of a dam on a layered foundation was first solved by Wilson (1969) by constructing a large planar finite element mesh through the entire system and analyzing the response to prescribed base rock motion using the step-by-step integration procedure. Soil-structure interaction analysis is either done by substructure method (Vaish & Chopra 1974, Chopra et al. 1980, Hall & Chopra 1982, Fenves & Chopra 1984, Ghanaat 1993, Tan & Chopra 1995, Guan et al. 1996, 1997, Saini & Garg 1997 and Zhang et al. 1999) or direct method (Bycroft & Mork 1987, Liou & Huang 1994 and Kim & Yun 2000).

A viscoelastic halfspace idealization (Chopra et al. 1980 and Chopra & Chakrabarti 1981) may be appropriate if the dam site consist of similar rock extending to great depth. Chopra & Chakrabarti (1981) employed the substructure technique to indirectly couple the dam-reservoir-foundation system while carrying out a dynamic

analysis in frequency domain. The dam is idealized as a two-dimensional finite element system that could account for the arbitrary geometry of the dam. However the hydrodynamic effects were determined analytically assuming the upstream face of the dam to be vertical. For the purpose of including the dam-rock interaction effects, the surface of the viscoelastic foundation rock was assumed to be horizontal. The reservoir bed was also assumed to be horizontal and absorption effect at the reservoir bottom was considered in the analysis. The forces at the base of the dam due to dam-rock interaction have been expressed in terms of interaction displacements and hydrodynamic forces through dynamic stiffness matrices of the foundation rock region. The hydrodynamic forces are expressed in terms of accelerations of the upstream face of the dam and the bottom of the reservoir.

In a dynamic analysis, the interaction effect of such unbounded medium can be accounted for by complex valued and frequency dependent dynamic stiffness matrix (Fenves & Chopra 1984). Analysis procedures were mostly in the frequency domain for determining the earthquake response of two-dimensional elastic concrete gravity dam including hydrodynamic effects due to compressible water. The effect of considering foundation flexibility was to reduce the stresses near the base of the dam.

A combination of BEM and FEM (Touhei & Ohmachi 1993) may be an alternative technique for determining the response of dam-foundation-reservoir system. The weighted residual procedure is applied while coupling the equations of motion for solid and fluid in the FE and BE region. This algorithm accounts for the interaction effects of the dam-reservoir, dam-foundation and the reservoir foundation interfaces; and the absorption of elastodynamic and hydrodynamic waves at the dam-foundation and dam-reservoir interfaces.

The extreme values of dam crest displacements and accelerations for different impedance ratios (E_f/E_d) as obtained by Yazdchi et al. (1999) in an analysis of dam-foundation systems are reproduced in Table 2.1. The modulus of the foundation was varied from 0.5 to 4.0 times the modulus of the dam and compared with rigid foundation. The Poisson's ratio and the mass density of the foundation were assumed to be same as those of the dam. The results indicate that the dam–foundation interaction is significant

when the E_f/E_d ratio is less than 2.0. However, the displacements and accelerations of the dam do not vary much when E_f/E_d varies between 2.0 to ∞.

Table 2.1 Effect of Flexible Foundation on Dam (Yazdchi et al. 1999)

E_f/E_d	0.5	1.0	2.0	4.0	∞
Displacement (mm)	-7.53	-4.41	-3.85	-3.70	-3.64
Acceleration (a/g)	-3.41	-3.18	-3.48	-4.19	-4.25

The peak horizontal crest displacement of Pine Flat dam-foundation-reservoir system considering the coupled and uncoupled approaches (Chandrashaker & Humar 1993) are presented in Table 2.2 for $E_f/E_d = 1.0$. It is interesting to note that the difference between the results obtained by the coupled and uncoupled method is very small. Further, the stresses obtained at the base and neck of the dam due to earthquake ground motions were compared by simplified and rigorous approaches and found to be very close.

Table 2.2 Peak Horizontal Crest Displacement (mm) of Pine Flat Dam (Chandrashaker & Humar 1993)

Ground Motion	Coupled Response	Uncoupled Response
Taft S69E, Horizontal	40.98	44.63
Taft S69E, Vertical	13.90	15.68
El Centro S90W	81.40	84.34

Chavez & Fenves (1995) presented the hybrid frequency-time domain (HFTD) procedure to compute the nonlinear earthquake response of concrete gravity dams including sliding along the interface between the dam base and foundation rock. The solution procedure considers the effect of non-linear base sliding behavior due to the frequency dependent interaction effects of the reservoir and flexible foundation. The non-linear sliding behavior in the complex interface zone is represented by the Mohr-Coulomb relationship for friction. The authors states that although no criteria have been established for acceptable base sliding in an extreme event, it is reasonable to expect that dams can tolerate a sliding on the order of 100-150 mm computed from this model.

Medrano et al. (1995) analyzed the transient response of reservoir-dam-soil systems by direct time domain numerical procedures. Emphasis was given to dam-soil interaction. The dam was modelled by finite element method and a displacement based

Lagrangian element was used to model the reservoir. The foundation was considered (i) by assuming it to be rigid; (ii) including a significant massless portion of the foundation rock; (iii) considering it to be viscoelastic and representing it by a stiffness and a damping matrix, neglecting the frequency dependent dynamic stiffness of the soil; (iv) considering it to be viscoelastic and neglecting damping and (v) using analytical solution in frequency domain and Fourier synthesis. The authors concludes from the comparative study that inspite of considering a rigid foundation, reasonable results were obtained, especially concerning the vertical stresses at the heel. But considering a large massless portion of the foundation resulted in large vertical stresses near the heel as the stiffness matrix was frequency independent. Modelling the foundation using stiffness and damping matrix for the first eigen-frequency resulted in overdamped solution. Introducing only the stiffness matrix for the first eigen-frequency showed results that were in good agreement with the general analytical solution.

In a dam-reservoir-foundation system (de Araújo & Awruch 1998) a probabilistic methodology was adopted to determine the safety of concrete gravity dam due to dynamic interaction. The stochastic characteristic of seismic excitation as well as the variation of concrete properties was considered using Monte Carlo method. It was found to be disadvantageous due to more computational effort as the structural stiffness matrix had to be defined for every simulation. Results were obtained for Tucuruj Dam due to mean earthquake of acceleration 0.1g, where g is the gravitational acceleration. Safety factors for sliding, crushing and cracking were used to define structural performance.

It is important to consider the nonlinear behavior of the foundation rock supporting the dam, if the rock is fractured and discontinuous. The nonlinear behavior of the foundation rock will affect the static and dynamic response of the dam. The sub-regions where these nonlinearities occur are modelled with finite elements (von Estorff and Firuziann 2000), while transient boundary elements are used to ensure that the radiation of waves to infinity is taken into account. Such a formulation having the advantages of finite and boundary elements may be suitable to handle semi-infinite systems with local nonlinearities.

Bouaanani et al. (2002) considered the effect of interaction forces at the dam-foundation interface that are related to the dam displacements through the complex valued dynamic stiffness (impedance) matrix as derived by Fenves & Chopra (1984).

Hence, it is observed from the available literature that if the elastic modulus of the dam foundation is more than the dam, the accuracy of the analysis procedure may not be affected while the foundation of the dam is considered to be rigid.

2.1.6 Earthquake Excitation Concepts

To evaluate the earthquake performance of concrete dams, it is important how the earthquake input motion is specified (National Research Council 1990). Because of the great extent of the dam, and recognizing the wave propagation mechanisms by which earthquake are propagated through the foundation rock, it is important to account for spatial variation of the earthquake motions at the dam-foundation interface. In a Standard Base Input Model, the seismic input is defined as a history of motion of a rigid base (Chavez & Fenves 1995). But the motion at a particular depth is not the same as free-field motions recorded at ground surface. The Massless Foundation Rock Model is an improved version of the preceding model, which neglects the mass of the rock in the deformable foundation region (Vitharana et al. 2002). This has the effect of eliminating the wave propagation mechanism in the deformable rock. Hence, the motions prescribed at the rigid base are transmitted directly to the dam interface. GDAP (Ghanaat et al. 2000) and ADAP-88 (Fenves et al. 1989) and other arch dam analysis programs commonly use this type of foundation model. In a Deconvolution Base Rock Input Model (DBRIM), a deconvolution analysis is performed on a horizontally uniform layer of deformable rock to determine motions at the rigid base boundary. This is then used in the standard base input model. This procedure permits the wave propagation in the foundation rock, but requires an extensive model for the foundation rock, which is computationally expensive. In a Free Field Input Model, the deconvolved rigid base motion is applied to a model of deformable foundation rock without the dam in place. The calculated interface free field motion account for scattering effects of canyon topography on earthquake waves and are used as input to the combined dam-foundation rock system. Free-field motion is defined as the motion of the dam-foundation contact surface due to seismic excitation without the presence of the dam. Such an input model

has been used in the dynamic analysis of gravity dams by several researchers such as Vaish & Chopra (1974), Dasgupta & Chopra (1979) and Tan & Chopra (1995).

Though various theoretical models have been developed for prediction of free-field input motion at the surface, no verification of such predictions has yet been achieved by comparison with actually recorded earthquake motions. The existing strong motion instrumentation at concrete dams is not designed to provide essential data. Some effective instrumentation schemes have been proposed by Darbre (1995) to record free field motions at dam sites, effective motions at the abutments and global dam responses that can help in determine dynamic properties of dam. The parameters that can be recorded from such instrumentation schemes are base input motion, free-field motion, crest deformation, response of neighborhood blocks, abutment motions, wave propagation, base rotation of blocks, and tri-dimensional response due to longitudinal excitations.

For seismic analysis of a dam-reservoir system, the time variation of ground acceleration (a_g) is the most useful way of defining the shaking of the ground during an earthquake (eq. 2.29). In an accelerogram, the ground motion is defined by numerical values at discrete time instants. Typically the time interval is chosen to be 1/100 to 1/50 of a second (Chopra 1998). A seismic analysis can be carried out either in the time-domain, using time-histories of acceleration or in the frequency domain, calculating frequency content using Fast Fourier Transforms (FFT). Each of these techniques can reveal important information about the behavior of the situation investigated; however, each technique loses some information. Earthquakes are transient and non-stationary events. This means that either the input acceleration or the behavior of the system at different moments in time is not identical. When an accelerogram is converted into the frequency domain using an FFT, the time-dependent behavior is lost. However, when the ground acceleration input is used as a time history, the frequency dependent response of a system can not be determined.

Haigh et al.(2002) used the harmonic wavelet analysis as a tool for the analysis of non-stationary signals in the time-frequency domain. This technique is adopted in the investigation of earthquake accelerograms and the performance of liquefiable slopes in centrifuge model earthquakes. This tool was found to be convenient for the analysis and

visualisation of the ground acceleration data combining the best features of both time-histories and Fourier transforms in giving information on the variability of signals with time and frequency. This technique helped in interpreting the behavior of geotechnical structures under earthquake loading. Harmonic wavelet analysis was shown to be a versatile tool that can reveal information unavailable in traditional time or frequency domain analysis.

Nagarajaiah & Varadarajan (2005) developed a semi-active variable tuned mass damper for wind response control of buildings using a Short Time Fourier Transform (STFT) algorithm. The basic idea of STFT is to break up the non-stationary signal into small time segments and obtain the FFT of each time segment to ascertain the frequencies that exist in it. The dominant frequency is extracted and is used to retune the semi-active variable tuned mass damper.

The difficulty in incorporating the frequency dependent foundation impedance functions in a standard time-history analysis of structures was encountered by Safak (2006). Impedance functions represent the dynamic stiffness of the soil media surrounding the foundation. A simple method was proposed to convert frequency-dependent impedance functions into time-domain filters. The method is based on the least-squares approximation of impedance functions by ratios of two complex polynomials. Such ratios are equivalent, in the time-domain, to discrete-time recursive filters, which are finite-difference equations giving the relationship between foundation forces and displacements. These filters can easily be incorporated into standard time-history analysis programs.

It is evident from (Haigh et al. 2002 and Safak 2006) that it is important to account for the frequency content of an earthquake excitation, when the dynamic response of the system analyzed is frequency dependent. The STFT algorithm used by Nagarajaiah & Varadarajan (2005) is an effective technique that may be used to determine the time-frequency distribution of an earthquake excitation.

2.1.7 Shake Table Test

Model tests have been found to be useful to investigate nonlinear aspects of dam response viz., cracking, joint opening, sliding and cavitation. Special materials are

required to model the concrete dam that maintained the similitude with the prototype. When the experiment is conducted under normal gravity, the strength and stiffness of the model materials compared to the prototype must be reduced by the product of the density and length ratios. Approximate small scale models of concrete dam have been developed that is plaster based with a high water content and lead powder added to increase density (Niwa and Clough 1980, Oberti & Castoldi 1980). Harris et al. (2000) designed a new concrete mix for the non-linear similitude modelling. A two-dimensional model of Koyna Dam at 1/50 scale was used on a shake table to simulate the effects and serve as data for non-linear computer model calibration. The first model with initial crack at the top failed in a sliding mode. The observations showed that the crack has to overcome some bonding before sliding can occur. The uncracked model failed due to material failure, a crack was initiated in less than 1/30 second and sliding occurred for a number of cycles before the top of the model toppled.

In the shaking-table test carried out by Niwa and Clough (1980) on a single monolith of Koyna dam, a single crack was formed which extended all the way through the neck. The top block rocked back and forth but remained stable and continued to withstand the water load even under intense excitations. It was observed from a series of shaking table tests on single monoliths of Pine Flat Dam under full reservoir condition (Donlon 1989) that no failure occurred inspite of cracks extending all the way through the neck in each model. The cracking patterns in each model were different indicating that prototype dams may be sensitive to parameters describing the existing state of the dam and the excitation.

Tinawi et al. (2000) conducted shake table test to obtain the sliding response and cracking response due to simple acceleration pulses. Experiments were carried out on a 3.4m high concrete dam model with cold joints, which were allowed to slide after breaking. These test helped to investigate the robustness, or to highlight the deficiencies of existing numerical procedure. Similar experiments were conducted by Morin et al. (2002) on post tensioned gravity dams to obtain load-displacement, dam sliding and rocking responses. It was concluded that more experimental data are required to derive empirical expressions applicable to actual dam structures for defining shear stiffness parameter. Variations in system properties, water depth, concrete properties, joint surface

properties, post-tensioning, hole size and presence of water inside the cracks or lift joints affected the results.

2.2 DISCUSSION ON REVIEW

The state of the art in the analysis of dam-reservoir interaction problems is reviewed. From the review of the literature cited above the areas, which apparently need further attention of research are: (i) Modelling of aged dam (ii) Modelling of infinite reservoir and (iii) Modelling of dam-reservoir coupled system.

2.2.1 Modelling of Aged Dam

Earlier, the effects of earthquakes on dams were represented considering dam to be a rigid system supported on a rigid foundation. But most of the recent work has incorporated the elastic properties of the dam materials into the mathematical model, which influences the vibration properties of the dam and influences the earthquake response behavior. In a dam-reservoir system, when flexibility of dam is considered, the hydrodynamic responses show high peaks at the natural frequencies of the system. Saini et al. (1978) concluded from their study: "*The effect of flexibility of the dam and compressibility of water shows that the response of the system is highly resonant at the fundamental natural frequency but is significantly less at higher natural frequencies*". Analysis of the dam was carried out by modelling it in three dimension (Fok et al.1986) and two-dimension (Proulx and Paultre 1997). Concrete degradation has been investigated due to various factors like the thermodynamic imbalance (Ulm and Coussy 1995), concrete creep (Bazant et al. 1997) and the growth of inelastic strains (Meschke and Grasberger 2003).

Concrete gravity dams being porous and in a constant state of submergence are susceptible to a state of damage that may be induced already by exposure to harsh environmental conditions, various types of loading induced by earthquakes, impacts due to blasts, freezing and thawing that may affect material degradation during its lifetime, loss of material strength and increased permeability of the material with age. Hence, it is important to estimate material degradation with ageing while predicting the dynamic behavior of an ageing dam.

It is apparent from the past literature that extensive research has been carried out in the field of nonlinear analysis of dams, where various techniques have been explored to predict the origin and propagation of cracks. Though various non-linear analysis procedures have been developed to determine the effect of degradation on the responses of the dam due to seismic excitation, primary mechanisms or factors that can produce premature deterioration of concrete dams needs to be identified. El-Aidi & Hall Part I & II (1989), Cervera et. al. (1995) and Ghaemian & Ghobarah (1999) had considered the dam-reservoir-interaction with an isotropic damage model while developing a non-linear damage model. The damage index used in the above procedures is mainly evaluated based on relation between the strain energy of the damaged material and elastic energy of the undamaged material.

The evolution of damage index has been treated by researchers in various manners (Ghrib & Tinawi 1995a & 1995b, Hubert et al. 2001 and Mazzotti et al. 2001). A damage index indicates the initiation and propagation of cracks in a concrete structure. The propagation of cracks and its effect on nonlinear behavior is generally determined for a seismic loading corresponding to the duration of the earthquake. The durability of concrete in dam is considerably affected by the loss of concrete strength induced by the time variant external loading in conjunction with environmental loading processes such as moisture and heat transport, freeze-thaw action, dissolution processes such as calcium leaching, chemical expansive reactions (alkali-silica reaction) due to presence of silt deposited on the upstream face. Although considerable progress has been achieved in carrying out dynamic analysis by modelling concrete gravity dam considering the non-linear behavior of concrete including cracks, environmental effects are still accounted for by more or less heuristic evaluations of the degradation process and its influence on the residual structural safety. Due to ageing, the dams are subjected to severe environmental effects, which lead to degradation of the dam concrete. Since the dam face is in constant contact with water, concrete degradation due to hygro-mechanical loading is inevitable and should be considered in the analysis procedure. Hence, an accurate method of analysis is required to predict the behavior of aged dam-reservoir system that can effectively account for the degradation of concrete.

2.2.2 Modelling of Infinite Reservoir

A concrete gravity dam being a structure in close proximity to the reservoir, the hydrodynamic pressure developed in the reservoir affects its dynamic behavior. Therefore, it is important to adopt a technique that can yield accurate estimation of hydrodynamic pressures. The hydrodynamic pressure distribution on the vertical face of a dam was first determined analytically by Westergaard in 1933. Since then, the various techniques and procedures have been proposed.

Analytical methods or closed-form solutions of determining hydrodynamic pressure are suitable only for the vertical dam-reservoir interface and a horizontal reservoir bed surface. This difficulty has led to the development of other numerical techniques such as finite element method (Zienkiwicz & Bettess 1978, Hamdi et al. 1978, Sharan 1992), boundary element method (Hanna & Humar 1982), finite difference method (Hung & Wang 1987), coupled finite element and boundary element method (von Estorff & Antes 1991, Touhei & Ohmachi 1993). There is a common belief that the boundary element method is superior over finite element for the modelling of infinite or semi-infinite domains. However, in the reported literature (Yang et al. 1993) the efficiency of boundary element method in time domain analysis is not ascertained. This is because of the presence of the convolution integral and the singularity of the kernels of the formulation which requires large storage space and computational time for the evaluation of the effect of past time history and numerical integration. The finite difference method suffers from two severe drawbacks. Firstly, this method is inefficient for the calculation of hydrodynamic pressure on dam having irregular upstream faces. Secondly, a large number of grid points are required to model the infinite or semi-infinite fluid domain into a finite one.

Due to complex topographical condition of the dam or other like structures, the finite element method is recognised as one of the powerful numerical tools in most of the practical problems to obtain the hydrodynamic pressure distribution in the fluid domain. In the finite element analysis, the governing equation of the fluid may be expressed in terms of either displacement (Hamdi et al. 1978), pressure (Sharan 1987a), velocity potential (Feng & Quevat 1990) or both pressure and displacement (Fenves & Vargas-Loli 1988).

Some drawbacks are observed in the displacement based finite element formulation in the fluid domain. Firstly, a penalty function is required to be introduced for satisfying the irrotationality condition; otherwise zero frequency spurious modes may occur. Secondly, the degrees of freedom for the fluid domain increase significantly (especially for 3D problems). Thirdly, it is difficult to model an infinite fluid domain properly into a finite one.

The governing equation for fluid has also been expressed using both the displacement and pressure as the nodal variables (Fenves et al. 1988). The formulation of this kind of variables facilitates the solution if non-linear convective term is also taken into account. However, the effect of the non-linear convective term is significantly small for the type of problem being addressed at present. Hence, formulation with these variables may not be appropriate, as the number of degrees of freedom increases. There are some distinct advantages on the pressure based formulation, especially for infinite or semi-infinite fluid domain, where the degrees of freedom are reduced significantly compared to the other formulations.

In the finite element analysis, difficulties arise mainly because of the large extent of the fluid domain, where the fluid is practically unbounded. Hence, it is necessary to arbitrarily truncate the reservoir region in order to have a comparatively smaller computational domain. A number of far-boundary conditions have been reported in the literature and they may be broadly categorised into two types, non-local and local. Both the types have their own merits and demerits. Both the conditions are concerned on establishing a relation between water pressures and their normal gradients. The non-local boundary conditions establish pressure-normal gradient relations along the full boundary surface (Saini et al. 1978, Tsai and Lee 1989). Although non-local conditions may be used for a broad frequency range, they share the common shortcoming that the analytical solution used to derive non-local conditions depends on the discretization process that is carried out along the boundary. As a consequence, boundary discretization should be refined sufficiently in order to obtain reliable results in the high frequency range, thus increasing the computation cost. On the other hand, the pressure-normal gradient relation for a local condition is applicable pointwise, such as the well known Sommerfeld radiation condition. This condition is inappropriate for frequencies of excitation lower than the first natural frequency of the reservoir. To overcome this shortcoming, another

local condition has been developed by Sharan (1987a) which seems to be also approximate. However, it is observed from the literature that the local type boundary condition is relatively simpler to adopt in the finite element program. The far boundary condition proposed by Maity & Bhattacharyya (1999) is found to be effective in modelling the effects of radiation damping of the infinite reservoir. The principle advantages of this technique are that it is quite simple to implement in the finite element formulation, which does not disturb the symmetrical and banded form of the matrix coefficients in the fluid equation. However, for the case of absorptive reservoir bottom beyond the truncated boundary, it can not accurately represent the infinite reservoir for the finite element analysis. Further, this boundary condition can not account for excitation frequency greater than the resonant frequency. Thus, modification of the truncation boundary condition proposed by Maity & Bhattacharya (1999) will lead to a more appropriate boundary condition representing the realistic behavior of a reservoir.

For linear problems, the near field and the far field can be analyzed rigorously in the frequency domain. Transfer functions relating the response to the excitation can be calculated and using Fourier transform, the corresponding response in the time domain can be obtained. These boundaries are frequency dependent and are referred to as consistent boundaries. The truncated boundaries may be formulated in time domain as convolutions when they are called consistent, non-local boundaries (Wepf et al. 1988). Convolution methods are computationally inefficient, though Tsai and Lee (1990) and Yang et al. (1990) further improved the technique by reducing the computational effort substantially. The boundary element method (Antes and Estorff 1987) can also be directly formulated in time domain but requires similar computational effort as convolution integral.

The effect of reservoir bottom absorption on hydrodynamic response of dam reservoir system has been investigated by several researchers both numerically (Hall & Chopra 1982, Chuhan at el. 2001) and experimentally (Ghanaat et al. 2000). However, the final conclusions concerning the practical significance of the compressibility effect of the reservoir and reservoir bottom absorption on the dam was not conclusive. The reflection coefficient is the fundamental parameter that characterizes the absorption effect that can be either considered to be frequency independent (Hall & Chopra, 1982 and Sharan, 1992) or frequency dependent (Hatami 1997 and Chuhan et al. 2001). Use of

such frequency dependent reflection coefficient may affect the hydrodynamic pressure determined using a dynamic solution procedure in the frequency domain. Studies conducted by Chuhan et al. (2001) reveal that consideration of a viscoelastic or a porous model of the sediment layer gives similar results. The effect of reservoir bottom absorption has been considered in frequency domain solutions (Sharan 1992 and Hatami 1997) but the time domain solutions (Yang et al. 1996) do not show any significant changes in the response of the system due to ramp load or seismic excitation. This is because, the reservoir bottom absorption effect is frequency dependent and the time domain solution procedure cannot account for the frequency content at every time instant of the seismic excitation. Hence, it is important to estimate the frequency content of an earthquake signal to effectively account for radiation damping and reservoir bottom absorption effect.

2.2.3 Modelling of Dam-Reservoir Coupled System

The dam-reservoir system is a complex system consisting of more than one subsystem. The accurate prediction of its dynamic behavior necessitates proper modelling of interaction effects between the subsystems i.e., the dam, the reservoir and the foundation. The dynamic interaction between an elastic dam and its adjacent reservoir has been the subject of intensive investigations in recent years. Depending on the relative rigidity of the dam and the foundation material, the dam-foundation interaction effects may be neglected without much loss of accuracy but the dam-reservoir effects cannot be neglected. Some simplified approaches are available in which the dam-reservoir system is studied in a decoupled manner. In this type of analysis, the reservoir response is first obtained assuming the dam as rigid and the resulting pressure field is imposed on the dam to obtain its response. But such type of analysis does not always lead to a conservative design of the dam. If resonance between the structure and the energy release mechanism in the fluid occur it can lead to the development of unsound design. Moreover, if coupled modes are excited, this approach gives non-conservative results. Thus it is necessary to study the dam-reservoir interaction problems in a coupled manner considering the elastic effect of the dam.

It is evident from the literature that various techniques such as mixed variational principles (Pinsky & Abboud 1989), coupled finite element-boundary element procedure

(von Estorff and Antes 1991), substructure technique in the frequency domain (Fenves & Chopra 1983) and substructure method in the time domain (Yang & Tsai 1996) have been adopted for the analysis of coupled fluid-structure systems. The variational principles accommodated the dissipation associated with viscoelastic constitutive properties of the structure as well as the radiation boundary condition of fluid. The vectorial formulation required a penalty constraint to inhibit spurious rotational modes.

The most common approach being adopted at present is that both the systems are coupled and solved as one system (Zienkiewicz & Bettess 1978, Fenves & Vargas-Loll 1988). Formulations based on displacement variables are generally chosen for the structure while fluid is described by different variables such as displacement, pressure, velocity potentials etc. Use of pressure-based formulation (Zienkiewicz & Newton 1969) for fluid elements results in equations for coupled system that are unsymmetrical and require special purpose computer program (Sandberg 1995). This difficulty can be overcome with the displacement-based formulation (Chen & Taylor 1990, Olson & Bathe 1983 and Bermúdez et al. 1995) where the fluid elements can easily be coupled to the structural elements using standard finite element assembly procedures. But in the analysis of dam-reservoir system this leads to a large coupled matrix as it consists of degrees of freedom from both the systems. Moreover, the fluid displacements must satisfy the irrotationality condition, otherwise zero frequency spurious modes may occur. The variables such as velocity and pressure have also been used for representing the governing equations for fluid (Fenves & Vargas-Loli 1988). However, requirement of computational time becomes higher as the number of unknown parameters increase in the fluid domain. Thus the need of a large computer storage and expense of vast computer time usually make the analysis impractical.

To overcome these limitations, the analysis of the coupled dam-reservoir interaction problem can be accomplished by solving the two systems separately with the interaction effects enforced by iteration (Chopra & Chakrabarti 1981, Paul et al. 1981, Singh et al. 1991 and Maity & Bhattacharyya 2003). The major advantage of this method is that the coupled problem can be solved in a sequential manner. The analysis is carried out for each field and interaction effect is accommodated by updating the variables of the fields in the respective coupling terms. The effectiveness of this method depends on the number of iteration for each time-step in the analysis.

2.3 COMMENTS ON EXISTING LITERATURE

After reviewing the existing literature on the dynamic analysis of concrete dam, the following pertinent points emerge out.

1. The finite element method has the distinct advantage of being straightforward in implementation in the analysis of dam-reservoir interaction problems and representing any arbitrary geometry, heterogeneity in the dam body and the reservoir bed profile.

2. 3-D analysis requires more computational effort, though little loss of accuracy has been reported compared to the 2-D analysis in the computation of amplitude in the first resonance. The necessity of a 3D analysis might be essential depending on the length to height ratio of the dam.

3. It is important to account for temperature stresses due to heat of hydration for massive concrete structures at an early age. This helps to predict the effect of some major variables such as the placing temperature, the starting date and the placing speed on the construction process. The consideration of creep is significant if the stress analysis includes simulation of construction process. However, in the long term, ageing of concrete is affected by the concentration of various constituents in the concrete, chemical reactions such as calcium leaching or alkali-silica reaction, moisture transport and loading due to submergence in water.

4. Nonlinear analysis is necessary to study the formation and extension of cracks and sliding of dams. Failure may occur due to crushing of toe material, cracking of upstream material with an increase in uplift pressure and reduction in shear resistance that may result in sliding instability of the dam. Consideration of nonlinear behavior of the dam-foundation interface may be important for the seismic analysis of the coupled system depending on site conditions. Cracks tend to initiate near stress concentration zones of the dam. Therefore, the performance of cracked dams subjected to earthquake excitation need to be obtained by nonlinear analysis.

5. The governing equations of the structure are generally preferred to express in terms of displacement variables while the fluid equations are described by different variables such as displacement, pressure, velocity potential etc.

6. The compressibility of water in the reservoir may not be neglected in the analysis. Non-linear effect of the fluid motion is insignificant for the kind of problems being investigated. Viscosity effect of water is negligibly small.

7. When pressure or velocity potential is taken as the nodal unknown, prohibitive computational efforts with a special purpose computer program are required to solve the unsymmetrical and unbanded mass and stiffness matrix of the coupled dam-reservoir system. Formulation with displacement variable for the fluid lead to the development of some spurious modes.

8. Consideration of reservoir bottom absorption alters the hydrodynamic responses of concrete gravity dams. The parameter that characterizes the damping at the reservoir bottom is the reflection coefficient which depends upon the physical properties and thickness of the sediment layer lying at the reservoir bottom. Though a frequency independent reflection coefficient has been used by most of the researchers to account for the presence of sediment layer, a more rigorous approach of determining the frequency dependent reflection coefficient is recommended for considerable thickness of sediment layers.

9. Most of the far-boundary conditions proposed to date in time domain analysis appears to be approximate and does not account for the reservoir bottom absorption effects. Further, most of the boundary conditions are effective within a certain range of excitation frequencies. A far-boundary condition which takes care of absorptive reservoir bottom under all range of excitation frequencies needs to be developed for the seismic analysis of dam-reservoir coupled system.

10. To calculate the design force quantities accurately, the effect of fluid-structure interaction is necessary to be considered. Realistic yet simplified modelling of the coupled system is essential to estimate the dynamic response of the concrete gravity dam.

11. The dam-reservoir systems are analysed in two ways: (*i*) Both the systems are coupled and solved as one system. As a result, size of the matrix for the whole system becomes large. Also, the matrix will be unsymmetrical if pressure is

considered as a variable parameter in the fluid domain. (*ii*) The two systems are solved separately and the interaction effects are imposed at the dam-reservoir interface by iterative process.

12. In general gravity dams are constructed on rocky foundation. Therefore, the assumption of a rigid boundary at the dam-foundation interface will not result in serious distortion. Nonlinear foundation interaction effects may be considered if significant material nonlinearity or any faults and fissures are detected in the dam foundation.

13. The consideration of cavitations leads to reduction of responses. However, the cavitations effects on the response of the gravity dams are negligibly small.

14. Strong-motion instrumentation should be deployed at sites being considered for construction of concrete dams to obtain the free field motions at a canyon location without the interference of an existing dam. The motions recorded can be utilized in analyses intended to verify the various input methods.

15. The research on earthquake safety of dams is still young, as new lessons are learnt from each strong earthquake. There are uncertainties in the dynamic behavior of concrete gravity dams due to strong ground motions because of unavailability of sufficient recorded data. Further research is required to determine the dynamic behavior of ageing concrete gravity dams due to strong ground shaking. Prediction of the safety of existing dams due to the degradation of the structural material with age is important to justify efficient seismic strengthening of existing dams.

16. Coupled analysis of aging dam-reservoir system which takes care of degradation effects of the concrete material and absorptive effects due to sediments in the reservoir bed with age is necessary to predict the possible generation of stresses in the existing dams for retrofitting.

17. Seismic analysis of dam-reservoir systems are generally carried out either in frequency or in time domain. It is necessary to account for the frequency content of an earthquake excitation to increase the accuracy in the analysis, since the boundary conditions at the reservoir bottom and at the truncated boundary of the reservoir is frequency dependent.

2.4 SCOPE OF THE PRESENT INVESTIGATION

The detailed review of the existing literature reveals the fact that the dynamic analysis of concrete gravity dam attracted the researchers for the last few decades, although the focus of attention kept changing with the passage of time. It is apparent from the discussions that there lies a broad scope of research in this field particularly for the problems of the kind being discussed. To fulfil the objectives of the present investigation stated before and considering the areas still unexplored, the scope of the present investigation is limited to the following.

1. Finite element analysis of a concrete gravity dam idealizing the same as two-dimensional plane strain problem considering the geometrical non-linearity as well.
2. Development of a suitable numerical scheme to predict the dynamic behavior of aged concrete dams considering the material degradation due to long-term ageing.
3. Finite element formulation of the governing equation for water in the reservoir, using pressure as nodal variable parameter and incorporating the effect of reservoir bottom absorption.
4. Development of an efficient truncation boundary condition that can be effectively used in a finite element model of infinite reservoir at all excitation frequencies in time domain.
5. Development of an algorithm to evaluate the frequency dependent response of the dam-reservoir coupled system subjected to seismic excitation by applying the dominant frequencies of an earthquake excitation extracted using Short Time Fourier Transform (STFT).
6. Development of an iterative scheme for the solution of the dam-reservoir coupled system, to obtain divergence free hydrodynamic pressure and structural displacement simultaneously.
7. Evaluation of the stress distribution in the dam, pressure and velocity distribution in the reservoir in time domain that can efficiently and reliably be used to evaluate the safety of the existing aged dam due to seismic excitation.

CHAPTER 3

THEORETICAL FORMULATION

3.1 INTRODUCTION

The assessment of response of an aged concrete dam is important for the prediction of its behavior during earthquakes, so that remedial measures can be taken at the right time to withstand future earthquakes. Appropriate and effective measures can be recommended if the results obtained from the dynamic analysis are accurate. The accuracy of the results will depend on the approximations used in the development of the mathematical models to represent the dam-reservoir system. Due to ageing, the dams are subjected to severe environmental effects, which may lead to loss of strength due to material degradation. Since the dam face is in constant contact with water, concrete degradation due to hygro-mechanical loading is inevitable and should be considered in the analysis procedure. Hence, an accurate method of analysis is required to predict the behavior of aged dam-reservoir system that can effectively account for the degradation of concrete. An approach to include the time dependent degradation of concrete owing to environmental factors and mechanical loading in terms of isotropic degradation index is presented. The design of seismic resistant concrete dam necessitates accurate determination of hydrodynamic pressure developed in the adjacent reservoir. The hydrodynamic pressure developed on the dam is dependent on the physical characteristics of the boundaries surrounding the reservoir including reservoir bottom. The sedimentary material in the reservoir bottom absorbs energy at the bottom, which will affect the hydrodynamic pressure at the upstream face of the dam. The absorption of pressure waves at the bottom of the reservoir due to the presence of sediments has been incorporated in the hydrodynamic pressure equation. Both the aged dam and infinite reservoir with sediments are modelled and analyzed by finite element technique.

To evaluate the hydrodynamic response of a dam-reservoir system, the formulation of the radiation condition of the unbounded reservoir is the key issue in the finite element analysis. The hydrodynamic forces in the reservoir are affected by radiation of waves towards infinity and wave absorption at the reservoir bottom. An

accurate evaluation of hydrodynamic pressure on the dam must consider the effect of sediments of the reservoir bottom. A far-boundary condition considering the effect of sediment layers at the bottom of the reservoir is implemented for the finite element analysis to evaluate the dynamic response of the infinite reservoir. The boundary condition at the bottom of the reservoir is formulated accounting for the characteristics of sediment layers above the reservoir bottom.

The coupled effects of the dam-reservoir system are obtained by introducing an iterative scheme that ensures the interactions. The solution of the coupled system is accomplished by solving the two systems separately with the interaction effects at the fluid-solid interface enforced by the developed iterative scheme.

The theoretical formulations for the dam-reservoir coupled systems are presented in three parts. Part A, B and C contain the formulations of the aged dam, reservoir and the coupled dam-reservoir system.

3.1.1 Suitability of Finite Element Technique

For the dam and reservoir having simple boundary, classical solution treating the dam and reservoir as continuum may be used effectively. However, if the dam geometry and reservoir boundary is not regular, numerical methods such as finite element technique may be used effectively. Due to varied geometric forms of the dam and irregular geometry of the reservoir, the finite element method (FEM) is recognized to be one of the most powerful numerical tools for solving such problems. However, a computational difficulty exists if the length of the reservoir is infinite for FE discretization. In such practical situation, the infinite reservoir is truncated by imposing an artificial boundary at a certain distance away from the structure. A suitable boundary condition must be imposed at truncation surface to evaluate the effect of radiation damping, so that no spurious wave reflection occurs from the boundary.

3.1.2 Selection of Finite Element Technique

In finite element method, a body or a structure is analyzed as an assemblage of a number of smaller subdivisions of finite dimensions called *finite elements*. These finite elements are connected at a finite number of *nodes* or *nodal points*. The properties of the

individual elements are formulated and assembled to obtain the solution for the entire body or structure. Here, the dam and the reservoir are discretized into eight noded and four noded isoparametric elements respectively. The isoparametric element is oriented in the natural coordinate system (ξ,η) and is transformed to the Cartesian coordinate system using Jacobian matrix. The elements in both the above-mentioned coordinate systems are shown in Figs. 3.1 and 3.2.

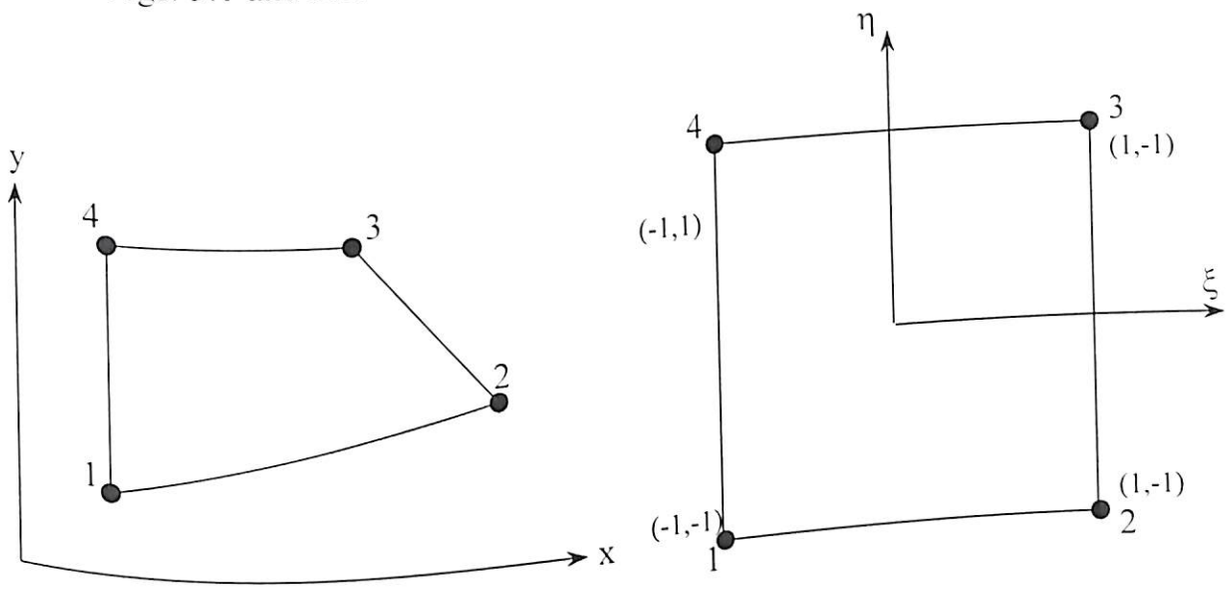

(a) Cartesian coordinate **(b) Natural coordinate**

Fig. 3.1 Transformation from Cartesian coordinates to Natural coordinates for four noded quadrilateral element

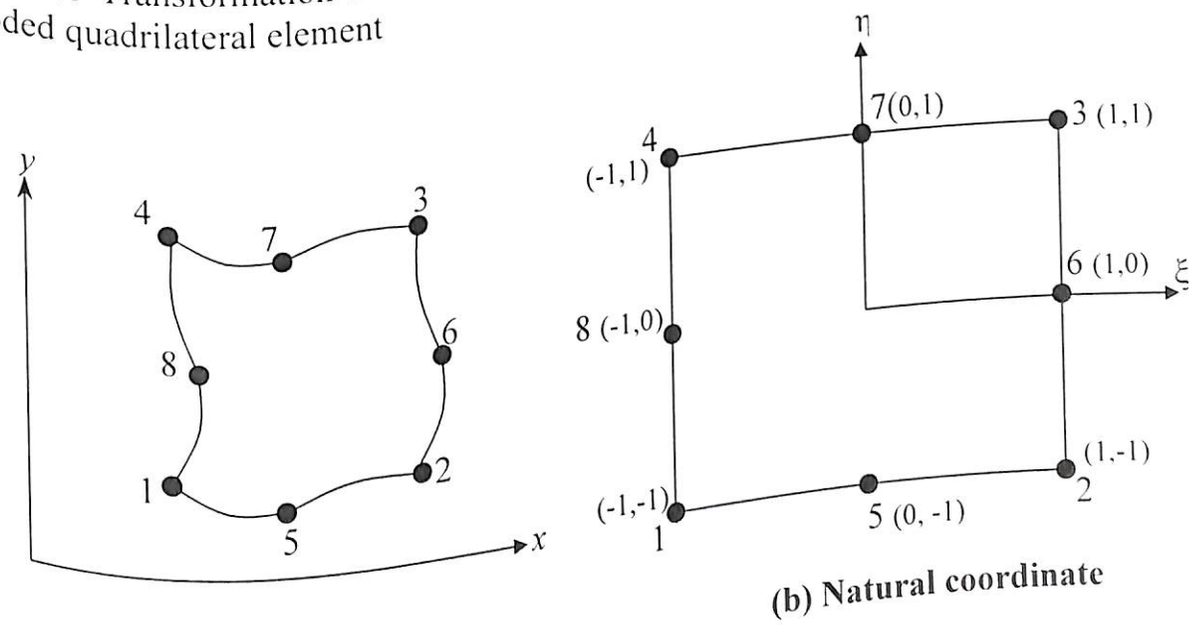

(a) Cartesian coordinate **(b) Natural coordinate**

Fig. 3.2 Transformation from Cartesian coordinates to Natural coordinates for eight noded quadrilateral element

3.1.3 Selection of Shape Function

The advantage of using isoparametric formulation is that it can generate non-rectangular elements having curved sides and arbitrary shapes. Isoparametric elements are formulated using an intrinsic coordinate system (ξ-η), which is defined by the element geometry and not by the element orientation in the global coordinate system. The natural coordinates are always attached to the element and are scaled so that the sides of the parent element are defined by $\xi = \pm 1$ and $\eta = \pm 1$.

3.1.3.1 Shape Functions for the Reservoir

A typical four noded quadrilateral element as shown in Fig.3.1 is considered for FE discretization of the reservoir. The shape functions are derived from an interpolation polynomial in terms of the natural coordinates to represent pressure at any point as nodal pressures. The interpolation polynomial is a function of ξ and η and can be written as

$$p(\xi,\eta) = A_0 + A_1\xi + A_2\eta + A_3\xi\eta \tag{3.1}$$

The shape functions derived from the interpolation polynomial are

$$N_{ri} = \frac{1}{4}(1+\xi\xi_i)(1+\eta\eta_i) \qquad i = 1,2,3,4 \tag{3.2}$$

Here, N_{ri} denotes the shape function at the i^{th} node of the element having natural coordinates ξ_i and η_i.

3.1.3.2 Shape Functions for the Dam

An eight noded quadrilateral element as shown in Fig.3.2 is considered for the discretization of the dam. The shape functions are derived from an interpolation polynomial in terms of natural coordinates so that the displacements are represented as a function of nodal displacement. The interpolation polynomial has the following form

$$u(\xi,\eta) = A'_0 + A'_1\xi + A'_2\eta + A'_3\xi^2 + A'_4\xi\eta + A'_5\eta^2 + A'_6\xi^2\eta + A'_7\xi\eta^2 \tag{3.3}$$

The shape functions derived from the interpolation polynomial are as

$$\left.\begin{aligned} N_{di} &= \frac{1}{4}(1+\xi\xi_i)(1+\eta\eta_i)(\xi\xi_i+\eta\eta_i-1) && i=1,2,3,4 \\ N_{di} &= \frac{1}{2}(1+\xi\xi_i)(1-\eta^2) && i=5,7 \\ N_{di} &= \frac{1}{2}(1+\eta\eta_i)(1-\xi^2) && i=6,8 \end{aligned}\right\} \tag{3.4}$$

Here, i denotes the node number of the element. The correctness of the shape functions is checked from the relations:

$$\sum N_{di} = 1, \quad \sum \frac{\partial N_{di}}{\partial \xi} = 0 \text{ and } \sum \frac{\partial N_{di}}{\partial \eta} = 0 \tag{3.5}$$

3.1.4 Relationship between Cartesian and Natural coordinates

The displacements u and v are expressed through the interpolation functions as

$$u = \sum N_{di} u_i \text{ and } v = \sum N_{di} v_i \tag{3.6}$$

The shape functions for the dam, N_{di} are functions of the natural coordinates ξ, η. Here, i represents the node numbers. Since the element is isoparametric, the same interpolation functions are used to represent the geometry in terms of the Cartesian coordinates x_i and y_i as

$$x = \sum N_{di} x_i \text{ and } y = \sum N_{di} y_i \tag{3.7}$$

Similarly, the pressure p may be expressed by the nodal pressure, p_i through the shape functions of the reservoir as:

$$p = \sum N_{ri} p_i \tag{3.8}$$

The relationship between the two coordinate systems may be computed by using the chain rule of partial differentiation as:

$$\begin{pmatrix} \frac{\partial}{\partial \xi} \\ \frac{\partial}{\partial \eta} \end{pmatrix} = \begin{pmatrix} \frac{\partial x}{\partial \xi} & \frac{\partial y}{\partial \xi} \\ \frac{\partial x}{\partial \eta} & \frac{\partial y}{\partial \eta} \end{pmatrix} \begin{pmatrix} \frac{\partial}{\partial x} \\ \frac{\partial}{\partial y} \end{pmatrix} = [J] \begin{pmatrix} \frac{\partial}{\partial x} \\ \frac{\partial}{\partial y} \end{pmatrix} \tag{3.9}$$

where $[J]$ is the Jacobian matrix. The derivative operators with respect to Cartesian coordinate system may be represented as

$$\begin{pmatrix} \frac{\partial}{\partial x} \\ \frac{\partial}{\partial y} \end{pmatrix} = [J]^{-1} \begin{pmatrix} \frac{\partial}{\partial \xi} \\ \frac{\partial}{\partial \eta} \end{pmatrix} \tag{3.10}$$

3.1.5 Time History Analysis

In a dynamic problem the equation of motion can be expressed as

$$[M]\{\ddot{d}\} + [C]\{\dot{d}\} + [K]\{d\} = \{F\} \tag{3.11}$$

The time history analysis is carried out using a suitable time stepping scheme. In eq.(3.11), $[M]$, $[C]$ and $[K]$ are the mass, damping and stiffness matrices of the system. In a linear dynamic system, these values remain constant throughout the time history analysis. The force vector is given by $\{F\}$. To obtain the transient response at time t_N, the time axis can be discretized into N equal time intervals ($t_N = \sum_{j=1}^{N} j\Delta t$), where displacement $\{d\}$, velocity $\{\dot{d}\}$ and acceleration $\{\ddot{d}\}$ are functions of time. The choice of method for time-history analysis is strongly problem dependent. Various direct time integration methods exist for time history analysis that are expedient for structural dynamics and wave propagation problem. Amongst these, the Newmark family of methods is most popular and is given by

$$\{d\}_{j+1} = \{d\}_j + \Delta t\{\dot{d}\}_j + \frac{\Delta t^2}{2}\left[(1-2\vartheta)\{\ddot{d}\}_j + 2\vartheta\{\ddot{d}\}_{j+1}\right] \tag{3.12}$$

$$\{\dot{d}\}_{j+1} = \{\dot{d}\}_j + \Delta t\left[(1-\gamma)\{\ddot{d}\}_j + \gamma\{\ddot{d}\}_{j+1}\right] \tag{3.13}$$

Here, ϑ and γ are chosen to control stability and accuracy. It is evident from the literature that the integration scheme is unconditionally stable if $2\vartheta \geq \gamma \geq 0.5$.

3.1.5.1 Stability Analysis of Newmark Method

The aim of the numerical integration of time in the finite element system equilibrium equations is to approximate the actual dynamic response of the structure under consideration. Stability of an integration scheme implies that the initial conditions for the equations with a large value of $\Delta t / T$ must not be amplified artificially and thus make the integration of lower modes worthless. In a stable scheme, there is no abrupt increase of any errors in displacements, velocities and accelerations at time t, due to rounding off during computation. Stability is acquired if the time step chosen is small enough to integrate accurately the response in the highest frequency component. It is important to optimize the size of the time step, so as to obtain accuracy but at the same time avoid an increase in computational cost.

3.1.5.2 Accuracy Analysis of Newmark Method

In a practical analysis, the choice of the integration operator depends on the cost of solution that can be determined by the number of time step required in the integration.

For a conditionally stable algorithm such as central difference, the time steps for a given time range considered is determined by the critical time step Δt_{cr} and not many choices are available.

The errors in the integration may be measured in terms of period elongation and amplitude decay. When the time step to period ratio is larger, the various integration methods exhibit quite different characteristics. For a given $\Delta t / T$, the Wilson-θ method with $\theta = 1.4$ introduces less amplitude decay and period elongation than the Houbolt method, and the Newmark average acceleration method introduces only period elongation and no amplitude decay. If the Newmark constant average acceleration is employed, the high frequency response is retained in the solution. It is observed that the method corresponding to $\gamma = 0.5$ and $\vartheta = 0.25$ has the most desired stability. Therefore, in the present work, the dynamic equilibrium equations are solved using the values of γ and ϑ as 0.5 and 0.25 respectively.

PART – A

3.2 THEORETICAL FORMULATION FOR DAM

The structural system considered for the present investigation, has been analyzed using two dimensional plane strain formulations. Since the problem considered here involves a long body, whose geometry and loading do not vary in the longitudinal direction, it can be analyzed by this idealization appropriately. However, plane stress formulations may become appropriate for strong motions where keyed joints fail and each monolith vibrates as a two dimensional plate. The formulation of the structure requires the following steps to be performed:

i) Selection of appropriate shape functions
ii) Relationship between the Cartesian and natural coordinates
iii) Strain-displacement relations
iv) Building of the constitutive matrix
v) Evaluation of degradation effect with age
vi) Modification of constitutive matrix to incorporate degradation effect

vii) Building the stiffness, mass and damping matrices

viii) Selection of a suitable numerical scheme for time history analysis

ix) Computation of stresses

The selection of shape functions for discretization of the dam, the relationship between the Cartesian and natural coordinates and selection of a suitable numerical scheme for time history analysis are as explained in sections 3.1.3.2, 3.1.4 and 3.1.5 respectively.

3.2.1 Strain Displacement Relations

The relation between strain and displacement is of utmost importance in the finite element formulation for stress analysis problems. The generalized strain-displacement relations for the two-dimensional plane strain problems may be written as

$$\left.\begin{aligned}
\varepsilon_x &= \frac{\partial u}{\partial x} + \frac{1}{2}\left[\left(\frac{\partial u}{\partial x}\right)^2 + \left(\frac{\partial v}{\partial x}\right)^2\right] \\
\varepsilon_y &= \frac{\partial v}{\partial y} + \frac{1}{2}\left[\left(\frac{\partial u}{\partial y}\right)^2 + \left(\frac{\partial v}{\partial y}\right)^2\right] \\
\gamma_{xy} &= \frac{\partial v}{\partial x} + \frac{\partial u}{\partial y} + \left[\frac{\partial u}{\partial x}\frac{\partial u}{\partial y} + \frac{\partial v}{\partial x}\frac{\partial v}{\partial y}\right]
\end{aligned}\right\} \qquad (3.14)$$

Using eq.(3.6) the elemental strain may be written as

$$\left.\begin{aligned}
\frac{\partial u}{\partial x} &= [B_1]\{\bar{u}\} \\
\frac{\partial v}{\partial x} &= [B_1]\{\bar{v}\} \\
\frac{\partial u}{\partial y} &= [B_2]\{\bar{u}\} \\
\frac{\partial v}{\partial y} &= [B_2]\{\bar{v}\}
\end{aligned}\right\} \qquad (3.15)$$

Here, $[B_1]$ and $[B_2]$ are the derivative of the shape function $[N_d]$ with respect to x and y respectively. The vectors $\{\bar{u}\}$ and $\{\bar{v}\}$ represent the nodal displacements vectors in x and y directions respectively. The vector of strains at any point inside an element, $\{\varepsilon\}$ may be expressed in terms of nodal displacement as

$$\{\varepsilon\} = [B_0]\{d\} \qquad (3.16)$$

where $[B_0]$ is the strain displacement matrix. $\{d\}$ is the nodal displacement vector and may be expressed as

$$\{d\} = \begin{Bmatrix} \{\bar{u}\} \\ \{\bar{v}\} \end{Bmatrix} \tag{3.17}$$

The matrix $[B_0]$ may be expressed as

$$[B_0] = [B_l] + [B_{nl}] \tag{3.18}$$

where, $[B_l]$ and $[B_{nl}]$ are the linear and nonlinear part of the strain-displacement matrix respectively and are expressed as follows:

$$[B_l] = \begin{bmatrix} [B_1] & [0] \\ [0] & [B_2] \\ [B_2] & [B_1] \end{bmatrix} \tag{3.19}$$

and

$$[B_{nl}] = \begin{bmatrix} \frac{1}{2}\{\bar{u}\}^T[B_1]^T[B_1] & \frac{1}{2}\{\bar{v}\}^T[B_1]^T[B_1] \\ \frac{1}{2}\{\bar{u}\}^T[B_2]^T[B_2] & \frac{1}{2}\{\bar{v}\}^T[B_2]^T[B_2] \\ \{\bar{u}\}^T[B_2]^T[B_1] & \{\bar{v}\}^T[B_2]^T[B_1] \end{bmatrix} \tag{3.20}$$

3.2.2 Solution Scheme to Include the Effect of Geometrical Non-Linearity

The nonlinear geometric effect of the structure at a particular instant of time can be obtained by performing the following steps.

1. Calculation of displacement $\{d\}_1$ considering linear part of strain matrix $[B_l]$.
2. Evaluation of nonlinear part of the strain matrix $[B_{nl}]$ (eq. 3.20) adopting $\{d\}_1$ from previous step.
3. Evaluation of total strain matrix $[B_0] = [B_l] + [B_{nl}]$.
4. Calculation of displacement $\{d\}_2$ considering both linear and nonlinear part of strain matrix $[B_0]$.
5. Repetition of steps 2 to 4 with $\{d\}_2$, from which modified displacement, $\{d\}_3$ are obtained.
6. Step 5 is carried out until the displacements for two consecutive iteration converge *i.e.*,

$$\left| \frac{\{d\}_j - \{d\}_{j-1}}{\{d\}_j} \right| < \varepsilon'$$

where ε' is any preassigned small value and j is the number of iterations.

3.2.3 Constitutive Matrix

For the plane strain formulations, a constant longitudinal displacement corresponding to a rigid body translation and rigid body rotations having displacements linear in a direction perpendicular to the cross-section of the dam, do not result in strain. This implies that

$$\varepsilon_z = \gamma_{zx} = \gamma_{xz} = 0 \tag{3.21}$$

Therefore, the constitutive relation for elastic isotropic material can be written as

$$\{\sigma\} = [D]\{\varepsilon\} \tag{3.22}$$

In the above equation, $\{\sigma\}^T = \{\sigma_x, \sigma_y, \tau_{xy}\}$ and $\{\varepsilon\}^T = \{\varepsilon_x, \varepsilon_y, \gamma_{xy}\}$ are the vectors of stress and strain respectively , and $[D]$ is the constitutive matrix defined as

$$[D] = \frac{E_d}{(1+\mu)(1-2\mu)}\begin{bmatrix} (1-\mu) & \mu & 0 \\ \mu & (1-\mu) & 0 \\ 0 & 0 & (1-2\mu) \end{bmatrix} \tag{3.23}$$

for a material with elastic modulus E_d and Poisson's ratio μ.

3.2.4 Degradation Model for Concrete

The concept of degradation of concrete strength is based on the reduction of the net area capable of supporting stresses. The loss of rigidity of the material follows as a consequence of material degradation due to various environmental and loading conditions. Adopting an analogy given by Ghrib & Tinawi (1995) to measure the extent of damage in concrete, the orthotropic degradation index can be determined as

$$d_{gi} = 1 - \frac{\Omega_i - \Omega_i^d}{\Omega_i} = 1 - \frac{\Omega_i^n}{\Omega_i} \tag{3.24}$$

where Ω_i = tributary area of the surface in direction i; and Ω_i^d = area affected by degradation. In a scale of 0 to 1, the orthotropic degradation index, $d_i = 0$ indicates no degradation and $d_{gi} = 1$ indicates completely degraded material. The index $i = 1,2$ corresponds with the Cartesian axes x and y in two-dimensional case. The effective plane strain material matrix can be expressed as

$$[D_d] = \frac{E_d}{(1+\mu)(1-2\mu)}\begin{bmatrix} (1-\mu)\Lambda_1^2 & \mu\Lambda_1\Lambda_2 & 0 \\ \mu\Lambda_1\Lambda_2 & (1-\mu)\Lambda_2^2 & 0 \\ 0 & 0 & (1-2\mu)\Lambda_1^2\Lambda_2^2/\left(\Lambda_1^2+\Lambda_2^2\right) \end{bmatrix} \tag{3.25}$$

where $\Lambda_1 = (1 - d_{g1})$ and $\Lambda_2 = (1 - d_{g2})$. In the above equation, E_d is the elastic modulus of the material without degradation. If $d_{g1} = d_{g2} = d_g$, the isotropic degradation model is expressed as

$$[D_d] = (1 - d_g)^2 [D] \tag{3.26}$$

where $[D_d]$ and $[D]$ are the constitutive matrices of the degraded and un-degraded model respectively.

3.2.5 Evaluation of Degradation Index

The compressive strength of concrete is expected to decrease with age due to chemical and mechanical material degradation. But it is also a known fact that concrete gains compressive strength with age. Various relations are available in the literature to predict gain in strength only for a short span of time, but no such relations exist to predict its strength during its entire lifetime. Generally, empirical relations are based on experimental results. To the author's knowledge, such experimental result for mass concrete which is generally used in a concrete dam does not exist, mainly because of difficulties that arise in testing mass concrete consisting of 152 mm maximum size aggregate (MSA). However, mix design of mass concrete is reported (Andrade et al. 1981, Bittencourt et al. 2001 and Deb & Borsaikia 2006) using smaller size of aggregates having the same fineness modulus as in mass concrete. The two concrete mixes consisting of different aggregate size but same geometrical gradation and fineness modulus gives the same compressive strength. Therefore, the present formulation strategy is based on experimental results of fifty years concrete (Washa et al.1989). While determining the degradation index at a particular age, the corresponding strength gain in concrete is also considered.

3.2.5.1 Degradation with Age

To consider the interaction phenomena of chemical and mechanical material degradation, the total porosity of concrete is taken as a measure to determine the degradation parameter. The total porosity ϕ is defined as the sum of the initial porosity, ϕ_0 the porosity due to matrix dissolution, ϕ_c and the apparent mechanical porosity, ϕ_m. The method of determining the chemically induced porosity can be found in the references Bangert et al. (2003) and Kuhl et al. (2004) as

$$\phi = \phi_0 + \phi_c + \phi_m \tag{3.27}$$

The apparent mechanically induced porosity, ϕ_m considers the influence of mechanically induced micro-pores and micro-cracks on the macroscopic material properties of the porous material. It is obtained as

$$\phi_m = [1 - \phi_0 - \phi_c]d_m \tag{3.28}$$

where d_m is the scalar degradation parameter. The strain based exponential degradation function as proposed by Simo and Ju (1987) is given as

$$d_m = a_s - \frac{\kappa^0}{\kappa}\left[1 - \alpha_c + \alpha_c e^{\left(\beta_c\left[\kappa^0 - \kappa\right]\right)}\right] \tag{3.29}$$

where κ^0 and κ are values of strain that represents the initial threshold degradation and the internal variable defining the current damage threshold depending on the loading history. κ^0 is given by f_t / E_0, where f_t is the static tensile strength and E_0 is the elastic modulus of the un-degraded material before any mechanical loading is imposed. The value of d_m at any age can be determined from eq. (3.29) that will vary with κ caused by the mechanical loading history. In the absence of degradation due to mechanical loading, $\kappa^0 = \kappa$, which makes $d_m = 0$ and hence $\phi_m = 0$. α_c and β_c are material parameters that can be obtained experimentally (Bangert et al. 2003). In eq. (3.29), the value of a_s is considered to be 1.0 by Simo and Ju (1987), which is the maximum allowable degradation due to mechanically induced porosity.

To study the effect of time on the degradation process, an analogy given by Atkin (1994) is adopted. Ageing process may be described by a normalized process extent with $\varsigma = 0$ for a freshly laid concrete and $\varsigma = 1$ for its completely aged state. Thus the kinetic law for the ageing process may be stated as

$$\dot{\varsigma} = \frac{1}{\tau_a}(1 - \varsigma)_m \tag{3.30}$$

where $\dot{\varsigma}$ is the time derivative of ς and τ_a is the characteristic time of the ageing process, which can be assumed to be the design life of the structure. Integrating eq. (3.30) with respect to time, the following expressions will be obtained:

$$1 - \varsigma = e^{\left(-\frac{t}{\tau_a}\right)} \tag{3.31}$$

Replacing ς with degradation index d_g in eq. (3.31), variation of degradation index with time can be given as

$$d_g = 1 - e^{\left(-\frac{t}{\tau_a}\right)} \tag{3.32}$$

At a constant ambient humidity, the reaction extent, ξ_γ for the corresponding characteristic time, τ_r as given by Steffens et al. (2003) is

$$\xi_\gamma = 1 - e^{\left(-\frac{t}{\tau_r}\right)} \tag{3.33}$$

Substituting t from eq. (3.33) in eq.(3.32) following relation will be arrived,

$$1 - d_g = (1 - \xi_\gamma)^{\frac{\tau_r}{\tau_a}} \tag{3.34}$$

The relation between degraded elastic modulus due to porosity of concrete, E_m and the elastic modulus of concrete considering strength gain at a particular age, E_0 can be given as $E_m = (1-d_g)E_0$. Using the dimensionless value of total porosity obtained by multiplying the scalar degradation variable, as reaction extent, the variation of degradation with respect to time can be given as

$$E_m = (1 - \phi)^{\frac{t_a}{\tau_a}} E_0 \tag{3.35}$$

The value of τ_a is the characteristic age for which the structure is designed and t_a is the time corresponding to which the degradation index is determined. Once the value of degraded elastic modulus is obtained from eq. (3.35), the isotropic degradation index, d_g can be determined as

$$d_g = 1 - \frac{E_m}{E_0} \tag{3.36}$$

3.2.5.2 Gain in Compressive Strength with Age

The gain in compressive strength of concrete is predicted by curve fitting of the experimental data published by Washa et al. (1989). Test results of various concrete specimens of different proportions were published in the referred literature. These specimens were moist cured for 28 days before placing outdoors. Outdoor storage was on level ground in an uncovered cage in an open location. The specimens were subjected to harsh weather conditions of 25 cycles of freezing and thawing each winter, annual precipitation including snowfall of about 0.813 cm and air temperature variation between

-32.0°C and 35.0°C.

In engineering problems, an experiment produces a set of data points (x_1, y_1), ..., (x_n, y_n), where the abscissas $\{x_k\}$ are distinct. The objective of using a numerical technique is to determine a formula $y = f(x)$ that relates these variables. There are many possibilities for the type of functions that can be used. Often, there is an underlying mathematical model, based on the physical situation that determines the form of the function. Many experiments are done with equipment that is reliable only to three or fewer digits of accuracy. This leads to experimental error in measurements. Therefore, the actual value $f(x_k)$ (Mathews 2001) satisfies

$$f(x_k) = y_k + e_k \tag{3.37}$$

where e_k is the measured error. Some of the methods that can determine how far the curve $y_{ls} = f(x)$ lies from the data are:

$$\left.\begin{array}{ll} \text{Maximum error:} & E_\infty(f) = \max\limits_{1\le k\le N'} \{|f(x_k) - y_k|\} \\ \text{Average error:} & E_1(f) = \dfrac{1}{N'} \sum\limits_{k=1}^{N'} |f(x_k) - y_k| \\ \text{Root-mean-square error:} & E_2(f) = \left[\dfrac{1}{N'} \sum\limits_{k=1}^{N'} |f(x_k) - y_k|^2 \right]^{1/2} \end{array}\right\} \tag{3.38}$$

The *best fitting* line is found by minimizing one of the quantities in eq.(3.38). Out of the three best fit lines that can be determined from the above equation, $E_2(f)$ is the traditional choice because it is much easier to minimize $E_2(f)$ computationally. The *least squares line* is the line that minimizes the root-mean-square error $E_2(f)$ and is given as

$$y_{ls} = f(x) = Ax + B \tag{3.39}$$

In the above equation, A and B can be determined from N' sets of experimental data as follows:

$$A = \frac{\sum\limits_{k=1}^{N'} x_k y_k}{\sum\limits_{k=1}^{N'} x_k} \quad , \quad B = \frac{\sum\limits_{k=1}^{N'} y_k}{N'} - A \frac{\sum\limits_{k=1}^{N'} x_k}{N'} \tag{3.40}$$

For the present analysis, the set of results corresponding to concrete of mix proportion 1:2.51:5.34 (cement:sand:gravel by weight) with water cement ratio of 0.49 is considered. There are various possibilities for curves used in data linearization. Here, the following forms are considered for curve fitting:

$$\left.\begin{array}{ll} \text{I.} & y = C'' e^{Dx} \\ \text{II.} & y = C'' x e^{Dx} \\ \text{III.} & y = A \ln(x) + B \end{array}\right\} \qquad (3.41)$$

In the above expressions, $C'' = e^{B}$ and $D' = -A$. Data linearization is carried out by transforming points (x_k, y_k) in the xy plane to $(X_k, Y_k) = (x_k, \ln(y_k))$ in the XY plane. Then the least squares line is fitted to the points $\{(X_k, Y_k)\}$ to give the predicted results. The predicted results using the above expressions (eq. 3.41) are plotted in Fig. 3.3.

It is observed from Fig. 3.3 that the relation $y = A \ln(x) + B$ represented by curve III is close to the experimental data. According to Washa et al. (1989), the specimen showed an increase in compressive strength roughly proportional to the logarithm of age during the first 10 years and small variation thereafter. Hence, the curve III is adopted for predicting the increase in compressive strength expressed as a function of age of concrete as

$$f(t_a) = 3.57 \ln(t_a) + 44.33 \qquad (3.42)$$

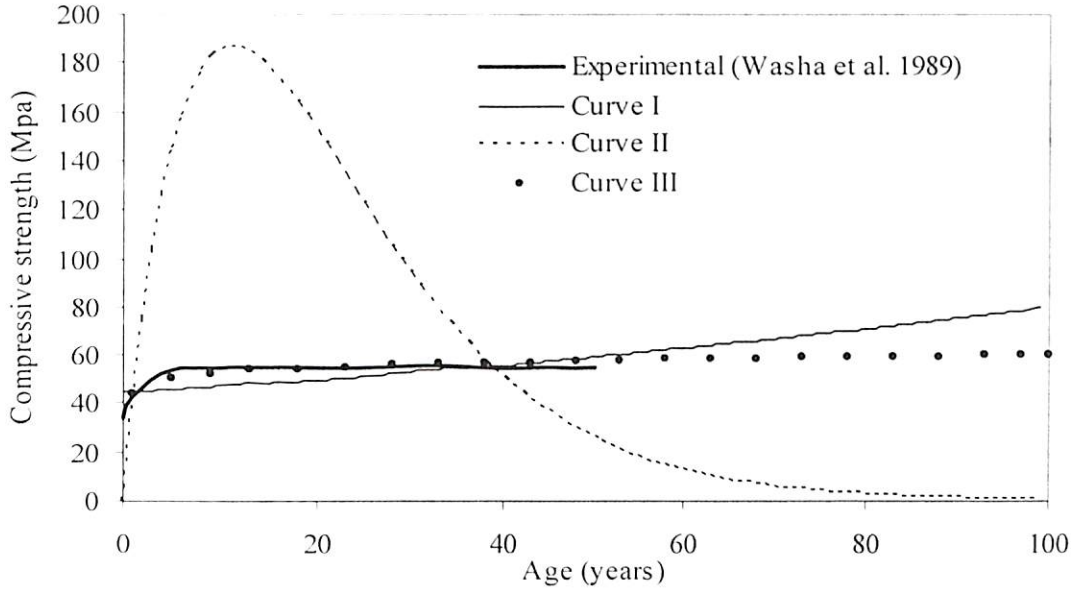

Fig. 3.3 Curve fitting of experimental data

The value of compressive strength obtained is in SI units and t_a is age of concrete in years. The value of static elastic modulus of concrete in SI units (Neville and Brooks 1987) is obtained from

$$E_0 = 4733\sqrt{f(t_a)} \qquad (3.43)$$

3.2.6 Stiffness, Mass and Damping Matrices

The dynamic response of a structure may be derived by minimizing the work of internal, inertial and viscous forces for any small kinematically admissible motion. For a single element, this work balance becomes

$$\int_{\Omega_e}\{\delta u\}_i^T\{F\}d\Omega+\int_{\Gamma_e}\{\delta u\}_i^T\{\Phi\}d\Gamma+\sum_{i=1}^{n_i}\{\delta u\}_i^T\{F_c\}_i = \int_{\Omega_e}\left(\{\delta\varepsilon\}_i^T\{\sigma\}+\{\delta u\}^T\rho_d\{\ddot{u}\}+\{\delta u\}^T k_d\{\dot{u}\}\right)d\Omega \tag{3.44}$$

Here, $\{\delta u\}$ and $\{\delta\varepsilon\}$ are small arbitrary displacements and their corresponding strains respectively, $\{F\}$ are the body forces, $\{\Phi\}$ are the prescribed surface tractions, $\{F_c\}_i$ are the concentrated loads that act at a total of n_c points on the element, $\{\delta u\}_i^T$ is the displacement of the point at which load $\{F_c\}_i$ is applied, ρ_d is the mass density of the dam material, k_d is the material damping parameter analogous to viscosity, and volume integration is carried out over the element volume Ω_e. The displacement field $\{u\}$ and its first two derivatives may be expressed as

$$\{u\}=[N_d]\{d\};\qquad \{\dot{u}\}=[N_d]\{\dot{d}\};\qquad \{\ddot{u}\}=[N_d]\{\ddot{d}\} \tag{3.45}$$

In the above equation, shape functions $[N_d]$ are functions of space and the nodal degree of freedom $\{d\}$ are functions of time only. Combining eq. (3.44) and (3.45) gives

$$\{\delta d\}^T\left[\int_{\Omega_e}[B_0]^T[D][B_0]d\Omega\{d\}+\int_{\Omega_e}[N_d]^T\rho_d[N_d]d\Omega\{\ddot{d}\}+\int_{\Omega_e}[N_d]^T k_d[N_d]d\Omega\{\dot{d}\}-\int_{\Omega_e}[N_d]^T\{F\}d\Omega-\int_{\Gamma_e}[N_d]^T\{\Phi\}d\Gamma-\sum_{i=1}^{n_c}\{F_c\}_i\right]=0 \tag{3.46}$$

It is assumed that the locations of concentrated load $\{F_c\}_i$ are coincident with node point locations. Since, $\{\delta d\}$ is arbitrary, eq. (3.46) can be written as

$$[M]\{\ddot{d}\}+[C]\{\dot{d}\}+[K]\{d\}=\{F_d\} \tag{3.47}$$

where the element mass, damping and stiffness matrices are defined as

$$\left.\begin{aligned}[M] &= \int_{\Omega_e} [N_d]^T \rho_d [N_d] d\Omega \\ [C] &= \int_{\Omega_e} [N_d]^T k_d [N_d] d\Omega \\ [K] &= \int_{\Omega_e} [B_0]^T [D][B_0] d\Omega \end{aligned}\right\} \quad (3.48)$$

The external load vector is defined as

$$\{F_d\} = \int_{\Omega_e} [N_d]^T \{F\} d\Omega + \int_{\Gamma_e} [N_d]^T \{\Phi\} d\Gamma + \sum_{i=1}^{n_c} \{F_c\}_i \quad (3.49)$$

For plane strain formulation, considering b as the dimension along the longitudinal direction of the structural element, the stiffness and mass matrix may be written as

$$\left.\begin{aligned}[K] &= b \int_A \int [B_0]^T [D][B_0] dx dy \\ [M] &= b \int_A \int [N_d]^T \rho_d [N_d] dx dy \end{aligned}\right\} \quad (3.50)$$

The elemental area in Cartesian coordinates may be expressed in terms of natural coordinate as

$$dx\,dy = |J|\, d\xi\, d\eta \quad (3.51)$$

The area integral is computed using Gauss quadrature technique.

Damping in a continuous structure like a concrete dam is generally due to mechanisms such as hysterisis in the material. Due to computational difficulty in incorporating this mechanism in equations of structural dynamics, the actual damping mechanism is approximated by viscous damping (Cook et al. 1989). In computational analyses damping can be determined either by phenomenological or spectral damping methods. In the phenomenological approach, the actual physical dissipative mechanism is modelled in details. In the spectral method, viscous damping is introduced as a specified fraction of critical damping. This specific fraction may be determined from (i) experimental observations of vibratory response of the structure; (ii) as a function of frequency; or (iii) a single damping fraction for entire frequency range of a structure.

In the present analysis, a popular spectral damping scheme called Rayleigh or proportional damping scheme is adopted. Here, the damping matrix [C] is formed as a linear combination of the stiffness and mass matrices as

$$[C] = \alpha'[K] + \beta'[M] \tag{3.52}$$

where α' and β' are the stiffness and mass proportional damping constants respectively. The relationship between the fraction of critical damping ratio, ξ', α' and β' at frequency ω is given by

$$\xi' = \frac{1}{2}\left(\alpha'\omega + \frac{\beta'}{\omega}\right) \tag{3.53}$$

Damping constants α' and β' are determined by choosing the fractions of critical damping (ξ_1' and ξ_2') at two different frequencies (ω_1 and ω_2) and solving simultaneously as follows

$$\left.\begin{aligned} \alpha' &= 2\left(\xi_2'\omega_2 - \xi_1'\omega_1\right)\left(\omega_2^2 - \omega_1^2\right) \\ \beta' &= 2\omega_1\omega_2\left(\xi_1'\omega_2 - \xi_2'\omega_1\right)\left(\omega_2^2 - \omega_1^2\right) \end{aligned}\right\} \tag{3.54}$$

3.2.7 Computation of Stresses

In a general finite element analysis, once the nodal displacements of an element are known, the stresses $\{\sigma\}$ can be calculated as

$$\{\sigma_e\} = [D][B_0]\{d_e\} \tag{3.55}$$

where $[D]$ is the constitutive matrix, $[B_0]$ is the strain displacement matrix, $\{\sigma_e\}$ is the elemental stress vector and $\{d_e\}$ is the elemental displacement vector. While using displacement method in finite element analysis, the stresses are discontinuous between adjacent elements because of the nature of assumed displacement variation. Although, one would like to get the stresses evaluated at the nodal points, they appear to be the worst sampling points (Zienkiewicz and Taylor 1991). Barlow (1976) has shown that for two dimensional isoparametric elements, the 2 × 2 Gauss points are the optimal sampling points. The 'local stress smoothing' is a technique that can be used to extrapolate stresses computed at Gauss points to nodal points (Hinton and Campbell 1974).

The stresses are computed at four Gauss points (I, II, III and IV) of an element as shown in Fig. 3.4. For example, at point III, $r = s = 1$ and $\xi = \eta = 1/\sqrt{3}$. Therefore the factor of proportionality is $\sqrt{3}$; *i.e.*,

$$r = \xi\sqrt{3} \text{ and } s = \eta\sqrt{3} \tag{3.56}$$

Stresses at any point P in the element are found by the usual shape function as

$$\sigma_P = \sum N'_{di}\sigma_i \quad \text{for } i = 1,2,3,4 \tag{3.57}$$

In the above equation, σ_P is σ_x, σ_y and τ_{xy} at point P. N'_{di} are the bilinear shape functions written in terms of r and s rather than ξ and η as

$$N'_{di} = \frac{1}{4}(1 \pm r)(1 \pm s) \tag{3.58}$$

N'_{di} are evaluated at r and s coordinates of point P. Let the point P coincides with the corner 1. To calculate stress σ_{x1} at corner 1 from σ_x values at the four Gauss points, substitution of r and s into the shape functions will give

$$\sigma_{xI} = 1.8666\sigma_{xI} - 0.500\sigma_{xII} + 0.134\sigma_{xIII} - 0.500\sigma_{xIV} \tag{3.59}$$

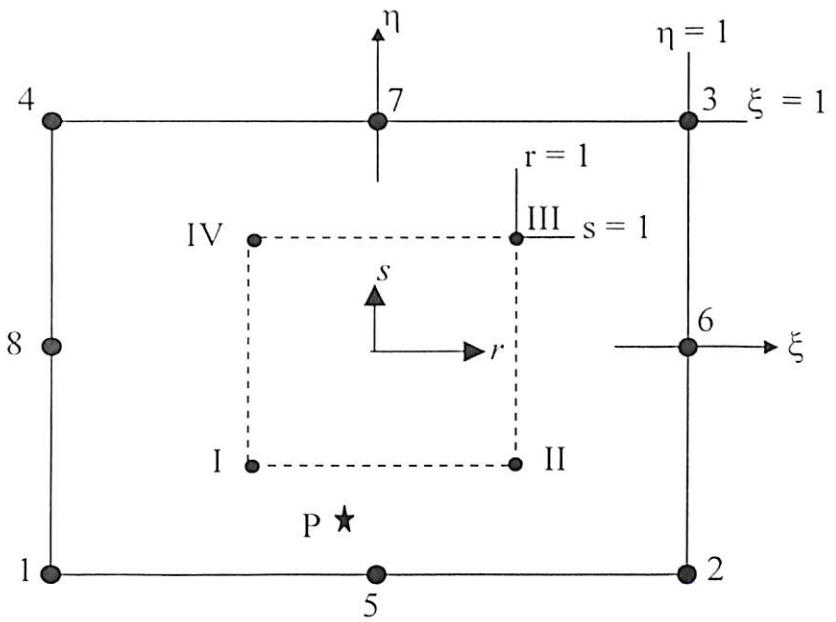

Fig. 3.4 Natural coordinate systems used in extrapolation of stresses from Gauss points

The resultant extrapolation matrix thus obtained may be written as

$$\begin{bmatrix}\sigma_1\\ \sigma_2\\ \sigma_3\\ \sigma_4\\ \sigma_5\\ \sigma_6\\ \sigma_7\\ \sigma_8\end{bmatrix} = \begin{bmatrix} (1+\sqrt{3}/2) & -0.5 & (1-\sqrt{3}/2) & -0.5 \\ -0.5 & (1+\sqrt{3}/2) & -0.5 & (1-\sqrt{3}/2) \\ (1-\sqrt{3}/2) & -0.5 & (1+\sqrt{3}/2) & -0.5 \\ -0.5 & (1-\sqrt{3}/2) & -0.5 & (1+\sqrt{3}/2) \\ (1+\sqrt{3})/4 & (1+\sqrt{3})/4 & (1-\sqrt{3})/4 & (1-\sqrt{3})/4 \\ (1-\sqrt{3})/4 & (1+\sqrt{3})/4 & (1+\sqrt{3})/4 & (1-\sqrt{3})/4 \\ (1-\sqrt{3})/4 & (1-\sqrt{3})/4 & (1+\sqrt{3})/4 & (1+\sqrt{3})/4 \\ (1+\sqrt{3})/4 & (1-\sqrt{3})/4 & (1-\sqrt{3})/4 & (1+\sqrt{3})/4 \end{bmatrix} \begin{Bmatrix}\sigma_I\\ \sigma_{II}\\ \sigma_{III}\\ \sigma_{IV}\end{Bmatrix} \tag{3.60}$$

Here, σ_1, σ_2 ..... σ_8 are the smoothened nodal values and $\sigma_I \ldots \sigma_{IV}$ are the stresses at the Gauss points. The smoothened stress resultants are then modified by finding the average of resultants of all elements meeting at a common node.

PART – B

3.3 THEORETICAL FORMULATION FOR RESERVOIR

The water in the reservoir is considered as non-viscous, linearly compressible and is of small amplitudes of motion. The reservoir water is modelled by finite element technique considering pressure as nodal degrees of freedom.

3.3.1 Governing Equation for Water

The motion of a viscous, Newtonian fluid in two-dimension may be expressed by the Navier-Stokes equation as:

$$\dot{V}_i + V_j V_{i,j} + \frac{1}{\rho_f} p_{,i} - \nu V_{i,jj} = f_i \tag{3.61}$$

where V_i are the velocity components, p is the hydrodynamic pressure, ρ_f is the mass density of fluid and ν is the kinematic viscosity. Considering the fluid as inviscid and neglecting nonlinear convective term for small amplitude of vibration and the body forces, the simplified form of eq. (3.61) is

$$\rho_f \dot{V}_i + p_{,i} = 0 \tag{3.62}$$

The continuity equation of the fluid can be expressed as

$$\rho_f c^2 V_{k,k} + \dot{p} = 0 \tag{3.63}$$

where c is the acoustic wave speed in water. In the above expression, velocity and pressure are the variables that describe the behavior of fluid. Eqs. (3.62) and (3.63) are combined to obtain a single variable formulation for the fluid. To obtain an equation to determine the magnitude of hydrodynamic pressure generated due to small amplitude vibration of compressible but non-viscous water, the following steps are performed. Eq. (3.63) is differentiated with respect to the time variable t and eq. (3.62) with respect to x_i and the resulting equations are subtracted to yield the wave equation for a two-

dimensional reservoir. This equation is generally referred to as the Helmholtz wave equation and can be expressed as

$$\nabla^2 p(x,y,t) = \frac{1}{c^2}\ddot{p}(x,y,t) \tag{3.64}$$

Here $p(x,y,t)$ is hydrodynamic pressure, x and y are space variables. For incompressible fluid c becomes infinitely large. Hence for incompressible fluid, eq. (3.64) can be written as

$$\nabla^2 p(x,y,t) = 0 \tag{3.65}$$

3.3.2 Boundary Conditions

Boundary conditions of the reservoir are shown in Fig. 3.5. The origin of the horizontal x-axis and vertical y-axis is considered at the bottom of the dam-reservoir interface and accordingly the boundary conditions have been defined.

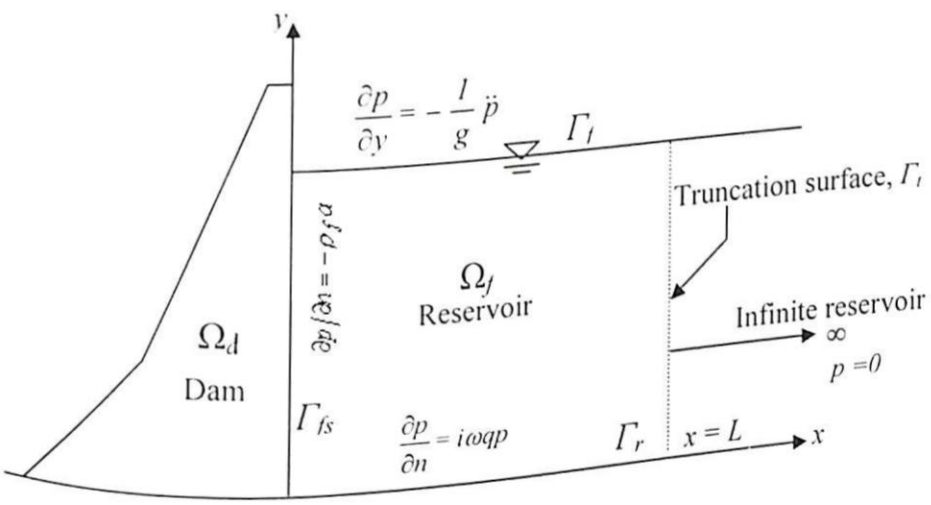

Fig. 3.5 Reservoir and its boundary conditions

(i) At the free surface (Γ_f)

Neglecting the effects of surface waves of the water, the boundary condition of the free surface may be expressed as

$$p(x, H_f, t) = 0 \tag{3.66}$$

Here, H_f is the depth of the reservoir. If the effects of surface waves of the water are considered, the boundary condition of the free surface is more elaborate and may be included. This can be approximated by assuming the actual surface to be at an elevation η relative to the mean surface. Hence,

$$p = \rho_f g \eta_y \tag{3.67}$$

where g is the gravitational acceleration. Differentiating eq.(3.67) twice with respect to time leads

$$\ddot{\eta}_y = \frac{1}{\rho_f g} \ddot{p} \tag{3.68}$$

Considering the y-axis in the vertical direction, eq. (3.62) may be written as

$$\frac{\partial p}{\partial y} + \rho_f \dot{V}_y = \frac{\partial p}{\partial y} + \rho_f \ddot{\eta}_y = 0 \tag{3.69}$$

Combination of eq.(3.68) and (3.69) leads to the following linearised free surface condition

$$\frac{1}{g} \ddot{p} + \frac{\partial p}{\partial y} = 0 \tag{3.70}$$

(ii) At the dam-reservoir interface (Γ_{fs})

At the dam-reservoir interface, the pressures should satisfy

$$\frac{\partial p}{\partial n}(0, y, t) = \rho_f a e^{i\omega t} \tag{3.71}$$

where $ae^{i\omega t}$ is the horizontal component of the ground acceleration in which, ω is the circular frequency of vibration and $i = \sqrt{-1}$, n is the outwardly directed normal to the elemental surface along the interface. In case of vertical dam-reservoir interface $\partial p/\partial n$ may be written as $\partial p/\partial x$ as both will represent normal to the element surface. For an inclined dam-reservoir interface $\partial p/\partial x$ cannot represent the normal to the element surface. Therefore, to generalize the expressions $\partial p/\partial n$ is used in eq. (3.71).

(iii) At the reservoir bed interface (Γ_r)

At the interface between the reservoir and the elastic foundation below the reservoir, the accelerations cannot be specified as rigid foundation case because they depend on the interaction between the reservoir and the foundation. The accelerations are therefore composed of free field acceleration part and an interaction part. When a pressure wave traveling in fluid strikes an elastic but stationary foundation medium, the incident pressure wave is partially reflected since a part of it refracts into the foundation. The absorption of pressure waves at the bottom of the reservoir is modelled by using the technique proposed by Hall & Chopra (1982). Here the reservoir and the reservoir

bottom are modelled as one-dimensional system, since the absorptive effect due to the presence of sediment layers do not vary along x-direction. Thus the pressures in the reservoir and displacements in the foundation medium is given by $p(y,t)$ and $u_f(y,t)$ respectively. The excitation may be provided by an incident displacement wave travelling upward through foundation medium. The one-dimensional pressure equation may be obtained from eq.(3.64) as:

$$\frac{d^2 p}{dy^2} = \frac{1}{c^2}\ddot{p} \tag{3.72}$$

Considering the reservoir bed interface (i.e., at $y = 0$), the accelerating boundary condition due to vertical acceleration can be expressed (eq. 3.62) as

$$\frac{dp}{dy}(0,t) = -\rho_f \ddot{u}_f(0,t) \tag{3.73}$$

If $u_f = u_{f0}\, e^{-i\omega t}$, in the above equation, $\ddot{u}_f(0,t) = \omega^2 u_f(0,t)$, where ω is the excitation frequency Thus, eq. (3.73) can be written as

$$\frac{dp}{dy}(0,t) = -\rho_f \omega^2 u_f(0,t) \tag{3.74}$$

The displacements within the sediment layer having compressional wave velocity c_s are also governed by the one-dimensional wave equation:

$$\frac{d^2 u_f}{dy^2} = \frac{1}{c_s^2}\frac{d^2 u_f}{dt^2} \tag{3.75}$$

The general solution of eq.(3.75) is

$$u(y,t) = C_1 e^{iky} + C_2 e^{-iky} \tag{3.76}$$

Here, $k = \omega/c_s$, C_1 is the unknown amplitude of the reflected displacement wave C_2 is the specified incident wave. For a fully reflective surface at the reservoir bed i.e., at $y = 0$, $C_1 = C_2$. If a' is the free-field acceleration in a direction normal to the reservoir bed, the amplitude of the incident wave can be obtained (Hall & Chopra 1982) as

$$C_2 = -\frac{1}{2\omega^2}a' \tag{3.77}$$

The value of C_1 can be evaluated by equating the pressure in the reservoir at the reservoir bed interface and the normal foundation stress at the reservoir bed surface (Hall & Chopra 1982),

$$p(0,t) = -E_s \frac{du_f}{dy}(0,t) \tag{3.78}$$

where E_s is the elastic modulus of the foundation medium consisting of sediment layer and is given as

$$E_s = \rho_s c_s^2 \tag{3.79}$$

Substituting eqs. (3.76), (3.77) and (3.79) in eq. (3.78) yields solution for C_1 as

$$C_1 = -\frac{1}{2\omega^2} a' + \frac{i}{\omega \rho_s c_s} p(0,t) \tag{3.80}$$

Substituting eqs. (3.76), (3.77) and (3.80) in eq.(3.74) yields the boundary condition at the reservoir bottom interface, which may be expressed as:

$$\frac{\partial p}{\partial n}(x,0,t) = -\rho_f a' + i\omega q p(x,0,t) \tag{3.81}$$

Here, the first term on the right hand side of the equation, $\rho_f a' = 0$, when only horizontal excitation is considered. In eq. (3.81), n is the outwardly directed normal to the elemental surface along the interface. In case of a horizontal reservoir bed interface $\partial p/\partial n$ may be written as $\partial p/\partial y$. For an inclined reservoir bed interface, $\partial p/\partial y$ cannot represent the normal to the element surface. Therefore, to generalize the expressions $\partial p/\partial n$ is used in eq. (3.81). The coefficient q is given by Hall & Chopra (1982) as

$$q = \frac{\rho}{\rho_s c_s} = \frac{1}{c}\left(\frac{1-\alpha}{1+\alpha}\right) \tag{3.82}$$

The frequency independent reflection coefficient, α as in the above equation can be evaluated as

$$\alpha = \frac{1 - \frac{\rho c}{\rho_s c_s}}{1 + \frac{\rho c}{\rho_s c_s}} \tag{3.83}$$

Here, ρ_s is the mass density of sediment. While considering the effect of sediment layers, the equivalent reflection coefficient (α) can be determined for sediment layers of thickness d_{s1} and d_{s2} and reflection coefficients α_1 and α_2 respectively as

$$\alpha = \frac{(\alpha_1 d_{s1} + \alpha_2 d_{s2})}{(d_{s1} + d_{s2})} \tag{3.84}$$

A more realistic value of frequency dependent reflection coefficient can be obtained by considering a layer of single-phase visco-elastic sediment layer of height d_s

over a rigid rock (Chuhan et al. 2001). The complex frequency dependent reflection coefficient, $B_{\omega 1}$ can be determined from the following equations given in matrix form as:

$$\begin{bmatrix} 1 & -iE_1k_1 & iE_1k_1 & 0 \\ ik & -\rho_f\omega^2 & -\rho_f\omega^2 & 0 \\ 0 & e^{-ik1ds} & e^{ik1ds} & -e^{-ik2ds} \\ 0 & -E_1k_1e^{-ik1ds} & E_1k_1e^{ik1ds} & E_2k_2e^{-ik2ds} \end{bmatrix} \times \begin{bmatrix} B_{\omega 1} \\ A_1 \\ B_{\omega 2} \\ A_2 \end{bmatrix} = \begin{bmatrix} -1 \\ ik \\ 0 \\ 0 \end{bmatrix} \tag{3.85}$$

In eq. (3.85) E_1 and E_2 are elastic modulus; k_1 and k_2 are wave numbers in sediment and rock respectively. A_1, A_2 and $B_{\omega 2}$ are constants obtained from the solution of one-dimensional wave equation. The detailed derivation can be found in the reference (Chuhan et al. 2001).

(iv) At the truncation boundary (Γ_t)

The specification of the far boundary condition is one of the most important features in the FE analysis of a semi-infinite or infinite reservoir. This is due to the fact that the developed hydrodynamic pressure, which affects the response of the structure, is dependent on the truncation boundary condition. Application of Sommerfeld radiation condition (Zeinkiwicz and Newton 1969) at the truncation boundary leads to

$$\frac{\partial p}{\partial x}(L, y, t) = 0 \tag{3.86}$$

L represents the distance between the structure and the truncation boundary. Incorporating the effect of reservoir bottom absorption, Sharan (1992) has incorporated the following condition.

$$\frac{\partial p}{\partial x}(L, y, t) = -\frac{\zeta}{H_f} p(L, y, t) \tag{3.87}$$

Here, ζ is a complex damping parameter imposed at the truncation boundary. The value of ζ as given by Sharan (1992) is

$$\zeta = \sqrt{\beta_1^2 - \Omega_s^2} \tag{3.88}$$

where $\Omega_s = \omega H_f / c$ and β_1 is the first complex root of solution of the wave equation (eq.3.64). The main drawback of the above condition is that it does not produce reasonably accurate results at second and third cutoff frequencies.

3.3.3 Proposed Truncation Boundary Condition (TBC)

The proposed condition along the truncation surface for the linearly compressible fluid domain is derived from the wave equation. The general solution of eq.(3.64) satisfying eqs. (3.70), (3.71), (3.81) and the radiation condition, can be solved by method of separation of variables (Bouaanani et al. 2003) to obtain pressure at any point *(x, y)* as

$$p(x,y,t) = -2\rho\, a\, H_f \sum_{m=1}^{\infty} \frac{\lambda_m^2 I_m}{\beta_m k_m} e^{(-k_m x)} (\Psi_m) e^{i\omega t} \tag{3.89}$$

where, a is the applied acceleration at the fluid-structure interface in the normal direction and

$$I_m = \frac{1}{H_f} \int_0^{H_f} \Psi_m dy \tag{3.90-a}$$

$$\Psi_m = \frac{1}{2\lambda_m} \left[(\lambda_m + \omega q) e^{i\lambda_m y} + (\lambda_m - \omega q) e^{-i\lambda_m y} \right] \tag{3.90-b}$$

$$\lambda_m^2 = \left(\frac{(2m-1)\pi}{2H_f} \right)^2 + i2\omega q / H_f \tag{3.90-c}$$

$$k_m = \sqrt{\lambda_m^2 - \Omega'^2} \tag{3.90-d}$$

$$\beta_m = \left(\lambda_m^2 - \omega^2 q^2 \right) \left(H - \frac{\chi}{\lambda_m^2 + \chi^2} \right) + i\omega q \tag{3.90-e}$$

$$\Omega' = \omega / c \tag{3.90-f}$$

$$\chi = \frac{\omega^2}{g} \tag{3.90-g}$$

The value of χ can be considered to be zero if the effect of gravity waves is neglected. For a rigid reservoir bottom, $q = 0.0$ and $\alpha = 1.0$, for which the pressure obtained is real valued. Generally, determination of the eigenvalues λ_m requires use of advanced programming techniques or specialized finite element program like Earthquake Analysis of Concrete Gravity Dams, EAGD (Fenves and Chopra, 1984). Here, an alternative strategy (Bouaanani et al. 2003) have been used to determine approximate values of λ_m. Differentiating the hydrodynamic pressure in eq. (3.89) with respect to x, one may arrive in the following expression:

$$\frac{\partial p}{\partial x}(x,y,t) = 2\rho\, a\, H \sum_{m=1}^{\infty} \frac{\lambda_m^2 I_m}{\beta_m} e^{(-k_m x)} (\Psi_m) e^{i\omega t} \tag{3.91}$$

To obtain a finite model of the infinite reservoir, it is truncated at a surface, where the normal pressure gradient may be expressed from eqs. (3.89) and (3.91) as:

$$\frac{\partial p}{\partial n} = \frac{\partial p}{\partial x} = \zeta_m \dot{p} \tag{3.92}$$

where ζ_m is obtained as follows:

$$\zeta_m = -\frac{i \sum_{m=1}^{\infty} \lambda_m^2 I_m e^{(-k_m x)} (\Psi_m)}{\Omega' c \sum_{m=1}^{\infty} \frac{\lambda_m^2 I_m}{\beta_m k_m} e^{(-k_m x)} (\Psi_m)} \tag{3.93}$$

The condition at the truncated boundary of the fluid domain considering the effect of non-reflective waves can be obtained from the plane wave equation (Zienkiewicz and Newton 1969) and can be expressed as

$$\frac{\partial p}{\partial n} = -\frac{1}{c} \dot{p} \tag{3.94}$$

To obtain a finite model of the infinite reservoir from the analytical solution and to incorporate the effects of non-reflecting wave at the truncation surface the eqs. (3.92) and (3.94) are combined, which gives the resulting relationship for $\partial p/\partial n$ at the truncation boundary as follows:

$$\frac{\partial p}{\partial n} = \left(\zeta_m - \frac{1}{c} \right) \dot{p} \tag{3.95}$$

The Helmholtz equation (eq. 3.64) can be solved (Chakrabarti & Chopra 1973) to obtain hydrodynamic pressure at the upstream face of the dam due to vertical ground acceleration, a' as

$$p = \frac{\rho_f c a'}{\omega} \frac{\sin \omega \left(\frac{H_f - y}{c} \right)}{\cos \left(\frac{\omega H_f}{c} \right) + iqc_f \sin \left(\frac{\omega H_f}{c} \right)} e^{i\omega t} \tag{3.96}$$

3.3.4 Finite Element Implementation

By the use of Galerkin process, and assuming pressure to be the nodal unknown the discretized form of eq. (3.64) may be written in two-dimension as

$$\int_{\Omega} N_{rj} \left[\nabla^2 \sum N_{ri} p_i - \frac{1}{c^2} \sum N_{ri} p_i \right] d\Omega = 0 \tag{3.97}$$

where N_{rj} is the interpolation function for the reservoir and Ω is the region under consideration. Using Green's theorem eq. (3.97) may be transformed to

$$-\int_{\Omega}\left[\frac{\partial N_{rj}}{\partial x}\sum\frac{\partial N_{ri}}{\partial x}p_i+\frac{\partial N_{rj}}{\partial y}\sum\frac{\partial N_{ri}}{\partial y}p_i\right]d\Omega$$
$$-\frac{1}{c^2}\int_{\Omega}N_{rj}\sum N_{ri}\,d\Omega\;\ddot{p}_i+\int_{\Gamma}N_{rj}\sum\frac{\partial N_{rj}}{\partial n}d\Gamma\;p_i=0 \qquad (3.98)$$

in which i varies from 1 to total number of nodes and Γ represents the boundaries of the fluid domain. The last term of the above equation may be written as

$$\{B\}=\int_{\Gamma}N_{rj}\frac{\partial p}{\partial n}d\Gamma \qquad (3.99)$$

The whole system of eq.(3.98) may be written in a matrix form as

$$[\overline{H}]\{\ddot{p}\}+[\overline{G}]\{p\}=\{B\} \qquad (3.100)$$

in which,

$$\left.\begin{aligned}[\overline{H}]&=\frac{1}{c^2}\sum\int_{\Omega}[N_r]^T[N_r]d\Omega\\ [\overline{G}]&=\sum\int_{\Omega}\left[\frac{\partial}{\partial x}[N_r]^T\frac{\partial}{\partial x}[N_r]+\frac{\partial}{\partial y}[N_r]^T\frac{\partial}{\partial y}[N_r]\right]d\Omega\\ \{B\}&=\sum\int_{\Gamma}[N_r]^T\frac{\partial p}{\partial n}d\Gamma=\{B_f\}+\{B_{fs}\}+\{B_r\}+\{B_t\}\end{aligned}\right\} \qquad (3.101)$$

Here the subscript f, fs, r and t stand for the free surface, fluid-structure interface, reservoir bottom-fluid interface and truncation surface respectively. According to the boundary conditions for the fluid domain, if linearised surface wave condition is adopted (eq. 3.70), the same may be written in finite element form as

$$\{B_f\}=-\frac{1}{g}[R_f]\{\ddot{p}\} \qquad (3.102)$$

in which,

$$[R_f]=\sum\int_{\Gamma_f}[N_r]^T[N_r]d\Gamma \qquad (3.103)$$

At the fluid-structure interface (eq.3.71), if $\{a\}$ is the vector of nodal accelerations of generalized coordinates, $\{B_{fs}\}$ may be expressed as

$$\{B_{fs}\}=-\rho_f[R_{fs}]\{a\} \qquad (3.104)$$

where,

$$[R_{fs}] = \sum \int_{\Gamma_{fs}} [N_r]^T [T][N_d] d\Gamma \tag{3.105}$$

Here, $[T]$ is the transformation matrix for generalized accelerations of a point on the fluid structure interface and $[N_d]$ is the matrix of shape functions of the dam used to interpolate the generalized acceleration at any point on the fluid-structure interface in terms of generalized nodal accelerations of an element. At the reservoir bed, $\{B_r\}$ may be expressed as

$$\{B_r\} = i\omega q[R_r]\{p\} - \rho_f [R_r]\{a'\} \tag{3.106}$$

where,

$$[R_r] = \sum \int_{\Gamma_r} [N_r]^T [N_r] d\Gamma \tag{3.107}$$

From the condition specified by eq. (3.100) at the truncation boundary, the following expression emerges.

$$\{B_t\} = \left(\zeta_m - \frac{1}{c}\right)[R_t]\{\dot{p}\} \tag{3.108}$$

where,

$$[R_t] = \sum \int_{\Gamma_t} [N_r]^T [N_r] d\Gamma \tag{3.109}$$

Substitution of all terms in eq. (3.100) gives

$$[H]\{\ddot{p}\} + [A]\{\dot{p}\} + [G]\{p\} = \{F_r\} \tag{3.110}$$

Here, $[H]$, $[A]$, $[G]$ and $\{F_r\}$ can be expressed as

$$\left.\begin{aligned} [H] &= [\overline{H}] + \frac{1}{g}[R_f] \\ [A] &= \left(\frac{1}{c} - \zeta_m\right)[R_t] \\ [G] &= [\overline{G}] - i\omega q[R_r] \\ \{F_r\} &= -\rho_f \left(\begin{bmatrix} R_{fs} \end{bmatrix}\{a\} + \begin{bmatrix} R_r \end{bmatrix}\{a'\} \right) \end{aligned}\right\} \tag{3.111}$$

For any prescribed acceleration at the dam-reservoir interface and reservoir bed interface, eq. (3.110) is solved to obtain the hydrodynamic pressure in the reservoir.

3.3.5 Time History Analysis with Frequency Dependent Boundaries

3.3.5.1 Frequency Dependent Boundary Condition

The effect of reservoir bottom absorption is an important parameter that influences the response of a dam-reservoir system during an earthquake. The available literature reveals that the dynamic problem of a dam-reservoir system has been rigorously analyzed in the frequency domain considering the effects of radiation damping and reservoir bottom absorption. Many time-domain models consider radiation damping with standard viscous dampers (Vargas-Loli & Fenves, 1989, El-Aidi & Hall, 1989 and Tsai et al.1990). The effect of reservoir bottom absorption has been accounted for in frequency domain solutions (Sharan 1992, Hatami 1997 and Chuhan et al. 2000) and in time domain solutions (Tsai et al. 1997). The reservoir bottom absorption effect is frequency dependent, which makes it difficult to incorporate in a time-history analysis as the solution procedure cannot account for the frequency content of the seismic excitation at every time instant. In an endeavor to understand the behavior of structural systems due to earthquake excitation various techniques are being developed to account for the frequency dependent parameters (Haigh et al. 2002, Safak 2006) in a time-history analysis. It is evident from the eqs. (3.81) and (3.93) that boundary conditions at the reservoir bottom and truncation surface are sensitive to excitation frequency. Hence, it is important to estimate the frequency content of an earthquake signal at every time step to effectively account for radiation damping and reservoir bottom absorption effect.

3.3.5.2 Short Time Fourier Transform

A Fourier transformation generally breaks down a signal into constituent sinusoids of different frequencies. While transforming a time-based signal to frequency-domain, the time information is lost and it is difficult to obtain the frequency information at a particular time instant. To overcome this deficiency, Gabor (1946) adapted the Fourier transform to analyze only a small section of the signal at a time - a technique called *windowing* the signal. Gabor's adaptation, called the *Short-Time Fourier Transform* (STFT), maps a signal into a two-dimensional function of time and frequency. However, the information obtained by STFT has limited precision, and that precision is determined by the size of the window.

Here, the technique commonly used in digital signal processing called Short Time Fourier Transformation (STFT) has been adopted to determine the frequencies at a time instant. To capture the time variation of the frequency contents of the signal, the signal $S(\tau)$ is multiplied by a sliding window $h(\tau\text{-}t)$, centered at time t, and taking the Fourier transform of the weighted signal. Mathematically,

$$S_t(\omega) = \int S(\tau) h(\tau - t) e^{-i\omega\tau} d\tau \tag{3.112}$$

gives the short time Fourier transform at every window. The spectral density of the modified signal at every time instant, t can be obtained by

$$P(t, \omega) = |S_t(\omega)|^2 \tag{3.113}$$

The instantaneous frequency at time t can be located from the center of the $S_t(\omega)$ by taking its first moment as

$$\omega_t = \frac{\int \omega |S_t(\omega)|^2 d\omega}{\int |S_t(\omega)|^2 d\omega} \tag{3.114}$$

This instantaneous excitation frequency of the earthquake signal so obtained can be incorporated in the boundary conditions at the reservoir-reservoir bed interface and truncation boundary defined by eqs. (3.81) and (3.93) respectively.

3.3.6 Computation of Velocity and Displacement of Fluid

The accelerations of the fluid particles can be calculated from eq.(3.62) after computing the developed hydrodynamic pressure in the reservoir. The velocity of the fluid particle may be calculated from the known values of acceleration at any instant of time using Gill's time integration scheme (Gill 1951), which is a step-by-step integration procedure based on Runge-Kutta method (Ralston & Wilf 1965). This procedure is advantageous over other available methods as (i) it needs less storage registers; (ii) it controls the growth of rounding errors and is usually stable and (iii) it is computationally economical. At any instant of time t, velocity will be

$$V_t = V_{t-\Delta t} + \Delta t \dot{V}_t \tag{3.115}$$

Velocity vectors in the reservoir may be plotted based on velocities computed at the Gauss points of each individual point. Similarly, the displacement of fluid particles in the reservoir, U at every time instant can also computed as

$$U_t = U_{t-\Delta t} + \Delta t V_t \tag{3.116}$$

PART - C

3.4 THEORETICAL FORMULATION FOR DAM-RESERVOIR SYSTEM

In the dam-reservoir interaction problems, the dam and the reservoir do not vibrate as separate systems under external excitations, rather they act together in a coupled way. Therefore, these problems have to be dealt in a coupled way. An iterative scheme is developed in the present study to achieve the coupled effect of dam-reservoir system.

3.4.1 Selection of the Numerical Technique

In most of the formulations developed for finite element analysis, the displacements representation of the structure is standard; but widely different formulations of the fluid are possible considering displacements, pressure, velocity potential or displacement potential as the unknown parameters. Although, formulation using displacement as unknown parameter in fluid leads to a symmetric system, it has two main drawbacks: (i) the degrees of freedom in fluid increase significantly (especially for 3D problems) and (ii) the fluid displacements must satisfy the irrotationality condition, otherwise zero frequency spurious modes may arise. In the formulation, using pressure as unknown parameter, the coupled matrix (Zienkiewicz and Newton 1969) can be obtained from eq. (3.47) and eq.(3.110) as

$$\begin{bmatrix} M & 0 \\ Q^T & H \end{bmatrix} \begin{Bmatrix} \ddot{d} \\ \ddot{p} \end{Bmatrix} + \begin{bmatrix} C & 0 \\ 0 & A \end{bmatrix} \begin{Bmatrix} \dot{d} \\ \dot{p} \end{Bmatrix} + \begin{bmatrix} K & -Q \\ 0 & G \end{bmatrix} \begin{Bmatrix} d \\ p \end{Bmatrix} = \begin{Bmatrix} F_d \\ F_r \end{Bmatrix} \tag{3.117}$$

In the above equation, $\{F_d\}$ and $\{F_r\}$ contain the forcing terms. The coupling term $[Q]$ in equation (3.117) arises due to the acceleration and pressure specified on the fluid-structure interface boundary (Zienkiewicz and Newton 1969) and can be expressed as:

$$[Q] = \int_{\Gamma_{fs}} [N_d]^T \, n [N_r] d\Gamma \tag{3.118}$$

Here n is the direction vector normal to the dam-reservoir interface. The coupled matrices are unsymmetric and therefore their simultaneous solver requires large computer storage and makes the standard use of finite element algorithm difficult. If the system is brought to a symmetric form, either the band structure properties of FEM are lost, leading to significant storage requirements, or the degrees of freedom of the

structure or the fluid are doubled (Morand and Ohayon 1979), or a damping matrix is artificially introduced (Everstine 1981), even if the system possesses no damping properties. Moreover, the computational implementation requires the development of special purpose computer programs, or extensive modifications of existing ones (Combescure et al. 1980). When incompressible fluid is considered, numerical problems may occur in extreme cases (Antoniadis and Kancharos 1988). Finally, in the analysis of the fluid-structure interaction problems in a coupled manner, the resulting coupled matrix becomes large, since degrees of freedom from both the systems are present in the matrices.

In view of the difficulties mentioned above, a systematic approach is followed. The two systems, i.e., the dam and the reservoir are analyzed separately and the interaction effects are enforced by a developed iterative scheme. The system under consideration as shown in Fig. 3.6 consists of a structural domain Ω_d and a fluid domain Ω_f with a common interface Γ_{fs}. Since the reservoir is very large and unbounded, it is necessary to artificially truncate the fluid domain at a boundary Γ_t to have a tractable computational domain. The developed truncation boundary condition is imposed at the truncation boundary Γ_t for the analysis of the coupled fluid-structure systems.

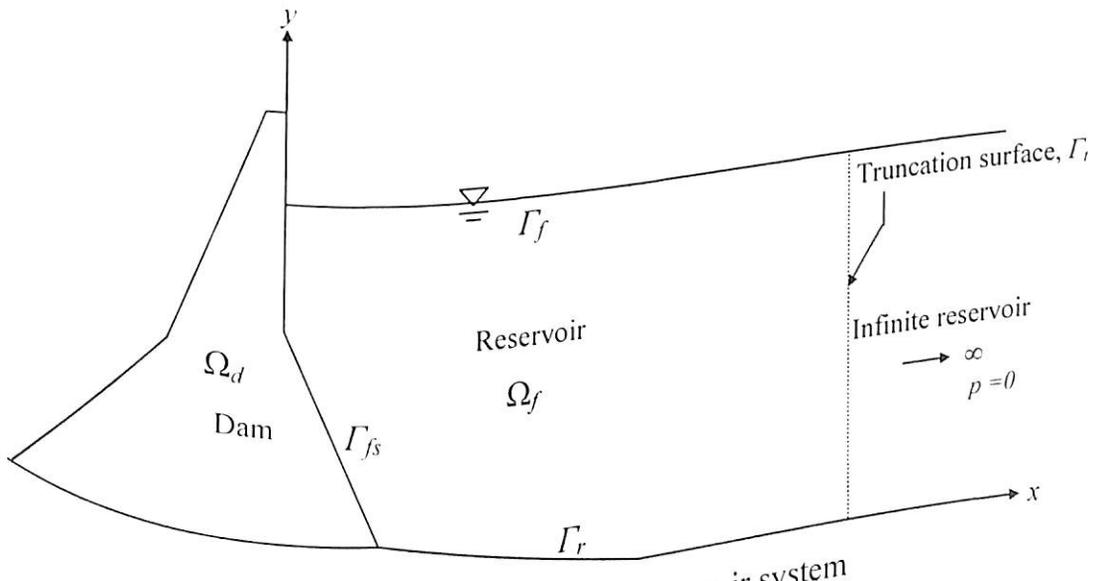

Fig. 3.6 Typical geometry of dam-reservoir system

3.4.2 Iterative Scheme

An efficient iterative scheme is developed for the present analysis to achieve the interaction effect of the coupled dam-reservoir system. Initially, the dam is assumed to be

rigid. The resulting hydrodynamic pressure is evaluated by solving the reservoir domain using eq. (3.110) with appropriate boundary conditions at any instant of time t. However, since the objective is to achieve a solution for an elastic dam-reservoir interaction, the resulting pressure is inaccurate. The developed pressures exert forces $\{F_r\}$on the adjacent dam. Hence, at the same time instant, the concrete dam is analyzed with the forces $\{F_r\}$, developed due to hydrodynamic pressures at the dam-reservoir interface, using the equation

$$[M]\{\ddot{d}\}+[C]\{\dot{d}\}+[K]\{d\}=\{F_d\}+\{F_r\} \tag{3.119}$$

where $\{F_d\}=-[M]a_g$. Due to these additional forces$\{F_r\}$, the dam undergoes a displacement $\{d\}_t$. As a result the dam-reservoir interface boundary changes and hence the solution of the reservoir domain. The reservoir domain is solved again at the same time instant with the changed conditions of displaced structural boundary. Consequently the structural system is also analyzed with the changed forces. Thus at time t, both the hydrodynamic pressure $\{p\}_t$ and the structural displacement $\{d\}_t$ are iterated simultaneously till a desired level of convergence is achieved. Thus, the iteration process is carried out till the conditions prescribed below are satisfied simultaneously

$$\left|\frac{\{p_{i+1}\}_t - \{p_i\}_t}{\{p_i\}_t}\right| \le \varepsilon'', \text{ and } \left|\frac{\{d_{i+1}\}_t - \{d_i\}_t}{\{d_i\}_t}\right| \le \varepsilon'' \tag{3.120}$$

i being the number of iteration. ε'' is a small preassigned tolerance value. The most costly operation involved in the above algorithm is to successively solve two linear equation systems at each iteration. But in the present case, matrices involved in the solution of the system equations are decomposed into triangular forms at the beginning of the iteration, and thereby only two forward-eliminations and back-substitutions are required at each iteration step. Thus, the time required to obtain the coupled response for a particular time instant is minimized in the present iterative scheme.

3.4.4 Flow Chart for the Analysis of Ageing Dam-Reservoir System

For an efficient and accurate analysis of the behavior of dam-reservoir coupled system, the steps to be followed are summarized in the form of flow chart given in Charts 3.1 – 3.4.

Chart 3.1 Flow chart for dynamic analysis of aged dam-reservoir system

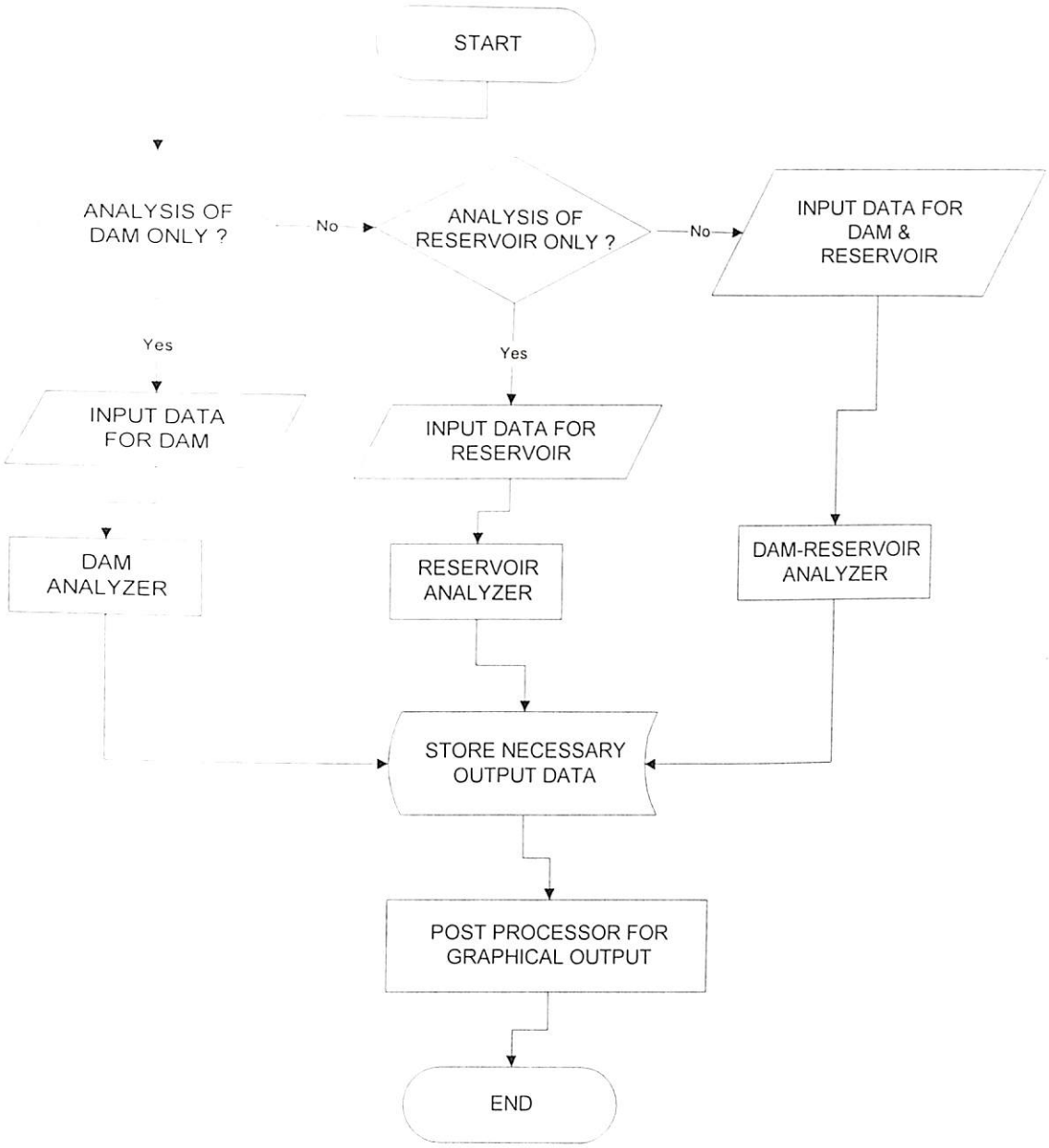

Chart 3.2 Flow chart for dam analyzer

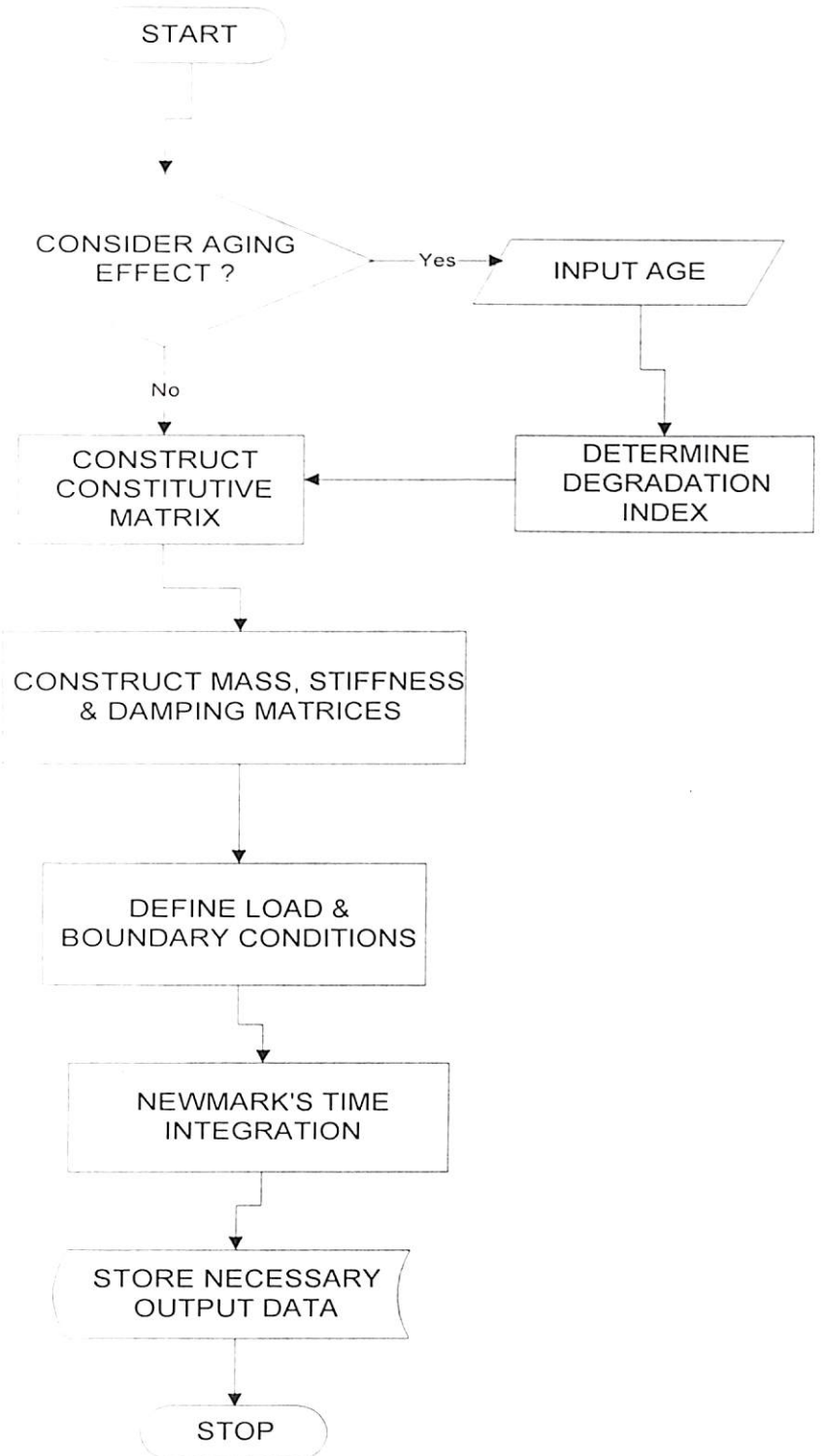

Chart 3.3 Flow chart for reservoir analyzer

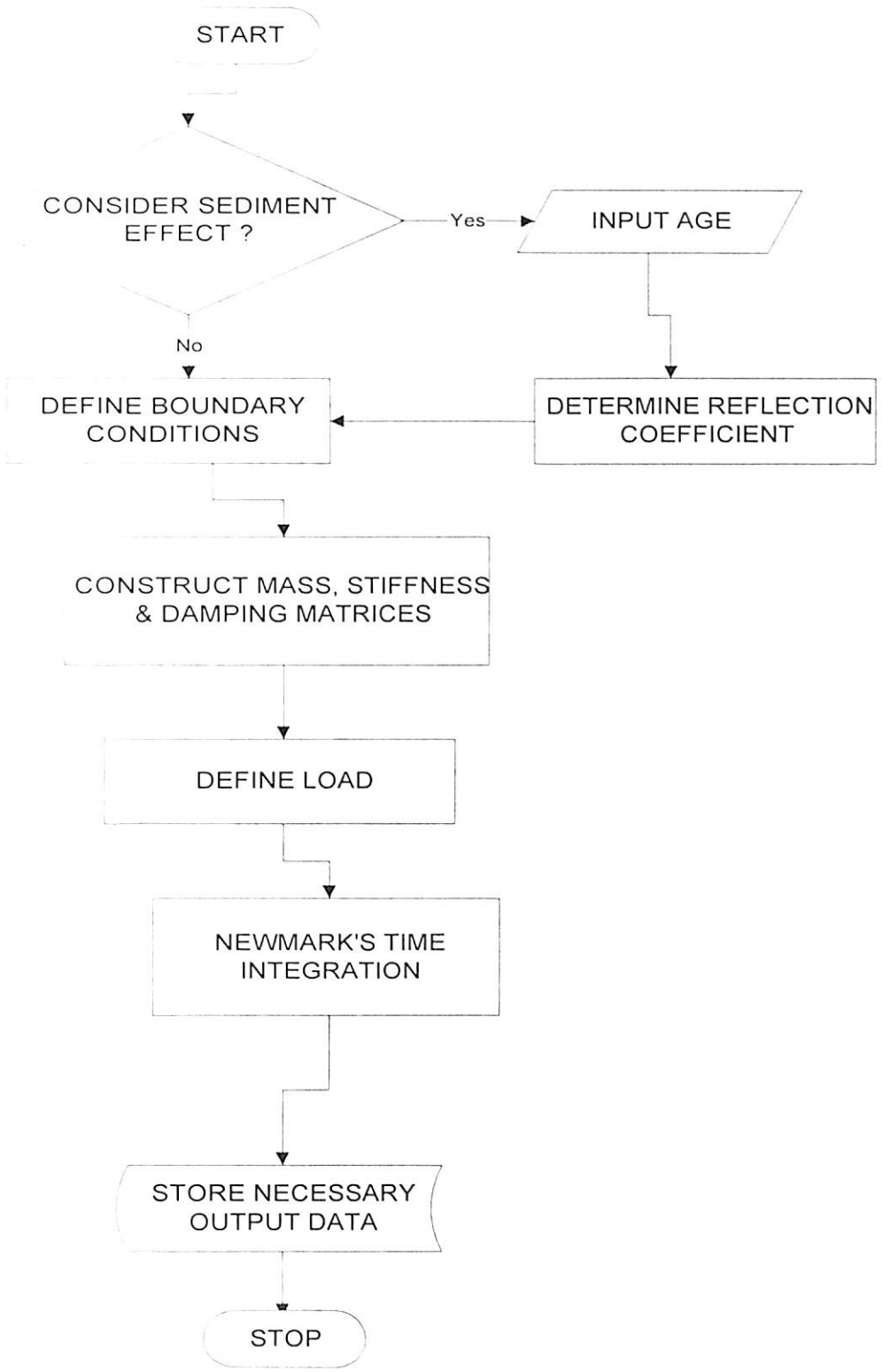

Chart 3.4 Flow chart for dam-reservoir analyzer

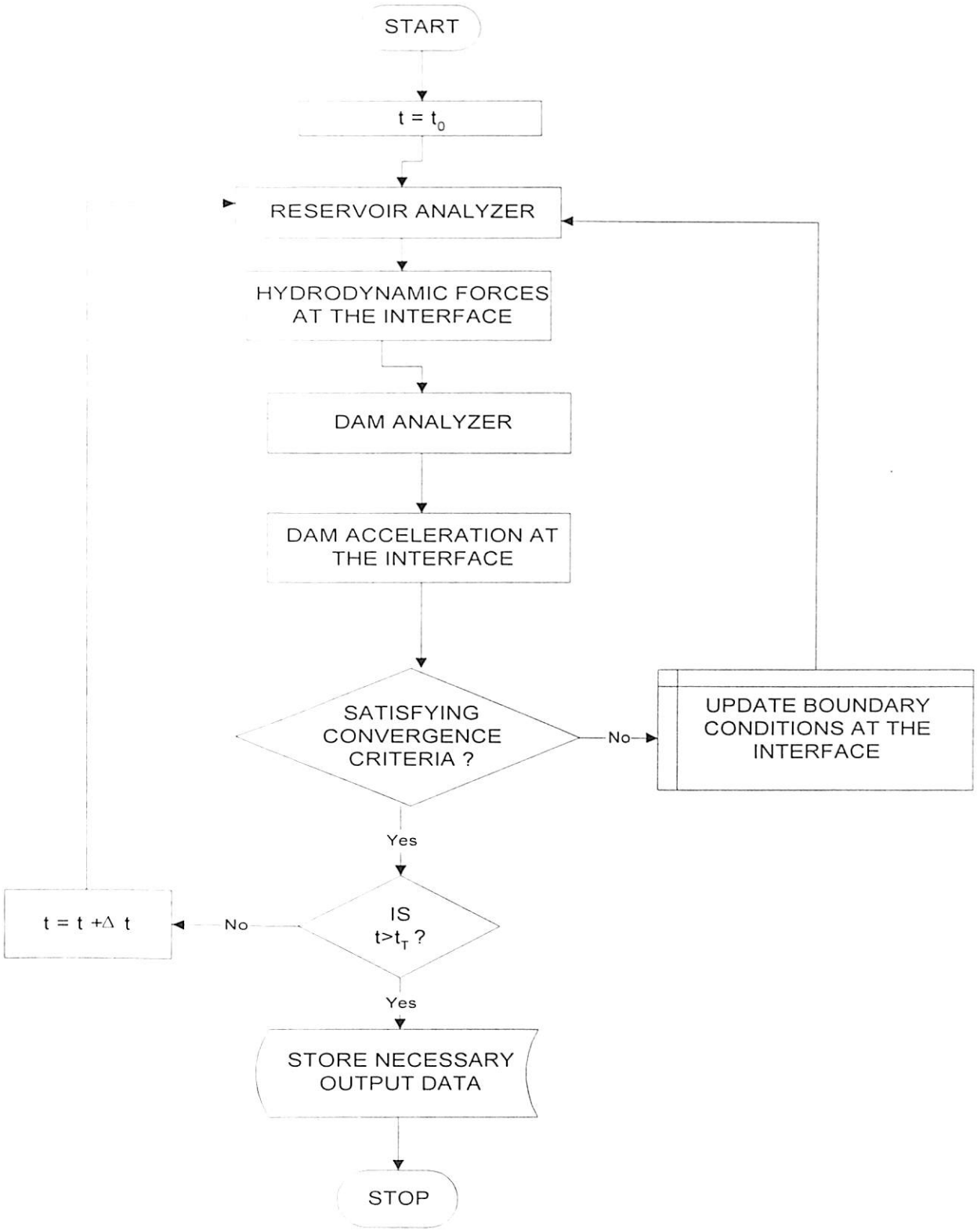

CHAPTER 4

NUMERICAL RESULTS AND DISCUSSIONS

In the present work, a technique to estimate the seismic response of an ageing concrete dam in the vicinity of a reservoir is developed. This approach includes the time dependent degradation of concrete owing to environmental factors and mechanical loading in terms of isotropic degradation index. To predict the dynamic behavior of an ageing concrete dam adjacent to an unbounded reservoir by the proposed algorithm, a set of computer codes have been developed. The self weight of the dam has not been included in the analysis deliberately to identify the other effects such as degradation of dam material, dam-reservoir interaction, absorption of reservoir bed etc under external excitations. A benchmark problem employing such a numerical algorithm for seismic analysis of an ageing concrete dam adjacent to infinite reservoir considering fluid-structure interaction does not exist in the available literature. Therefore, for the validation and critical evaluation of the computer codes developed in the present investigation as described in the formulation, different benchmark problems are solved separately for each part. The developed codes are used for the evaluation of hydrodynamic pressure in the reservoir and the stress distribution in the dam considering dam-reservoir interaction.

The problems are categorized in three different parts. The first part deals with the response of the concrete dam only, where a comparison of the response of the dam with and without ageing effect is presented. The second part consists of results and discussions on the effectiveness of the developed truncation boundary condition in the unbounded reservoir considering the presence of sediment layers. The results obtained by taking into account the frequency content of earthquake excitation are also another important component of this part. The response of the reservoir and the dam considering dam-reservoir interaction effects are presented in the third part.

PART – I

4.1 ANALYSIS OF DAM

The scope of the present investigation is to determine the effect of ageing on the seismic response of the dam. A parameter called degradation index is introduced, that varies from 0 to 1 with age and various other environmental and loading parameters that can cause concrete degradation. With an increase in age, the constitutive matrix used in determining the change in response of the dam is modified. The problem related to the dynamic response of the dam with and without degradation in the absence of the reservoir is discussed here.

4.1.1 Discretization of the Dam

In general, computed results in finite element method are rarely exact. This is because while representing a mathematical continuum by finite elements, the grading of the mesh, the number, type and the shape of the elements selected affect the accuracy of the solution. The approximation inherent in the procedure results in discretization error. This error can be minimized at the cost on increased computer time and cost which may not yield an optimized solution. In the present work, the structure *i.e.*, the dam is solved using plane strain formulation discretizing the domain with eight-noded isoparametric quadratic elements. Therefore, a solution with maximum accuracy and minimum discretization error is sought by selecting an economic number of divisions. Satisfactory solution may be arrived at either by (i) selecting the required number of subdivisions of the continuum from past experience or (ii) if an analysis is attempted for the first time, the convergence can be tested based on varied mesh grading and thereafter making a suitable choice.

To check the convergence of horizontal displacement at the crest of the structure obtained for various mesh grading, a simplified section of the Koyna dam has been chosen for the extensive analysis using finite element technique. The upstream face of the dam is assumed to be straight and vertical which is slightly different from the real configuration (Chopra & Chakrabarti 1972). The slope on the downstream face above the neck of the dam is also neglected in the present analysis. The dimension and the material

properties of the dam in the present case are: height of the dam = 103 m; width at the top of the dam is 14.8 m and at the base is 70.0 m, modulus of elasticity = 31500 MPa; Poisson's ratio = 0.235 and mass density = 2415.816 kg/m^3. Structural damping is considered as 3%. The dam is discretized with 8-noded quadratic elements as shown in Fig. 4.1 and is analyzed using plain strain formulation. A concentrated horizontal load of 1000 kN is applied at the crest of the structure. The structure is discretized with different number of meshes and the convergences of results for the natural frequencies and the crest displacements obtained for different discretisations are presented in Table 4.1. It is observed from the results that the solution converges sufficiently for a discretization of 5 × 3.

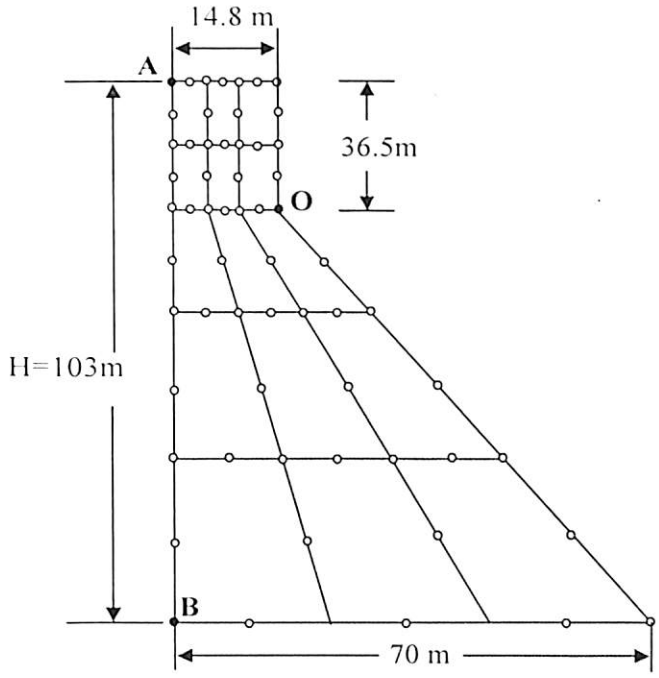

Fig. 4.1 Geometry and finite element discretization of Koyna dam

4.1.2 Selection of Time Step (Δt)

In order to choose a time step for the dynamic analysis of the dam, the example in Section 4.1.1 is considered with the same geometry and material parameters. Ramp acceleration of unit magnitude is applied at the dam base. The Newmark's average acceleration which is unconditionally stable is adopted for the present solution. A study is carried out with different time steps to obtain a convergent value of a particular

response in the present analysis. The initial time step Δt is chosen as the $1/100^{th}$ of the fundamental period. Time histories of horizontal displacements at the top of the structure subjected to ramp acceleration for different time steps are shown in Fig.4.2. From the results it is observed that a time step of 0.01 second may be considered, at which sufficient level of convergence is obtained.

Table 4.1 Convergence of natural frequency and horizontal crest displacement of Koyna dam

$N_v \times N_h$	Natural Frequency (rad/sec)		Crest Displacement (mm)
	Mode 1	Mode 2	
5 × 2	16.916	43.198	6.2
5 × 3	16.495	42.885	6.5
5 × 4	16.477	42.629	6.5
10 × 2	16.488	42.793	6.4
10 × 3	16.458	42.682	6.5
10 × 4	16.442	42.603	6.5
20 × 5	16.417	42.577	6.5
20 × 8	16.409	42.562	6.5

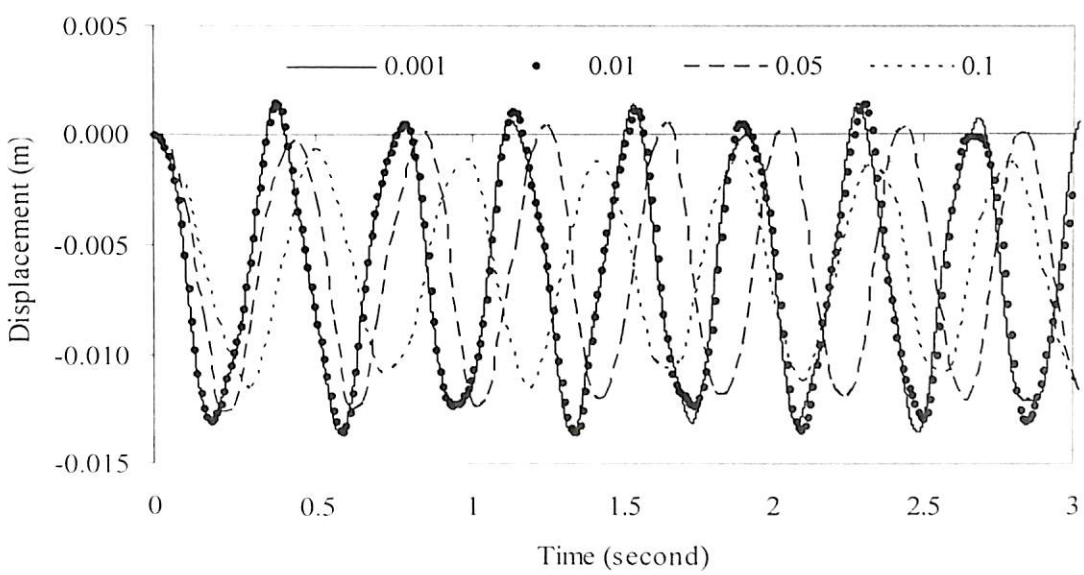

Fig.4.2 Horizontal displacement at the top of the dam subjected to ramp acceleration

4.1.3 Validation of the Algorithm

To check the accuracy of the present analysis procedure, the results available for Pine Flat dam (Fenves and Chopra, 1985) are considered. The maximum crest displacements due to the South East (S69E) component of the ground motion at Taft Lincoln School Tunnel on 21st July, 1952 are presented in Table 4.2 for comparison. A little variation in the results is observed which may be due to different finite element mesh sizes and other parameters for representing the dam.

Table 4.2 Fundamental period and maximum crest displacement of Pine Flat Dam.

Fundamental period (sec)		Max Crest Displacement (mm)	
Fenves & Chopra (1985)	Present	Fenves & Chopra (1985)	Present
0.317	0.320	26.93	26.58

4.1.4 Evaluation of Degradation Index

The degradation index is determined using compressive strength gain curve as given by Washa et al. (1989), assuming concrete of similar mix and compaction. The scalar degradation parameter d_m is evaluated by eq. (3.29) using material parameters $\alpha_m = 0.9$, $\beta_m = 1000$, and $\phi_0 = 0.2$ (Kuhl et al. 2004). The value of ϕ_c may be considered as 0.2 in the presence of chemical degradation and zero in the absence of silt deposited on the upstream face. The maximum allowable degradation due to mechanically induced porosity, a_s (eq. 3.29) can be predefined between 1.0 and 0.0, indicating 100 percent and no degradation respectively due to porosity developed in the concrete at the end of its design life. Here, the value of elastic modulus as obtained from eq. (3.43) without any degradation to 1.0. The value of a_s for a design life of 100 years is taken in the range of 0.4 is plotted in Fig. 4.3. The variation of elastic modulus of concrete with design life of 100 years, considering hygro-chemo-mechanical effect is plotted for comparison. It is observed that if degradation due to porosity in concrete ϕ is considered by eq. (3.35), the decrease in elastic modulus of the material can be predicted. It is interesting to note from Fig. 4.3 that considering $a_s = 1.0$ (as in Simo & Ju 1987) results in excessive reduction in

the elastic modulus of concrete. This implies that at 100th year, the concrete is reduced to a pile of sand which is practically not correct. Thus, to study the effect of maximum allowable degradation due to mechanically induced porosity during its design life on the strength of concrete, the elastic modulus is obtained for different values of a_s. It is observed that with a decreasing value of a_s the decrease in elastic modulus of concrete is reduced i.e., the extent of degradation is reduced. However, it is seen that if the material parameters are known, the proposed technique can be used effectively to estimate the degradation of concrete in the concrete gravity dam due to aggressive environmental effect.

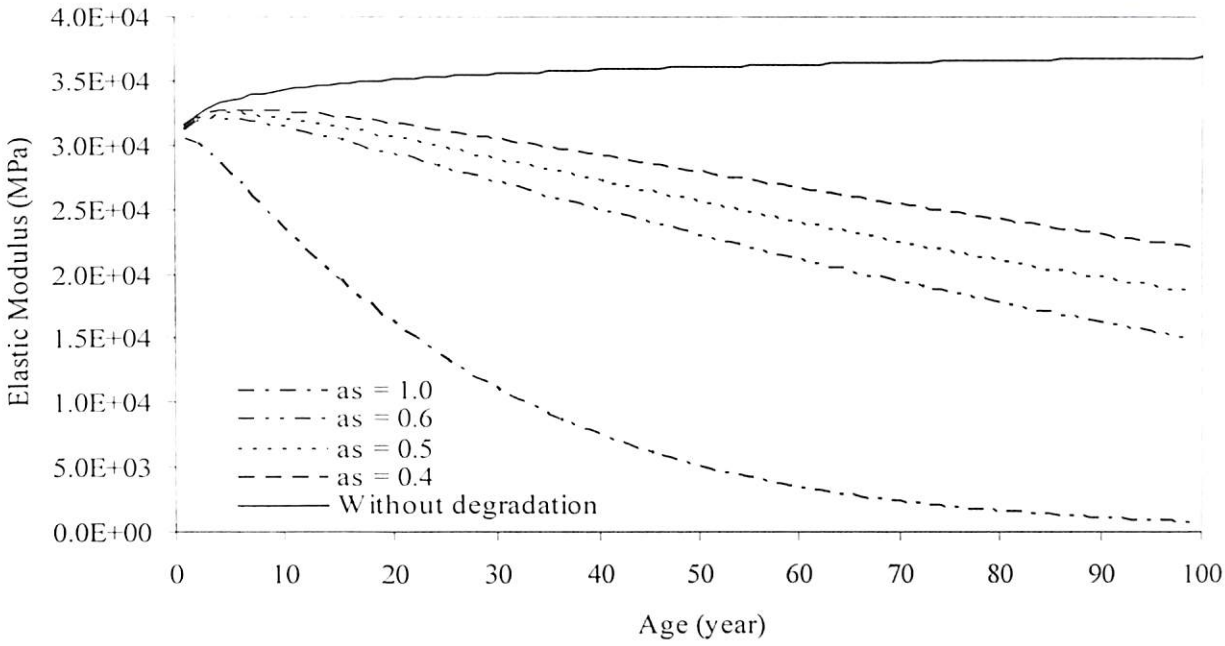

Fig. 4.3 Variation of elastic modulus of concrete with age

4.1.5 Response of Aged Dam

Structural degradation leads to the termination of the life of a structure. For prediction of dynamic behavior of an ageing dam, a new paradigm is introduced defining extent of degradation of the dam due to the effect of hygro-chemo-mechanical (HCM) effects. During the lifetime of the structure, the original safety margin will be reduced by deterioration of structural strength, reflected in the time evolution of the stiffness matrix, the most suitable assemblage of structural degradation information. The definition of degradation indicators d_{gl} is dependent on porosity of the degraded concrete. The value of d_{gl} = 0 to 1 represents a structure's life from birth to failure. Degradation generally

originates from numerous local material defects, but only their effects on structural stiffness or strength can be identified as structural damage. The formulation of material degradation phenomena is based on the constitutive relations. The developed concept is illustrated by analysis of two existing dams in India.

4.1.5.1 Koyna Dam

The Koyna dam is located on the western side of India, about 200 kilometers south of Mumbai, in the state of Maharashtra and was constructed in 1962. The ageing effect of the dam due to seismic excitation has been studied. Fig. 4.4 shows variation of the horizontal crest displacement of the dam with age due to a static horizontal load of 1000 kN applied at the top of the dam. The degradation index of the concrete material for different age are calculated corresponding to hygro-mechanical (HM) and hygro-chemo-mechanical (HCM) effect for design life of 50 years and 100 years for a comparison. Here, the value of allowable degradation due to mechanically induced porosity, a_s is considered to be 0.57 (eq. 3.29). When the chemical effect is ignored (HM), the degradation is reduced and hence the displacements are observed to be less.

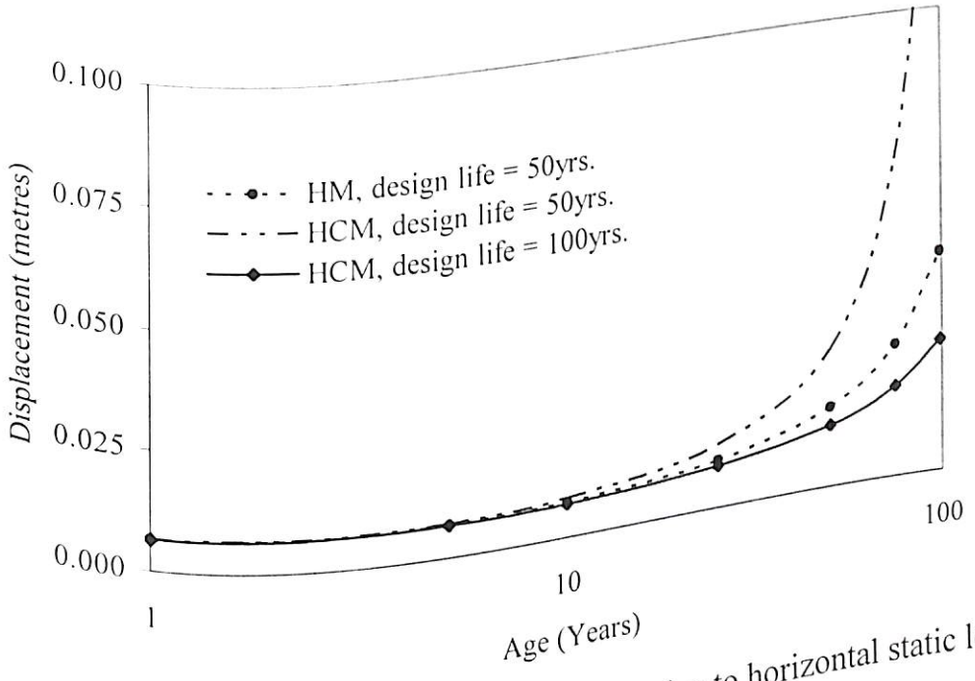

Fig. 4.4 Horizontal crest displacements due to horizontal static load

The effect of isotropic damage caused by degradation on the response of the dam due to horizontal component of Koyna earthquake (Fig. 4.5) is examined in the absence of reservoir. In the present work, the dynamic magnifications of strength and stiffness parameters of concrete due to rapid application of seismic strains are not considered. The analysis is carried out without any initial damage, after completion of construction,

considering one year old concrete strength. In the second and third case, an isotropic damage due to degradation of 34.5 % (d_g =1-E_m/E_0) and 19.1% at 25 years is estimated for the hygro-chemo-mechanical effect with a design life of 50 (HCM-50) and 100 (HCM-100) years respectively.

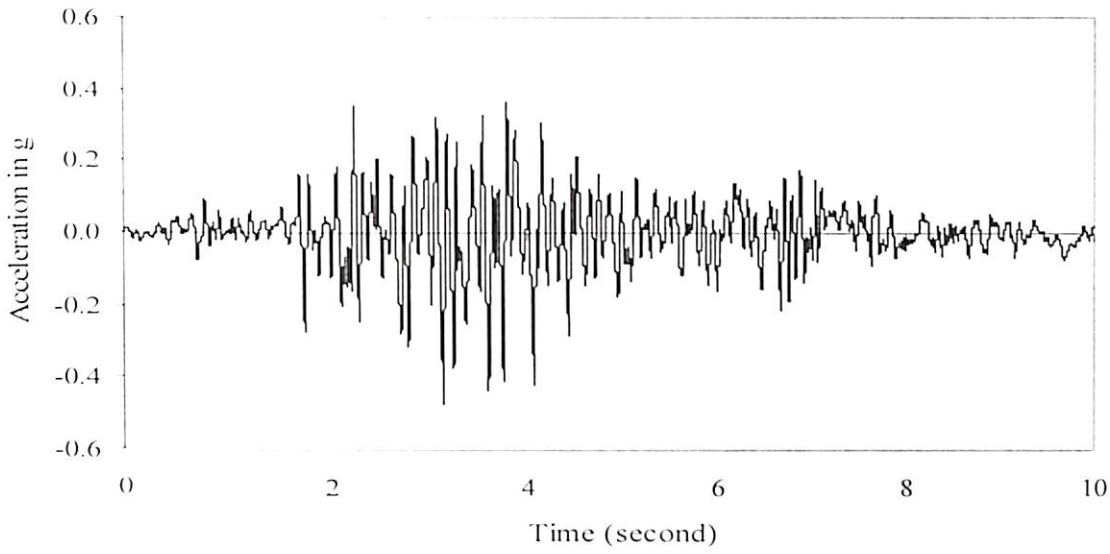

Fig.4.5 Horizontal accelerogram of Koyna earthquake, December 11, 1967

The degraded value of elastic modulus of concrete considering strength gain, E_m at a particular age is determined from eq. (3.35). The degradation index is then derived from eq. (3.36), which is used in the isotropic degradation model (eq.3.26). The displacements normalized with respect to gravitational acceleration, g is plotted in Fig. 4.6; which shows the effects of damage due to degradation on displacements of the dam due to seismic excitation. It is observed from the graphical results that the displacement is more in case of a lower design life. However, the peak responses are reached at a later time with a higher design life.

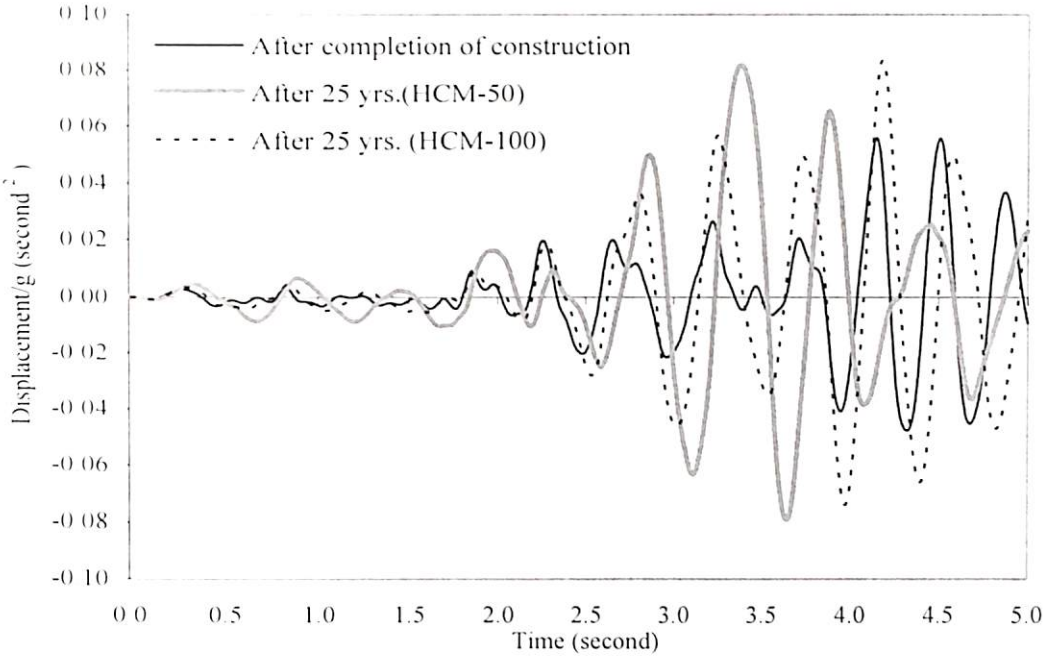

Fig. 4.6 Effect of degradation on horizontal crest displacement due to Koyna earthquake

Degradation of the dam material will lead to damage in the body of the dam that may result in loss of strength of the material along the horizontal, vertical or in both the directions. A study is carried out to evaluate the response of the dam due to damage along the width and height of the dam. It is observed from Fig. 4.7 that with an increase in damage caused by degradation, the natural frequency of the structure reduces. This behavior is mainly attributed to the reduced stiffness of the structure with increased degradation. Increase in degradation will thereby increase the time period of the structural system and will affect the deflection and stresses induced in the dam. Moreover, the decrement in frequency is high in case of isotropic damage model as compared to orthotropic one, as it affects the stiffness of the dam section in both horizontal and vertical directions. The damage along dam height also has a similar effect as that in the isotropic case, as this is the primary source of stiffness. The decrease in the frequency for the model having degradation variation along vertical direction is steeper than that of along horizontal direction.

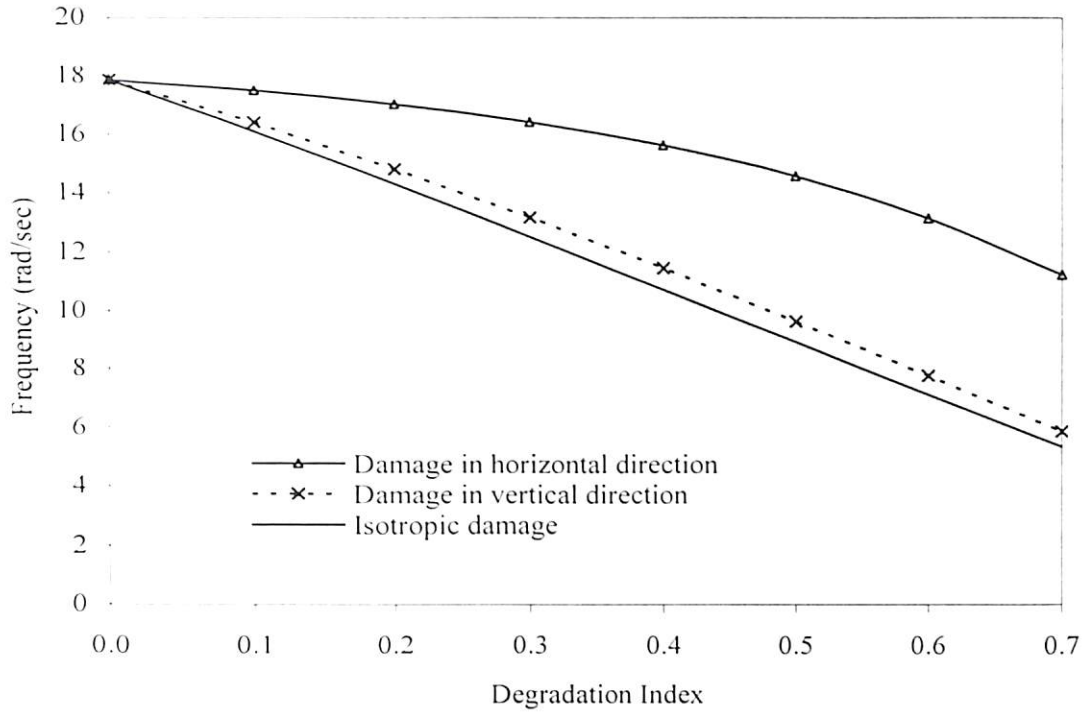

Fig. 4.7 Variation in frequency of dam with initial degradation

The variations of static displacements with respect to varying damage in the two mutually perpendicular directions are studied extensively under a point load of 1000 kN is applied at top of the dam. The horizontal and vertical displacements at the top of the dam under horizontal load at the top are plotted in Figs. 4.8 and 4.9 for comparison. The graphical results show that an isotropic damage model exhibits higher displacements as compared to that of orthotropic owing to the fact that the overall stiffness in an isotropic damage model is reduced along both the mutually perpendicular axes. But in case of orthotropic damage model, the displacements along both the directions are observed to be more when the damage is along vertical direction than when the damage is along horizontal direction. This is because the damage in vertical direction affects the stiffness of the dam comparatively more than that in horizontal direction. Also, it may be noted that the displacements of the dam increase with an increase in damage due to degradation no matter whether it is an orthotropic or an isotropic degradation model.

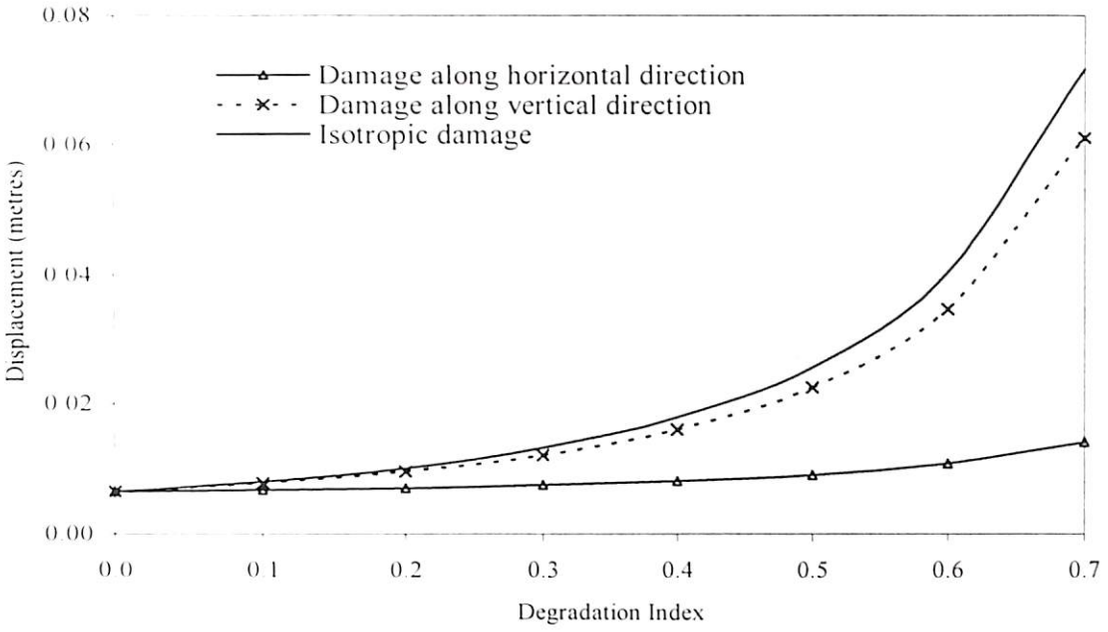

Fig. 4.8 Variation of horizontal crest displacements with degradation under horizontal loading

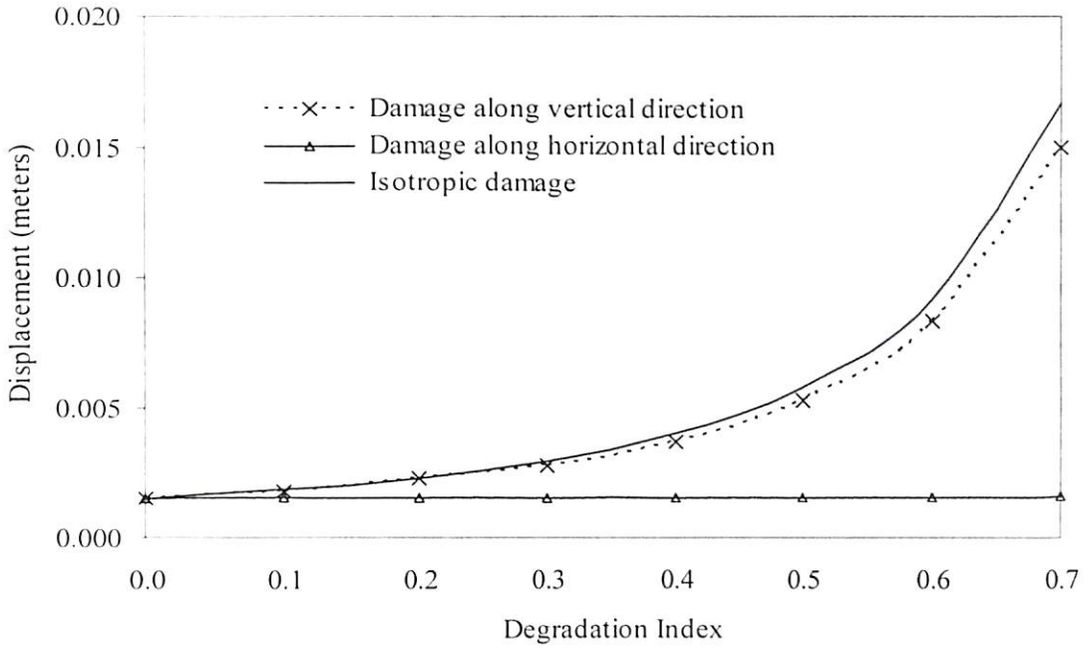

Fig. 4.9 Variation of vertical crest displacements with degradation under horizontal loading

The horizontal and vertical displacements at the top of the dam due to a vertical load of 1000 kN applied at the top of the dam are plotted in Figs. 4.10 and 4.11 for different types of damage. It is observed that the horizontal crest displacements due

isotropic damage are more than that for damage along vertical and horizontal direction. The effect of damage along horizontal direction on horizontal crest displacements is found to be less than damage along vertical direction.

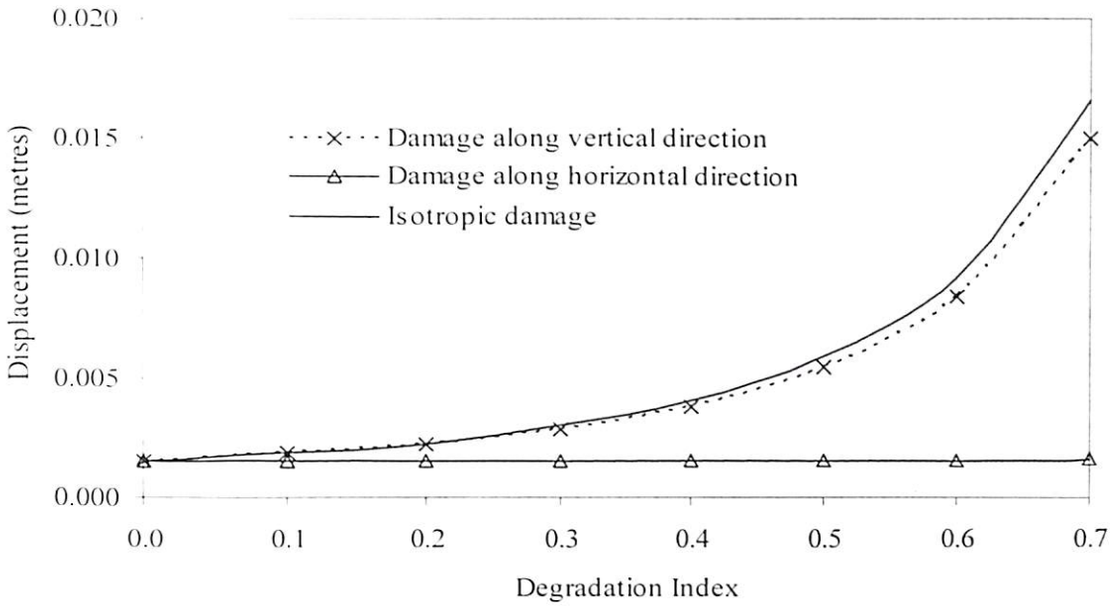

Fig. 4.10 Variation of horizontal crest displacements with degradation under vertical loading

Thus, it is observed that an isotropic damage causes an overall reduction in the stiffness of the dam and results in maximum displacement due to both horizontal and vertical loading. Comparing the damages along the horizontal and vertical directions it is observed that damage in vertical direction affects the stiffness of the dam and results in higher displacements than when the damage is in horizontal direction. This is because the lost area due to damage along its width is much less than the lost area due to damage along its height.

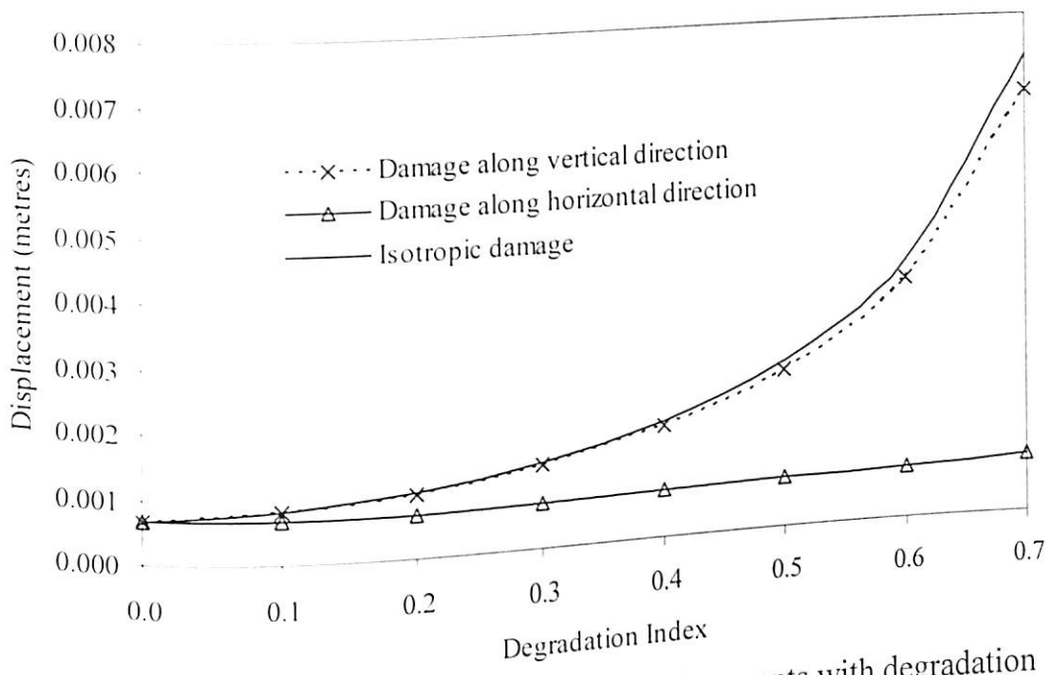

Fig. 4.11 Variation of vertical crest displacements with degradation under vertical loading

The maximum horizontal crest displacements of the dam for a design life of 50 and 100 years considering hygro-chemo-mechanical (HCM) and hygro-mechanical (HM) degradation due to Koyna earthquake are plotted in Fig.4.12. Due to degradation there is a rise in the crest displacements under seismic excitation for all the cases. The results show that the increase in displacements is gradual for a design life of 100 years and much less than that due to design life of 50 years. The effect of HM degradation is found to be less than that due to HCM degradation with design life of 50 years. A higher design life results in lower displacements even with both chemical and hygro-mechanical effect. The increased crest horizontal and vertical displacements due to degradation are primarily due to loss of vertical stiffness of the dam.

The principal stresses σ_{p1} (maximum tensile and minimum compressive) and σ_{p2} (maximum compressive and minimum tensile) developed in the Koyna dam due to Koyna earthquake (Fig.4.5), considering design life of 100 years with HCM degradation are plotted in Fig. 4.13 and Fig. 4.14 respectively. It is observed that as degradation increases with age, the percentage of damage increases in the dam. As a result the stresses developed in the dam body is less at the 75th year compared to its earlier age, i.e., at 1st year. At different instants of time during the earthquake excitation, the principal stress contours (σ_{p1} and σ_{p2}) are plotted in Figs. 4.15 to 4.20 for the 1st and 75th year after

the construction of the dam. The magnitudes of stresses indicated in the contour are in Pascal (Pa).

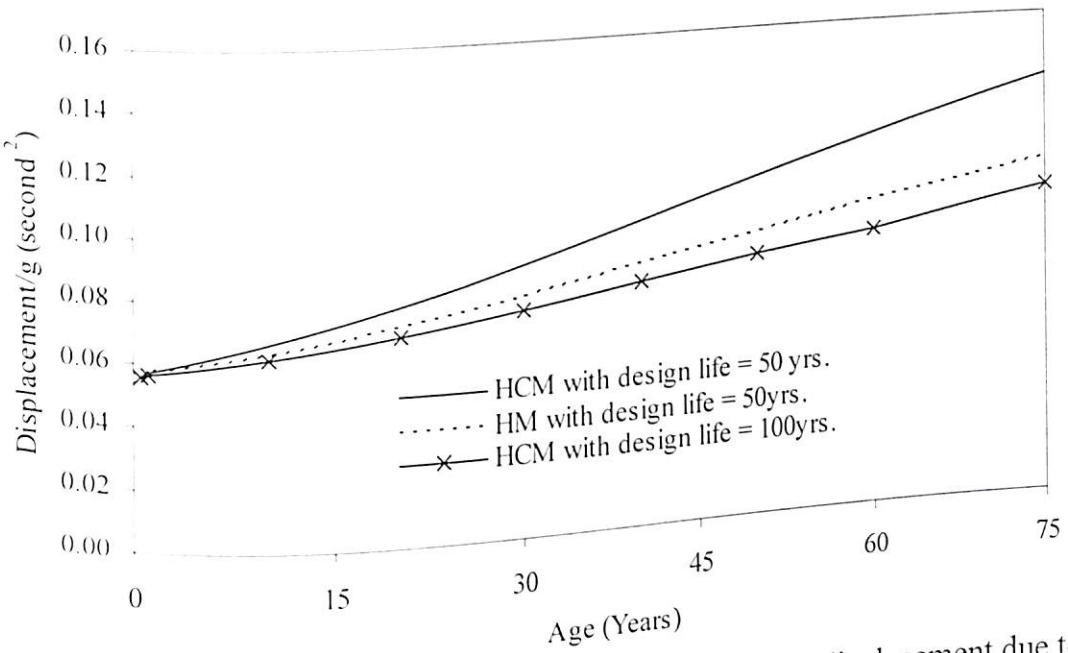

Fig. 4.12 Variation of maximum horizontal crest displacement due to Koyna earthquake

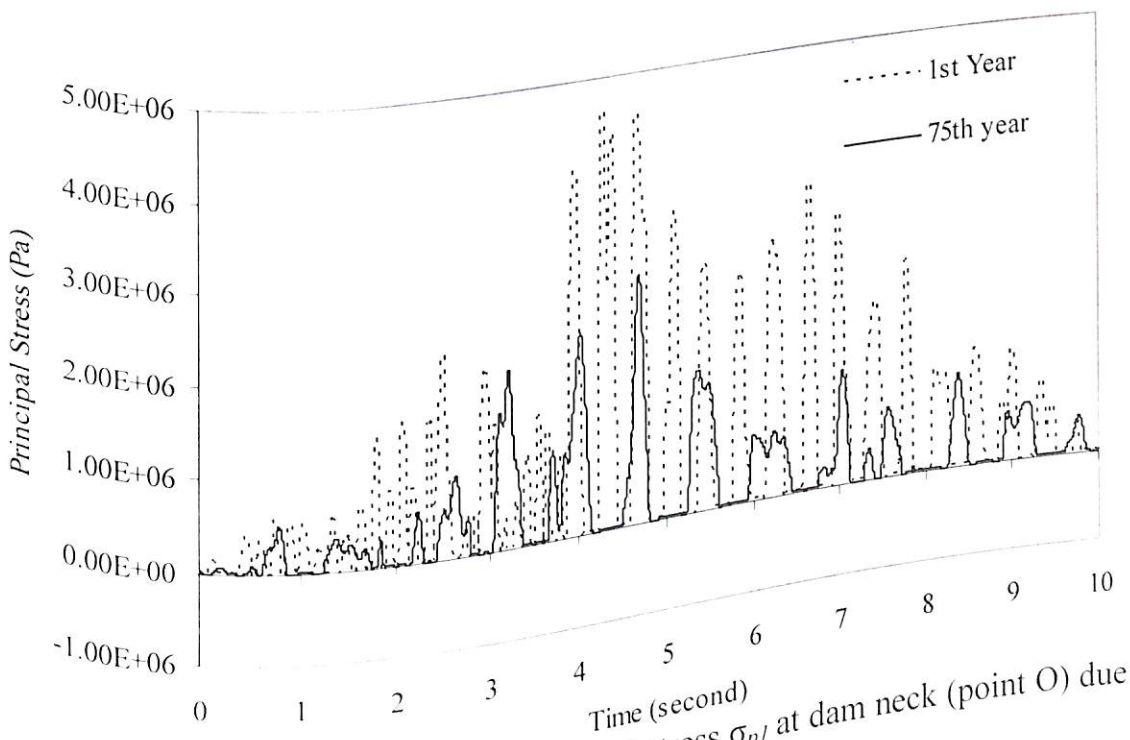

Fig. 4.13 Variation of principal stress σ_{pl} at dam neck (point O) due to Koyna earthquake

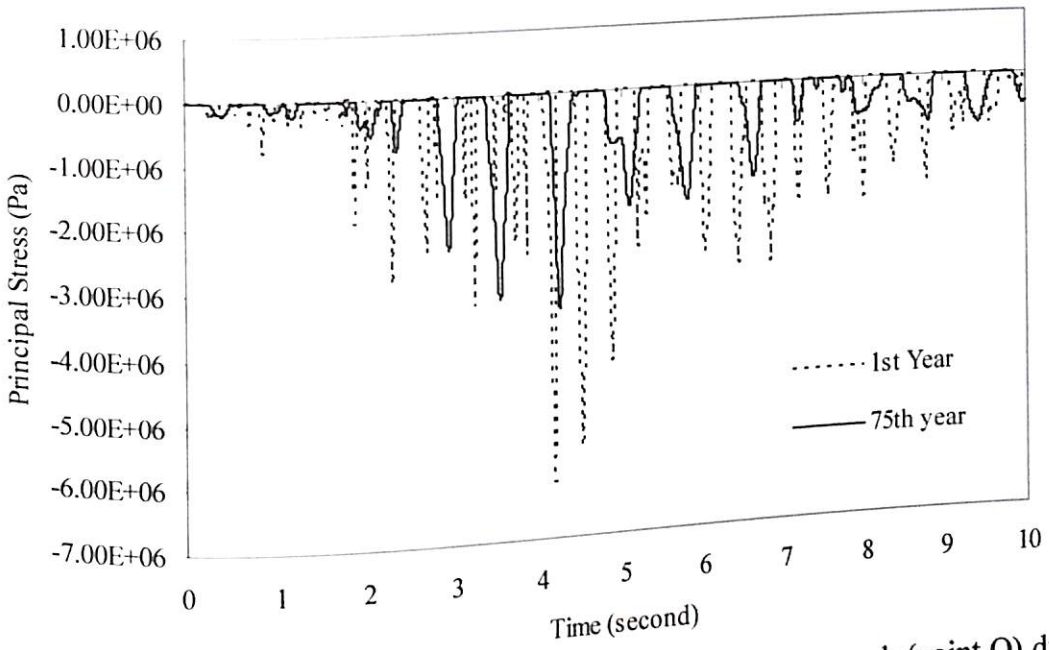

Fig. 4.14 Variation of principal stress σ_{p2} at at dam neck (point O) due to Koyna earthquake

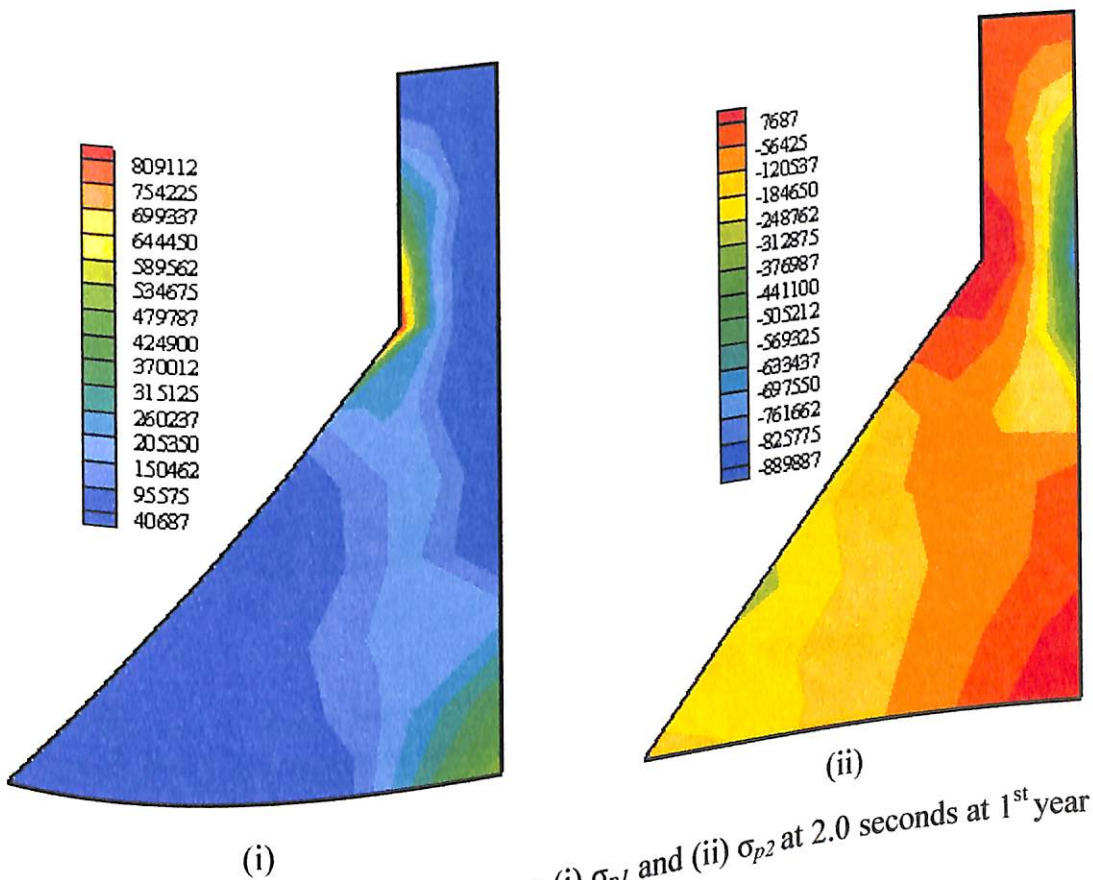

(i) (ii)

Fig. 4.15 Contour for principal stress (i) σ_{p1} and (ii) σ_{p2} at 2.0 seconds at 1st year due to Koyna earthquake

It is observed from Fig.4.15 (i) that at t = 2.0 seconds, the maximum tensile stresses are concentrated near the neck of the dam (point O) and at the heel of the dam (point B). The compressive stresses are higher near the point O (Fig. 4.15 (ii)) but along the vertical face of the dam. At t = 4.28 seconds, where the principal stresses (σ_{p1}) at point O reaches its peak (Fig. 4.13), it is observed that tensile stresses along the vertical face is much higher than in the other parts of the dam body (Fig.4.16(i)). The compressive stresses are concentrated around point O (Fig.4.16 (ii)). At t = 9.0 seconds, it is further observed that tensile stresses are higher along the vertical face of the dam, whereas the maximum compressive stresses are near the point O of the dam (Fig. 4.17).

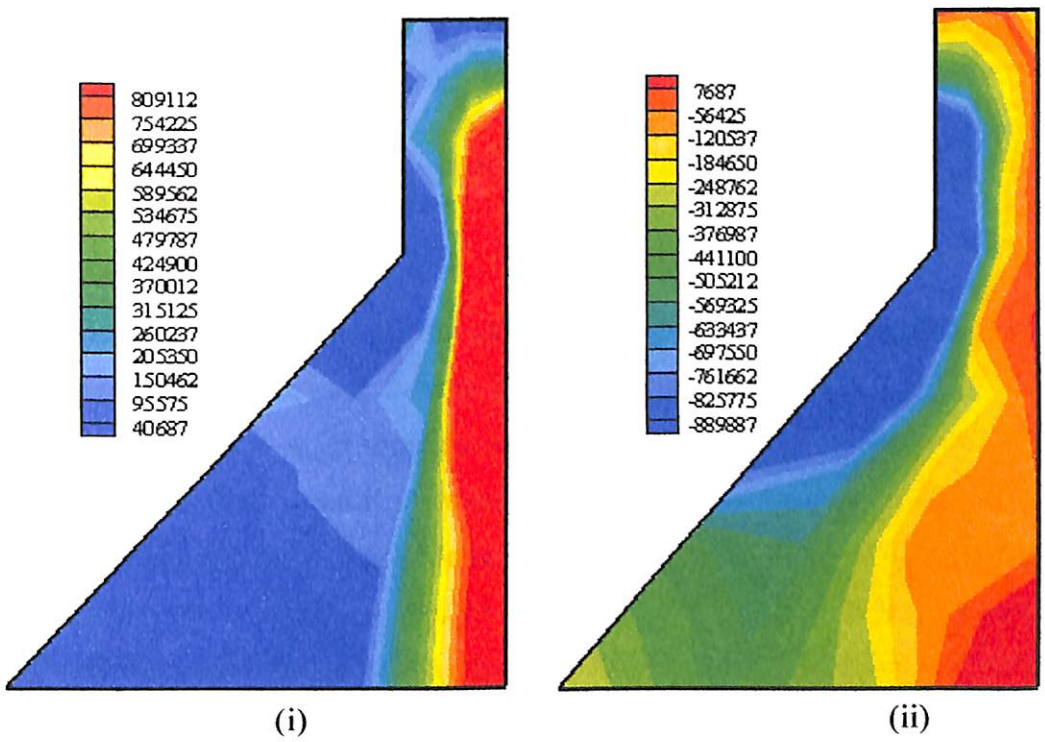

Fig. 4.16 Contour for principal stress (i) σ_{p1} and (ii) σ_{p2} at 4.28 seconds (1st year) due to Koyna earthquake

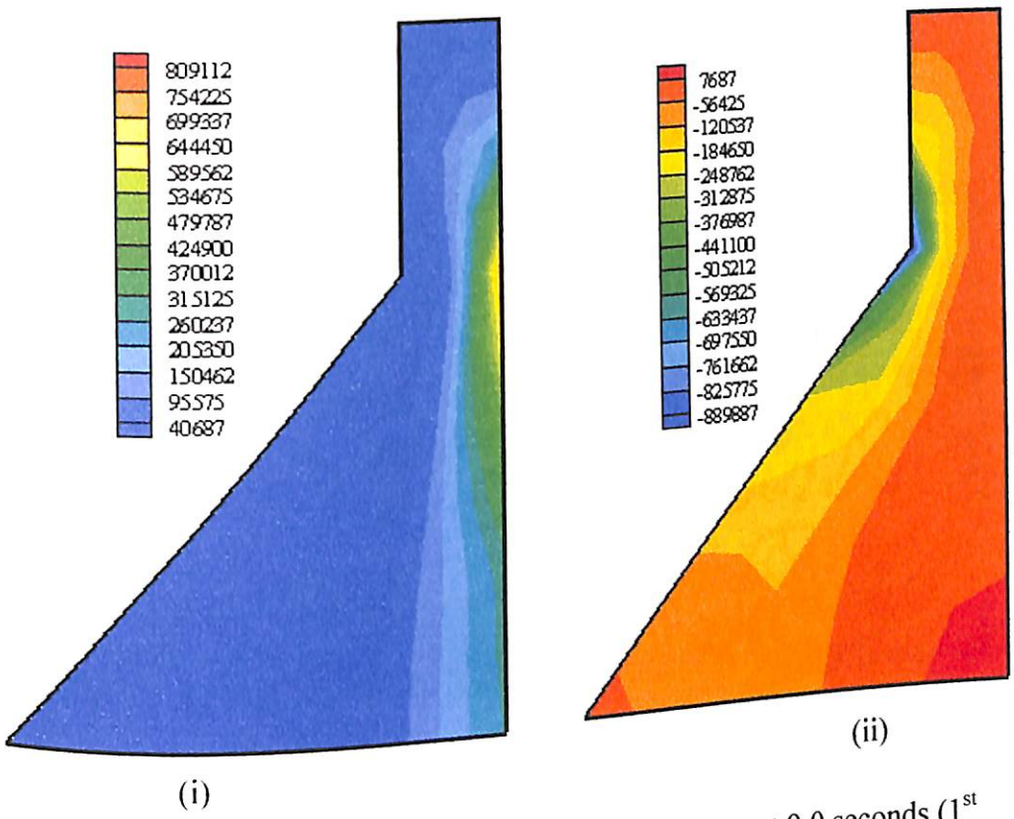

Fig. 4.17 Contour for principal stress (i) σ_{p1} and (ii) σ_{p2} at 9.0 seconds (1st year) due to Koyna earthquake

At the 75th year, at t = 2.0 seconds, the pattern of stress distribution in the dam body is similar to that as in the first year though the value of stresses are less than those in the first year (Fig.4.18). At t = 4.28 seconds, unlike the stress distribution pattern in the first year, it is observed that tensile stresses are concentrated around point O and the maximum compressive stresses are along the vertical face is much higher than in the other parts of the dam body (Fig.4.19). At t = 9.0 seconds, the tensile stresses are higher along the upstream vertical face of the dam, whereas the maximum compressive stresses are near the point O of the dam (Fig. 4.20). The values of stresses are less than those in the 1st year.

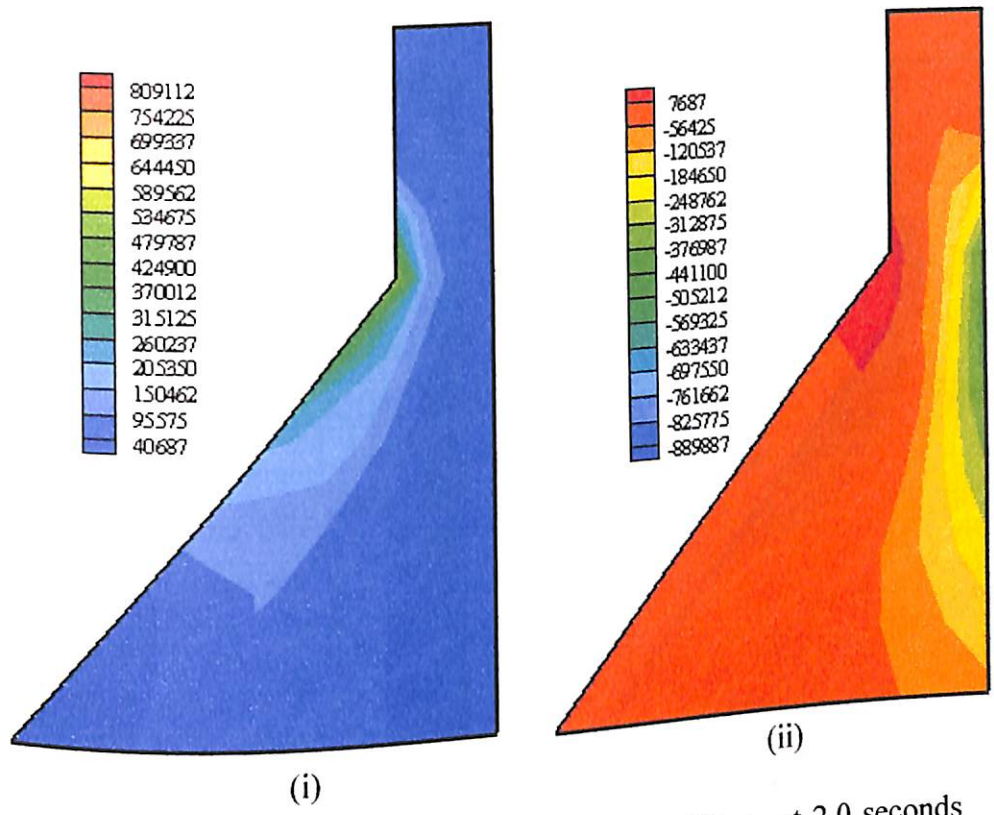

Fig. 4.18 Contour for principal stress (i) σ_{p1} and (ii) σ_{p2} at 2.0 seconds (75^{th} year) due to Koyna earthquake

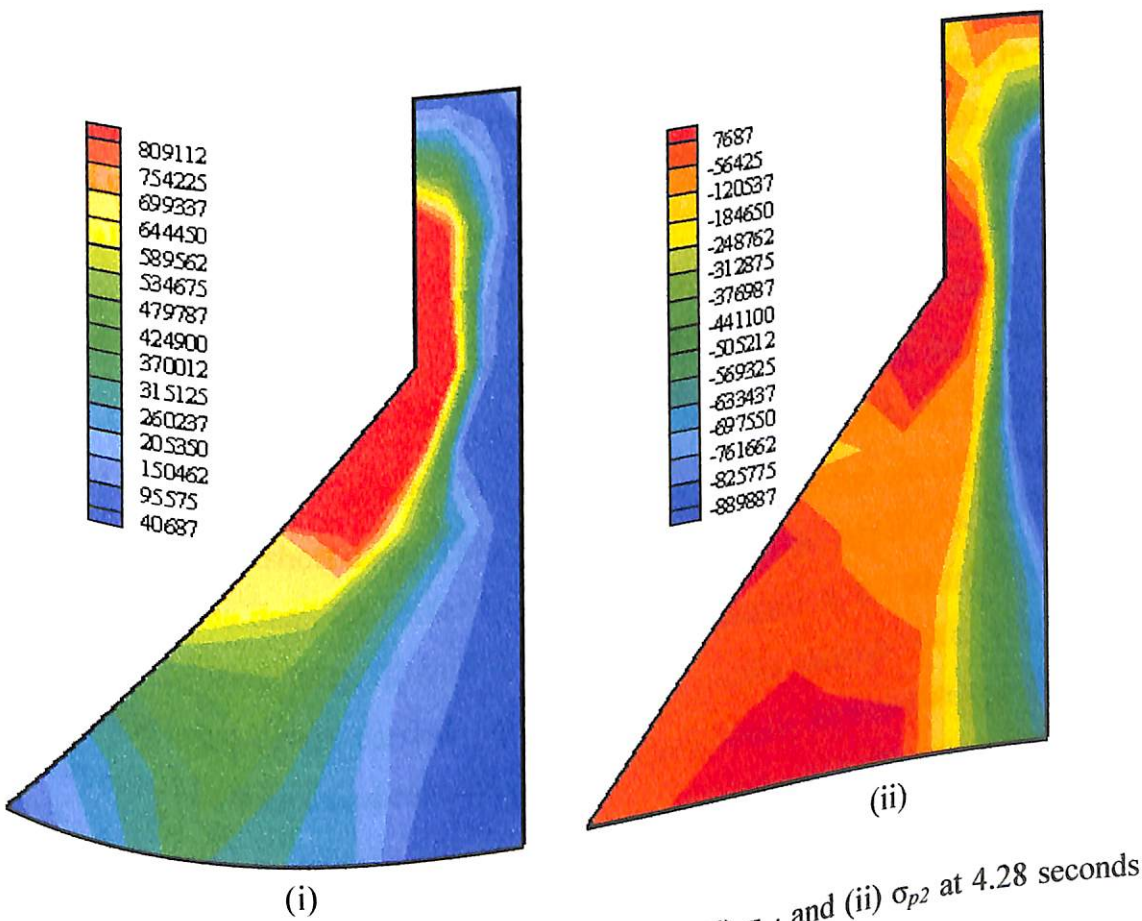

Fig. 4.19 Contour for principal stress (i) σ_{p1} and (ii) σ_{p2} at 4.28 seconds (75^{th} year) due to Koyna earthquake

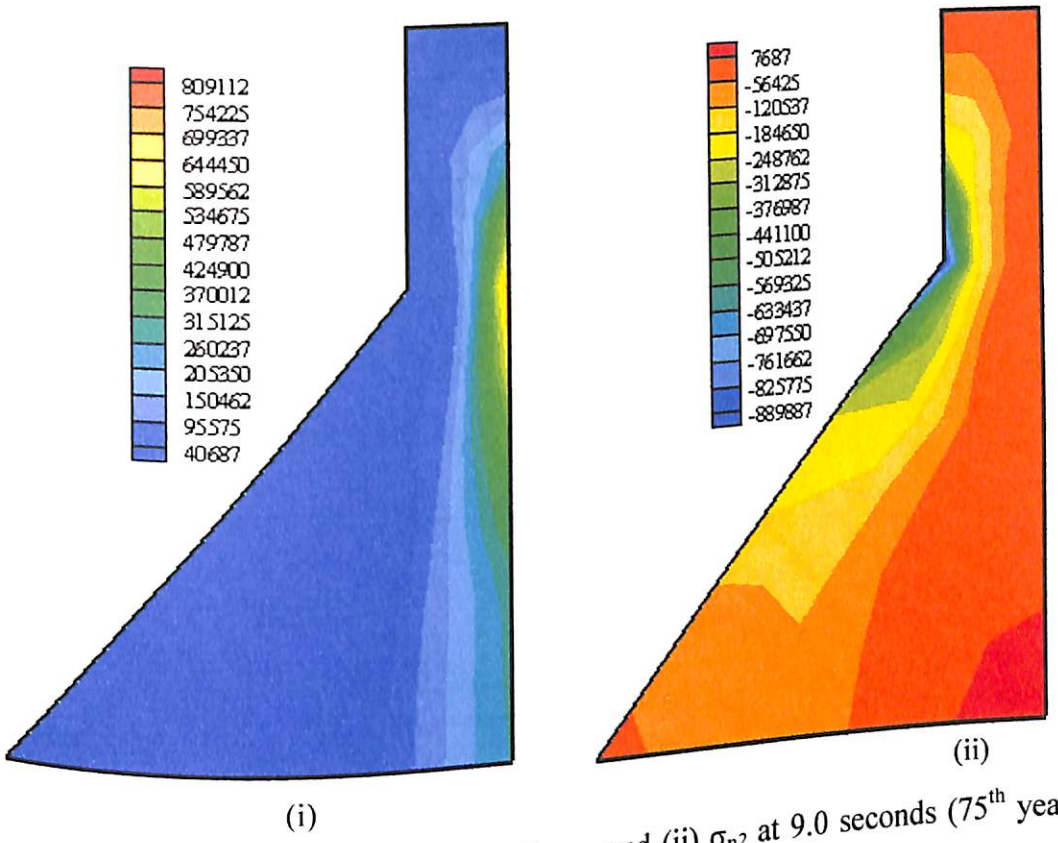

Fig. 4.20 Contour for principal stress (i) σ_{p1} and (ii) σ_{p2} at 9.0 seconds (75^{th} year) due to Koyna earthquake

4.1.5.2 Langpi Dam

It may not be wise to generalize the response results of the Koyna dam to arrive at a general conclusion. Hence, another dam located in the Karbi Anglong district of Assam, India called Langpi dam (Fig. 4.21) has been chosen for the extensive analysis using the same technique. The dimensions of a typical non-overflow section of the dam considered are: height of the dam = 46.5 m; width at the top of the dam is 9.1 m and at the base is 39.5 m. The Koyna dam has a height to width ratio of 1.47, whereas the Langpi dam has a height to width ratio of only 1.18 and hence in the present work, the Langpi dam will be referred to as a short dam. The material properties of the dam are considered same as in case of Koyna dam. The effect of isotropic damage on the response of the dam due to horizontal component of Koyna earthquake is examined in the absence of reservoir water. The analysis is carried out without any initial damage, after completion of construction. In the second case, after 25 years an isotropic damage due to degradation of 34.5% (eq. 3.36) is estimated due to hygro-chemo-mechanical effect for a design life of 50 years. In the third case, an isotropic damage of 19.1 % at 25 years is estimated due to hygro-chemo-mechanical effect for a design life of 100 years.

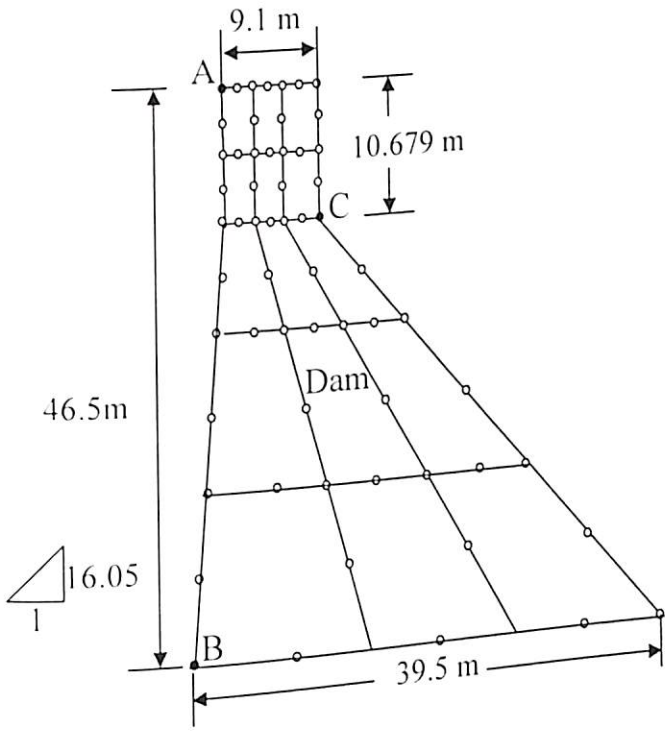

Fig. 4.21 Finite element mesh of Langpi dam

The results plotted in Fig. 4.22 show the effects of degradation on displacements of the dam due to seismic excitation (Koyna earthquake, 1967). It is observed from the results that the displacements are comparatively higher for a lower design life. The variation of fundamental frequency of the dam for various magnitude and types of damage are plotted in Fig. 4.23. The results show that even in the case of Langpi dam, with an increase in degradation, the natural frequency of the structure reduces. The decrement in frequency is high in case of isotropic degradation model as compared to orthotropic one, as it affects the stiffness of the dam section in both horizontal and vertical direction. However, the pattern of reduction in frequencies is not similar as in Koyna dam. This is because of different height to width ratio of the two dams. As the height to width ratio of the Langpi dam is 1.18 (for Koyna dam, it is 1.47), similar changes are observed for the damages in vertical and horizontal directions. Since the cross sectional area along the dam height is more than that along its width, damage along the dam height has prominent effect and rapid decline on the dam's natural frequency.

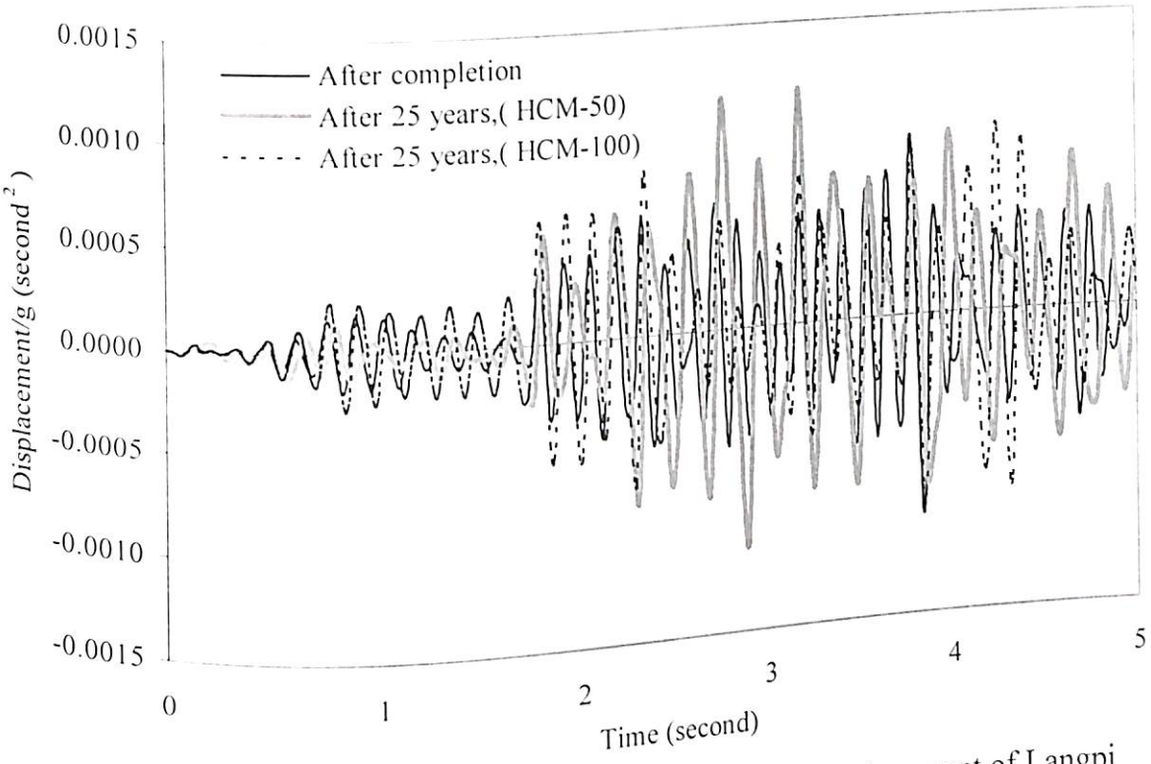

Fig. 4.22 Effect of degradation on horizontal crest displacement of Langpi dam due to Koyna earthquake

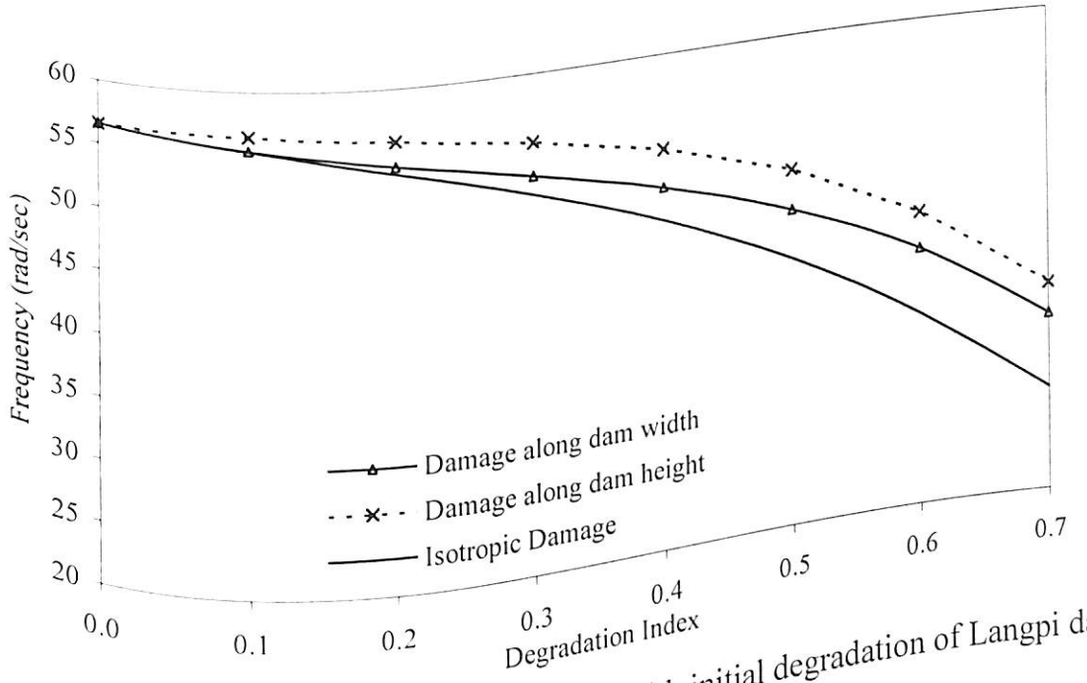

Fig. 4.23 Variation in frequency of dam with initial degradation of Langpi dam

The variations of static displacements with respect to varying damages in the two mutually perpendicular directions are also studied extensively for Langpi dam. The effect of degradation on horizontal and vertical displacements is compared in Fig. 4.24, when a horizontal load of 1000 kN is applied at the top of the dam. The four cases considered are: (1) horizontal displacement due to damage along dam width; (2) vertical

displacement due to damage along dam width; (3) horizontal displacement due to damage along dam height and (4) vertical displacement due to damage along dam height. The graphical results plotted in Fig.4.24 show that the variation of displacements are almost same having damages in horizontal and vertical directions.

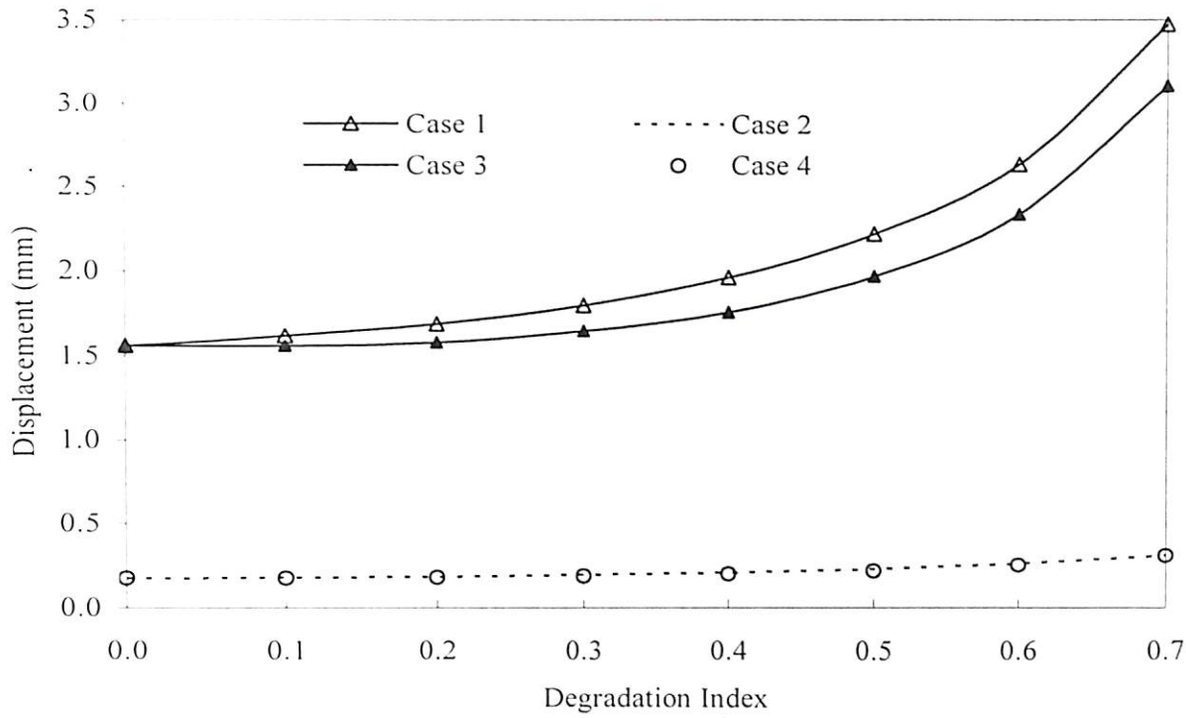

Fig. 4.24 Effect of degradation on crest displacement of Langpi dam

It may be interesting to note that the results obtained in case of Koyna dam due to vertical loading (Fig. 4.10) are different from those obtained in case of Langpi dam. Damage along the dam height has more pronounced effect on both the horizontal and vertical displacements in case of Koyna dam as it is comparatively slender having height to width ratio of 1.47. Thus, it can be concluded that for dams having higher height to width ratio, the damage along the dam height will influence the displacements more than the damage along the width of the dam. This is because the lost area due to damage along its width is much less than the lost area due to damage along its height. However, for the damage with height to width ratio approaching unity, will not vary much on the direction of damage.

4.1.6 Effects of Geometrical Nonlinearity

To study the effect of geometrical nonlinearity of the dam, the problem as considered in Section 4.1.1 is chosen. The modulus of elasticity is varied from 3.15×10^6 kN/m^2 to 3.5

$\times 10^8$ kN/m^2. The results for the horizontal deflection due to horizontal static load of 1000 kN at the top of the dam, with and without the effect of geometrical non-linearity are given in Table 4.3 for comparison. The tabular results show that the variation of results with geometric linear and non-linear analysis is very less as the height to width ratio is less (and in this case 1.47) at the base.

Table 4.3 Effects of geometrical nonlinearity of the dam

Modulus of Elasticity E_d (kN/m^2)	**Horizontal displacement linear (m)**	**Horizontal displacement nonlinear (m)**
3.15×10^6	0.064600	0.064563
3.15×10^7	0.006460	0.006459
3.15×10^8	0.000646	0.000646

The dynamic responses of the dam subjected to sinusoidal ground acceleration of 5.0 radians/second at different ages are shown in Figs. 4.25- 4.27. The magnitude of acceleration is considered as 1 m/sec^2. The time history results show that the effect of geometrical nonlinearity of the dam can be neglected without loosing much accuracy in the analysis.

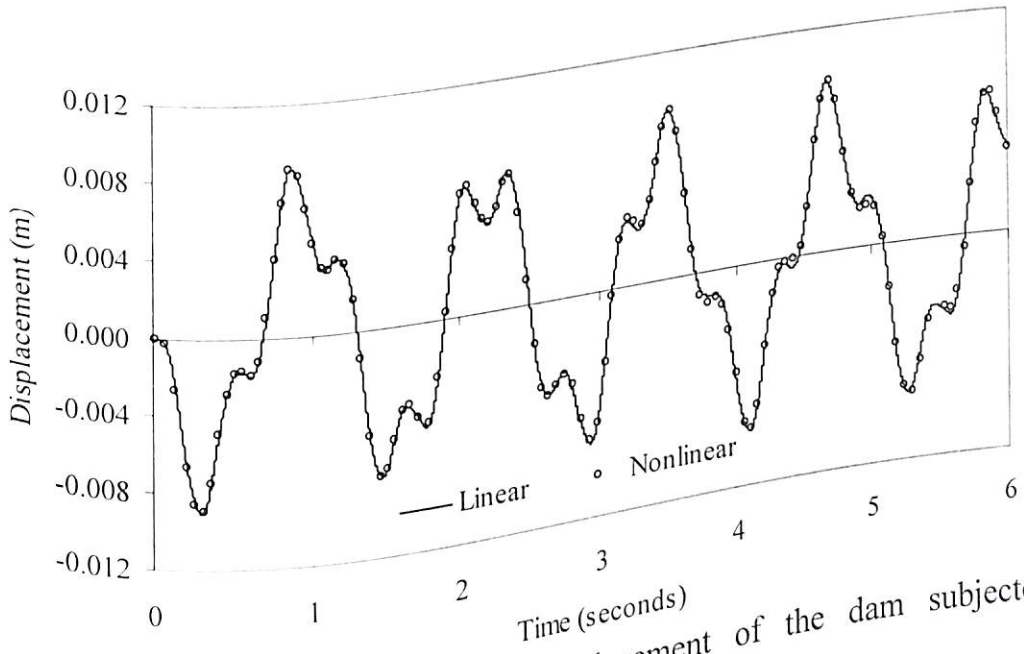

Fig. 4.25 Horizontal crest displacement of the dam subjected to sinusoidal acceleration at 1st year.

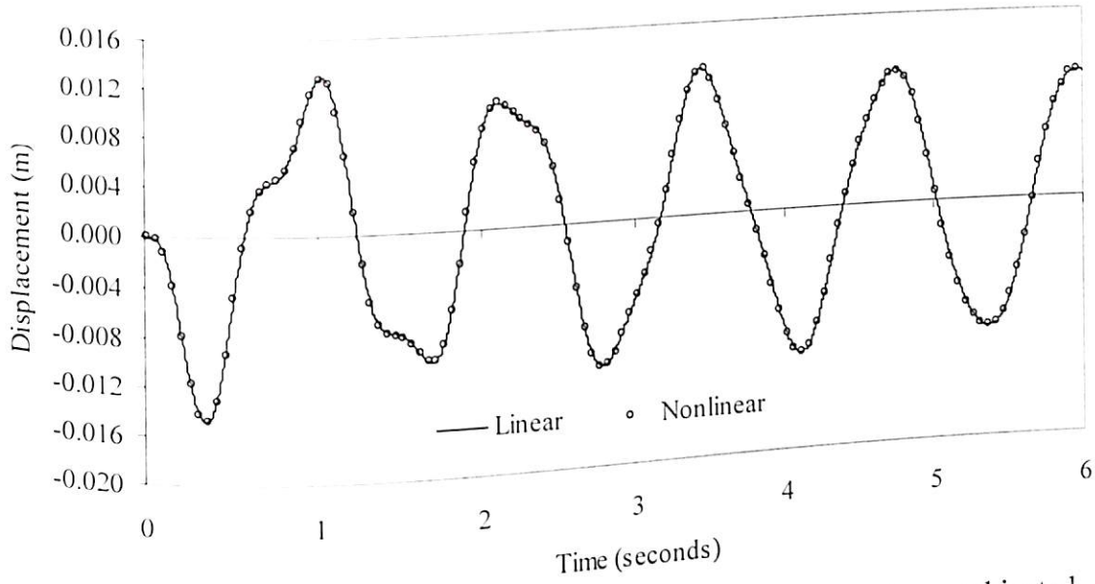

Fig. 4.26 Horizontal crest displacement of the dam subjected to sinusoidal acceleration at 25th year

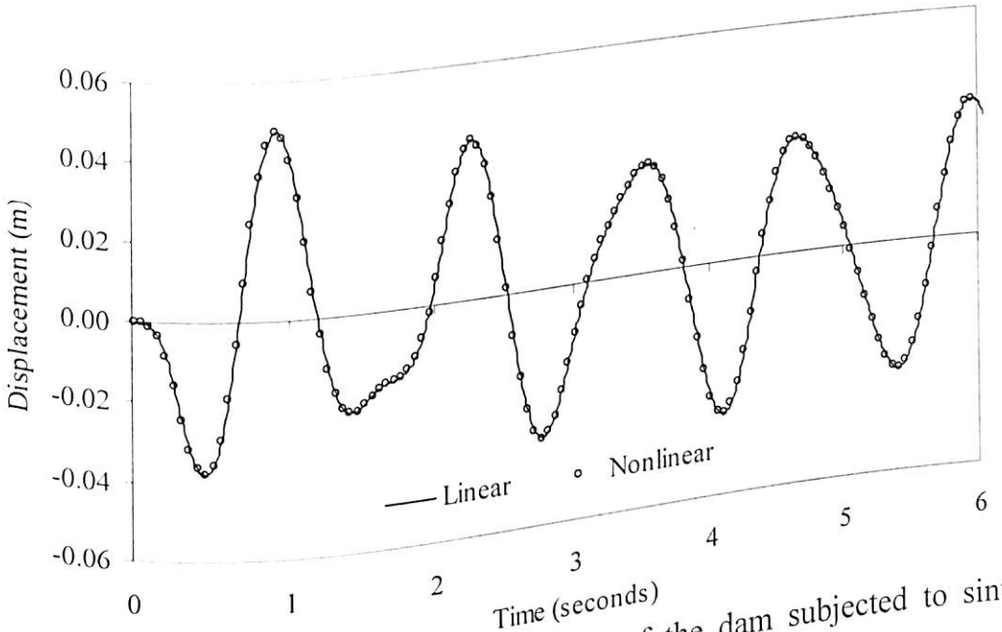

Fig. 4.27 Horizontal crest displacement of the dam subjected to sinusoidal acceleration at 75th year

The responses obtained by performing a geometrical nonlinear analysis of the same dam due to Koyna earthquake are compared with linear analysis at different ages in Figs. 4.28 – 4.31. The displacements normalized with respect to gravitational acceleration, g is plotted in Fig. 4.28 and 4.29. The variations in crest displacements and stresses at different ages under Koyna earthquake show that the geometric nonlinearity may confidently be neglected for the analysis of dam like structures.

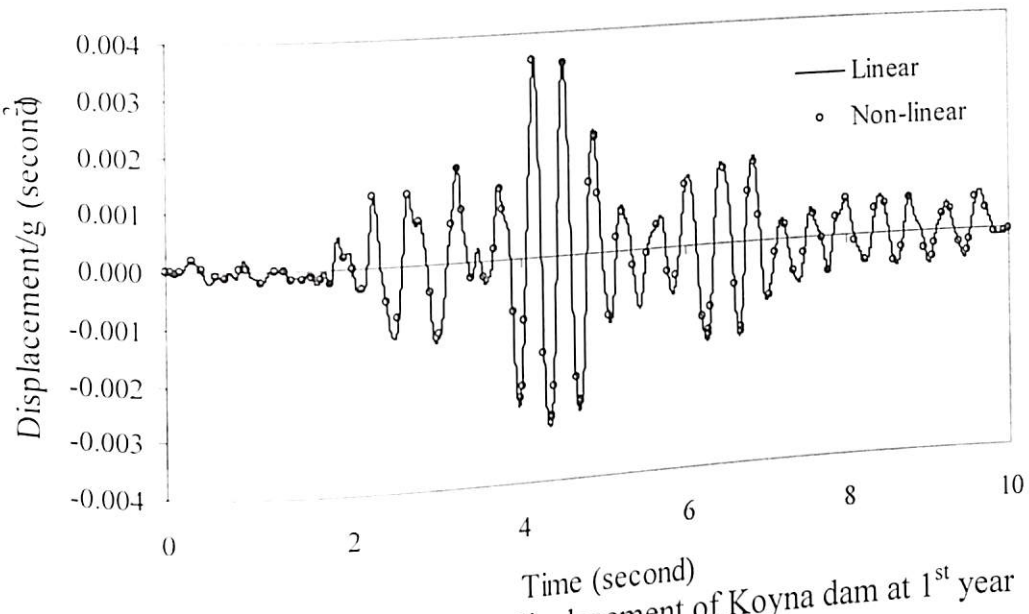

Fig. 4.28 Horizontal crest displacement of Koyna dam at 1st year subjected to Koyna earthquake

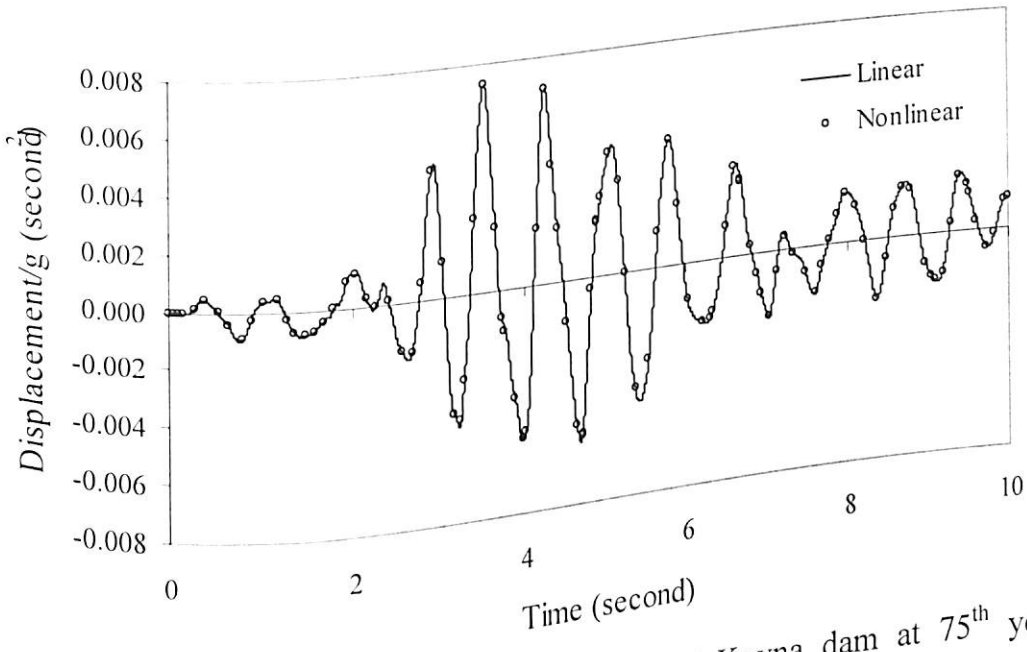

Fig. 4.29 Horizontal crest displacement of Koyna dam at 75th year subjected to Koyna earthquake

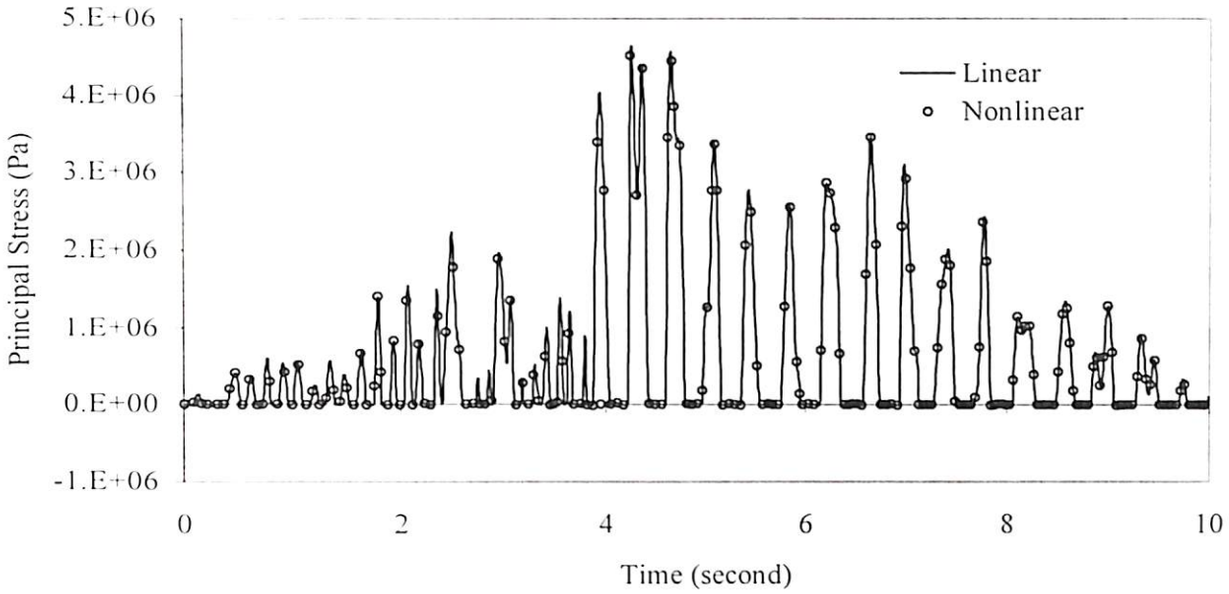

Fig. 4.30 Principal stress σ_{p1} at dam neck (point O) of the Koyna dam at 1st year subjected to Koyna earthquake

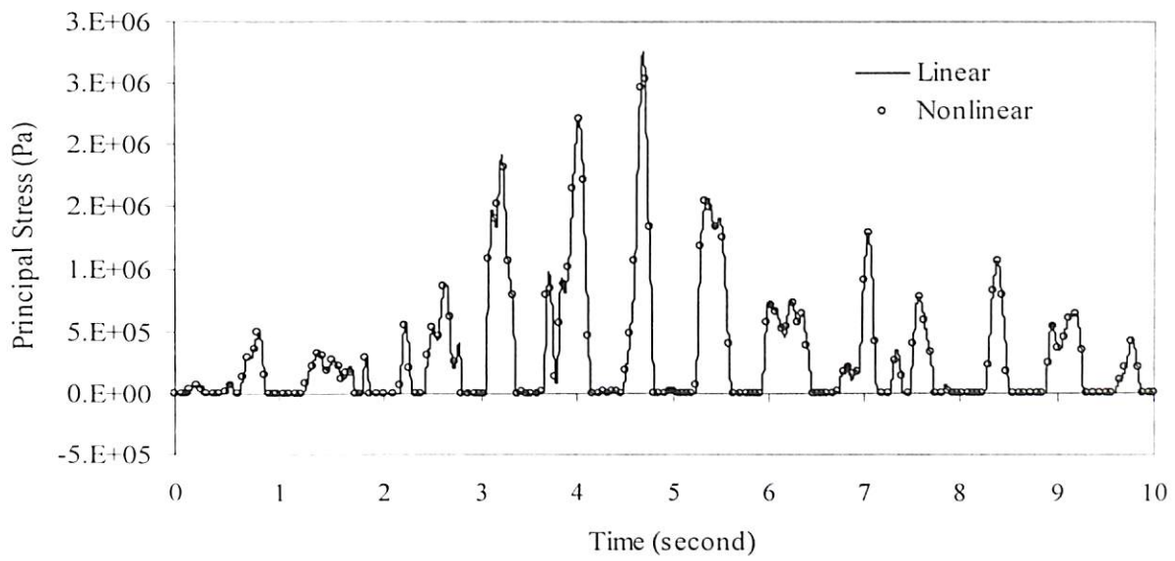

Fig. 4.31 Principal stress σ_{p1} at dam neck (point O) of the Koyna dam at 75th year subjected to Koyna earthquake

PART – II

4.2 ANALYSIS OF INFINITE RESERVOIR

In order to examine the feasibility and the accuracy of the proposed finite element model, few examples are solved using the computer code developed with the algorithm described in Chapter 3. The examples are related to the analysis of the hydrodynamic pressure distribution on two-dimensional structures exposed to infinite reservoir. The structure is considered in this particular case as rigid dam. An efficient truncation boundary condition has been developed and adopted for the finite element analysis of the infinite reservoir. The water in the present case considered is linearly compressible, inviscid and of small amplitude of motion. The proposed model for the dynamic analysis of an infinite reservoir utilizes the wave reflection coefficient approach to account for the sediment properties at the reservoir bottom. The effect of the depth of sediment layer lying over the reservoir bedrock on reflection coefficient is presented. The effect of reservoir bottom absorption and the gravity waves on the development of hydrodynamic pressure due to ground motion is also investigated. The efficiency of the proposed non-reflecting boundary condition imposed at the artificially truncated boundary of the reservoir with sediment layer is examined.

The full depth of the reservoir in the present analysis is considered as 70m. The mass density of water is considered as 1000 kg/m^3 and the acoustic velocity of water, c as 1440 m/sec. The amplitude of the external sinusoidal excitation is assumed to be equal to the gravitational acceleration g. The pressure coefficient at the bottom of the upstream face ($c_b = p_b/\rho a H_f$) is determined for different excitation frequency. p_b is the hydrodynamic pressure at the base of the dam-reservoir interface. The hydrodynamic pressure coefficient becomes generally maximum at the base of the dam-reservoir interface for $Tc/H_f \geq 4$. The reservoir domain has been discretized by four noded isoparametric elements for the finite element analysis. A typical finite element mesh has been shown in Fig. 4.32. N_v and N_h in Fig. 4.32 represent the number of elements in vertical and horizontal directions respectively and N_t represents the number of time steps per cycle of excitation.

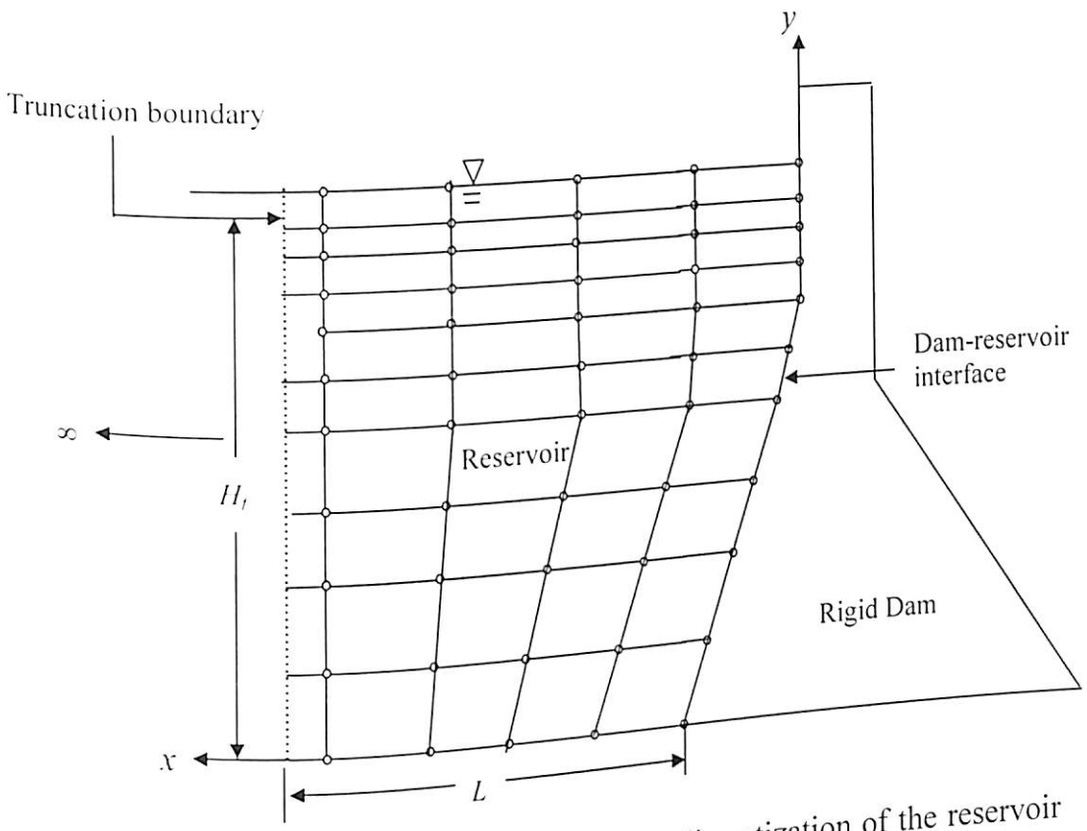

Fig. 4.32 A typical finite element discretization of the reservoir ($N_v = 10$, $N_h = 4$)

4.2.1 Convergence of coefficient, ζ_m

To get the effect of the unbounded reservoir domain at the truncation surface, the coefficient ζ_m in eq.(3.93) is determined numerically considering reservoir bottom absorption. The convergence of the coefficient ζ_m is tested first, prior to the evaluation of the hydrodynamic pressure distribution in the reservoir. The value of m is assumed to be a large number, which leads to precise determination of normal derivative of complex valued pressure at the truncation boundary. In the present analysis, ζ_m is determined considering first several terms of the infinite series till the value is sufficiently converged. A convergence study has been made to find the number of terms (m) of the infinite series to be considered for the finite element analysis of the infinite reservoir. The absolute values of the coefficient, ζ_m while truncating at a distance of $L = 0.5H_f$ and reflection coefficient of $\alpha = 0.5$ are calculated and plotted in Fig. 4.33 at different depths of the reservoir domain. Similarly, for $L = 0.1H_f$ and reflection coefficients of $\alpha = 0.95$, the coefficient ζ_m is plotted in Fig. 4.34. It is observed from the graphical results that the magnitude of ζ_m converges sufficiently for $m = 10$ for all the cases (i.e., at various

distance L and reflection coefficient, α). Thus, the coefficient, ζ_m for finding various results has been calculated by considering the value of m as 10 for all the cases unless it is mentioned. The variation of the absolute value of the coefficient, ζ_m along the reservoir depth is plotted in Fig.4.35 and Fig. 4.36 for different values of reflection coefficient which shows that the coefficient ζ_m is not constant at all along its height though the previous researchers have considered it as either constant (Sharan 1992) or zero (Sommerfeld). Also, the magnitude of ζ_m at a particular height is different for different position of truncation surface (L) using proposed truncation boundary condition (TBC). Hence, significant amount of error develops while the truncation boundary proposed by Sharan (1992) or Sommerfeld is imposed at a closer distance from the dam interface.

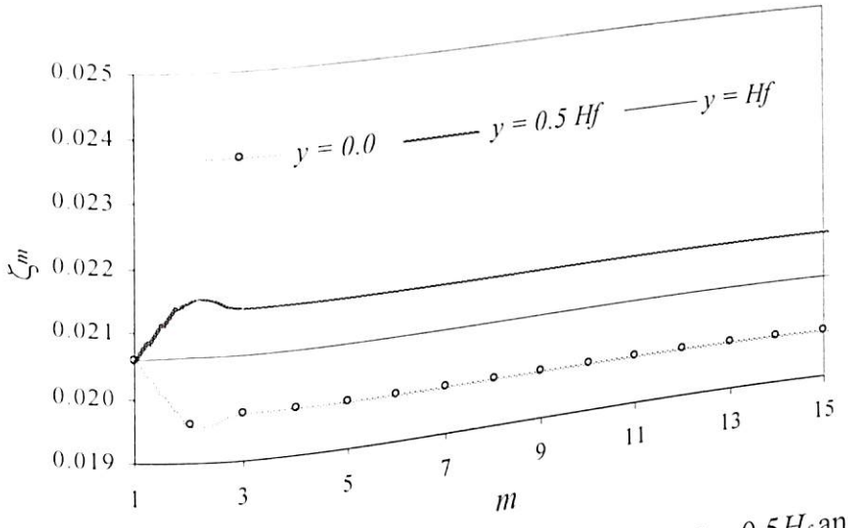

Fig. 4.33 Convergence of coefficient, ζ_m for $L = 0.5H_f$ and $\alpha = 0.5$

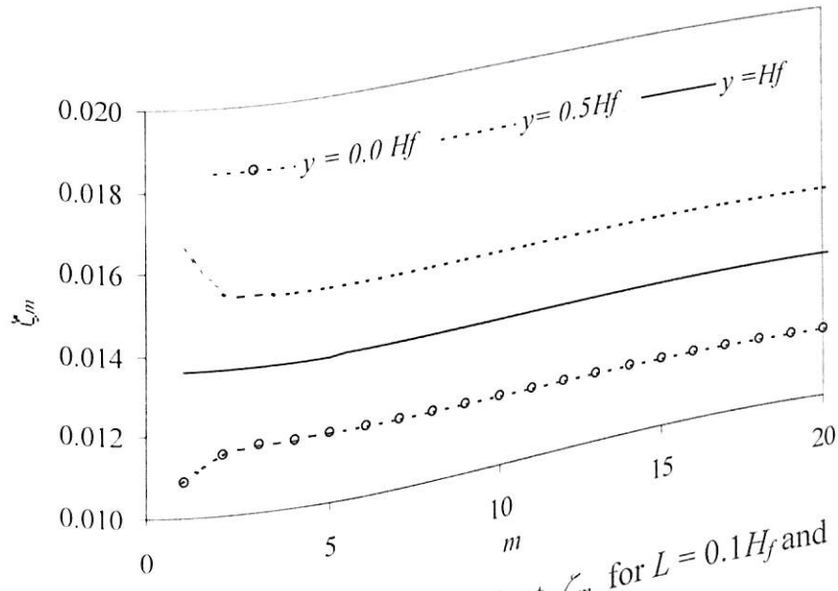

Fig. 4.34 Convergence of coefficient, ζ_m for $L = 0.1H_f$ and $\alpha = 0.95$

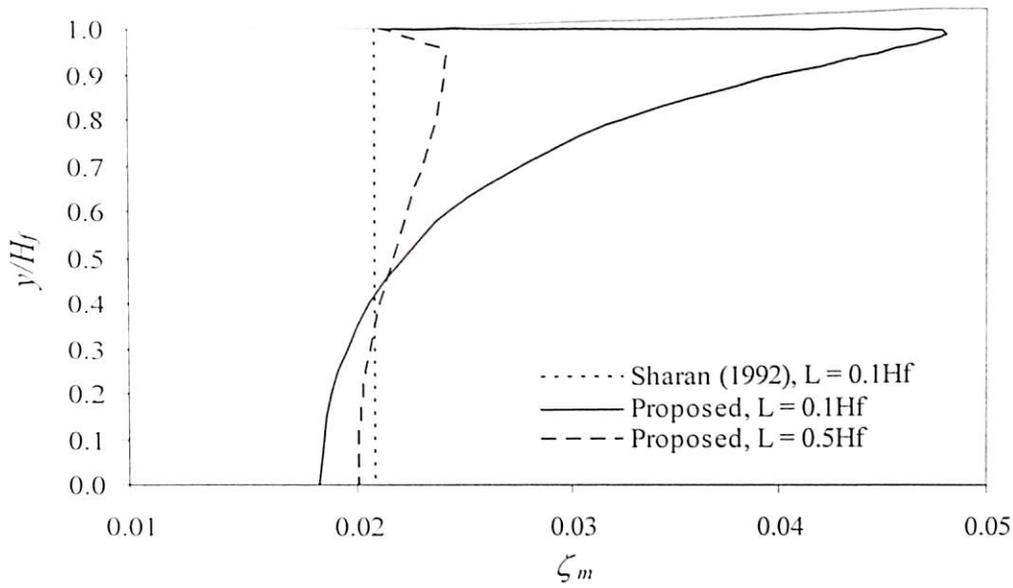

Fig. 4.35 Variation of coefficient ζ_m along dam height for $\alpha = 0.5$

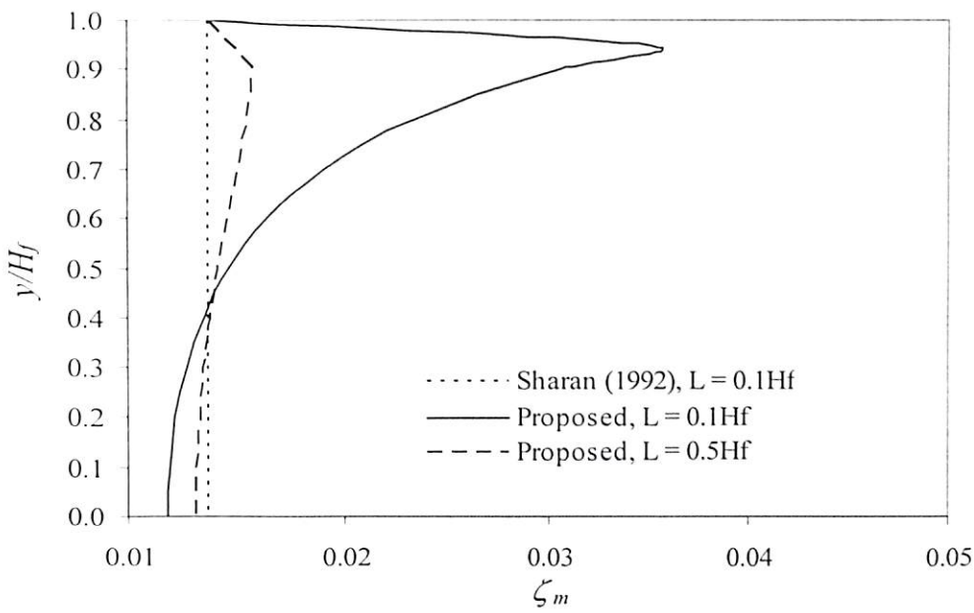

Fig. 4.36 Variation of coefficient ζ_m along dam height for $\alpha = 0.95$

4.2.2 Selection of Time Step

In order to choose the time step for the solution of the reservoir by the Newmark's integration technique, a convergence study is carried out. The results are shown in Table 4.4 for different values of Tc/H_f. In the table, N_t is the number of time steps per cycle of the excitation. Results shown in Table 4.4 are the maximum hydrodynamic pressure coefficients, $c_m = p_m / \rho_f a H_f$ at the bottom of the upstream face, at a time when the magnitude of the acceleration is maximum. p_m is the hydrodynamic pressure developed at

the bottom of the dam-reservoir interface at 0.75T. Thus, the results c_m presented in Table 4.4 correspond to 0.75T. Analyses are carried out adopting the present truncation boundary condition at a distance of $L = 0.2H_f$. N_v and N_h are taken as 20 and 4 respectively for the convergence test with the reflection coefficient of $\alpha = 0.5$. It is observed from the tabular results that the developed hydrodynamic pressure at a particular time instant for different values of Tc/H_f converge for values of $N_t = 32$. Thus, the time step (Δt) for the analysis of fluid domain is adopted as $T/32$ for all the case unless it is mentioned. For example, if the reservoir is vibrated at a frequency, such that Tc/H_f becomes 100, then the time step will be ($\Delta t = 100H_f/32c$) 0.15 second.

Table 4.4 Convergence of hydrodynamic pressure coefficients (c_m) for different time steps

N_t	$Tc/H_f = 100$	$Tc/H_f = 10$	$Tc/H_f = 4$	$Tc/H_f = 1$
8	0.7474	0.8204	0.9711	0.1323
16	0.7451	0.8146	1.1991	0.1398
24	0.7433	0.8116	1.2187	0.1411
32	0.7431	0.8097	1.2206	0.1414
64	0.7431	0.8097	1.2206	0.1414
128	0.7431	0.8097	1.2206	0.1414

4.2.3 Hydrodynamic Pressure with Vertical Dam-Reservoir Interface

The hydrodynamic pressure at the vertical upstream face of a dam is computed subjected to harmonic excitation. The maximum absolute hydrodynamic pressure can be obtained at an interval of 0.25T under harmonic excitation. However, to avoid initial unsteadiness, the maximum hydrodynamic pressure coefficient has been considered at a time of 0.75T. The results are compared with closed form and other methods (Bouaanani et al. 2003, Sharan 1992 and Sommerfeld).

A comparison of hydrodynamic pressure coefficient c_p ($= p/\rho a H_f$) along the dam height is plotted (Figs. 4.37 – 4.42) at various ratios of Tc/H_f and reflection coefficients α corresponding to 0.75T. It is evident from the literature (Hall & Chopra 1982) that the effect of reservoir bottom absorption is frequency dependent and is significant at the

resonant frequency. To investigate the effectiveness of the present boundary condition with absorptive reservoir bottom at resonance frequency ($Tc/H_f = 4$), the hydrodynamic pressure distribution is plotted for α varying from 0.95 to 0.25. It is interesting to note that the results obtained using the present far-boundary condition conform well to the closed-form analytical one, while those of Sharan (1992) have a large deviation for most of the cases. It may be worth to mention that accurate pressure coefficients are obtained by the proposed TBC even at a very short distance of $L = 0.02H_f$ when Tc/H_f becomes large, i.e., at 200 and 100 (Figs.4.37 & 4.38). The hydrodynamic pressure distribution in the reservoir domain at a particular time instant ($0.75T$) is shown in Fig. 4.43 in a contour form. The values indicated in the color bar are the magnitude of the hydrodynamic pressure coefficient c_p.

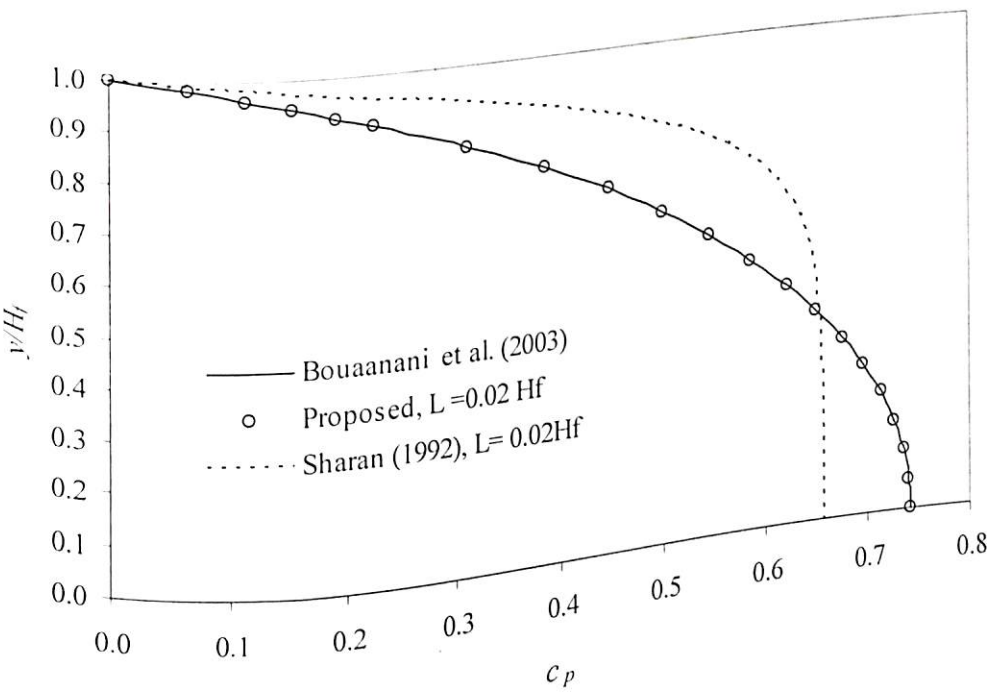

Fig. 4.37 Comparison of hydrodynamic pressure along the dam-reservoir interface for $Tc/H_f = 200$ and $\alpha = 0.5$

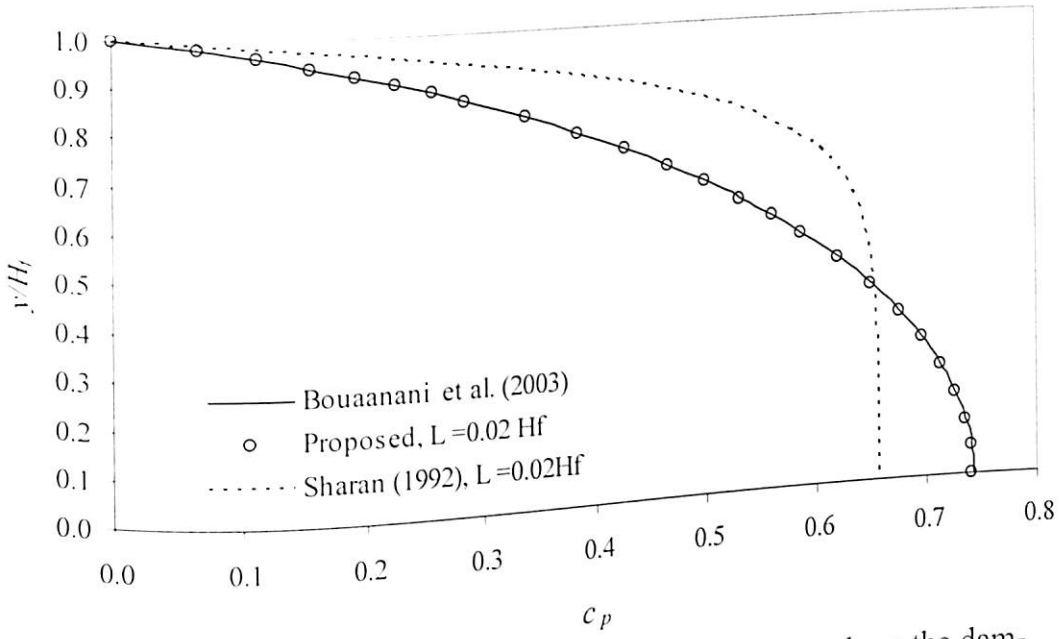

Fig. 4.38 Comparison of hydrodynamic pressure along the dam-reservoir interface for $Tc/H_f = 100$ and $\alpha = 0.5$

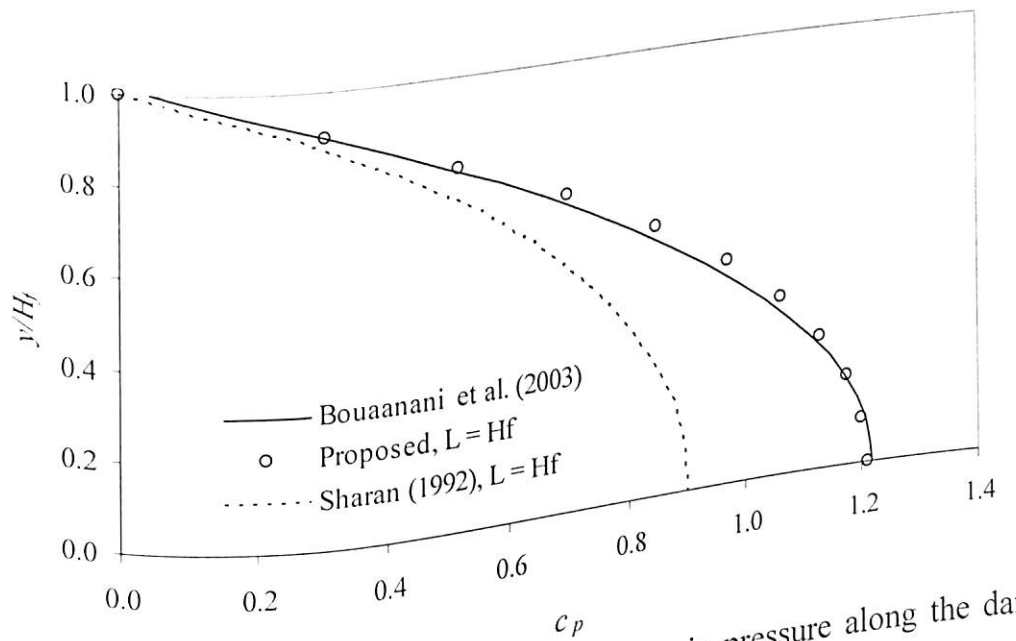

Fig. 4.39 Comparison of hydrodynamic pressure along the dam-reservoir interface for $Tc/H_f = 4$ and $\alpha = 0.5$

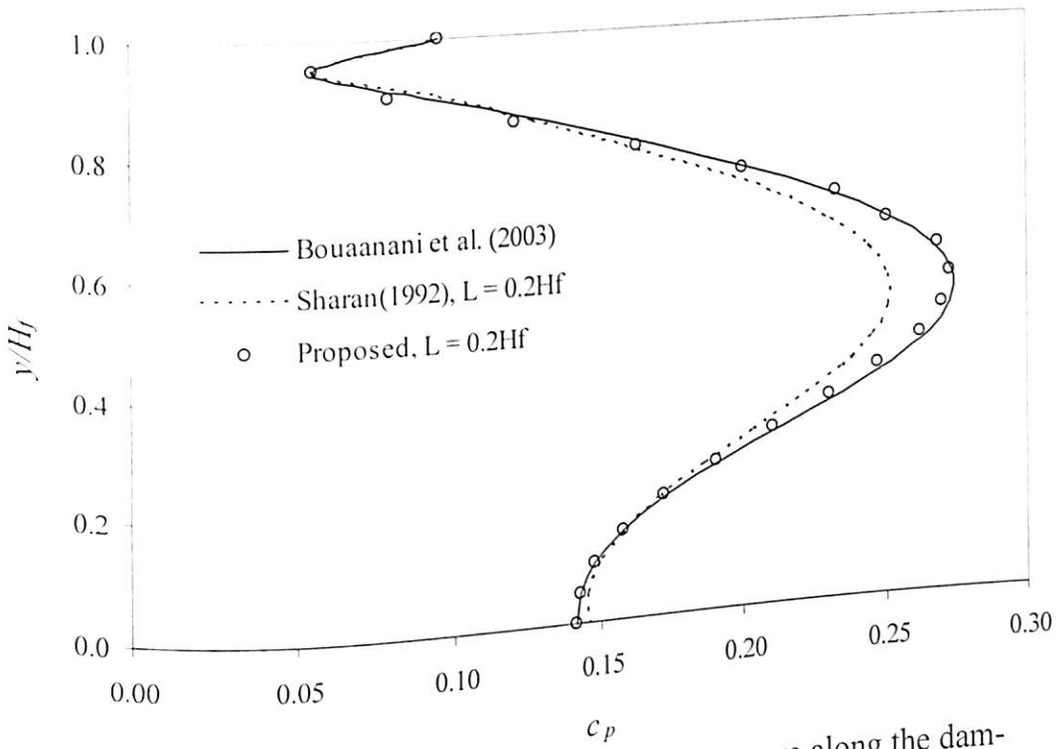

Fig. 4.40 Comparison of hydrodynamic pressure along the dam-reservoir interface for $Tc/H_f = 1$ and $\alpha = 0.5$

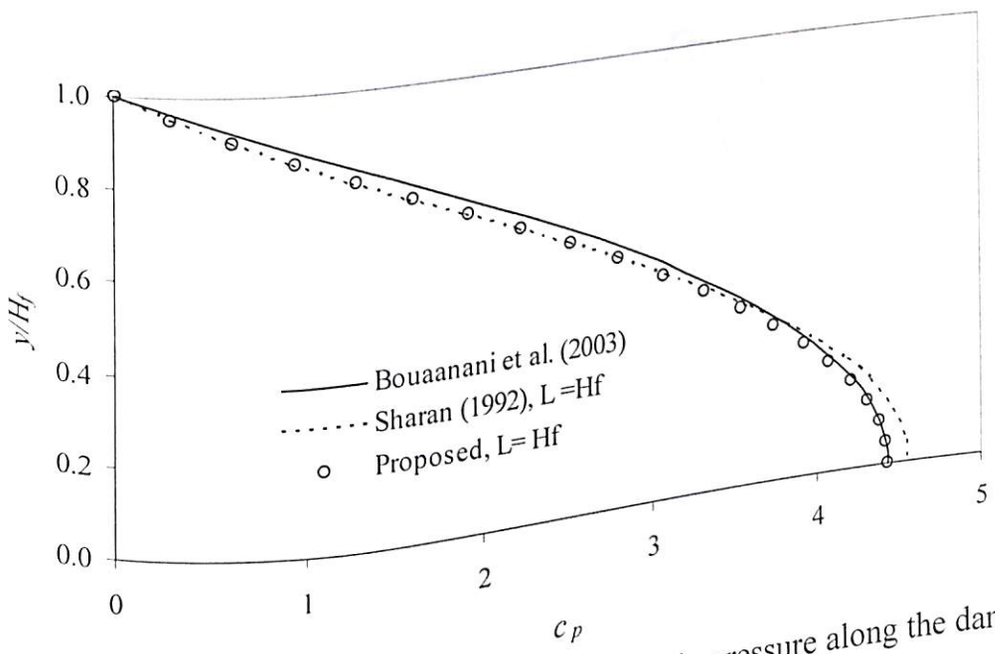

Fig. 4.41 Comparison of hydrodynamic pressure along the dam-reservoir interface for $Tc/H_f = 4$ and $\alpha = 0.95$

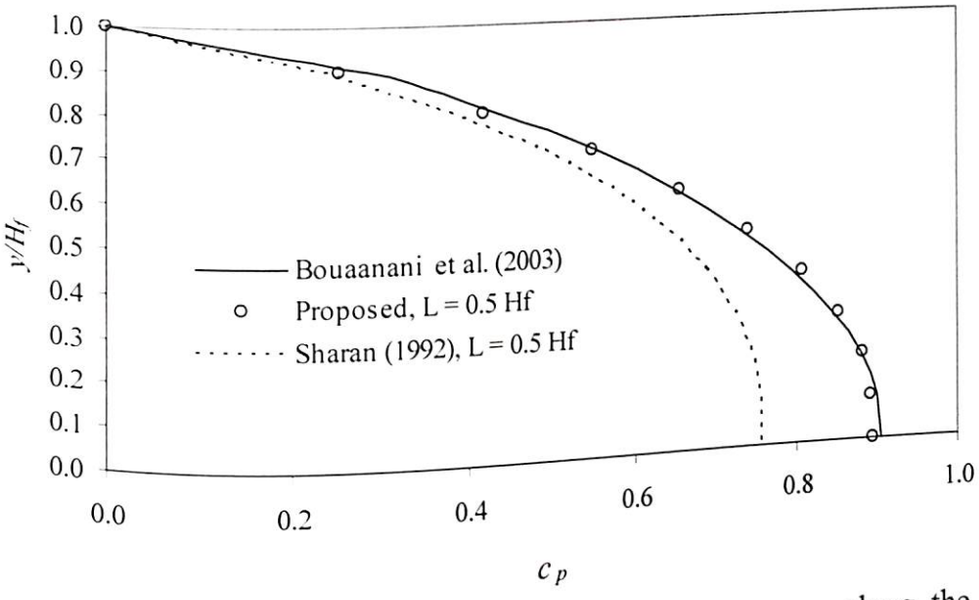

Fig. 4.42 Comparison of hydrodynamic pressure along the dam-reservoir interface for $Tc/H_f = 4$ and $\alpha = 0.25$

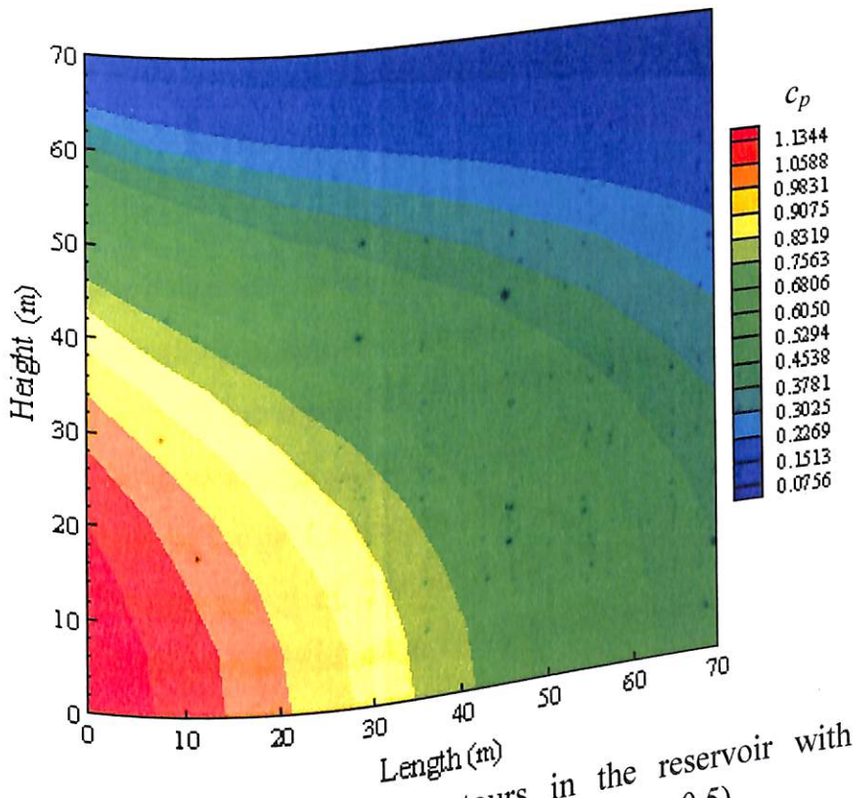

Fig. 4.43 Pressure contours in the reservoir with vertical upstream face of the dam ($Tc/H_f = 4$, $\alpha = 0.5$)

The total hydrodynamic pressure coefficient, c_t which is the ratio of total hydrodynamic pressure to total hydrostatic pressure at the dam reservoir interface is plotted with time in Fig. 4.44. It is interesting to note from the results that the present boundary condition is also effective at very short distance to calculate total

hydrodynamic pressure accurately. The plots in Fig. 4.45 and 4.46 show comparisons of total hydrodynamic pressure coefficient (c_t) at the dam interface for $\alpha = 0.5$ at Tc/H_f = 100, $L/H_f = 0.1$ and at $Tc/H_f = 4$, $L/H_f = 0.5$ respectively, which further confirms the accuracy of the proposed far boundary condition.

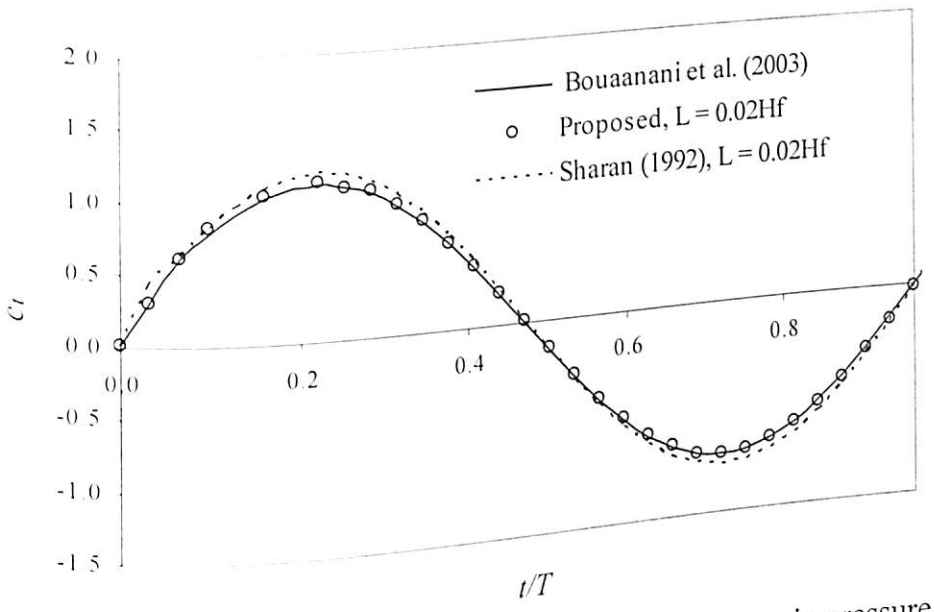

Fig. 4.44 Time history of the total hydrodynamic pressure coefficient on a vertical surface ($Tc/H_f = 200$, $\alpha = 0.5$)

Analyses are carried out for different values of Tc/H_f to study the effectiveness of the present far-boundary condition. The analyses of different cases are summarised in a tabular form along with the results for the maximum pressure coefficient c_m at the bottom of the upstream face, at a time when the magnitude of the acceleration is maximum. The results c_m presented in Table 4.5 correspond to $0.75T$, and are compared with the closed-form solution (Bouaanani et al. 2003). Table 4.5 shows the accuracy of the solution scheme using the proposed truncation boundary condition. The results indicate that the proposed far boundary condition is quite effective for all ranges of excitation frequencies. It is observed that the present far-boundary condition is capable of producing reasonably accurate results even for a relatively shorter distance away from the dam-reservoir interface, except at resonant frequency, i.e., at $Tc/H_f = 4$.

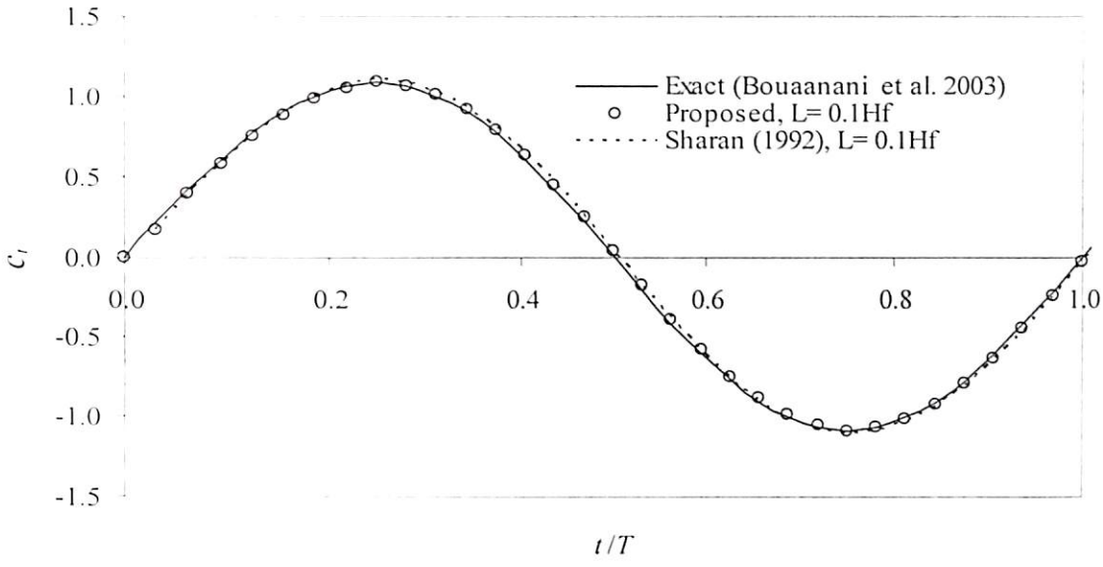

Fig. 4.45 Time history of the total hydrodynamic pressure coefficient on a vertical surface ($Tc/H_f = 100$, $\alpha = 0.5$)

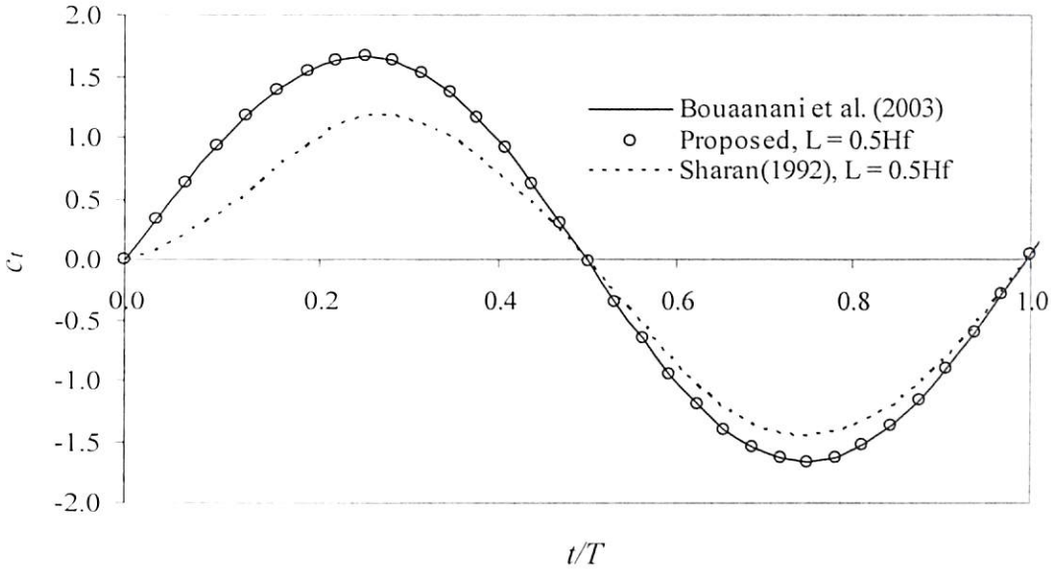

Fig. 4.46 Time history of the total hydrodynamic pressure coefficient on a vertical surface ($Tc/H_f = 4$, $\alpha = 0.5$)

Table 4.5 Comparison of truncation boundary condition for vertical surface

$\frac{Tc}{H_f}$	α	$\frac{L}{H_f}$	Mesh Size $N_v \times N_h$	Truncation Boundary Condition					
				Sommerfeld		Sharan (1992)		Proposed BC	
				c_m	% Error*	c_m	% Error*	c_m	% Error*
1	0.95	0.1	20 × 2	1.9892	1853.87	0.1552	44.64	0.1072	-0.09
		0.2	20 ×4	1.2883	1200.65	0.1251	16.59	0.1073	0.00
	0.5	0.1	20 × 2	1.2343	772.91	0.1397	-1.20	0.1397	-1.20
		0.2	20 × 4	0.2306	63.08	0.1430	1.13	0.1414	0.00
4	0.95	0.1	20 × 2	122.0610	2650.00	3.6767	-17.12	4.0648	-8.38
		0.2	20 ×4	60.7411	1270.00	4.0986	-7.61	4.3372	-2.24
		0.5	20 × 10	24.0546	442.00	4.4550	0.41	4.4368	0.01
		1.0	20 × 20	12.3857	179.00	4.4410	0.09	4.4364	0.00
	0.5	0.1	20 × 2	20.1202	1551.00	1.0129	-16.88	1.0182	-16.46
		0.2	20 × 4	9.6100	688.60	1.0299	-15.49	1.0458	-14.19
		0.5	20 × 10	1.0873	-10.74	1.2225	0.31	1.2210	0.19
		1.0	20 × 20	1.3319	9.34	1.2214	0.22	1.2204	0.14
10	0.95	0.1	20 × 2	1.7299	112.15	0.684	-16.12	0.7971	-2.26
		0.2	20 × 4	1.6351	101.21	0.8533	5.35	0.8155	0.00
	0.5	0.1	20 × 2	1.7514	116.30	0.7178	-14.16	0.7964	-1.64
		0.2	20 × 4	1.6493	103.69	0.7547	-6.79	0.8092	-0.06
100	0.95	0.02	50 × 1	8.7381	1075.96	0.6559	-11.73	0.7417	-0.18
		0.1	20 × 2	4.7213	535.39	0.7074	-4.80	0.7427	-0.06
	0.5	0.02	50 × 1	8.7410	1076.41	0.6559	-11.73	0.7417	-0.18
		0.1	20 × 2	4.7205	535.31	0.7073	-4.80	0.7424	-0.08

*Compared with closed form solution (Bouaanani et al. 2003) with values of
(i) $c_m = 0.1073$ and 0.1414 for $\alpha = 0.95$ and 0.5 respectively at $Tc/H_f = 1$
(ii) $c_m = 4.4364$ and 1.2187 for $\alpha = 0.95$ and 0.5 respectively at $Tc/H_f = 4$
(iii) $c_m = 0.8155$ and 0.8097 for $\alpha = 0.95$ and 0.5 respectively at $Tc/H_f = 10$
(iv) $c_m = 0.7431$ and 0.7430 for $\alpha = 0.95$ and 0.5 respectively at $Tc/H_f = 100$

It is further noted that the reflection coefficient of the reservoir bottom affects the accuracy of the solution at excitation frequencies higher than the fundamental frequency of the reservoir. These conclusions are in agreement with Sharan (1992) carried out in the frequency domain analysis. At lower excitation frequencies (Tc/H_f = 10, 100), the reflection coefficient does not have much effect on the accuracy of the results obtained. It can thus be concluded that the present truncation boundary condition can effectively

account for the effect of the reservoir bottom absorption for all the important frequency range that is significant in earthquake response analysis of dams.

A convergence test with respect to the truncated length of the reservoir (L/H_f) of the finite element model is conducted for different values of Tc/H_f. The maximum hydrodynamic pressure coefficients (c_m) obtained for different values of Tc/H_f and with different L/H_f are also plotted in Figs. 4.47- 4.50 for reflection coefficient values of 0.95 and 0.5. It is interesting to note that the results obtained by the present TBC are undistinguishable from the exact solution at $\alpha = 0.5$ and 0.95 for $Tc/H_f = 100$ (Figs. 4.47 and 4.49) even at a very closer distance. At the resonant frequency, having $\alpha = 0.5$ and 0.95, the present TBC and the Sharan's TBC are observed to be convergent at $L = 0.5H_f$ (Figs. 4.48 and 4.50). The proposed TBC has the advantage of producing accurate results for very low to very high ranges of frequencies including resonant frequency for both the highly absorptive and reflective reservoir bottom cases.

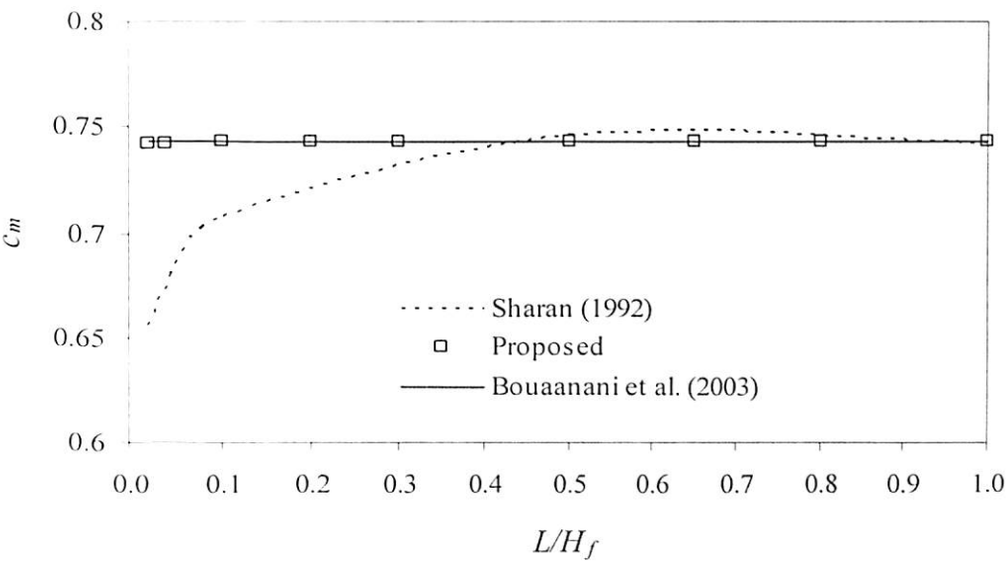

Fig. 4.47 Convergence of hydrodynamic pressure at the base ($Tc/H_f = 100$, $\alpha = 0.95$)

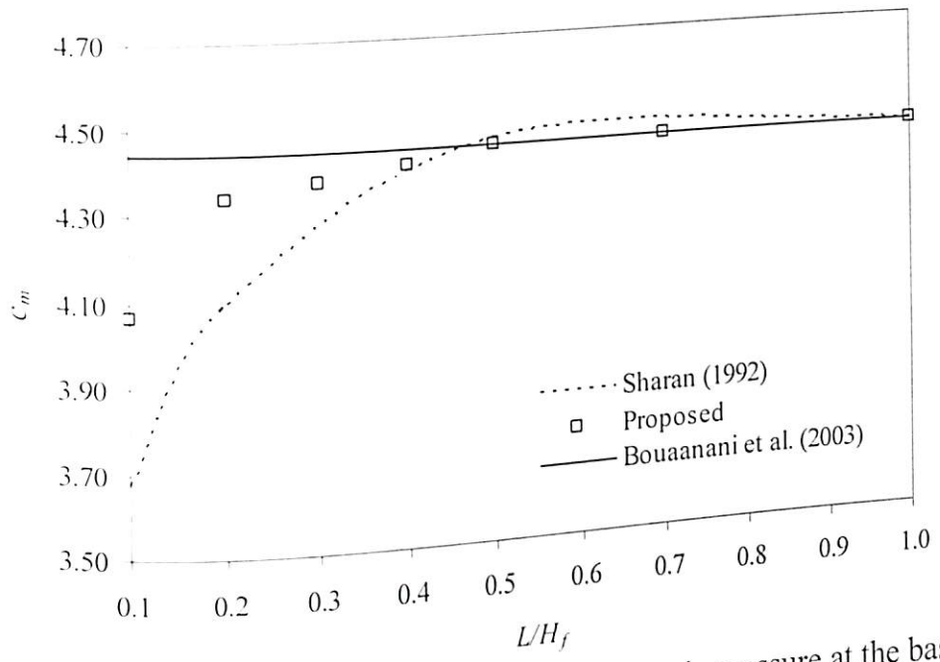

Fig. 4.48 Convergence of hydrodynamic pressure at the base ($Tc/H_f = 4,\ \alpha = 0.95$)

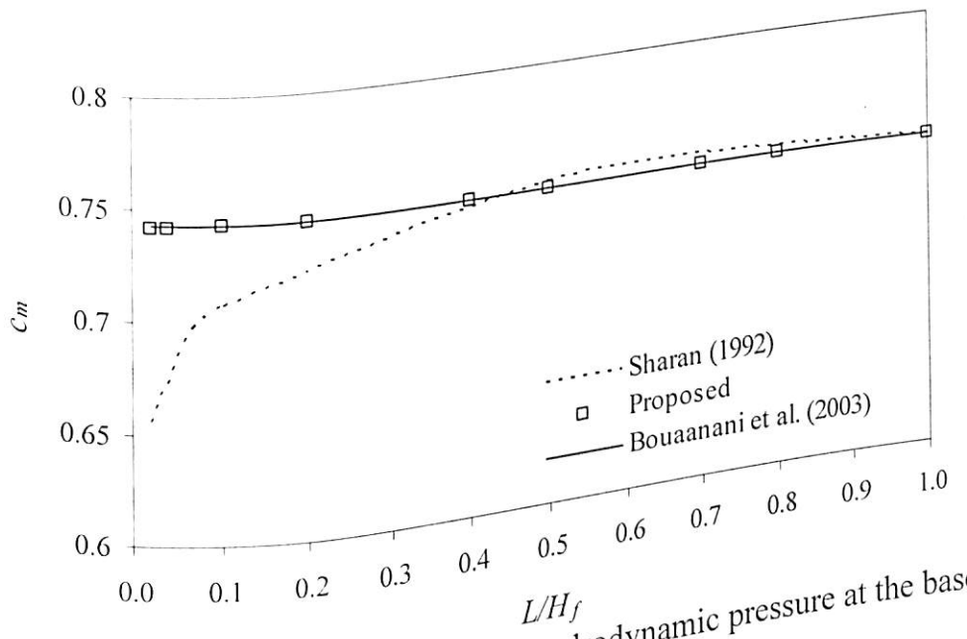

Fig. 4.49 Convergence of hydrodynamic pressure at the base ($Tc/H_f = 100,\ \alpha = 0.5$)

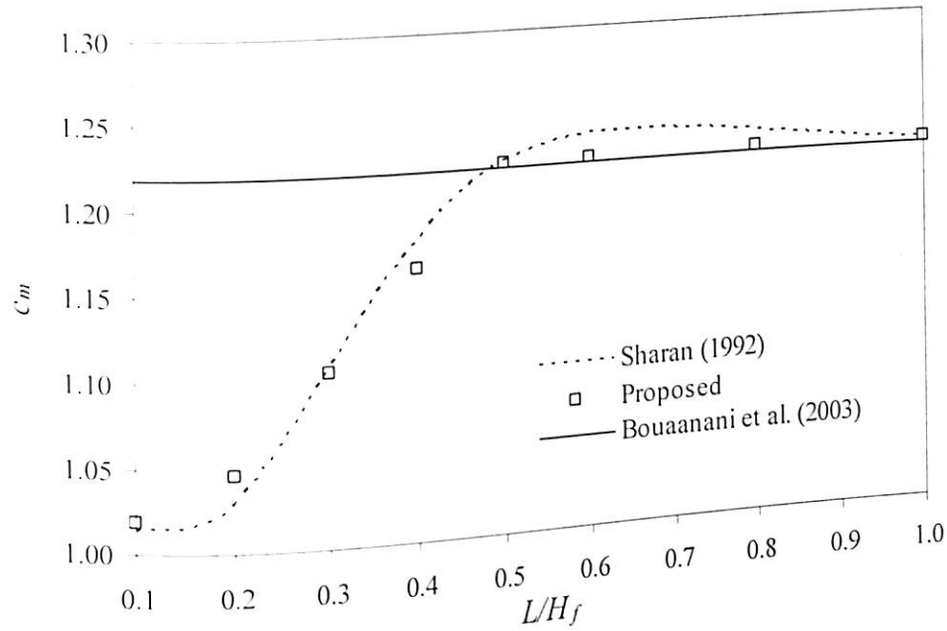

Fig. 4.50 Convergence of hydrodynamic pressure at the base (Tc/H_f = 4, α = 0.5)

4.2.4 Hydrodynamic Pressure with Inclined Dam-Reservoir Interface

The inclination of the dam-reservoir interface (Fig. 4.51) would have effect on the development of hydrodynamic pressure (Chwang 1978 and Sharan 1992). No classical solution considering reservoir bottom effect for inclined upstream face is observed in the open literature accessible to the author. The effectiveness of the proposed TBC is tested by comparing the hydrodynamic pressure coefficients ($c_b = p_b/\rho a H_f$) evaluated at a large distance ($L \geq 3.0H_f$) using Sommerfeld boundary condition. p_b is the hydrodynamic pressure at the bottom of the dam-reservoir interface. The hydrodynamic pressure at the base of the inclined upstream dam face for different Tc/H_f ratios and inclinations are presented in tabular form in Tables 4.6 - 4.7 and in graphical form in Figs. 4.52 - 4.59. The results show that the infinite reservoir may be truncated at a relatively closer distance away from the structure in case of lower excitation frequency i.e., at Tc/H_f = 100 (Figs. 4.52, 4.53). Further, it is observed that at resonant frequency i.e., at Tc/H_f = 4.0, the accuracy on the development of hydrodynamic pressure is less at a closer distance (Figs. 4.54 - 4.57). Thus, a length of reservoir equal to half of its depth should be considered for a fully inclined dam for accurate evaluation of hydrodynamic pressure at resonant frequency. At Tc/H_f =1.0, it is observed from Figs. 4.58 and 4.59 that convergence is obtained within a very short length of reservoir ($L = 0.1H_f$). However,

since the proposed TBC is derived assuming upstream face of the reservoir to be vertical, the accuracy and effectiveness of the TBC decreases with the increase in dam inclination. It is also noted that for higher absorption of the reservoir bottom and at excitation frequencies away from the first natural frequency of the reservoir, the error of the proposed TBC is reduced.

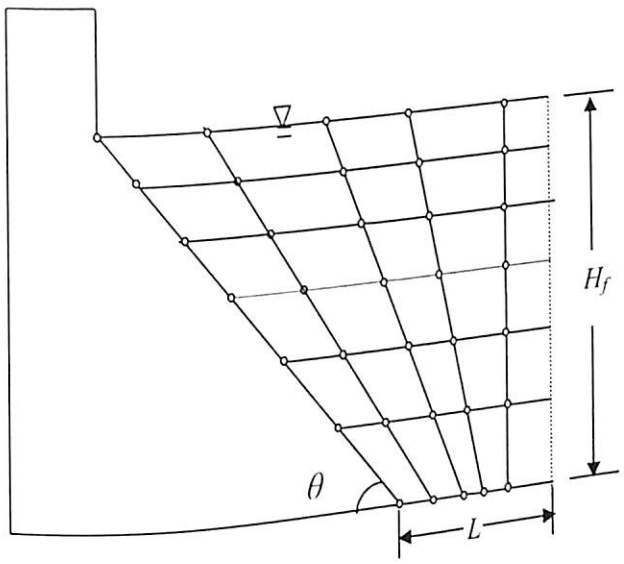

Fig. 4.51 Typical Finite element mesh of infinite reservoir with inclined upstream dam face

The hydrodynamic pressure distribution along the inclined dam-reservoir interface is shown in Figs. 4.60 to 4.62 for different cases under resonant frequency i.e., at $Tc/H_f = 4$ to study the effectiveness of the proposed truncation boundary condition (TBC). The graphical results show that the convergence of the results is quite impressive at resonant frequency also as compared to the existing far boundary conditions. The development of hydrodynamic pressure for different angles of dam inclination are plotted in Fig.4.63 for $Tc/H_f = 100$ and $\alpha = 0.5$, which show that the hydrodynamic pressure is decreased with the decrease of θ, i.e., with an increase of dam inclination. The pressure contours in the reservoir are plotted for inclined upstream face of the dam in Figs. 4.64 and 4.65. The plots show that the effect of sediment layers lying in the reservoir bottom is to reduce the magnitude of hydrodynamic pressure developed in the reservoir.

Table 4.6 Comparison of truncation boundary condition for inclined surface ($\theta = 60°$)

$\frac{Tc}{H_f}$	α	$\frac{L}{H_f}$	Truncation Boundary Condition					
			Sommerfeld		Sharan (1992)		Proposed BC	
			c_b	% Error*	c_b	% Error*	c_b	% Error*
1	0.95	0.10	0.1187	14.24	0.1056	1.64	0.1040	0.10
		0.50	0.1037	-0.19	0.1041	0.19	0.1039	0.00
	0.5	0.10	0.1420	2.53	0.1398	0.94	0.1391	0.43
		0.50	0.1390	0.36	0.1390	0.36	0.1390	0.36
4	0.95	0.10	0.6439	-45.64	0.5462	-53.89	0.7431	-37.27
		0.50	0.7195	-39.26	0.6519	-44.97	1.1954	0.91
		1.00	0.9942	-16.07	1.1914	0.57	1.1856	0.08
	0.5	0.10	0.6572	-27.68	0.4862	-46.49	0.5065	-44.26
		0.50	0.7091	-21.97	0.8401	-7.55	0.9080	-0.08
		1.00	0.8771	-3.48	0.9080	-0.08	0.9080	-0.08
10	0.95	0.1	0.8093	55.40	0.4765	-8.51	0.4788	-8.06
		0.5	0.6176	18.59	0.4953	-4.90	0.4954	-4.88
		1.0	0.5455	4.74	0.5251	0.83	0.5186	-0.42
	0.5	0.1	0.8091	57.02	0.4753	-7.76	0.4775	-7.34
		0.5	0.6172	19.77	0.4947	-4.00	0.5252	0.84
		1.0	0.5452	5.80	0.5183	0.58	0.5183	0.58
100	0.95	0.02	1.5045	219.40	0.4456	-5.40	0.4517	-4.11
		0.2	0.8925	89.47	0.4699	-0.24	0.4710	-0.00
	0.5	0.02	1.5045	219.41	0.4456	-5.40	0.4517	-4.10
		0.2	0.8925	89.48	0.4699	-0.24	0.4710	-0.00

*Compared with with values of c_b computed by FEM using Sommerfeld or Present TBC at $L = 3.0H_f$

(i) $c_b = 0.1039$ and 0.1385 for $\alpha = 0.95$ and 0.5 respectively at $Tc/H_f = 1$
(ii) $c_b = 1.1846$ and 0.9087 for $\alpha = 0.95$ and 0.5 respectively at $Tc/H_f = 4$
(iii) $c_b = 0.5208$ and 0.5153 for $\alpha = 0.95$ and 0.5 respectively at $Tc/H_f = 10$
(iv) $c_b = 0.4710$ and 0.4710 for $\alpha = 0.95$ and 0.5 respectively at $Tc/H_f = 100$

Table 4.7 Comparison of truncation boundary condition for inclined surface ($\theta = 30°$)

$\frac{Tc}{H_f}$	α	$\frac{L}{H_f}$	Truncation Boundary Condition					
			Sommerfeld		Sharan (1992)		Proposed BC	
			c_b	% Error*	c_b	% Error*	c_b	% Error*
1	0.95	0.1	0.0663	-7.30	0.0606	-15.30	0.0695	-2.80
		0.5	0.0715	0.00	0.0715	0.00	0.0715	0.00
	0.5	0.1	0.1288	-4.17	0.1336	-0.60	0.1335	-0.67
		0.5	0.1466	9.08	0.1336	-0.60	0.1339	-0.37
4	0.95	0.1	0.5242	-37.06	0.3310	-60.26	0.5164	-38.00
		0.5	0.6133	-26.37	0.4269	-48.75	0.5975	-28.26
		1.0	0.8090	-2.87	0.8332	0.04	0.8332	0.04
	0.5	0.1	0.3216	-36.88	0.1996	-60.82	0.2371	-53.46
		0.5	0.4572	-10.26	0.4675	-8.24	0.5073	-0.43
		1.0	0.5407	-6.12	0.5077	-0.35	0.5090	-0.09
10	0.95	0.1	0.3622	37.82	0.2291	-12.82	0.2292	-12.79
		0.5	0.3025	15.11	0.2493	-5.14	0.2581	-1.79
		1.0	0.2802	6.62	0.2605	-0.88	0.2605	-0.88
	0.5	0.1	0.3620	41.79	0.2287	-10.42	0.2287	-10.42
		0.5	0.3024	18.45	0.2490	-2.47	0.2550	-0.12
		1.0	0.2800	9.67	0.2588	1.37	0.2555	0.08
100	0.95	0.02	0.5311	121.29	0.1714	-28.58	0.1715	-28.54
		0.20	0.3794	58.08	0.2408	0.33	0.2393	-0 .29
	0.5	0.02	0.5311	121.66	0.1714	-28.46	0.1715	-28.42
		0.20	0.3794	58.35	0.2394	0.13	0.2394	0.13

*Compared with with values of c_b computed by FEM using Sommerfeld or Present TBC at $L = 3.0H_f$

(i) $c_b = 0.0715$ and 0.1344 for $\alpha = 0.95$ and 0.5 respectively at $Tc/H_f = 1$

(ii) $c_b = 0.8329$ and 0.5095 for $\alpha = 0.95$ and 0.5 respectively at $Tc/H_f = 4$

(iii) $c_b = 0.2628$ and 0.2553 for $\alpha = 0.95$ and 0.5 respectively at $Tc/H_f = 10$

(iv) $c_b = 0.2400$ and 0.2400 for $\alpha = 0.95$ and 0.5 respectively at $Tc/H_f = 100$

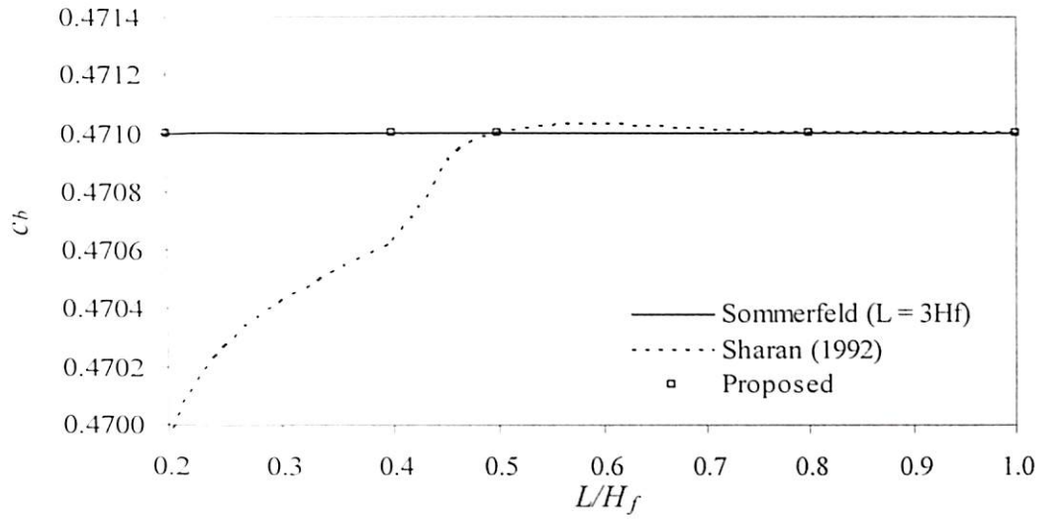

Fig. 4.52 Convergence of hydrodynamic pressure at the base of dam (Tc/H_f = 100, α = 0. 95, θ = 60°)

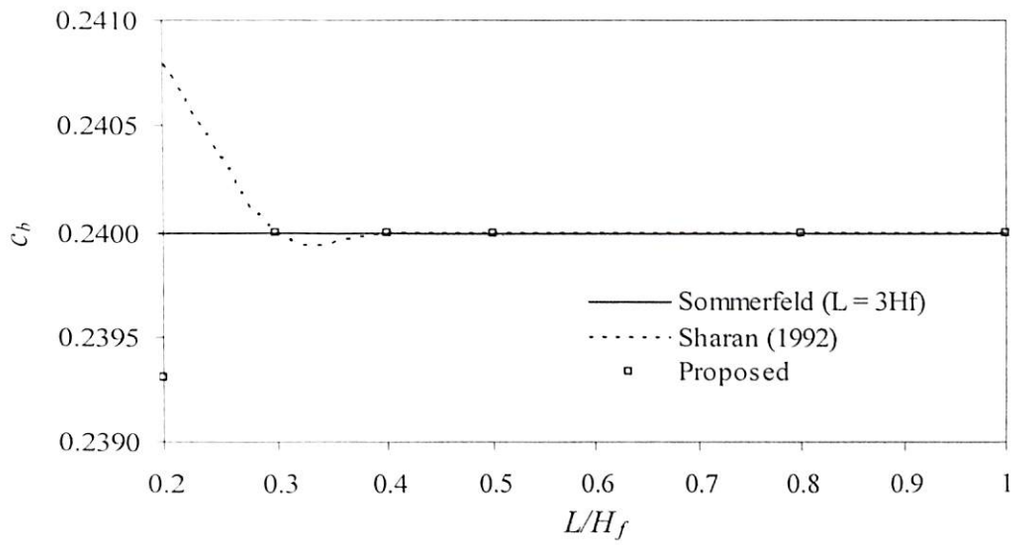

Fig. 4.53 Convergence of hydrodynamic pressure at the base of dam (Tc/H_f = 100, α = 0. 95, θ = 30°)

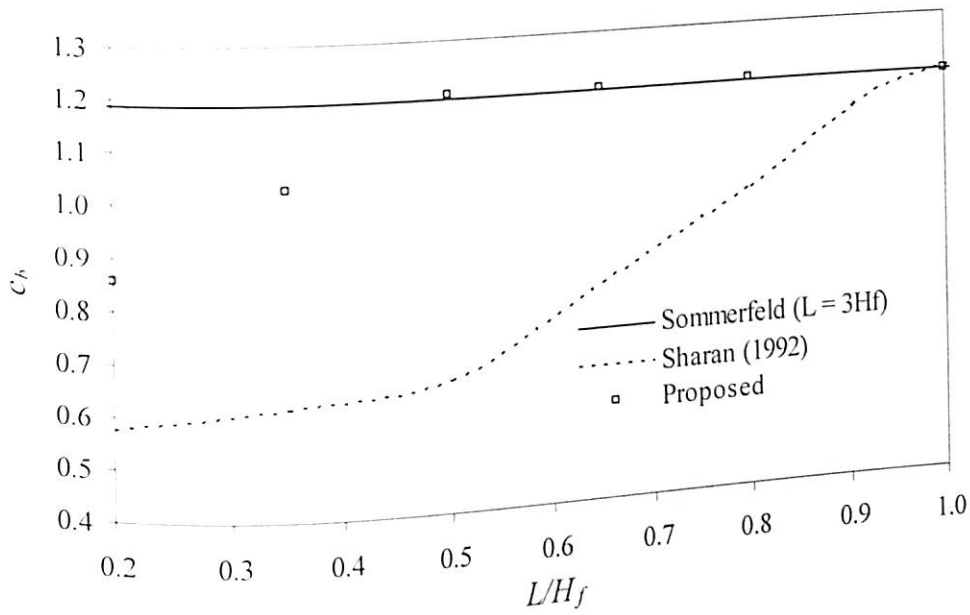

Fig. 4.54 Convergence of hydrodynamic pressure at the base of dam ($Tc/H_f = 4$, $\alpha = 0.95$, $\theta = 60°$)

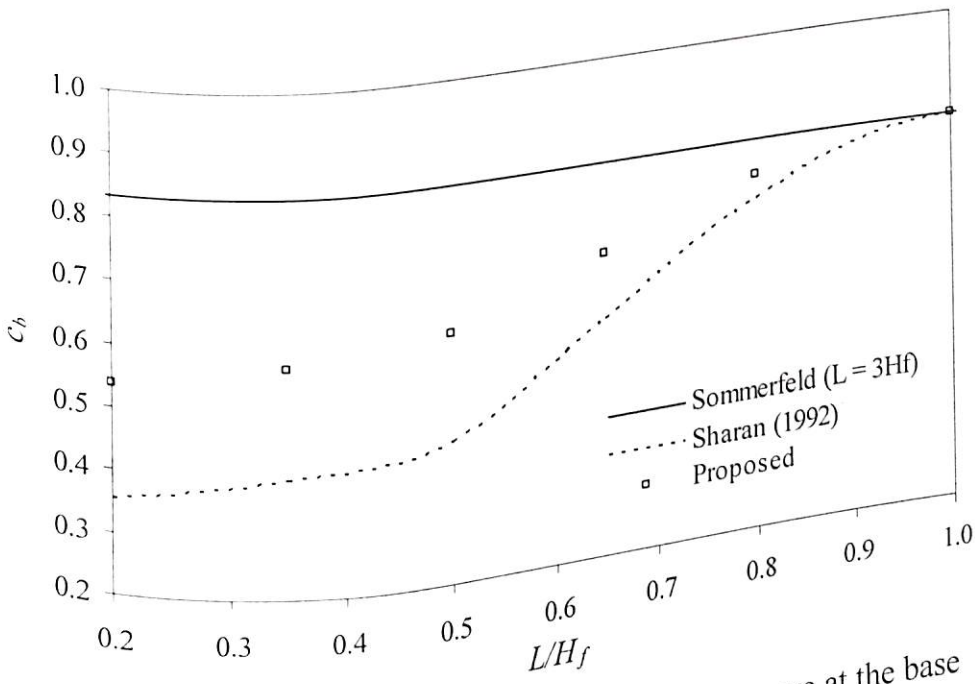

Fig. 4.55 Convergence of hydrodynamic pressure at the base of dam ($Tc/H_f = 4$, $\alpha = 0.95$, $\theta = 30°$)

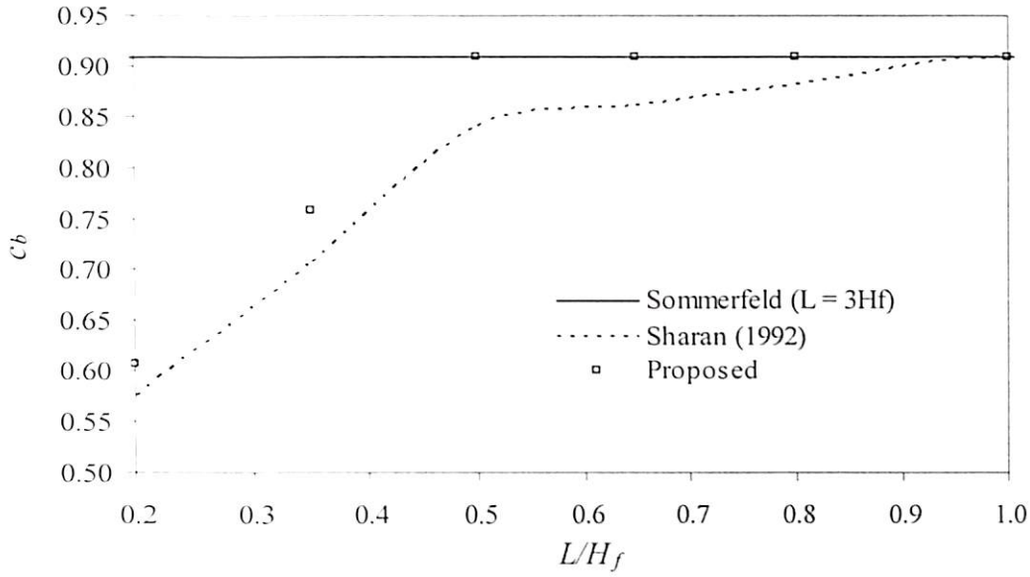

Fig. 4.56 Convergence of hydrodynamic pressure at the base of dam ($Tc/H_f = 4$, $\alpha = 0.5$, $\theta = 60°$)

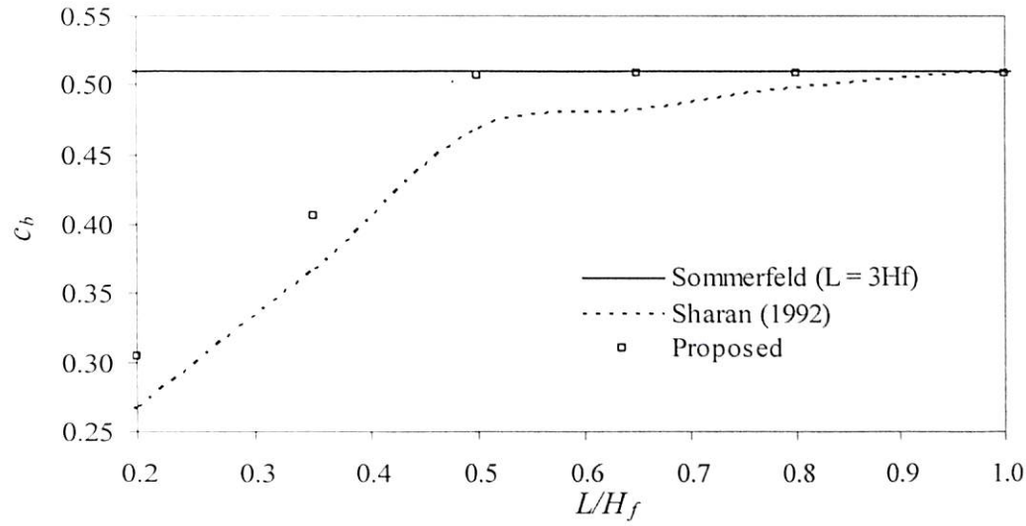

Fig. 4.57 Convergence of hydrodynamic pressure at the base of dam ($Tc/H_f = 4$, $\alpha = 0.5$, $\theta = 30°$)

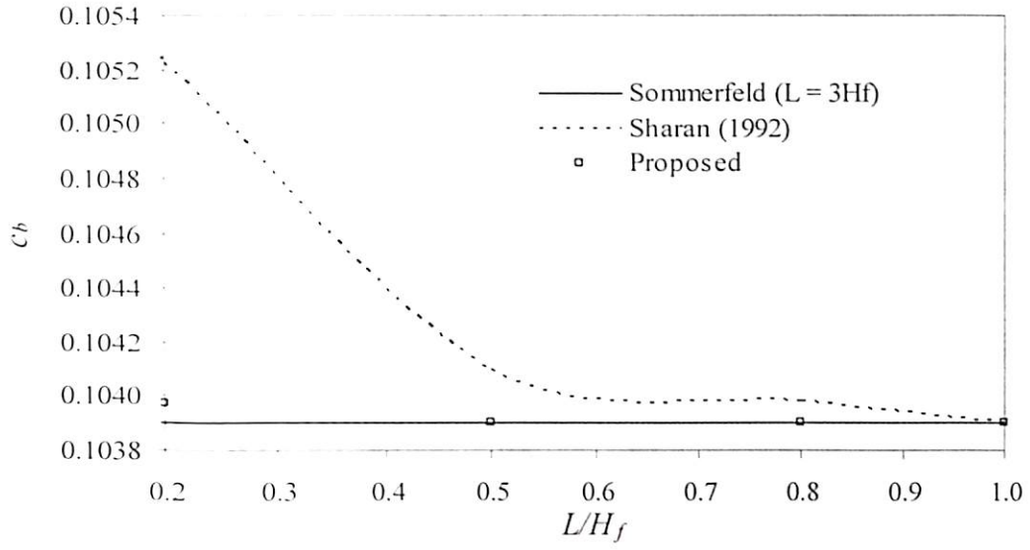

Fig. 4.58 Convergence of hydrodynamic pressure at the base of dam ($Tc/H_f = 1$, $\alpha = 0.95$, $\theta = 60°$)

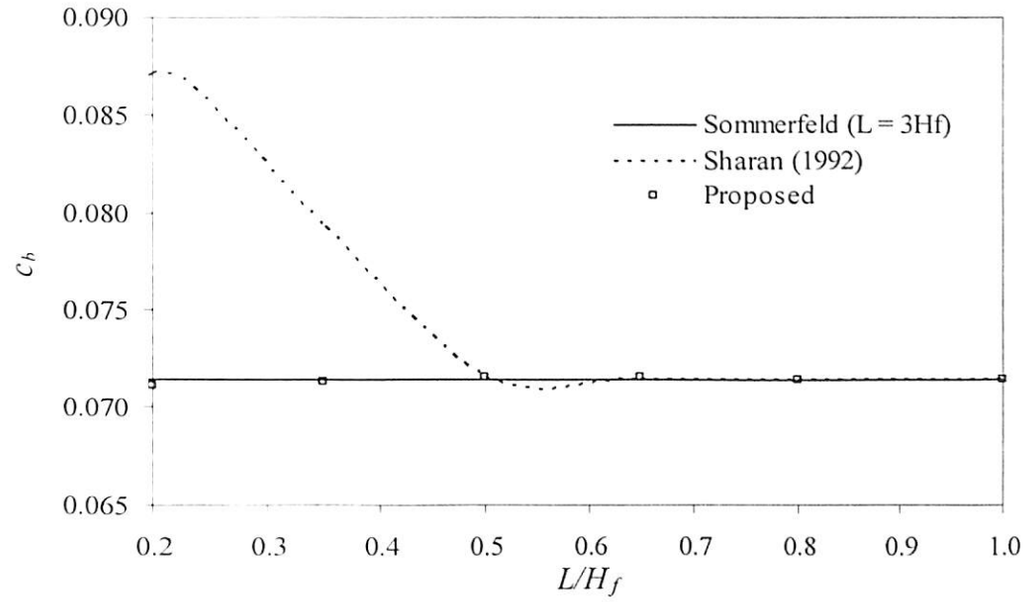

Fig. 4.59 Convergence of hydrodynamic pressure at the base of dam ($Tc/H_f = 1$, $\alpha = 0.95$, $\theta = 30°$)

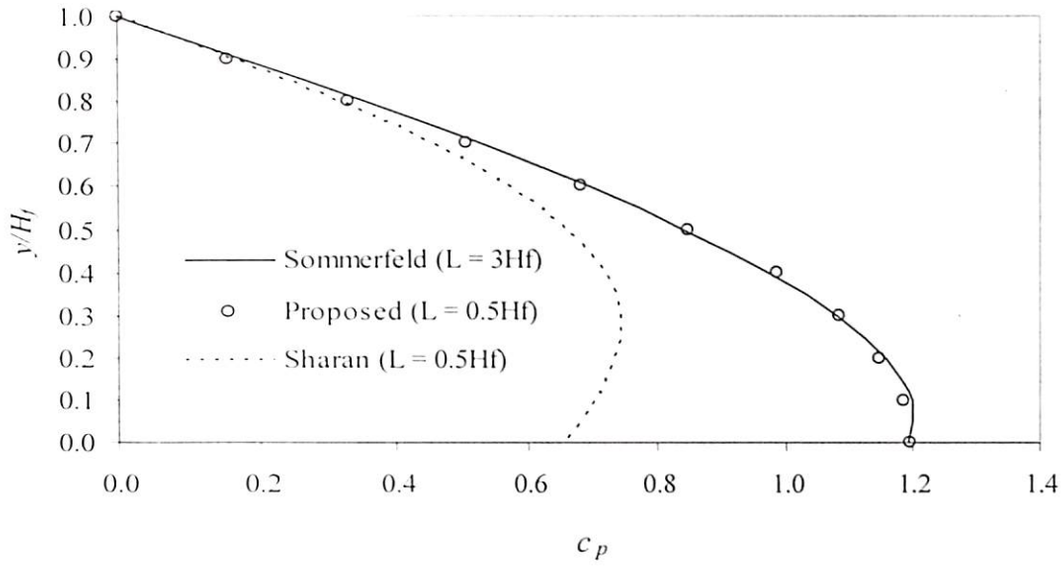

Fig. 4.60 Hydrodynamic pressure distribution along an inclined upstream dam face ($Tc/H_f = 4$, $\alpha = 0.95$, $\theta = 60°$)

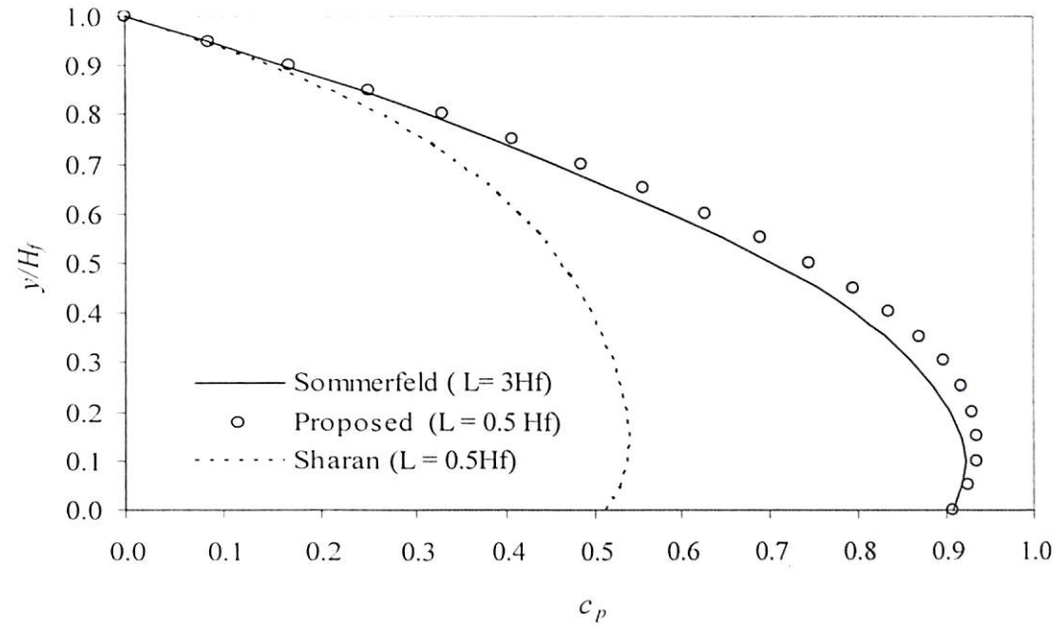

Fig. 4.61 Hydrodynamic pressure distribution along an inclined upstream dam face ($Tc/H_f = 4$, $\alpha = 0.5$, $\theta = 60°$)

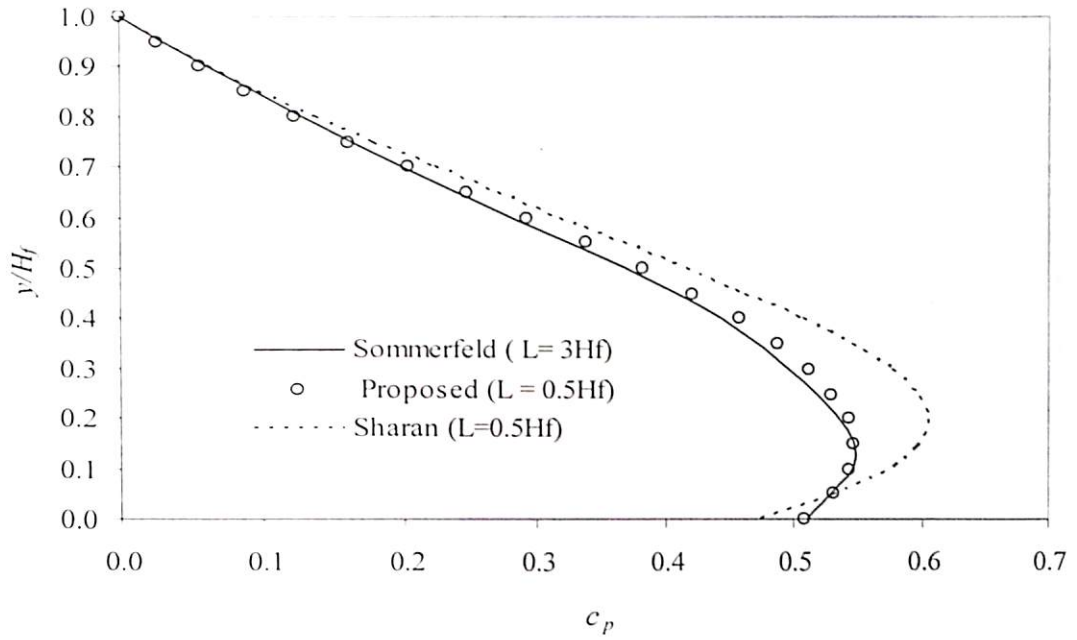

Fig. 4.62 Hydrodynamic pressure distribution along an inclined upstream dam face ($Tc/H_f = 4$, $\alpha = 0.5$, $\theta = 30°$)

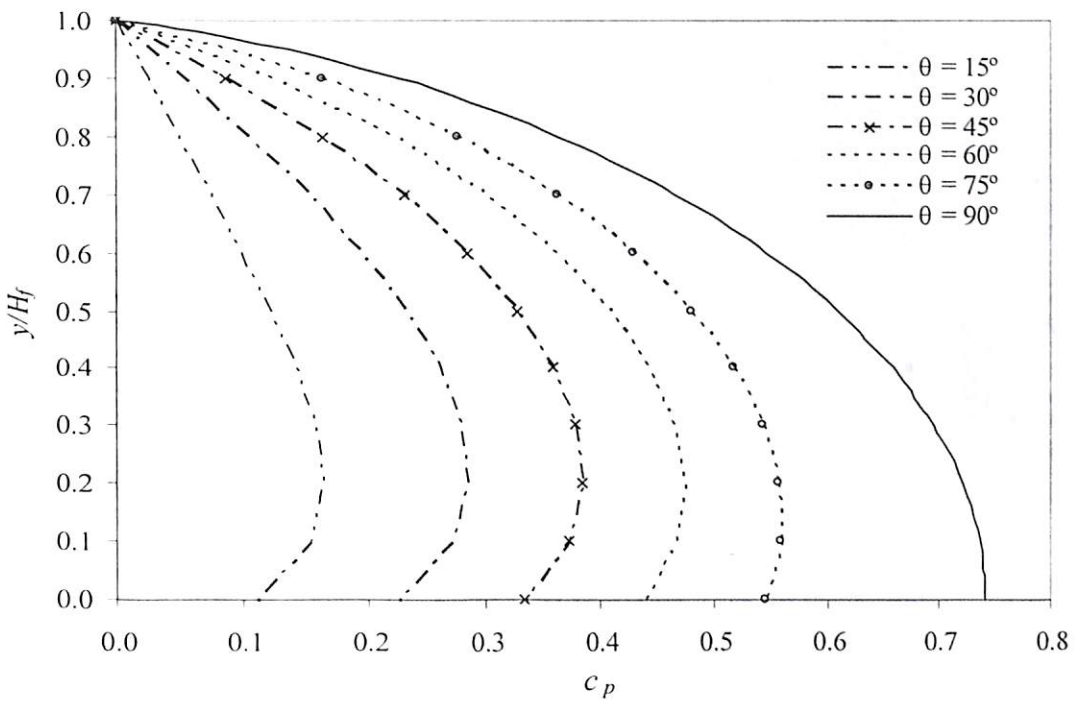

Fig. 4.63 Effect of dam-reservoir interface inclination on hydrodynamic pressure distribution ($Tc/H_f = 100$, $\alpha = 0.5$)

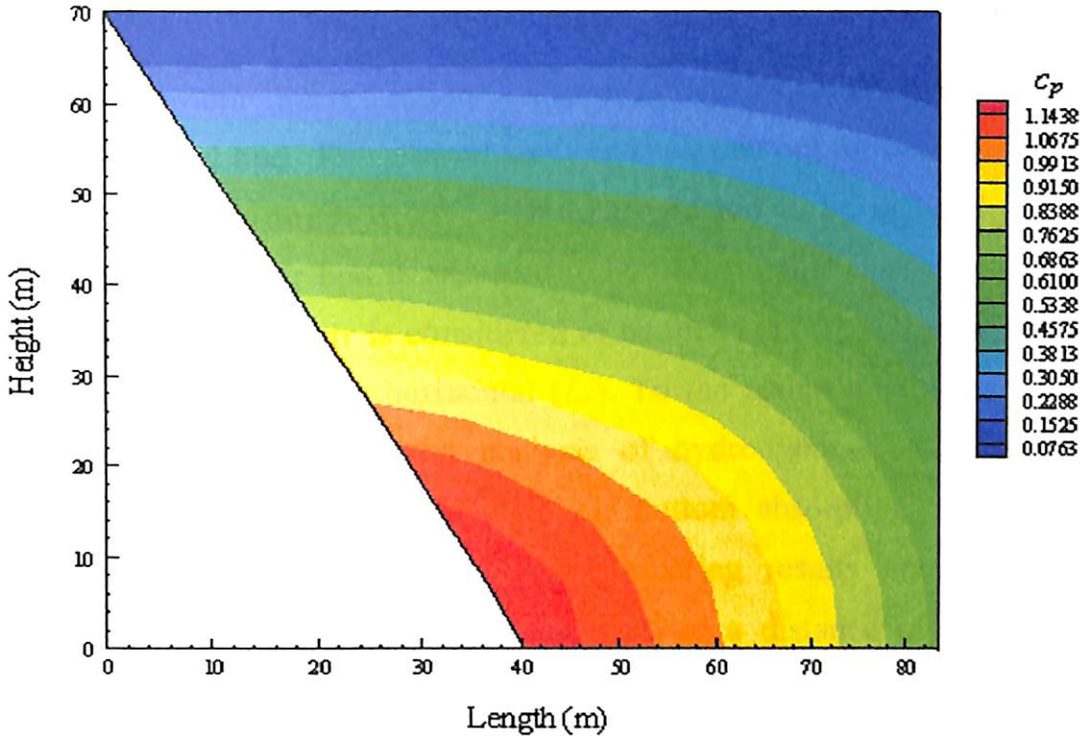

Fig. 4.64 Pressure contours in the reservoir with inclined upstream face of the dam ($Tc/H_f = 4$, $\alpha = 0.95$, $\theta = 60°$, $t = 0.75T$ seconds)

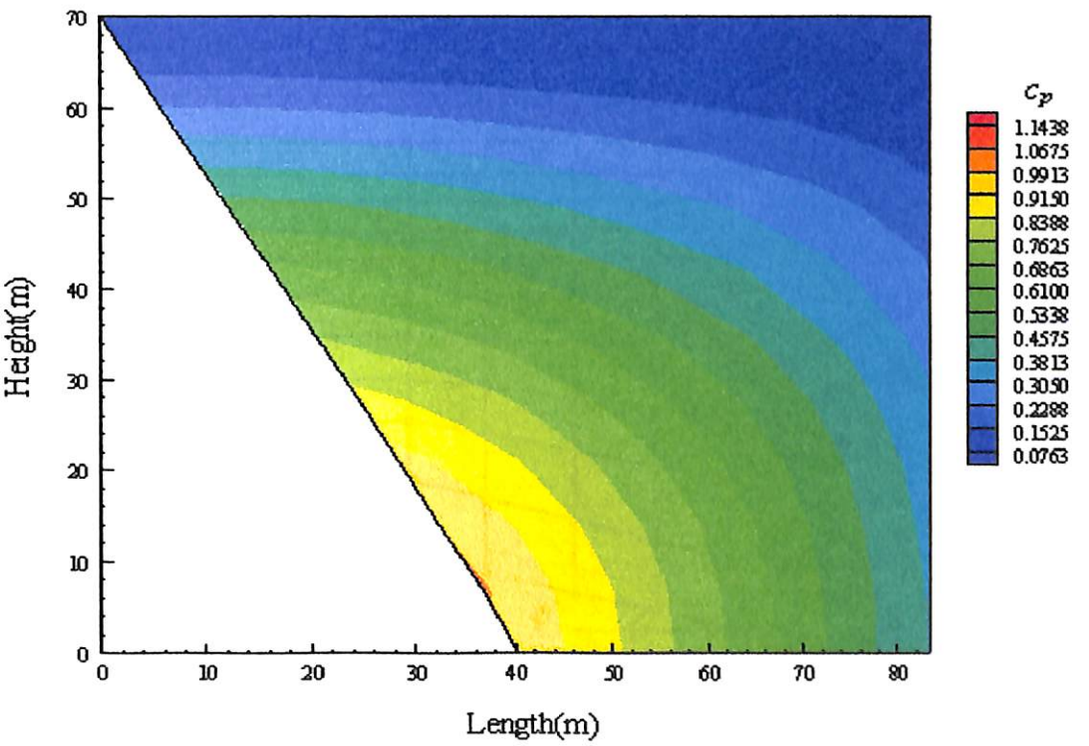

Fig. 4.65 Pressure contours in the reservoir with inclined upstream face of the dam ($Tc/H_f = 4$, $\alpha = 0.5$, $\theta = 60°$, $t = 0.75T$ seconds)

4.2.5 Hydrodynamic Pressure with Inclined Reservoir Bed

A typical finite element discretization is shown in Fig. 4.66 for the analysis of infinite reservoir with inclined bed. The present analysis is carried out for two cases: (i) length of reservoir up to half the depth of reservoir is considered to be inclined (L_{hi} = 0.5 H_f), beyond which the reservoir bed is assumed to be horizontal (L_h), (ii) length of reservoir equal to the depth of reservoir is considered to be inclined (L_{hi} = H_f), beyond which the reservoir bed is assumed to be horizontal (L_h). To the author's knowledge, there is no classical solution available for the analysis of hydrodynamic pressure for a non-horizontal reservoir bed considering reservoir bottom absorption effects. Hence, the parametric study has been conducted by comparing results obtained by applying Sommerfeld boundary condition or present TBC at a distance of $L = 3.0H_f$, which produce identical results. Since the effect of reservoir bottom is almost negligible for values of Tc/H_f very higher or lower than 4, as is evident from the preceding cases, here only Tc/H_f = 10, 4 and 1 is considered and results are shown in graphical forms. Here, the reservoir bed inclination is considered $+\phi'$ for upward and $-\phi'$ for downward direction.

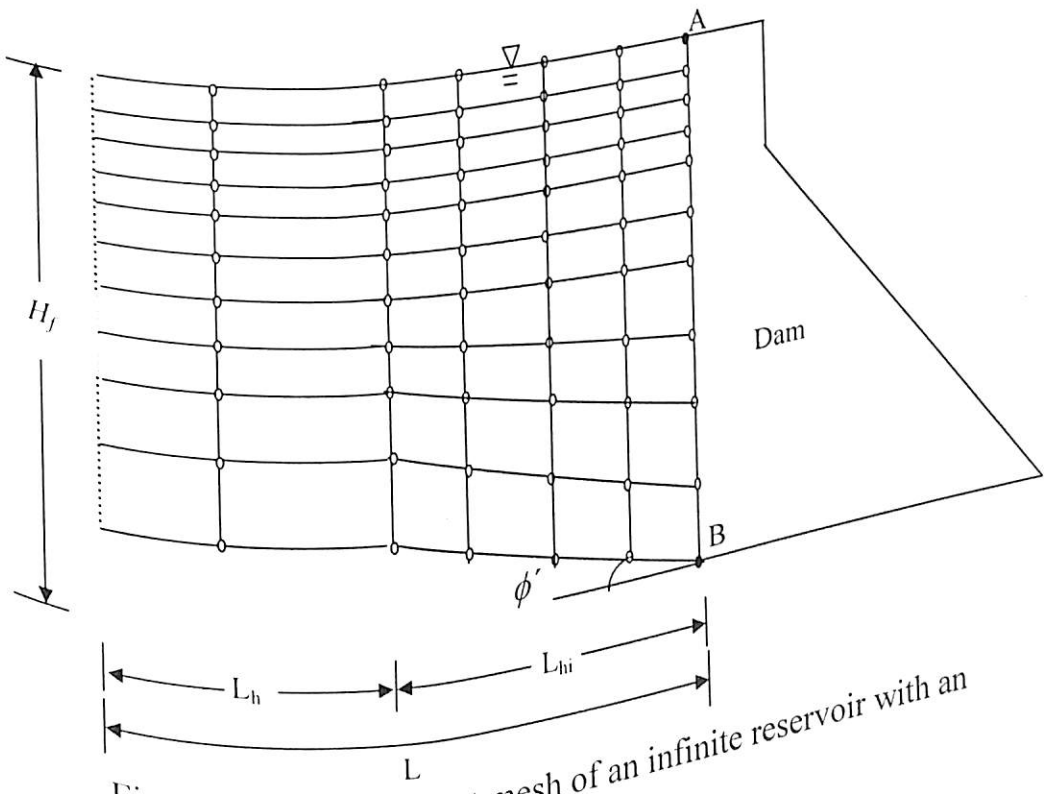

Fig. 4.66 Finite element mesh of an infinite reservoir with an inclined reservoir bed

For the first case when the length of inclined bed is equal to half the depth of the reservoir, the pressure distribution for $Tc/H_f = 10$ and $\alpha = 0.5$ are plotted in Figs. 4.67 to 4.74 for different directions (upward and downward) and magnitudes of bed inclinations. The hydrodynamic pressure distributions are obtained for the case when the length of the inclined reservoir bed is equal to half the depth of reservoir and are plotted from Figs. 4.67 to 4.74. It is observed from the graphical results that (i) the accuracy of pressure distribution obtained at the upstream dam face reduces with an increase in reservoir bed inclination; (ii) the hydrodynamic pressure increases with an upward inclination of the reservoir bed i.e., for $+\phi'$ whereas the hydrodynamic pressure reduces for a downward inclination of the reservoir bed i.e., for $-\phi'$ and (iii) a reservoir length equal to half of its depth gives pressure distribution along the depth of the reservoir with negligible error. The distribution of pressure coefficients in the reservoir for different directions of reservoir bed inclination are plotted in the form of contours in Figs. 4.75 and 4.76.

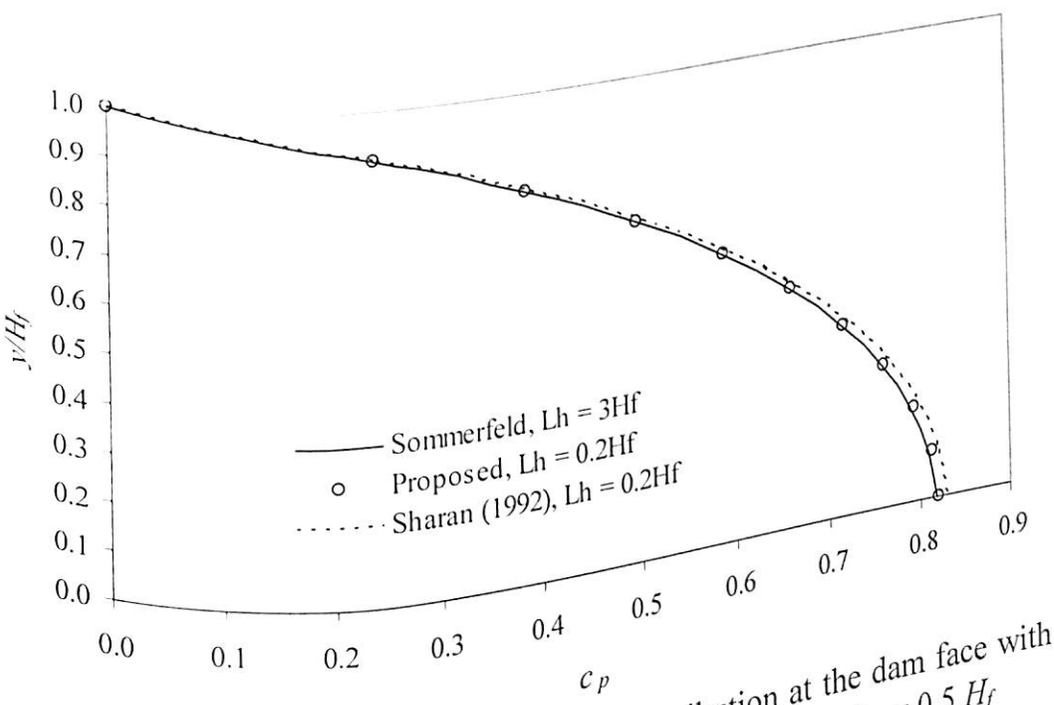

Fig. 4.67 Hydrodynamic pressure distribution at the dam face with reservoir bed slope of $\phi' = +1°$, $Tc/H_f = 10$, $\alpha = 0.5$, $L_{hi} = 0.5\ H_f$

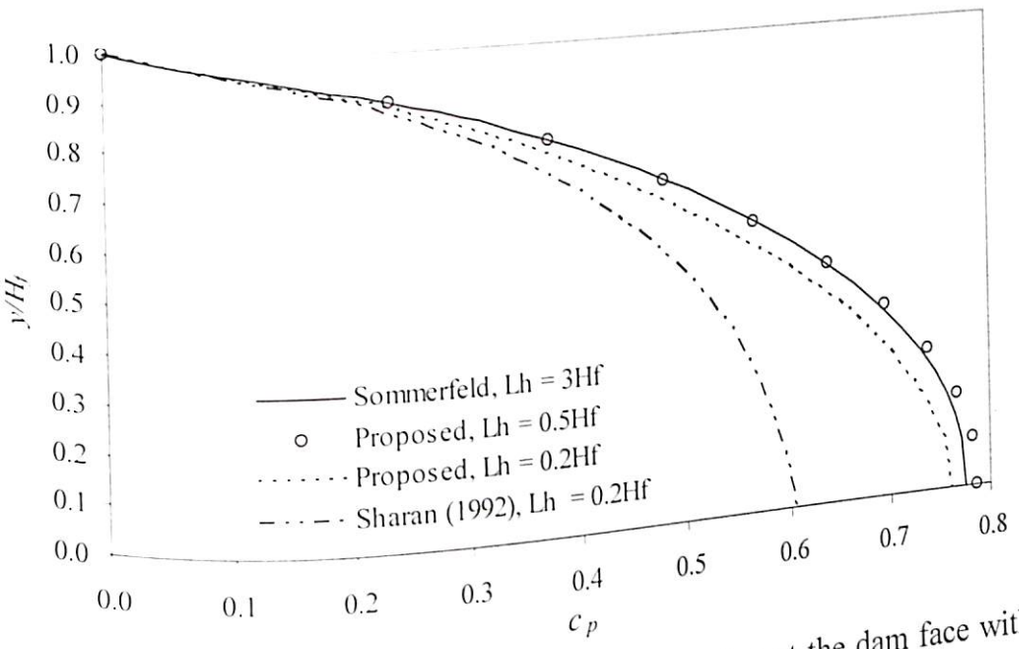

Fig. 4.68 Hydrodynamic pressure distribution at the dam face with reservoir bed slope of $\phi' = -1°$, Tc/H_f=10, $\alpha = 0.5$, $L_{hi} = 0.5\ H_f$

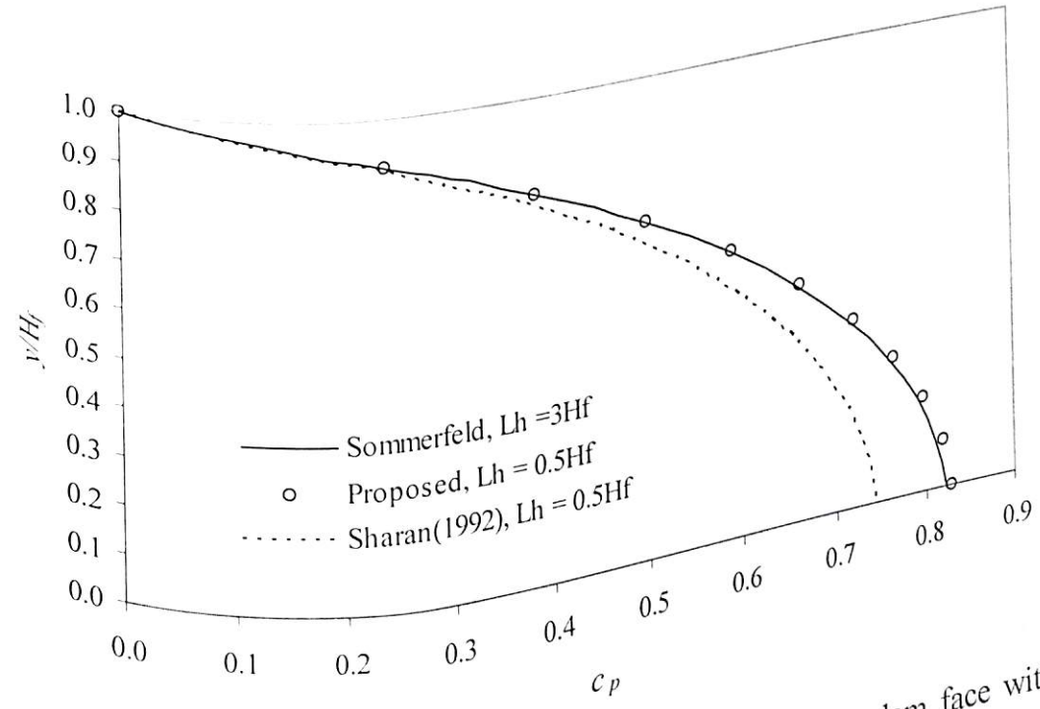

Fig. 4.69 Hydrodynamic pressure distribution at the dam face with reservoir bed slope of $\phi' = +3.3°$, Tc/H_f=10, $\alpha = 0.5$, $L_{hi} = 0.5\ H_f$

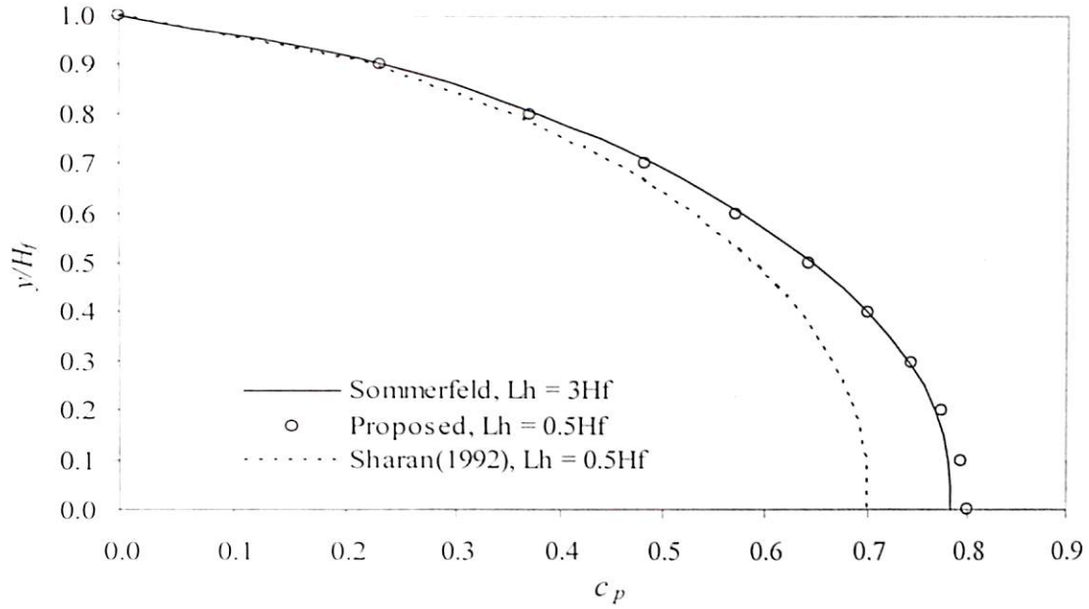

Fig. 4.70 Hydrodynamic pressure distribution at the dam face with reservoir bed slope of $\phi' = -3.3°$, $Tc/H_f = 10$, $\alpha = 0.5$, $L_{hi} = 0.5\ H_f$

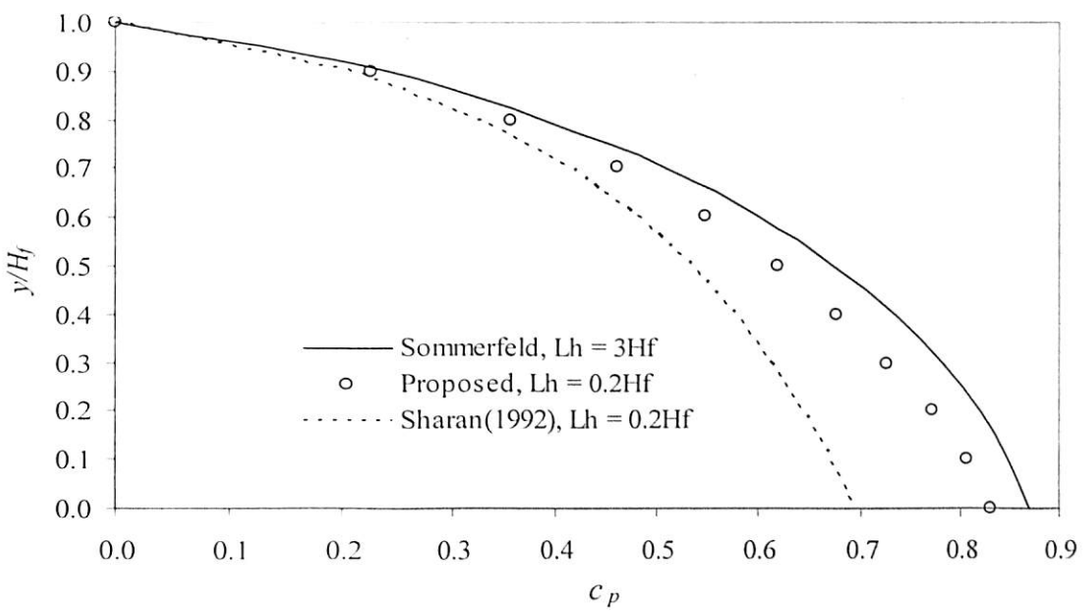

Fig. 4.71 Hydrodynamic pressure distribution at the dam face with reservoir bed slope of $\phi' = +10°$, $Tc/H_f = 10$, $\alpha = 0.5$, $L_{hi} = 0.5\ H_f$

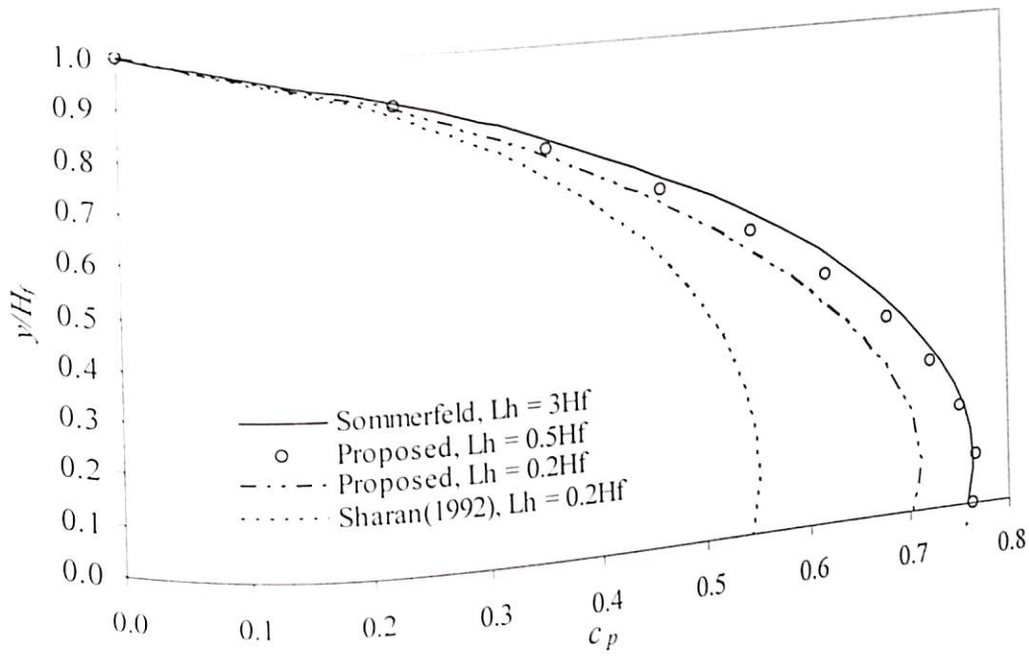

Fig. 4.72 Hydrodynamic pressure distribution at the dam face with reservoir bed slope of $\phi' = -10°$, $Tc/H_f = 10$, $\alpha = 0.5$, $L_{hi} = 0.5\ H_f$

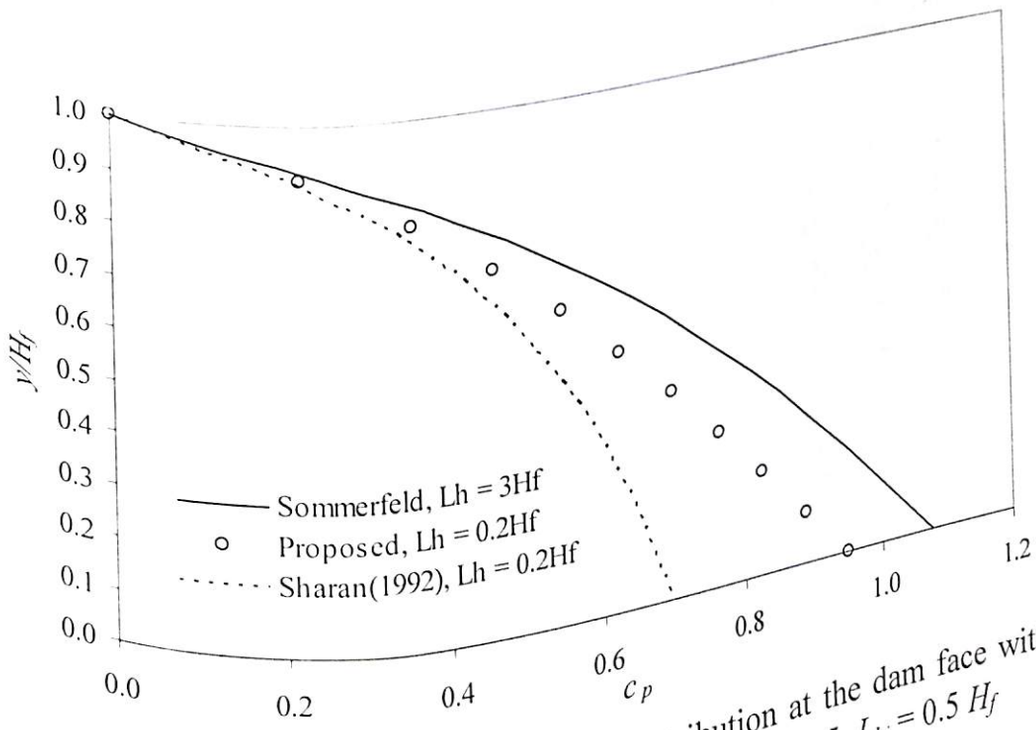

Fig. 4.73 Hydrodynamic pressure distribution at the dam face with reservoir bed slope of $\phi' = +30°$, $Tc/H_f = 10$, $\alpha = 0.5$, $L_{hi} = 0.5\ H_f$

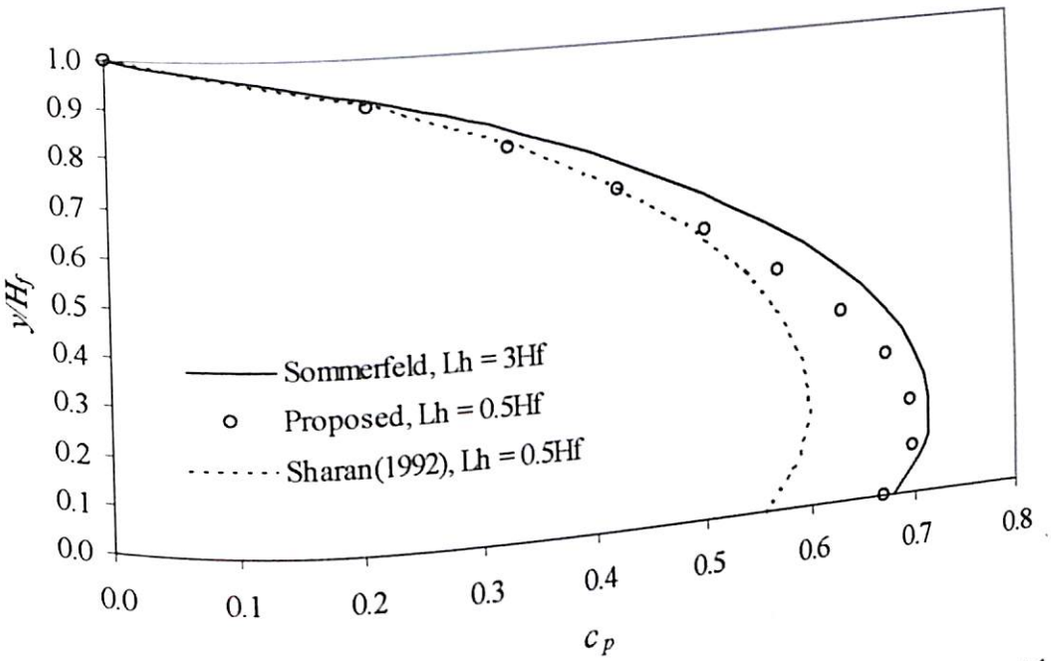

Fig. 4.74 Hydrodynamic pressure distribution at the dam face with reservoir bed slope of $\phi' = -30°$, Tc/H_f=10, $\alpha = 0.5$, $L_{hi} = 0.5\ H_f$

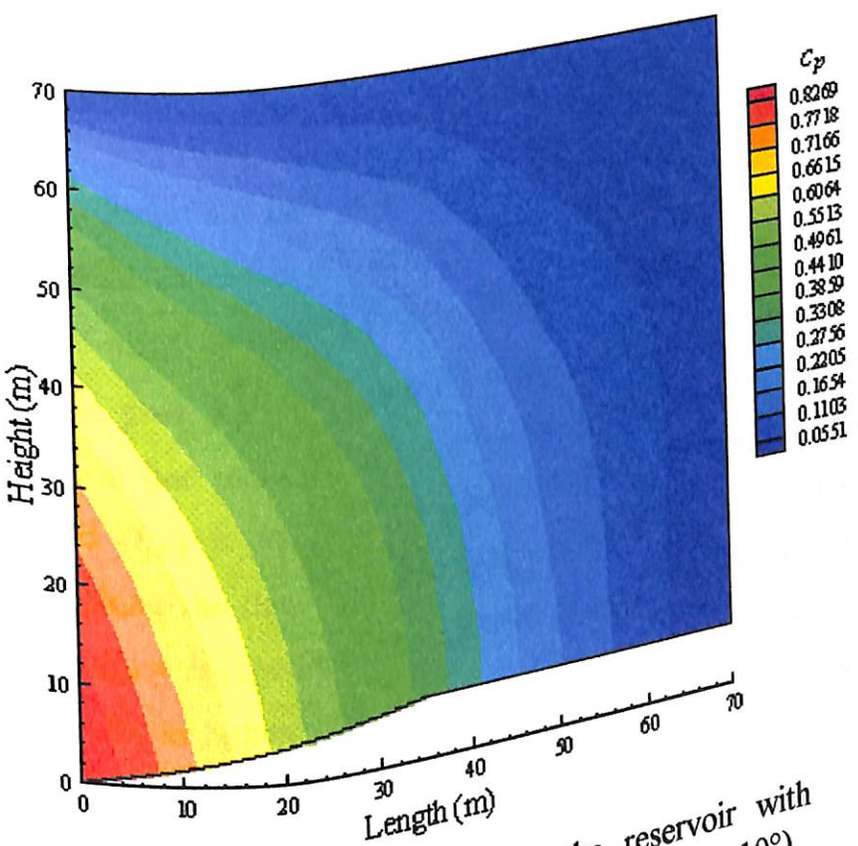

Fig. 4.75 Pressure contours in the reservoir with inclined reservoir bed (Tc/H_f= 10 $\alpha = 0.5$, $\phi' = +10°$)

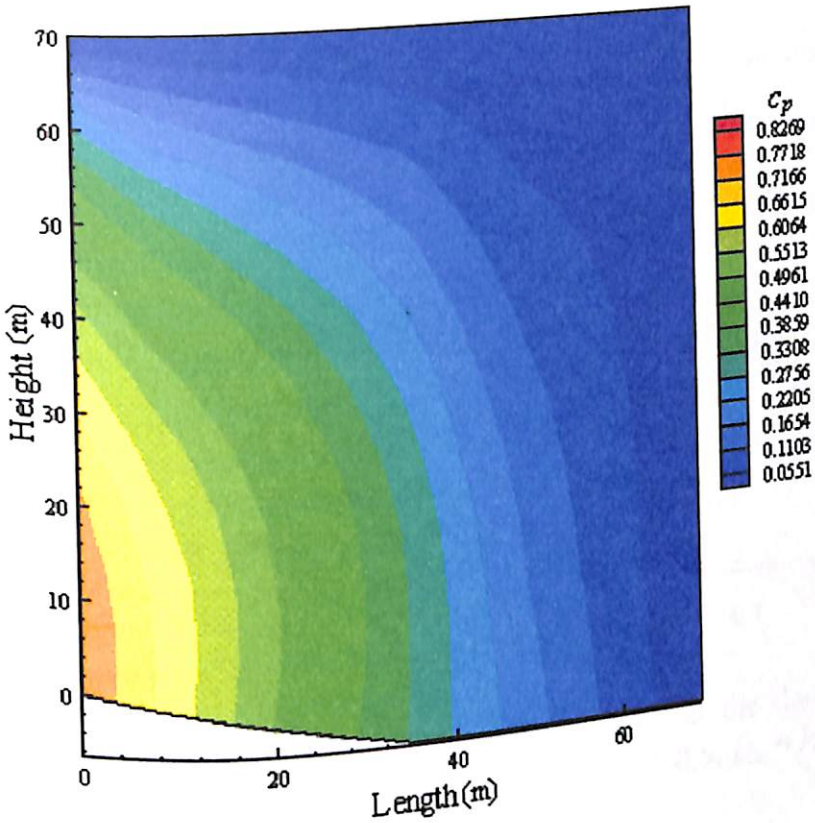

Fig. 4.76 Pressure contours in the reservoir with inclined reservoir bed ($Tc/H_f = 10$ $\alpha = 0.5$, $\phi' = -10°$)

The effect of reservoir bed inclination at $Tc/H_f = 10$, when the length of inclination (L_{hi}) is equal to the depth of the reservoir is studied and the results are presented in graphical forms in Figs. 4.77 to 4.80 at $\phi' = \pm 10°$ and $\pm 30°$. It is observed that the hydrodynamic pressure increases with reservoir bed inclination in upward and decreases with reservoir bed inclination in downward direction. When the length of the reservoir bed inclined (L_{hi}) is equal to its depth (H_f), the variation in hydrodynamic pressure distribution along the dam-reservoir interface is more than the case when $L_{hi} = 0.5\ H_f$. Further, when $L_{hi} = H_f$, the finite domain of the reservoir extends to length at least equal to H_f. This results in higher accuracy of the solution even when the reservoir is truncated at a considerably short distance of $L_h = 0.2H_f$. It is also interesting to note that more accuracy in the results is obtained at a shorter length of finite domain of the reservoir when the reservoir bed has upward inclination (Figs. 4.77 and 4.79). The hydrodynamic pressure distribution at a particular time instant ($0.75T$) in the reservoir domain has been shown in contour form in Figs. 4.81 and 4.82 for different directions of reservoir bed inclination.

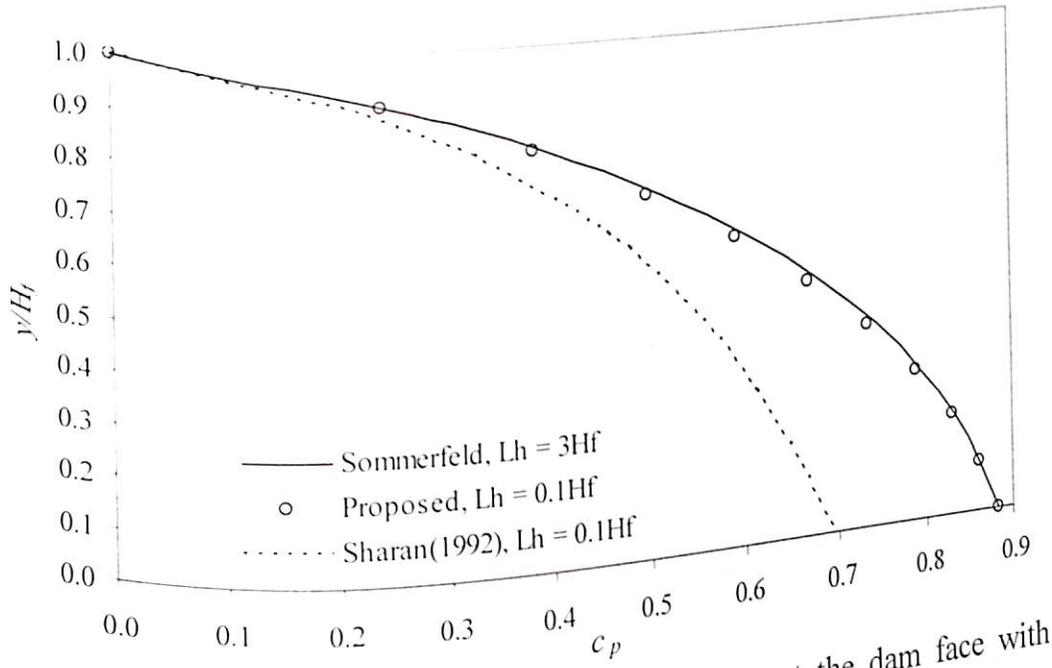

Fig. 4.77 Hydrodynamic pressure distribution at the dam face with reservoir bed slope of $\phi' = +10°$, $Tc/H_f = 10$, $\alpha = 0.5$, $L_{hi} = H_f$

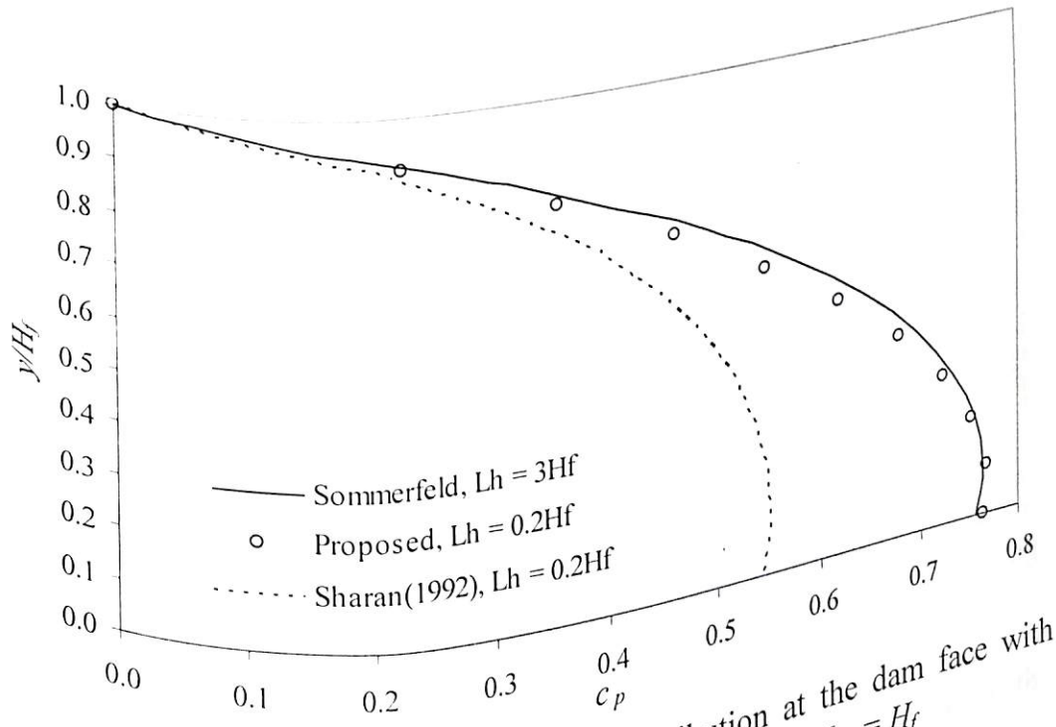

Fig. 4.78 Hydrodynamic pressure distribution at the dam face with reservoir bed slope of $\phi' = -10°$, $Tc/H_f = 10$, $\alpha = 0.5$, $L_{hi} = H_f$

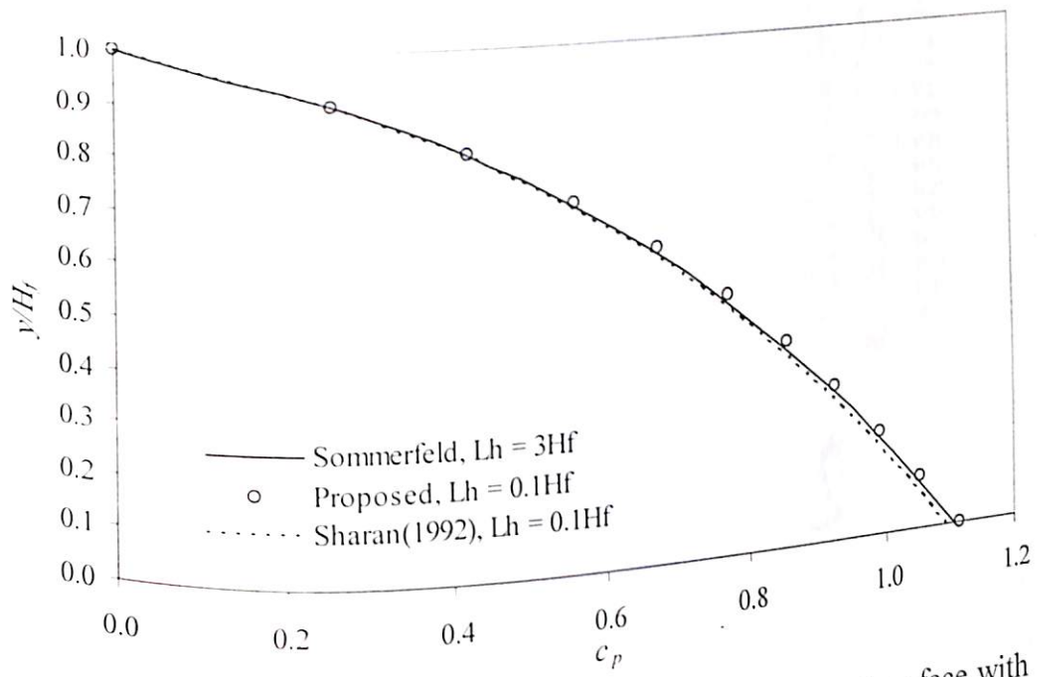

Fig. 4.79 Hydrodynamic pressure distribution at the dam face with reservoir bed slope of $\phi' = +30°$, $Tc/H_f = 10$, $\alpha = 0.5$, $L_{hi} = H_f$

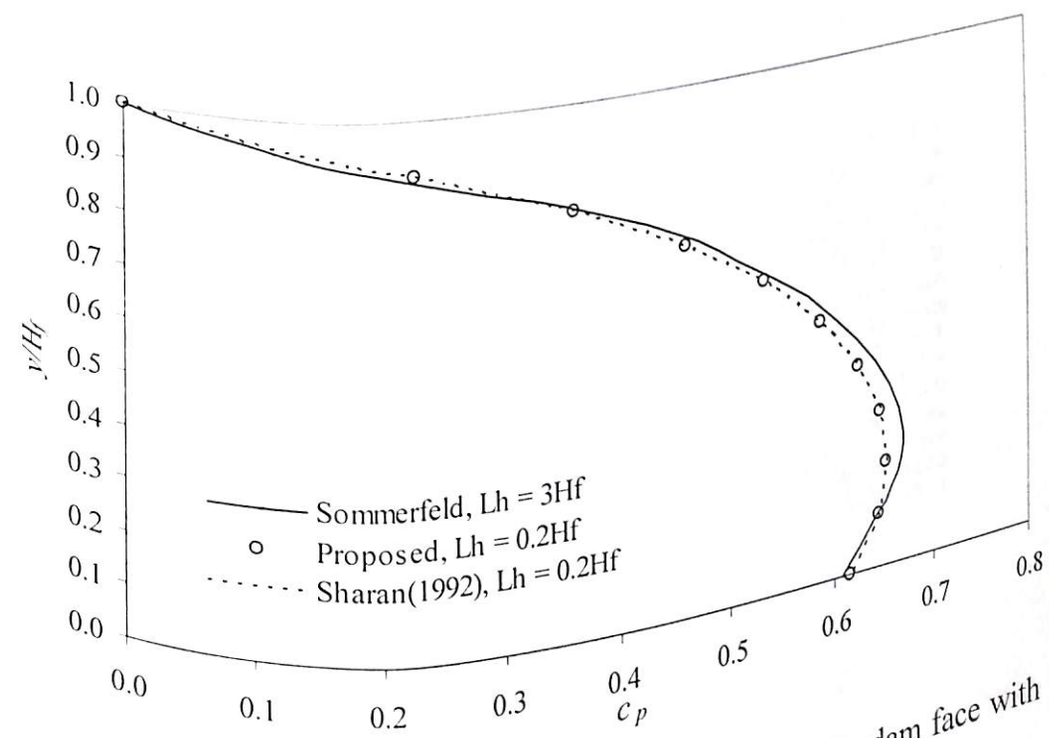

Fig. 4.80 Hydrodynamic pressure distribution at the dam face with reservoir bed slope of $\phi' = -30°$, $Tc/H_f = 10$, $\alpha = 0.5$, $L_{hi} = H_f$

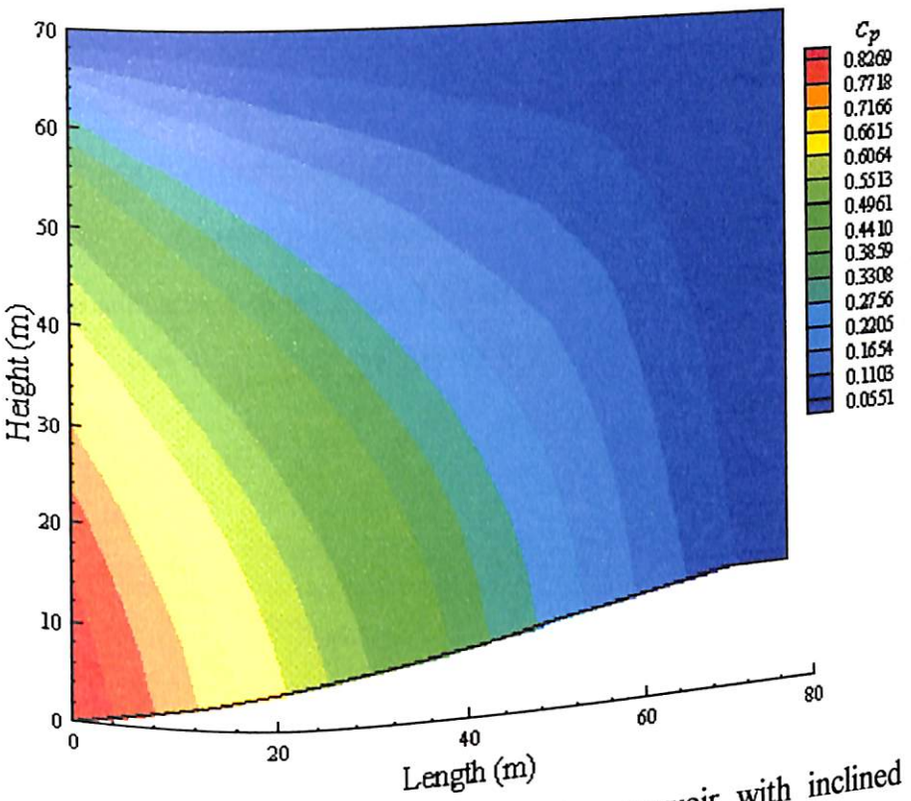

Fig. 4.81 Pressure contours in the reservoir with inclined reservoir bed ($Tc/H_f = 10$, $\alpha = 0.5$, $\phi' = +10°$, $t/T = 0.75$)

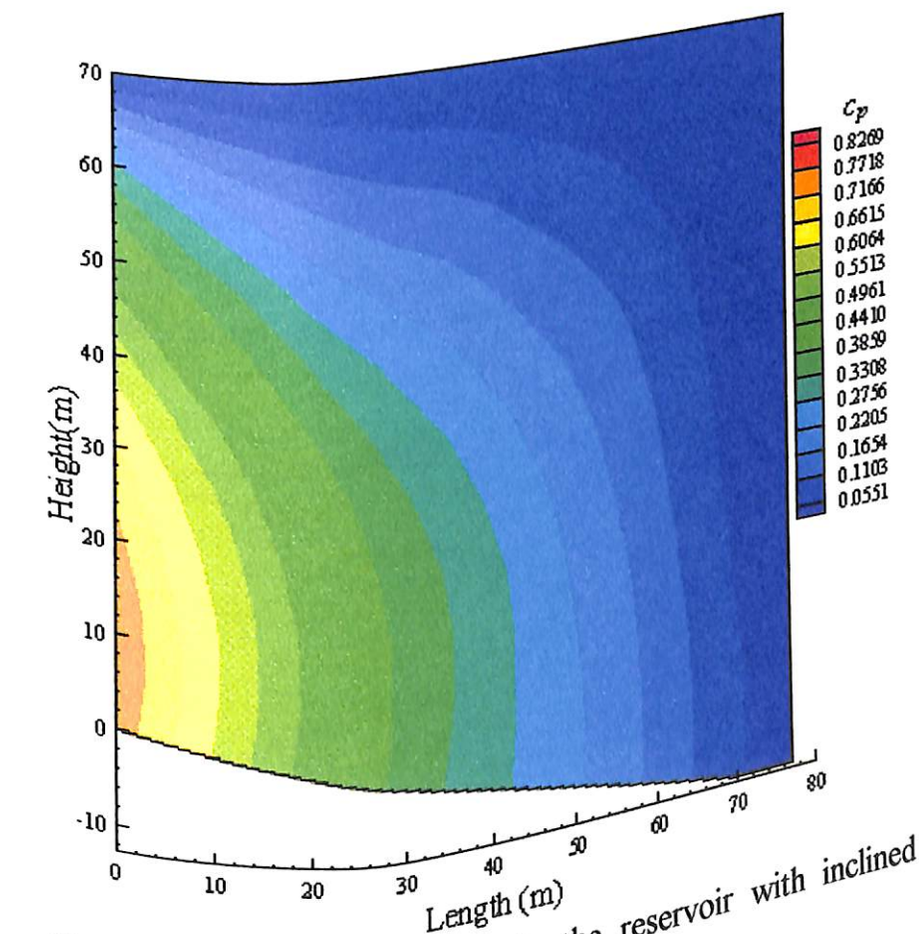

Fig. 4.82 Pressure contours in the reservoir with inclined reservoir bed ($Tc/H_f = 10$, $\alpha = 0.5$, $\phi' = -10°$)

To determine the effectiveness of the proposed truncation boundary condition in determining the hydrodynamic pressure at $Tc/H_f = 4$, a few cases are studied for different reservoir bed inclination considering the length of inclined reservoir bed, $L_{hi} = 0.5\ H_f$. The hydrodynamic pressure distribution is plotted for reflection coefficient, $\alpha = 0.5$ and at $t = 0.75T$. It is observed from Figs. 4.83 to 4.86 that sufficient accuracy can be arrived at a distance of $L_h = 0.5\ H_f$, if the reservoir is excited at its resonant frequency ($Tc/H_f = 4$).

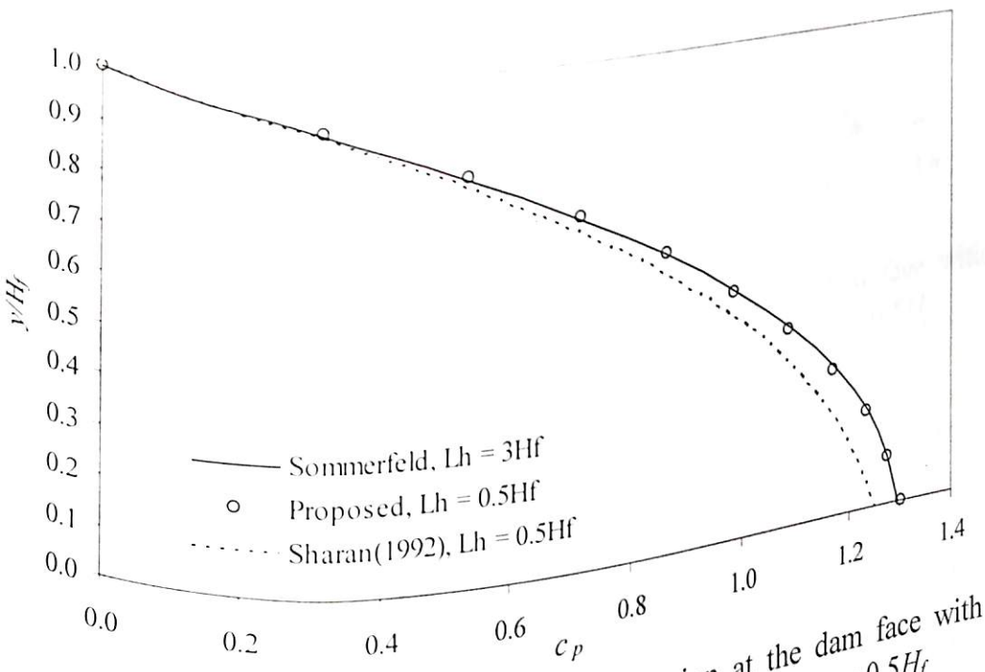

Fig. 4.83 Hydrodynamic pressure distribution at the dam face with inclined reservoir bed at $\phi' = +10°$, $Tc/H_f = 4$, $\alpha = 0.5$, $L_{hi} = 0.5H_f$

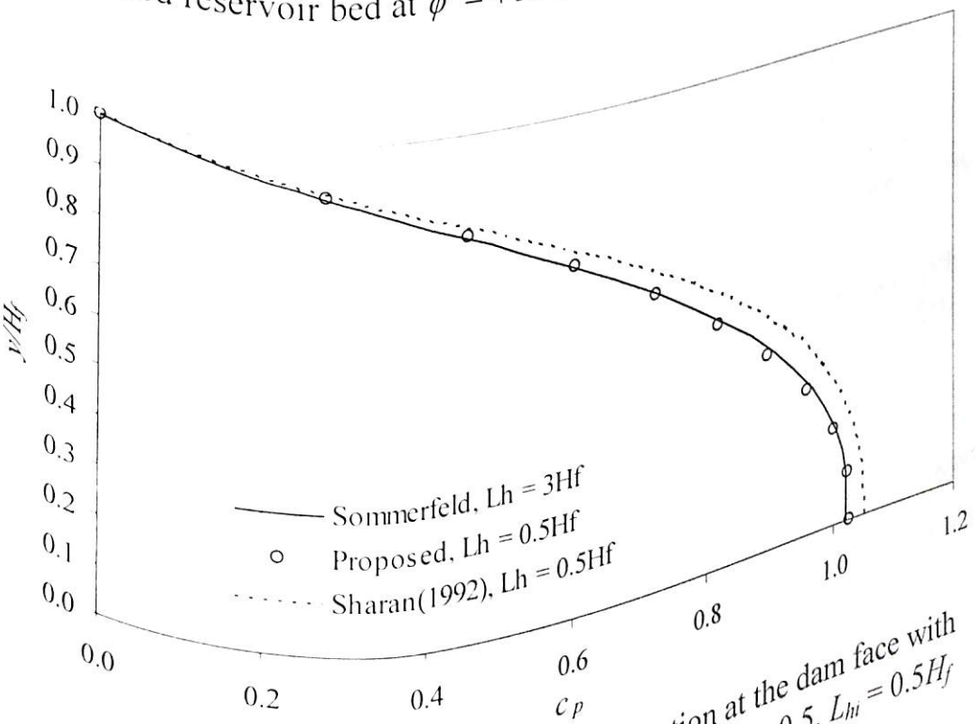

Fig. 4.84 Hydrodynamic pressure distribution at the dam face with inclined reservoir bed at $\phi' = -10°$, $Tc/H_f = 4$, $\alpha = 0.5$, $L_{hi} = 0.5H_f$

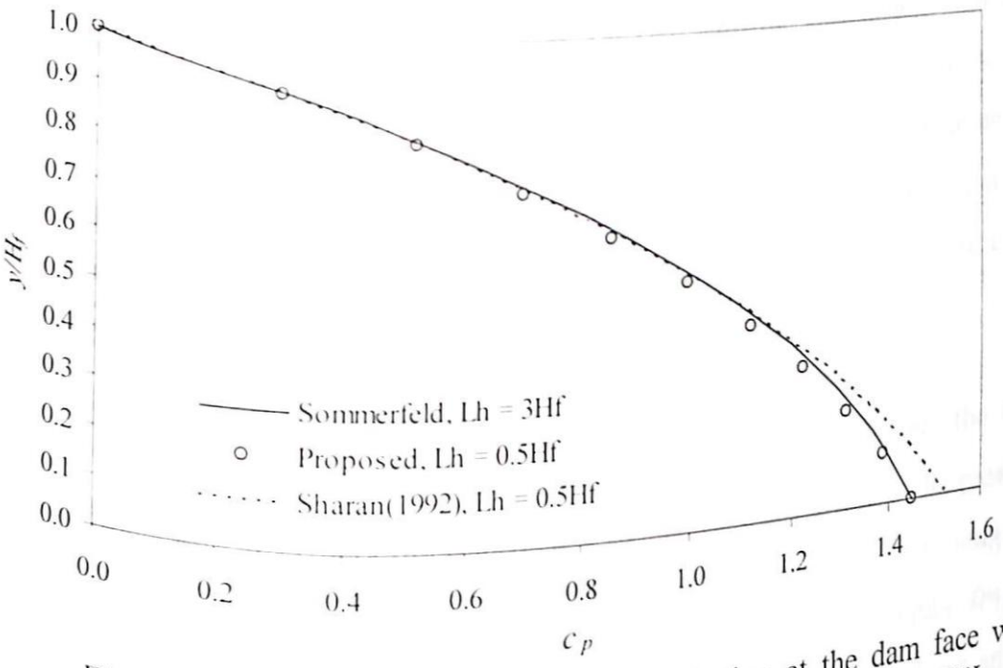

Fig. 4.85 Hydrodynamic pressure distribution at the dam face with inclined reservoir bed at $\phi' = +30°$, $Tc/H_f = 4$, $\alpha = 0.5$, $L_{hi} = 0.5H_f$

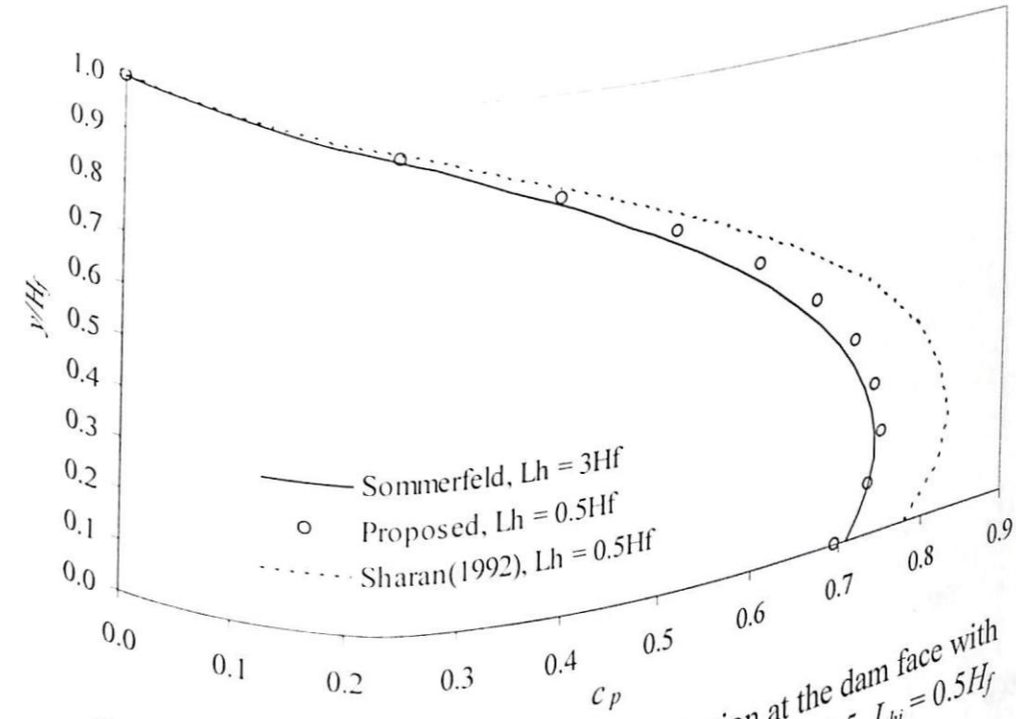

Fig. 4.86 Hydrodynamic pressure distribution at the dam face with inclined reservoir bed at $\phi' = -30°$, $Tc/H_f = 4$, $\alpha = 0.5$, $L_{hi} = 0.5H_f$

The accuracy of the developed truncation boundary condition has also been tested for the higher excitation frequency. The hydrodynamic pressure coefficient at the dam-reservoir interface has been plotted in Figs. 4.87 and 4.88 with a reservoir bed inclination of $\phi' = \pm 30°$. The inclined length of the reservoir bed has been considered here as $L_{hi} = 0.5H_f$ and the reservoir is excited at $Tc/H_f = 1$. The comparison of results show that the

present algorithm is capable enough to produce reasonable accurate results if the infinite reservoir is truncated at a distance of $L_h = 0.5H_f$ where as large deviation is observed if the boundary condition proposed by Sharan (1992). Similar conclusions can be drawn from Figs. 4.89 and 4.90 which show the comparison of the results when the reservoir bed is inclined up to its reservoir depth, i.e., for $L_{hi} = H_f$. The hydrodynamic pressure distribution inside the reservoir domain with inclined bed in different direction at higher excitation frequency (at $Tc/H_f = 1$) has been shown in the form of pressure contour in Figs. 4.91 and 4.92.

Thus, in summary, it is evident from the graphical results that the length of reservoir bed inclination affects the magnitude of pressure coefficient. The present study reveals that the proposed algorithm can effectively account for the reservoir bed inclination with reservoir bottom absorption for a wide range of excitation frequencies. An increase in upward inclination (i.e. ϕ' is +ve) of the reservoir bed shows an increase in hydrodynamic pressure, while an increase in downward inclination (i.e., ϕ' is -ve) shows a decrease in hydrodynamic pressure.

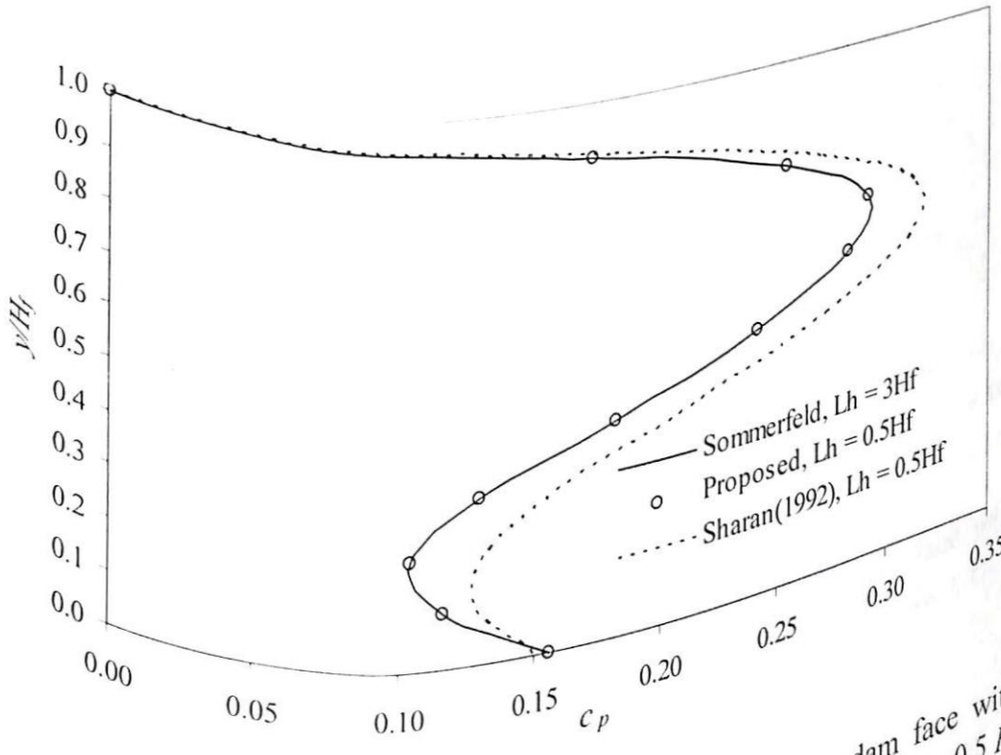

Fig. 4.87 Hydrodynamic pressure distribution at the dam face with inclined reservoir bed slope at $\phi' = +30°$, $Tc/H_f = 1$, $\alpha = 0.5$, $L_{hi} = 0.5\ H_f$

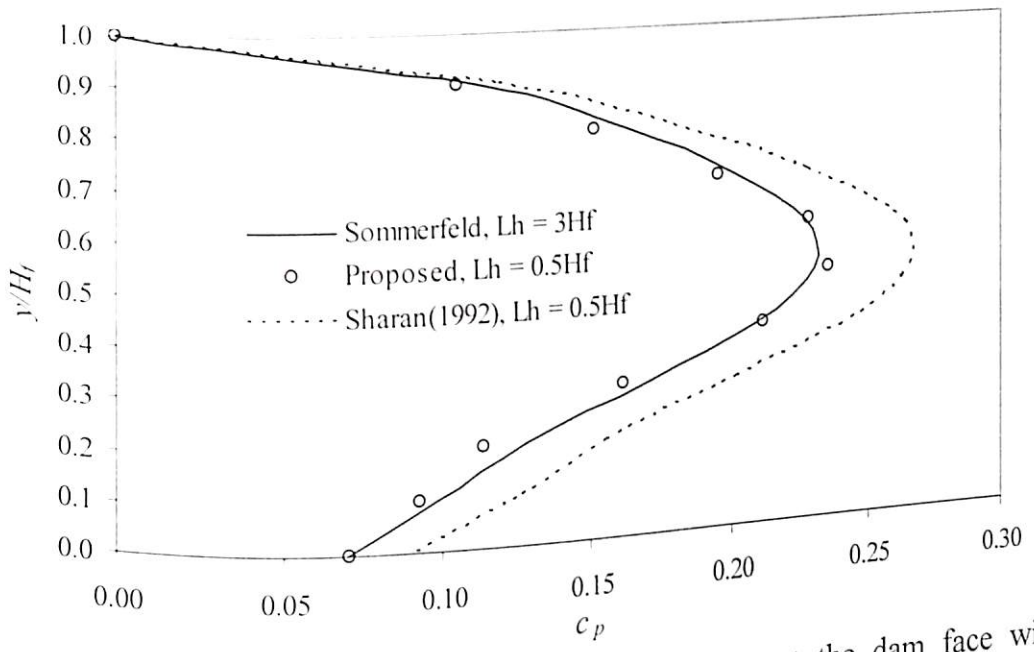

Fig. 4.88 Hydrodynamic pressure distribution at the dam face with inclined reservoir bed slope at $\phi' = -30°$, $Tc/H_f = 1$, $\alpha = 0.5$, $L_{hi} = 0.5\ H_f$

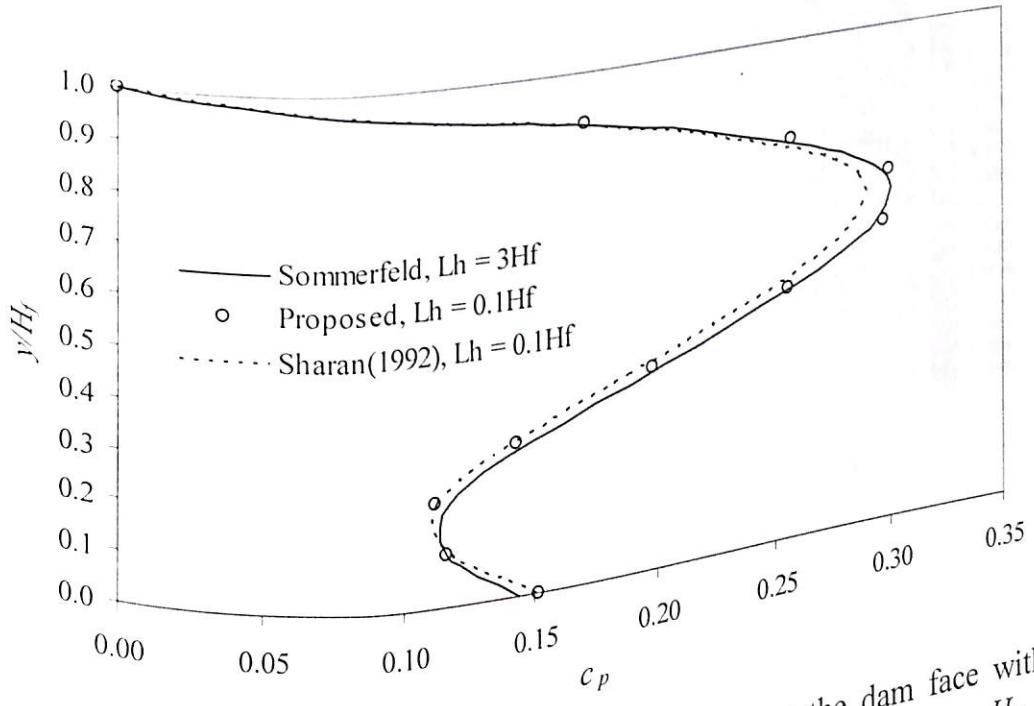

Fig. 4.89 Hydrodynamic pressure distribution at the dam face with inclined reservoir bed slope at $\phi' = +30°$, $Tc/H_f = 1$, $\alpha = 0.5$, $L_{hi} = H_f$

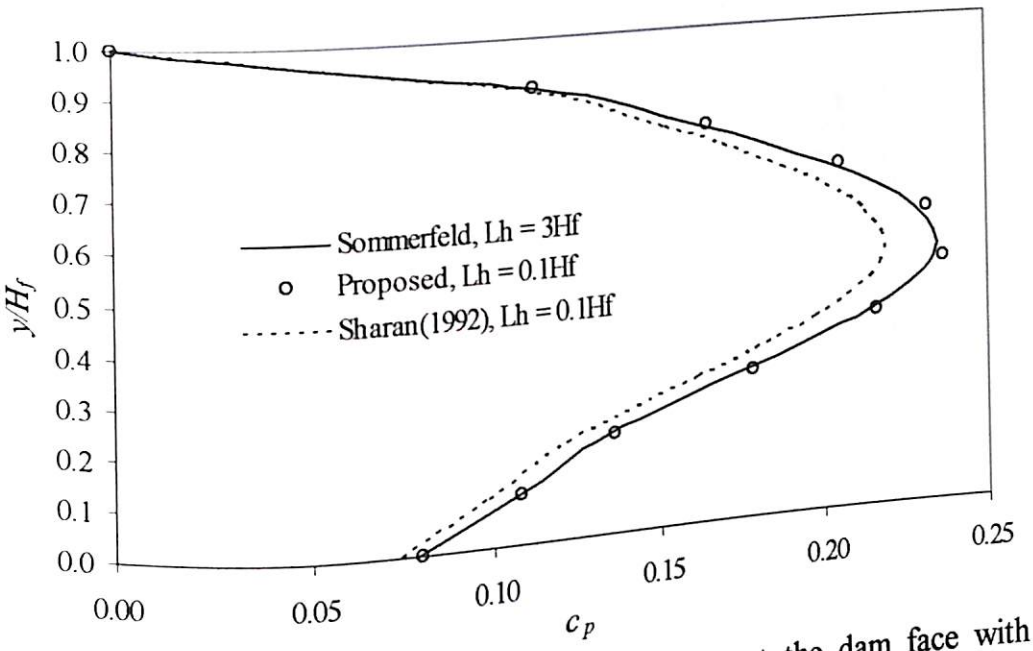

Fig. 4.90 Hydrodynamic pressure distribution at the dam face with inclined reservoir bed slope at $\phi' = -30°$, $Tc/H_f = 1$, $\alpha = 0.5$, $L_{hi} = H_f$

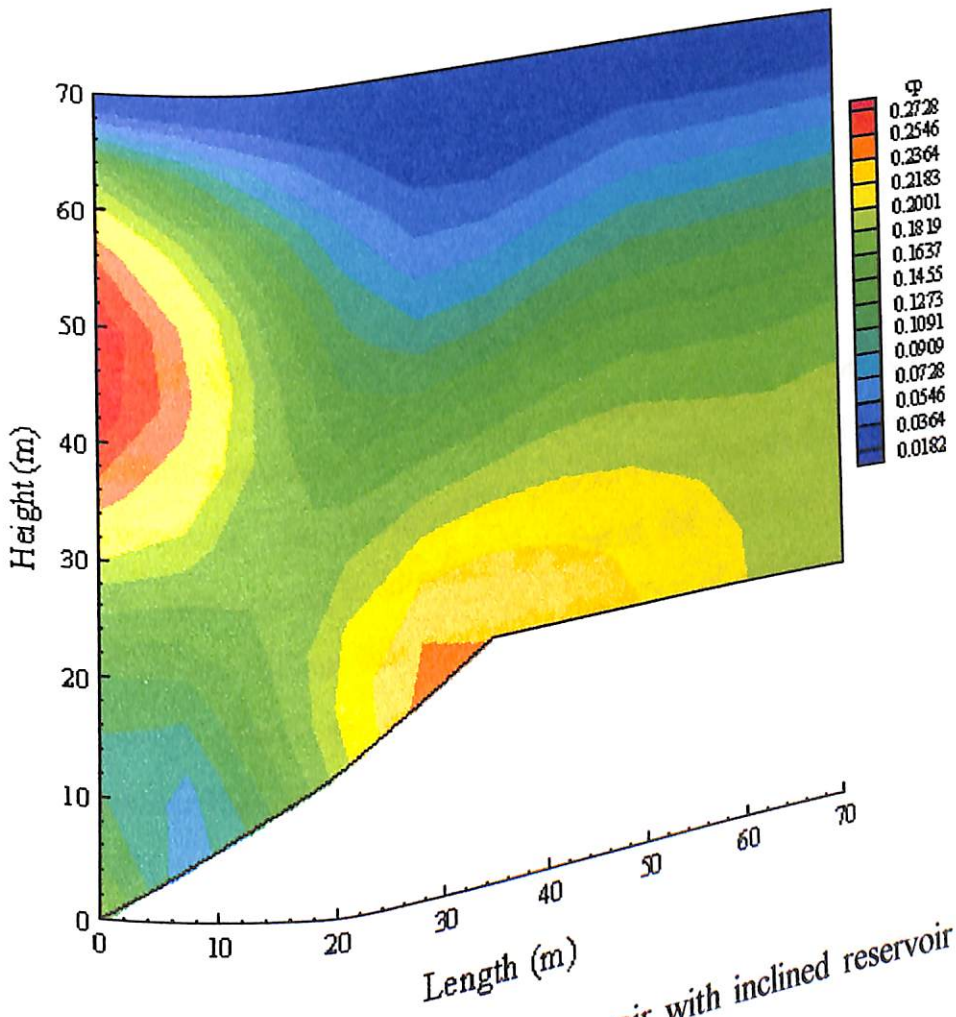

Fig. 4.91 Pressure contours in the reservoir with inclined reservoir bed ($Tc/H_f = 1$, $\alpha = 0.5$, $\phi' = +30°$, $t/T = 0.75$)

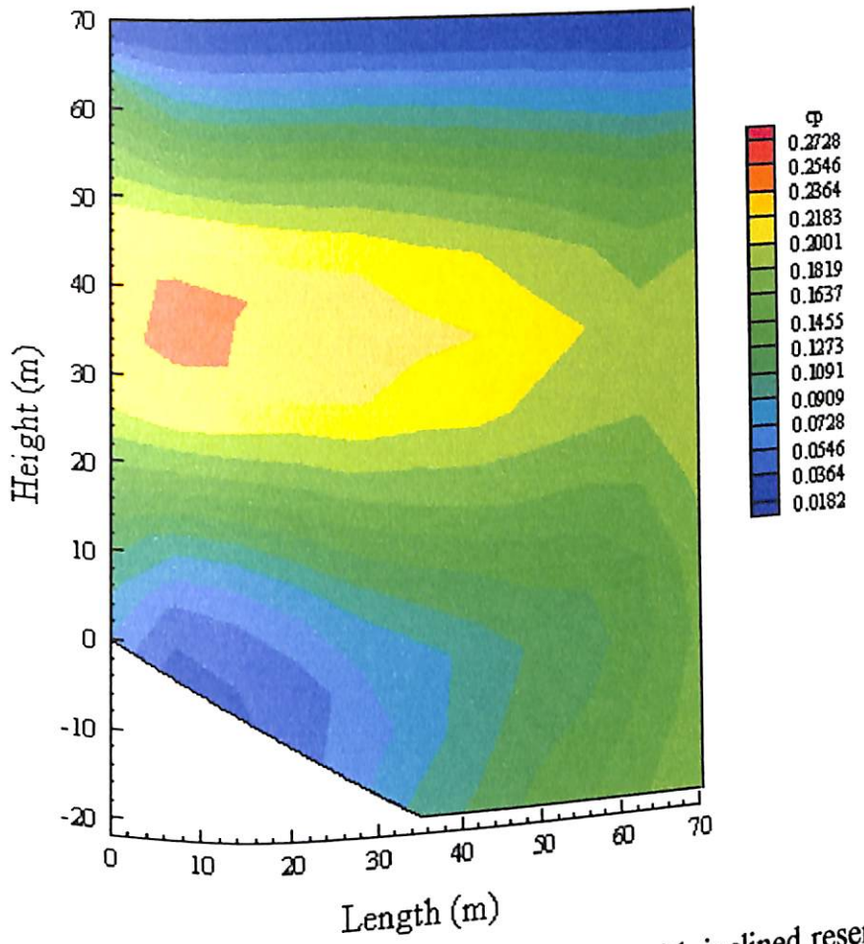

Fig. 4.92 Pressure contours in the reservoir with inclined reservoir bed ($Tc/H_f = 1$, $\alpha = 0.5$, $\phi' = -30°$, $t/T = 0.75$)

4.2.6 Effect of Gravity Waves on Hydrodynamic Pressure

The proposed algorithm accounts for the effect of gravity waves in the finite element analysis of infinite reservoir. The hydrodynamic pressure coefficients (c_b) obtained at the base of the vertical dam-reservoir interface is plotted for different values of χ and α. Here, χ ($= \omega^2/g$) is a coefficient that represents the effect of gravity waves (eq. 3.90). In the absence of gravity waves, the magnitude of χ will be equal to zero; otherwise the value of χ will be greater than zero and will vary with the excitation frequency. The value of α may vary from 1 to 0 depending on the rigidity of the reservoir bottom. Fig. 4.93 shows the influence of gravity wave in the development of hydrodynamic pressure at the base of a vertical dam-reservoir interface. Here, c_b ($= p_b/\rho a H_f$) is the pressure coefficient at the bottom of the upstream face of the dam, p_b is the hydrodynamic pressure at the base of the dam-reservoir interface, ω_r is the fundamental frequency of the reservoir and ω is the excitation frequency. It is interesting to note that a small peak occurs at an early stage ($\omega/\omega_r < 0.1$) due to the presence of gravity waves. However, the second peak

coincides with the first mode when the effects of gravity waves are not considered. The results show that there is a negligible influence of gravity waves in the hydrodynamic pressure beyond the excitation frequency ratio (ω/ω_r) of 0.1. It is also observed from Fig. 4.93 that the changes in reflection coefficient do not affect the amplitude of the first resonant peak considering the gravity waves. This is in agreement with findings reported by Bouaanani et al. (2002). The authors attribute the occurrence of this phenomenon to the presence of ice layer at the reservoir surface. However, it is observed from the present numerical results that the first peak may occur even in the absence of the ice layer.

A parametric study is carried out to study the effect of surface gravity waves on the development of hydrodynamic pressure for different values of χ. The results are presented in Table 4.8 that show the effect of gravity waves to be prominent at low frequencies (i.e., at $Tc/H_f = 200$ and 100) where the absorptive reservoir bottom does not have much effect. For higher excitation frequencies gravity waves have negligible effect and reservoir bottom absorption have more prominent effect on the development of hydrodynamic pressure.

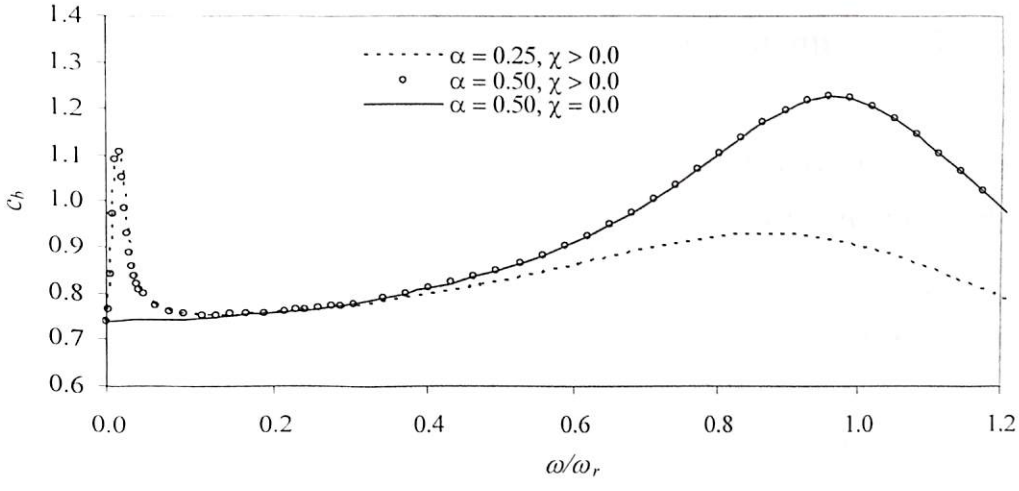

Fig. 4.93 Effect of gravity waves on hydrodynamic pressure coefficient

Table 4.8 Effect of gravity waves on hydrodynamic pressure coefficient

Tc/H_f	ω/ω_r	χ	α	c_b
200.0	0.02	0.00	1.0	0.7416
			0.5	0.7416
		0.04	1.0	1.0219
			0.5	1.0219
100.0	0.04	0.00	1.0	0.7431
			0.5	0.7430
		0.17	1.0	0.81039
			0.5	0.81034
4.0	1.0	0.00	1.0	54.8010
			0.5	1.2182
		106.42	1.0	54.8090
			0.5	1.2187
2.0	2.0	0.00	1.0	0.4781
			0.5	0.5053
		425.66	1.0	0.4781
			0.5	0.5053

4.2.7 Effect of Reservoir Bottom Absorption on Fundamental Frequency of Reservoir

The hydrodynamic pressure coefficient (c_b) at the base of a vertical dam-reservoir interface is plotted in Fig. 4.94 for varying frequency ratio (ω/ω_r) using eq. (3.89). Here, (ω_r) is the fundamental frequency of the reservoir with absorptive bottom. The natural frequencies of the reservoir are determined from the frequency ratios (ω/ω_r), where the magnitude of c_b is maximum. The natural frequencies thus obtained are presented in Table 4.9. The results show that the fundamental frequency of the reservoir (T) as the absorption at the reservoir bottom fundamental time period is reduced elongating the increases. It is observed from Fig. 4.94 and Table 9 that the hydrodynamic pressure coefficient at the base of the upstream face of the dam is reduced substantially for lower magnitudes of reflection coefficient.

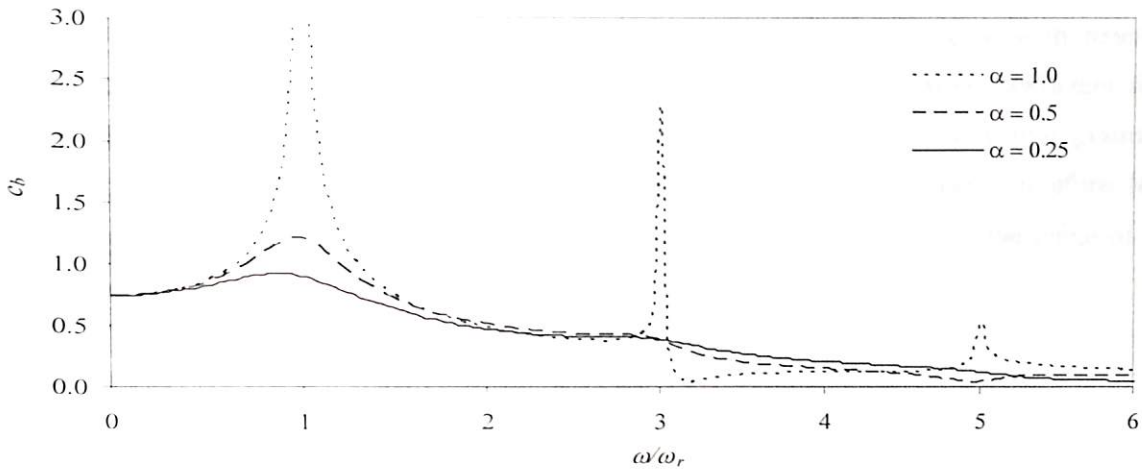

Fig. 4.94 Effect of reservoir bottom absorption on hydrodynamic pressure coefficient, without gravity waves

Table 4.9 Effect of reservoir bottom absorption on fundamental frequency of the reservoir

Reflection Coefficient, α	Fundamental Frequency, ω_r	Time Period, *T (sec)*
0.25	28.0	0.224
0.50	31.0	0.203
0.95	32.0	0.196
1.00	32.3	0.195

4.2.8 Effect of Sediment on Reflection Coefficient

The results presented in the previous sections emphasize that the development of hydrodynamic pressure is dependent on the reflection coefficient defined at the reservoir bottom. A value of $\alpha = 1.0$ implies a highly reflective reservoir bottom, which may yield exaggerated values of hydrodynamic pressure. In practical situation, a fully absorptive reservoir bottom with $\alpha = 0.0$ may not exists. The value of α is dependent on the density of the sediment layer (ρ_s) at the reservoir bottom (eq. 3.83). Hence, the characteristics of the overlying sediment layer play a significant role in determining the reflection coefficient and subsequently, the hydrodynamic pressure. Here, the effect of sediment

density on the reflection coefficient is studied, where a sediment layer having an elastic modulus of 35000 MPa is considered. The variation of reflection coefficient with density is plotted in Fig. 4.95. The results show a steep increase in reflection coefficient for sediment densities lower than 1000 kg/m^3. The density of underwater fine grained sediments (Leurer 1997), may range from a density equal to that of water. Therefore, for all the practical problems, with sediment density more than 1000 kg/m^3, the value of α may be considered in the range of 0.5 to 1.

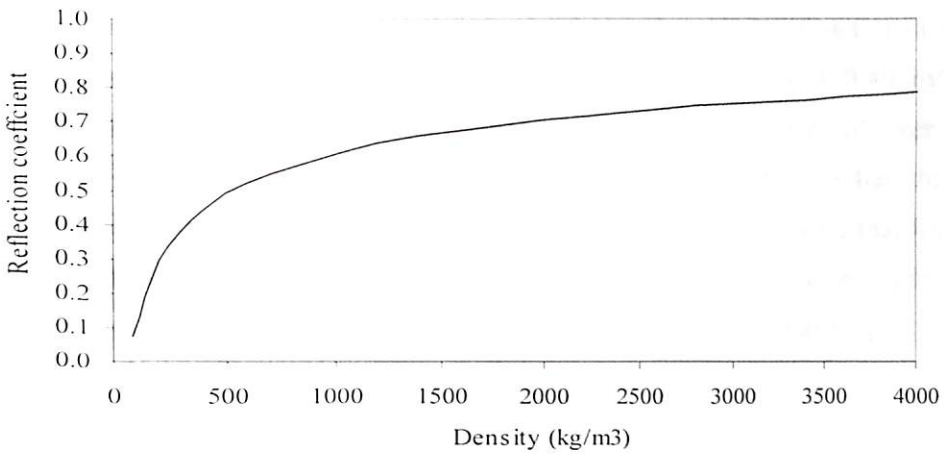

Fig. 4.95 Effect of sediment density on reflection coefficient

4.2.9 Effect of Sediment Layer Depth on Reflection Coefficient

To evaluate the dynamic behaviour of an ageing dam-reservoir system, it is important to study the variation of reflection coefficient and its effect on hydrodynamic pressure developed in the reservoir with age. It is evident from eq. (3.84) that the value of reflection coefficient will reduce with an increase in the depth of sediment layer. If the sediment is not flushed out of the reservoir at regular intervals, the depth of sediment layer will increase with ageing of the reservoir system. Hence, it is important to study the effect of increasing depth of sediment layer on the development of hydrodynamic pressure in the reservoir.

A simple yet effective approach to determine the reflection coefficient considering increasing depth of sediment layer with age is given by eq. (3.84). Here, d_{sl}

is considered to be the depth of a sediment layer lying over a rigid rock stratum of a very large depth, d_{s2}. A study is carried out to determine the variation of reflection coefficient with age for different properties of the underlying strata for a period of 100 years. The reflection coefficients obtained in the present analysis are compared with the frequency dependent reflection coefficients obtained by Hatami (1997) at an attenuation constant, b = 0.25, when excited at the resonant frequency of the reservoir. The material parameters considered in the present analysis is same as in the reference i.e., elastic modulus of sediment layer, E_{s1} = 4500 MPa and the elastic modulus of underlying rigid stratum, E_{s2} = 23000 MPa. The wave propagation velocity in sediment is considered to be 1500 m/sec. The reflection coefficients are evaluated with the depth of sediment increasing with age considering a rate of sedimentation as 0.15 m/year and 0.40 m/year. The sediment layer is considered to lie (i) over a rigid stratum (ORS), (ii) over a flexible stratum (OFS) (iii) neglecting rigidity of foundation rock (NFR) i.e., when the sediment layer is considered to be of infinite depth. It is observed from Fig. 4.96 that for sediment layer lying over a rigid stratum (ORS), the reflection coefficient varies from 1.0 to 0.9 and 1.0 to 0.75 at sedimentation rates of 0.15m/year and 0.40 m/year respectively within a period of 100 years.

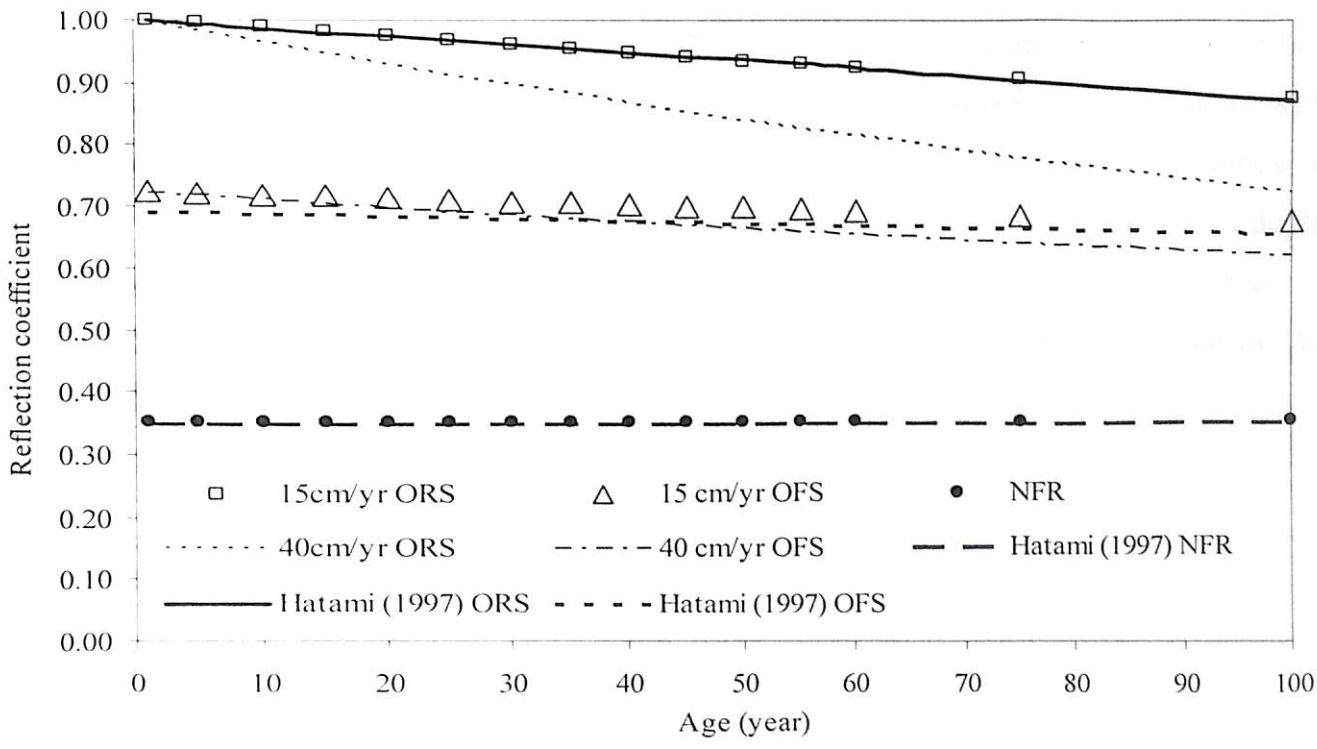

Fig. 4.96 Variation of reflection coefficient with age

To represent a flexible underlying stratum, the elastic modulus of the underlying layer (E_{s2}) is considered to be $0.2E_{s1}$, where E_{s1} is the elastic modulus of overlying sediment layer. It is observed from Fig 4.96 that for sediment layer overlying a flexible stratum (OFS), the reflection coefficient ranges from 0.73 to 0.7 for a sedimentation rate of 0.15m/year. At a sedimentation rate of 0.40 m/year the reflection coefficient ranges from 0.73 to 0.65. It is interesting to note that when the underlying foundation rock is neglected (NFR), the reflection coefficient remains constant at 0.35 for the entire period of 100 years.

The decrease in the reflection coefficient with age is significant when the sediment layer is considered to be deposited over a rigid stratum than when the sediment layer is considered to be deposited over a flexible stratum. If the underlying layer is considered to be a sediment layer of infinite depth, a constant value of reflection coefficient is obtained. As the flexibility of the underlying strata increases, the significance of the increasing depth of sediment layer reduces. These results are in agreement with those published by Hatami (1997).

The frequency dependent reflection coefficient (eq.3.85) is further studied considering the viscoelastic modeling of the sediment layer lying over a rigid rock. Here, the sediment is considered to be of density 1962 kg/m^3 and elastic modulus of 5.12×10^5 MPa. It is seen from Fig. 4.97 that at lower excitation frequency the variation with sediment depth (d_s) is almost negligible. In the figure, n_f is the excitation frequency in Hz. But for higher frequencies, the variation of reflection coefficient with sediment depth is pronounced. Hence, if the frequency content of an earthquake excitation is high, it would necessitate incorporating the effect of frequency dependent reflection coefficient in the analysis procedure.

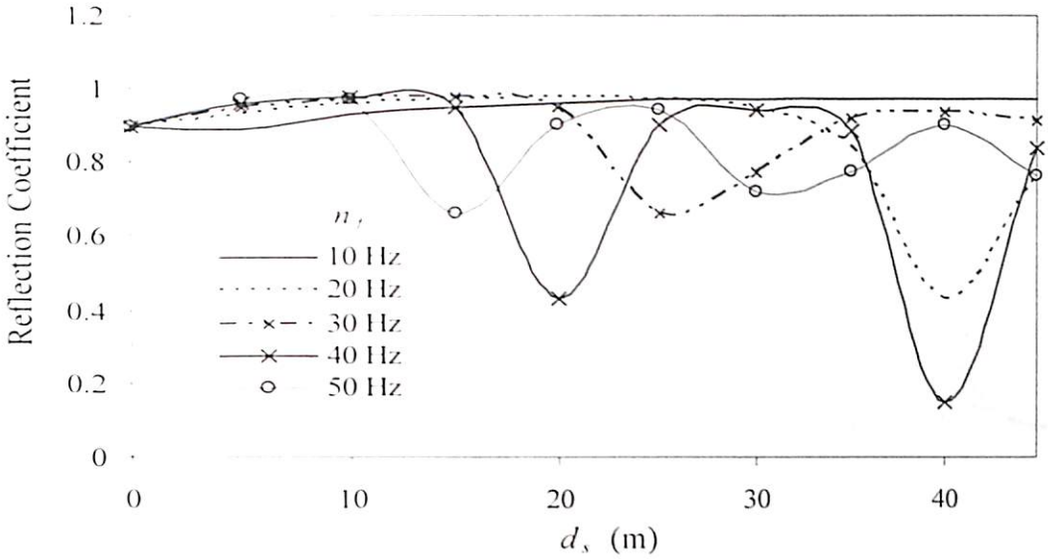

Fig. 4.97 Variation of frequency dependent reflection coefficient

4.2.10 Hydrodynamic Pressure due to Vertical Excitation

The hydrodynamic pressure developed on the upstream face of a vertical dam due to vertical excitation can be evaluated from the solution of the boundary value problem as given by the eq. (3.96). A finite element solution is required to evaluate the hydrodynamic pressure on the upstream face of a dam-reservoir system that may have a complicated geometry. It is evident from the literature (Nath 1969) that the hydrodynamic pressure coefficients due to vertical excitation is independent of the truncated length of the reservoir considered, when the upstream face of the rigid dam is vertical and the reservoir bottom is considered to be rigid.

An analysis is carried out to study the effect of reservoir bottom absorption on hydrodynamic response of a dam due to vertical excitation and compared with the exact solution as given by Chopra and Chakrabarti (1981). A reservoir depth of 70 m is considered with the other material parameters same as in preceding sections. Fig. 4.98 shows the variation of pressure coefficients at the base of the dam (c_b) with frequency ratio (ω/ω_r). Here, ω is the excitation frequency and ω_r is the fundamental frequency of the reservoir. The magnitudes of pressure coefficients are larger than those due to horizontal excitation.

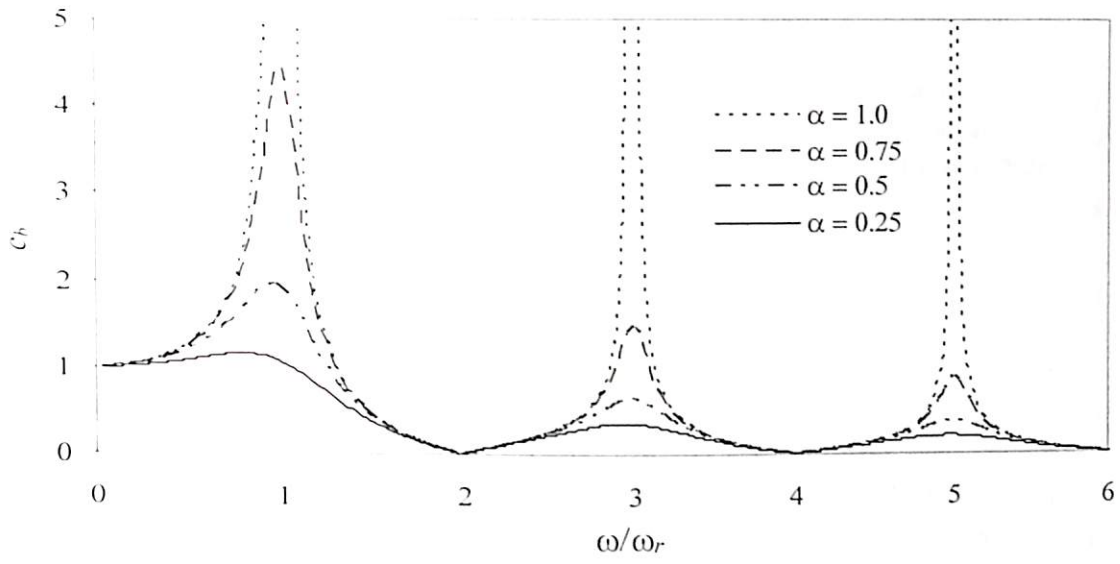

Fig. 4.98 Effect of reservoir bottom absorption on hydrodynamic pressure coefficient due to vertical excitation

The proposed algorithm for determination of hydrodynamic pressure due to vertical excitation is studied and compared with the exact solution for $\alpha = 1.0$ and $\alpha = 0.5$. Fig. 4.99 shows the hydrodynamic pressure along a vertical surface due to vertical excitation at $t = 0.75T$. It is observed that though the hydrodynamic pressure due to vertical excitation given by eq.(3.96) is independent of the horizontal length of the reservoir, the pressure distribution along the dam height determined by finite element method are affected by the horizontal length of the reservoir considered in the analysis. A comparison of the hydrodynamic pressure distribution along the vertical dam-reservoir interface considering a reservoir length $L = H_f$, (Fig. 4.99) shows that the performance of the proposed TBC at a particular instant of time is better than TBC proposed by Sharan (1992).

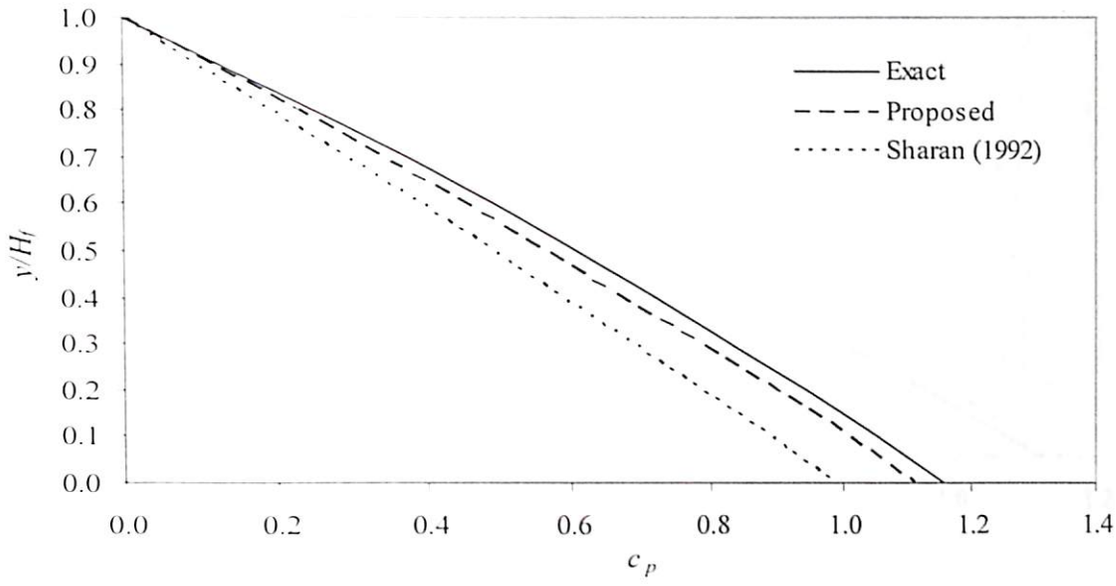

Fig. 4.99 Hydrodynamic pressure distribution along a vertical surface due to vertical excitation at $Tc/H_f = 10$, $\alpha = 1.0$

The hydrodynamic pressure along the dam-reservoir interface due to vertical excitation considering reservoir bottom effect at $Tc/H_f = 10$ and $\alpha = 0.5$ are presented in Fig. 4.100 for vertical ($\theta = 90°$) upstream face. The hydrodynamic pressure obtained along the dam-reservoir interface due to vertical excitation at an inclined dam-reservoir interface with $\theta = 45°$, $Tc/H_f = 10$ and $\alpha = 0.5$ is plotted at $L = 4.0H_f$ in Fig. 4.101. The pressure contours in Figs. 4.102 and 4.103 shows the hydrodynamic pressure developed in the reservoir due to vertical excitation. It is clearly seen from these contours that since the reservoir bed is the accelerating surface due to vertical excitation, the maximum hydrodynamic pressure developed is along the reservoir bed.

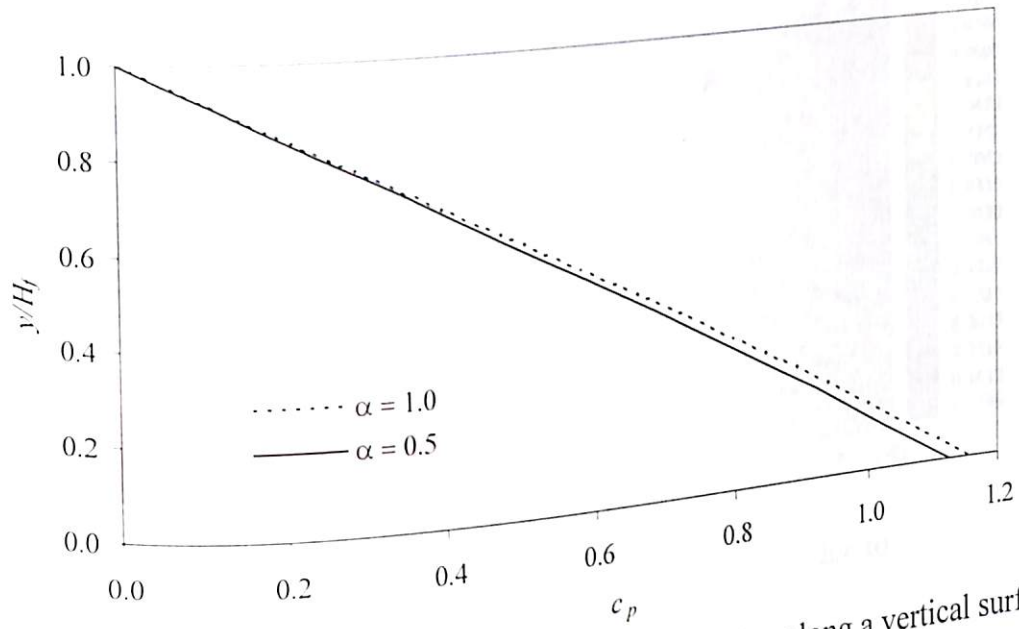

Fig. 4.100 Hydrodynamic pressure distribution along a vertical surface due to vertical excitation at $Tc/H_f = 10$

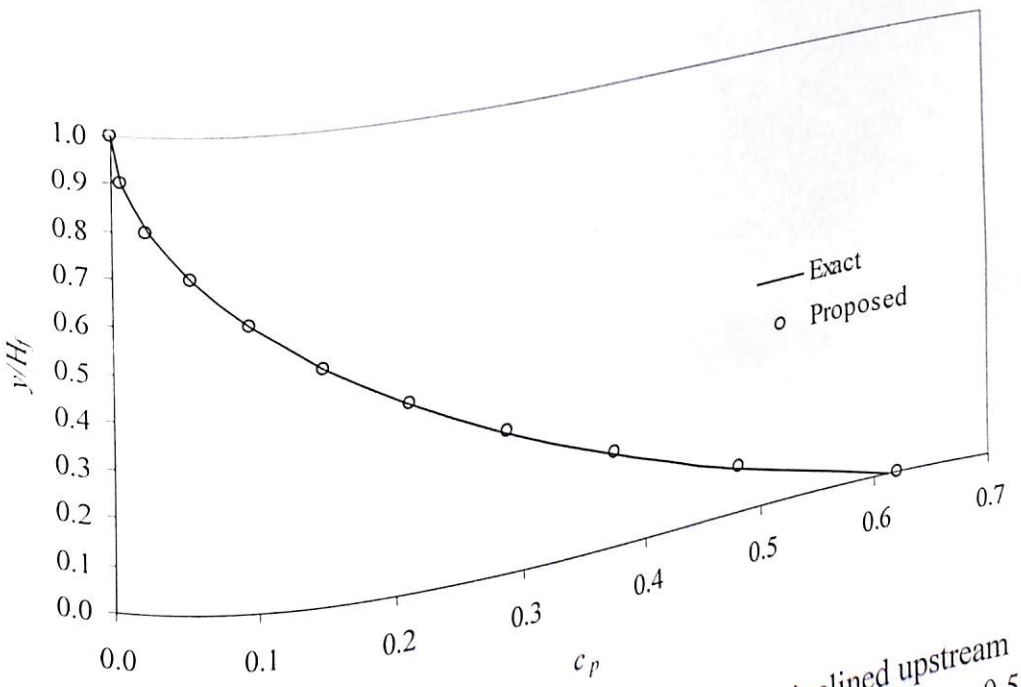

Fig. 4.101 Hydrodynamic pressure distribution with inclined upstream dam-reservoir interface due to vertical excitation at $Tc/H_f = 10$, $\alpha = 0.5$ and $\theta = 45°$

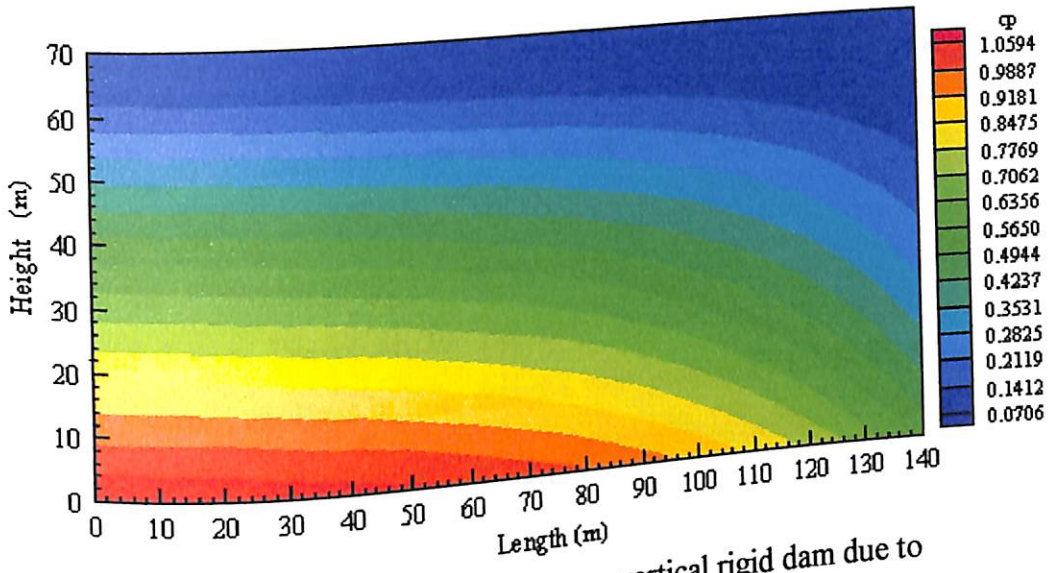

Fig. 4.102 Pressure contours along a vertical rigid dam due to vertical excitation at $Tc/H_f = 10$, $\alpha = 0.5$

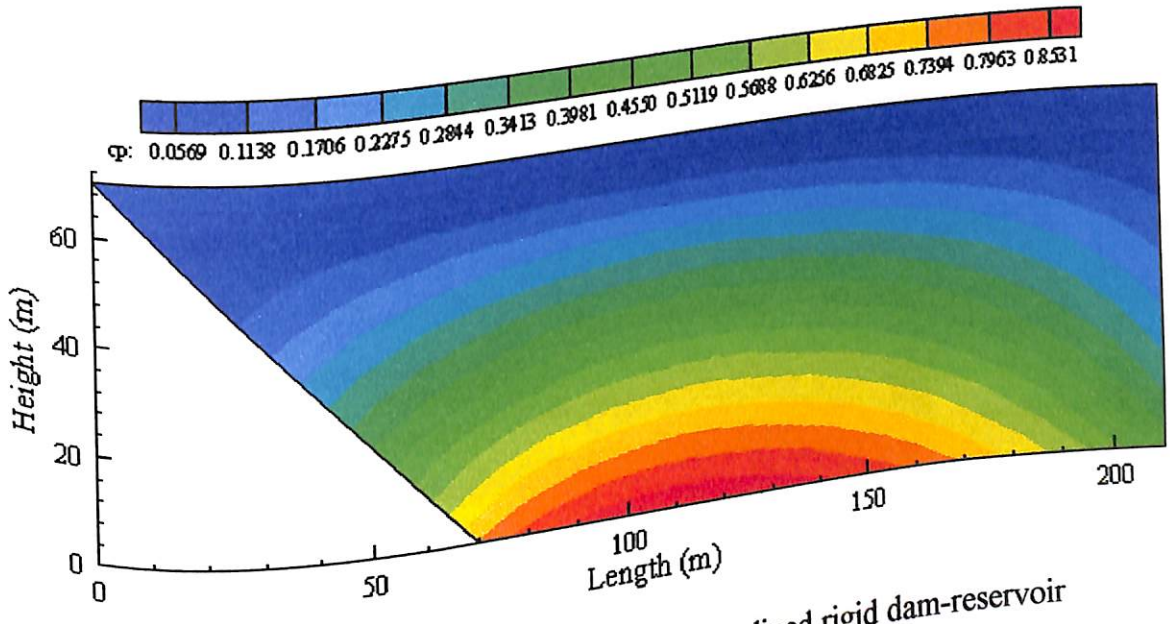

Fig. 4.103 Pressure contours along an inclined rigid dam-reservoir due to vertical excitation at $Tc/H_f = 10$, $\alpha = 0.5$ and $\theta = 45°$

Hence, it can be concluded that to determine the hydrodynamic pressure due to vertical excitation, the proposed algorithm can be effectively implemented in a finite element model of the reservoir in the case of vertical and inclined upstream face of the dam respectively. The extent of the reservoir to be considered while determining the pressure coefficients due to vertical excitation is more since the truncation boundary condition has been derived from equation for pressure coefficients due to horizontal excitation.

4.2.11 Seismic Analysis using Short Time Fourier Transform

A dynamic analysis procedure in time domain cannot account for the spectral contents of the seismic excitation when the input is in the form of time history. The present boundary conditions at the reservoir bottom and the truncated surface are frequency dependent (eqs. 3.81 and 3.93). Therefore, to increase the efficiency and accuracy of present algorithm for seismic analysis in time domain, the frequency dependent reservoir bottom absorption effect can be accounted for by using the excitation frequency (ω) of the earthquake at every time step. The spectral content of the seismic excitation is extracted and incorporated in the present analysis as explained in Section 3.3.5.

4.2.11.1 Extraction of Frequencies from Time History Data of Recorded Earthquake

The earthquake data represented by accelerograms as shown in Figs. 4.5 and 4.104 do not indicate the frequency components of the earthquake signal. A Fast Fourier Transform (FFT) converts the signal to frequency domain and can be used to obtain the power spectrum, which is a measurement of power at various frequencies (Fig. 4.105). The ground accelerations due to El Centro earthquake (1940) is recorded at a time step of $\Delta t = 0.02$. Therefore, this set of data is sampled at frequency, $f_n = 1/\Delta t$, i.e., 50 Hz. The accelerations due to Koyna earthquake (1967) are recorded at a time step, $\Delta t = 0.01$. Hence, this set of data is sampled at a frequency, $f_n = 100$ Hz. It is evident from the power spectrum of El Centro earthquake (Fig.4.105) that the energy of lower frequencies is dominant than those in the higher frequencies. Sometimes it may be useful to normalize the output of FFT so that a unit sinusoid in the time domain corresponds to unit amplitude in the frequency domain. A normalized discrete-time Fourier transform can be obtained as P_n = abs (FFT(**x**)) × 2/length(**x**) and is plotted in Fig. 4.106. Here **x** represents the earthquake excitation in time domain. It is apparent from these figures that the amplitude of the earthquake excitation is not significant at higher frequencies.

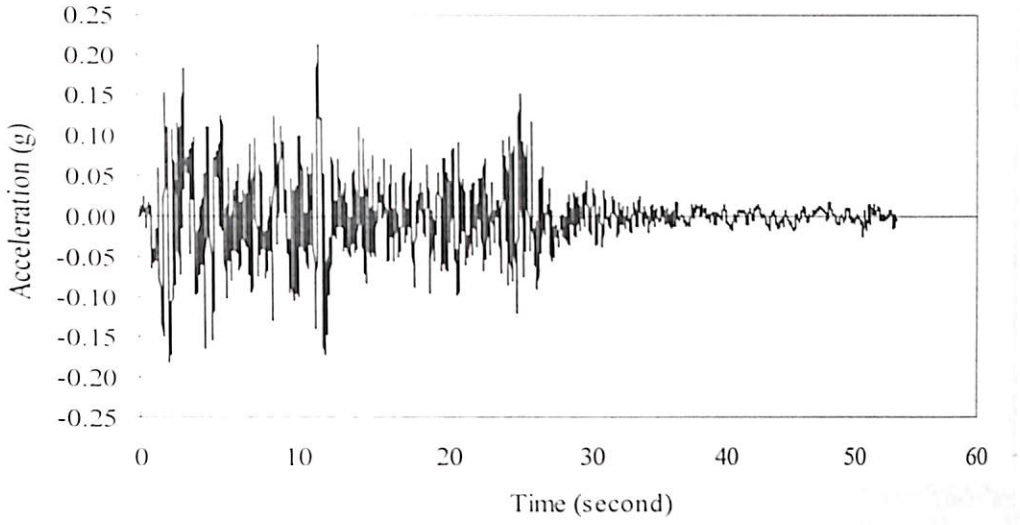

Fig. 4.104 East-West Component of El Centro Earthquake of May 18, 1940

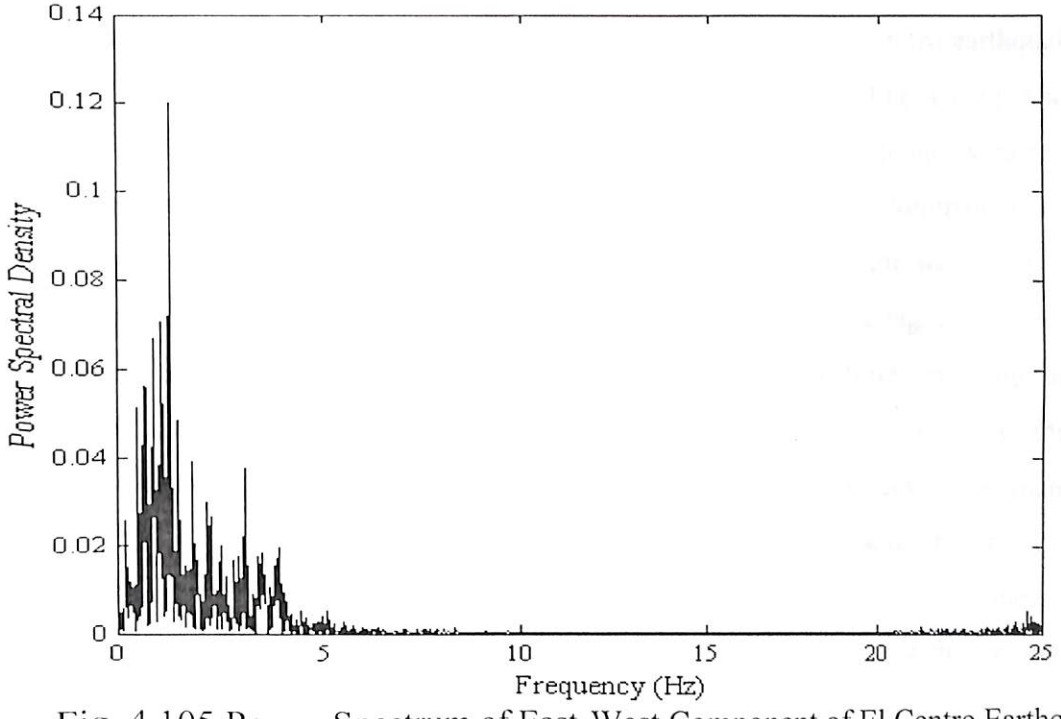

Fig. 4.105 Power Spectrum of East-West Component of El Centro Earthquake

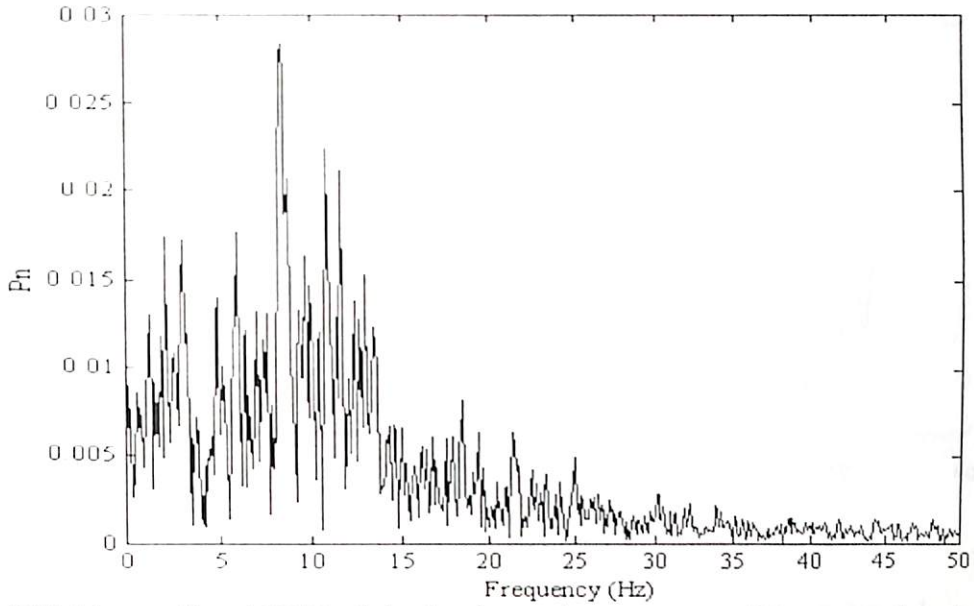

Fig. 4.106 Normalised FFT of the horizontal component of Koyna earthquake, 1967

The Short Time Fourier Transform (STFT) of the El Centro earthquake signal is evaluated at Δt = 0.02 sec (Fig. 4.107) and at Δt = 0.002 sec (Fig. 4.108). The frequency inputs in the proposed algorithm at each time step are the frequencies corresponding to the maximum spectral density in the moving window. These dominant frequencies are adopted as excitation frequency at each time step. When the time step is large (Δt = 0.02 sec), the number of samples per window is less than when the signal is sampled at Δt = 0.002 sec. It is observed from the figures that a larger time sampling may lead to inaccuracy in frequency evaluation, as it may not be possible to extract all the important frequencies present in the signal. It is seen that the peak frequency is less than 35 rad/sec when sampled at Δt = 0.02 sec (Fig.4.107), whereas the peak frequency reaches 70 rad/sec when sampled at Δt = 0.002 sec (Fig.4.108). Fig.4.109 shows the STFT of the Koyna earthquake (Fig.4.5) sampled at Δt = 0.005 seconds, where the frequencies of the Koyna earthquake reach a peak value of 80 rad/sec.

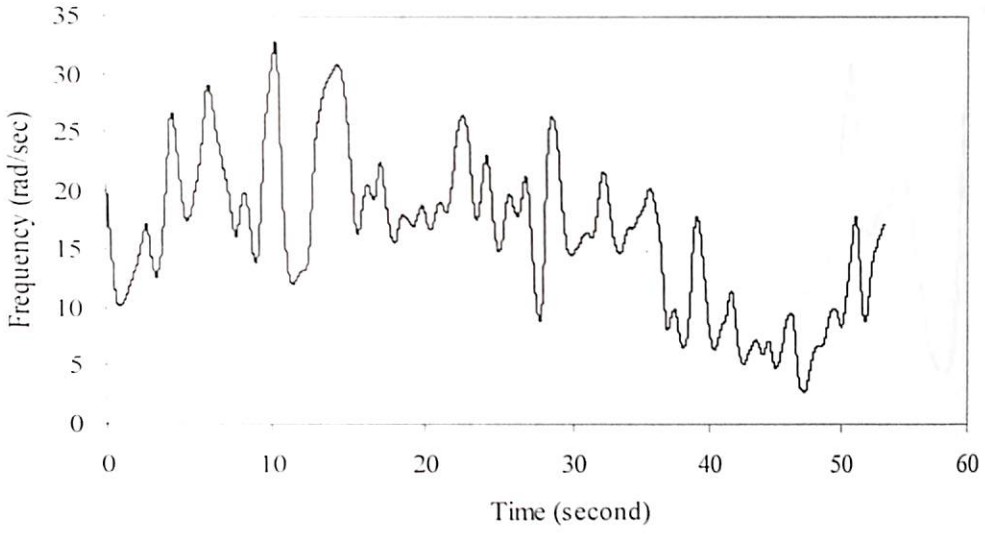

Fig. 4.107 STFT of El Centro earthquake, 1940 (Δt = 0.02 sec)

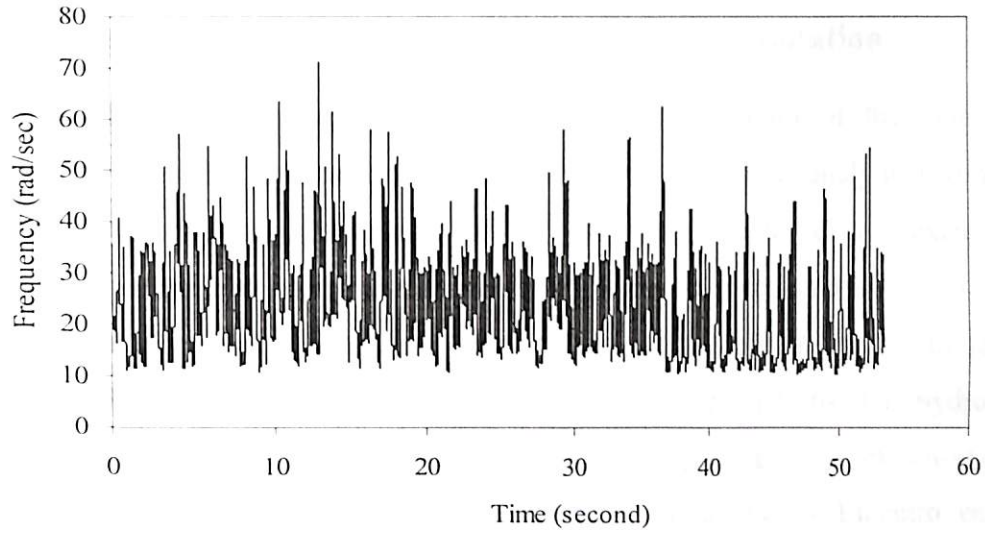

Fig. 4.108 STFT of El Centro earthquake, 1940 (Δt = 0.002 sec)

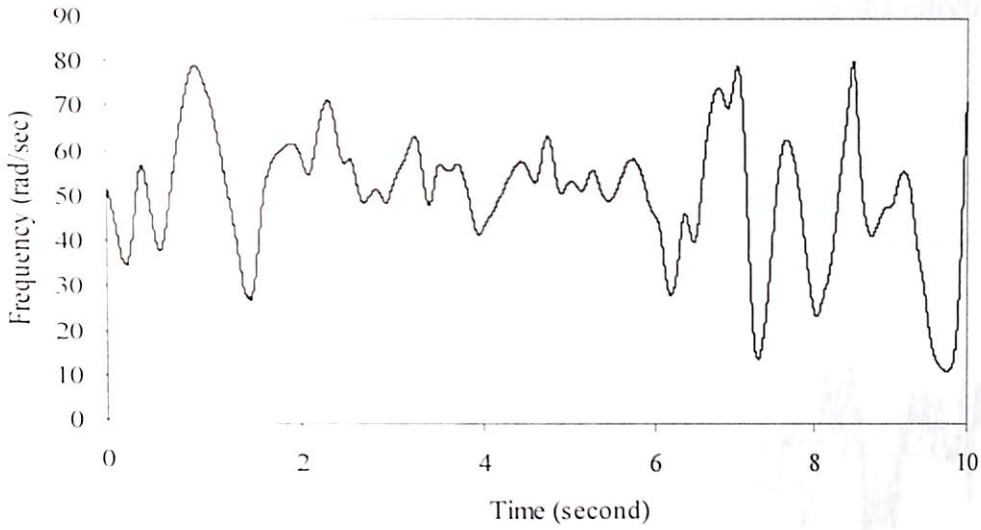

Fig. 4.109 STFT of Koyna earthquake, 1967 (Δt = 0.005 sec)

4.2.11.2 Hydrodynamic Pressure due to Seismic Excitation

The hydrodynamic pressure developed at the bottom of the dam-reservoir interface due to seismic excitation is evaluated. Due to lack of analytical technique to evaluate the hydrodynamic response of the reservoir due to seismic excitation, the accuracy of the proposed technique is verified by convergence study. The effectiveness of the proposed boundary condition using Short Time Fourier Transform (STFT) is examined for different reservoir depths and earthquake excitations. The hydrodynamic pressure coefficient is evaluated for a reservoir depth of (i) 30m and (ii) 150m considering the frequency content of East-West component of Elcentro earthquake (1940). At a reservoir depth of 30m, the fundamental frequency of the reservoir is 75.398 rad/sec, which is higher than the peak frequency content of the earthquake excitation (approximately 70 rad/sec as seen in Fig.4.108). At a reservoir depth of 150m, the fundamental frequency of reservoir becomes 15.07 rad/sec which is less than the peak frequency content of the earthquake excitation. It is observed from the results obtained in Section 4.2.3 that a reservoir length of $L = 0.5H_f$ is effective for all ranges of excitation frequencies to determine the hydrodynamic pressure in the reservoir due to harmonic excitation. Therefore, the hydrodynamic pressure coefficients are evaluated at the vertical upstream of the dam considering a length of the reservoir, $L = 0.5\ H_f$ for the first 6 seconds and compared with that obtained at $L = 3.0H_f$. The reflection coefficient is considered as 0.5 for the seismic analysis. It is interesting to note from Figs. 4.110 and

4.111 that consideration of STFT in the seismic analysis increases the effectiveness of the proposed truncation boundary condition.

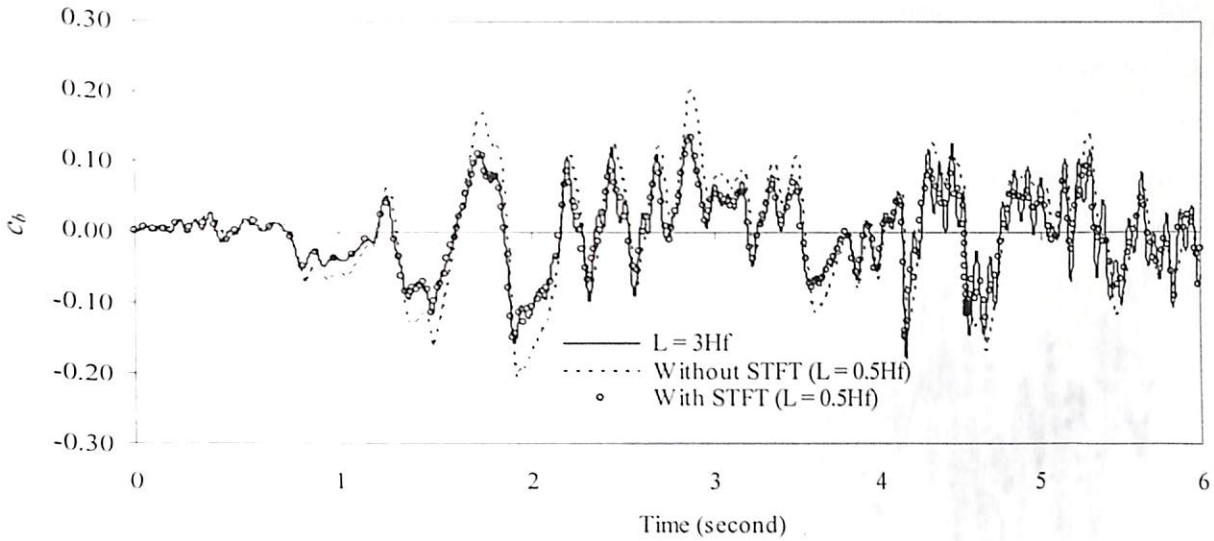

Fig. 4.110 Hydrodynamic pressure coefficient at the bottom of dam-reservoir interface due El Centro earthquake (H_f = 30 m)

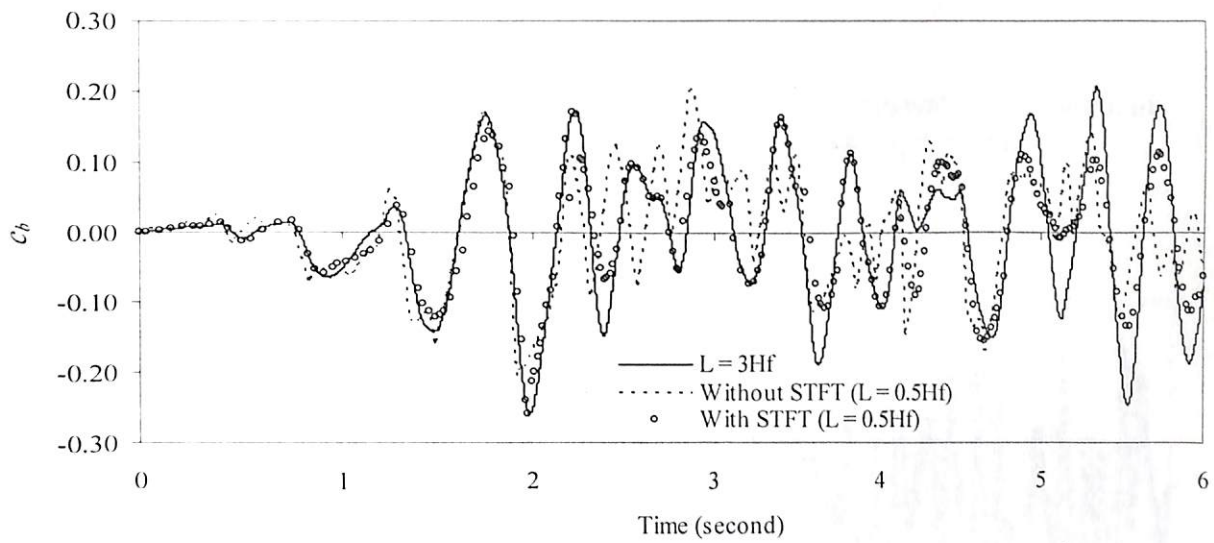

Fig. 4.111 Hydrodynamic pressure coefficient at the bottom of dam-reservoir interface due El Centro earthquake (H_f = 150 m)

The hydrodynamic pressure coefficients are determined for the reservoir having the same parameters as in the previous case considering the Koyna earthquake. It is seen from the Fig. 4.112 and 4.113, that the hydrodynamic response due to Koyna earthquake can be obtained accurately by imposing the proposed truncation boundary at a distance of

$L = 0.5H_f$. This is because the fundamental frequencies of the reservoir having depth of 30m and 150m are less than the peak frequency content of Koyna earthquake, which is approximately 80 rad/sec. When the STFT of the earthquake is not considered the effect of frequency dependent absorption at the reservoir can not be effectively accounted for, which as a result gives higher magnitudes of hydrodynamic response.

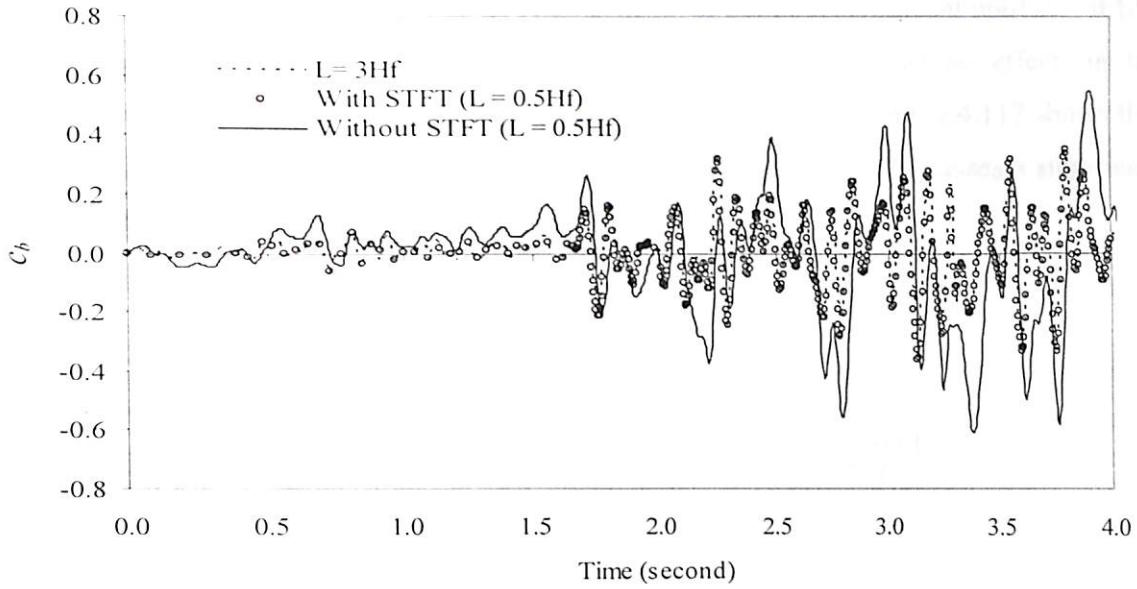

Fig. 4.112 Maximum hydrodynamic pressure coefficient at the bottom of dam-reservoir interface due to Koyna earthquake (H_f = 30 m)

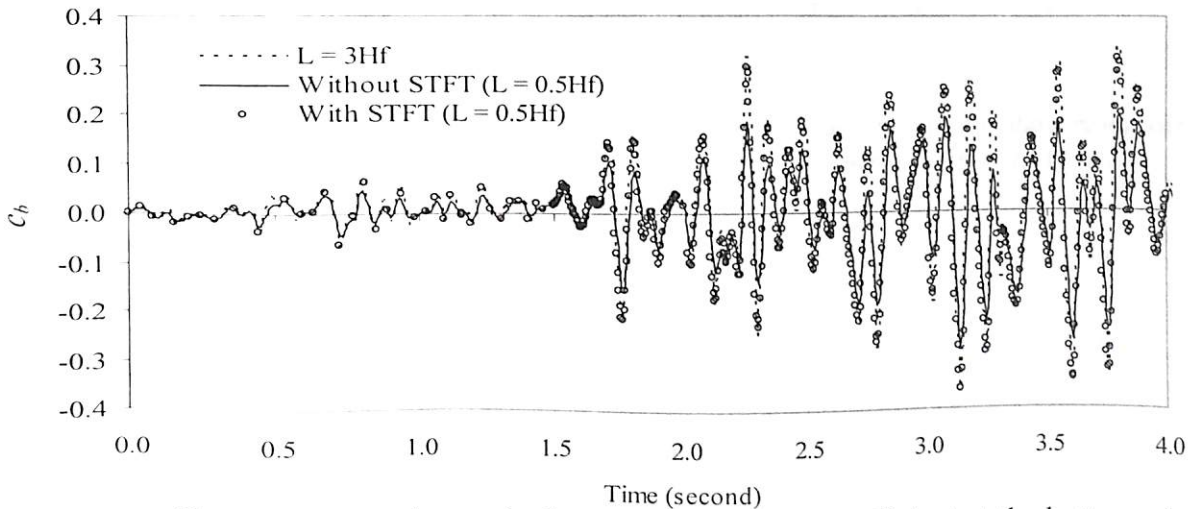

Fig. 4.113 Maximum hydrodynamic pressure coefficient at the bottom of dam-reservoir interface due to Koyna earthquake (H_f = 150m)

The hydrodynamic pressure distribution developed due to seismic excitation (Koyna earthquake, 1967) along the dam-reservoir interface is studied for different depths of sediment layer. The depth of the reservoir (H_f) is considered to be 150m. The depth of sediment layer (d_s) is expressed in terms of the reservoir depth (H_f). The infinite domain of the reservoir is truncated at $L = 0.5H_f$. It is observed from the results (Figs. 4.114-4.115) that effectiveness of the proposed algorithm in determining the hydrodynamic pressures is improved with the use of STFT. It is further observed from Fig.4.116 that the effect of increase in sediment layer depth is significant until $d_s = 0.1H_f$, beyond which an increase in sediment depth to $d_s = 0.5H_f$ has no effect on the hydrodynamic pressure developed. The pressure contours plotted in Fig.4.117 shows that an increase in the depth of sediment layer from $d_s = 0.01H_f$ to $0.1H_f$ causes a significant change in pressures developed in the reservoir.

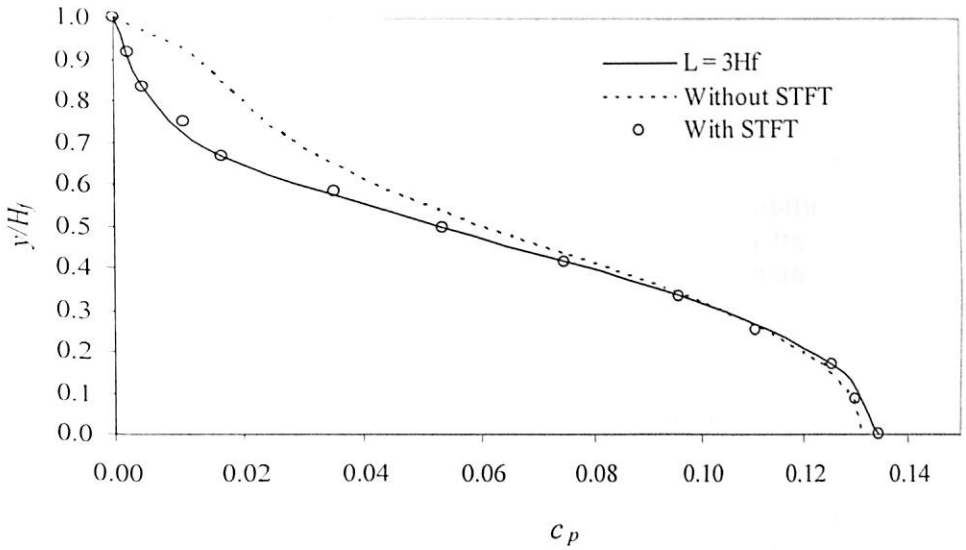

Fig. 4.114 Hydrodynamic pressure distribution along dam-reservoir interface due to seismic excitation at $t = 2.94$ seconds ($d_s = 0.01H_f$)

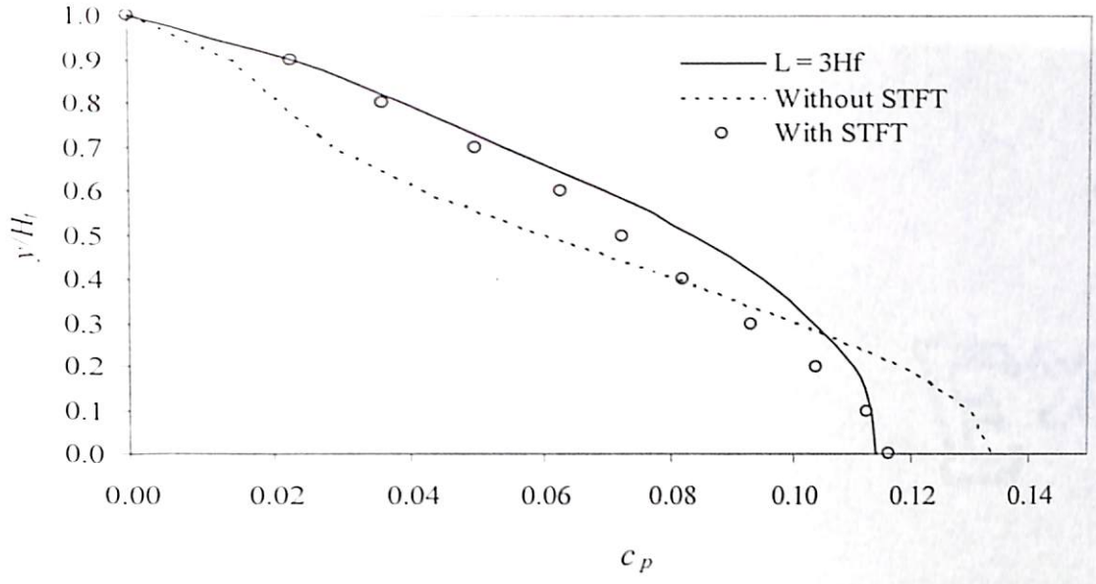

Fig. 4.115 Hydrodynamic pressure distribution along dam-reservoir interface due to seismic excitation, at t = 2.94 seconds ($d_s = 0.1H_f$)

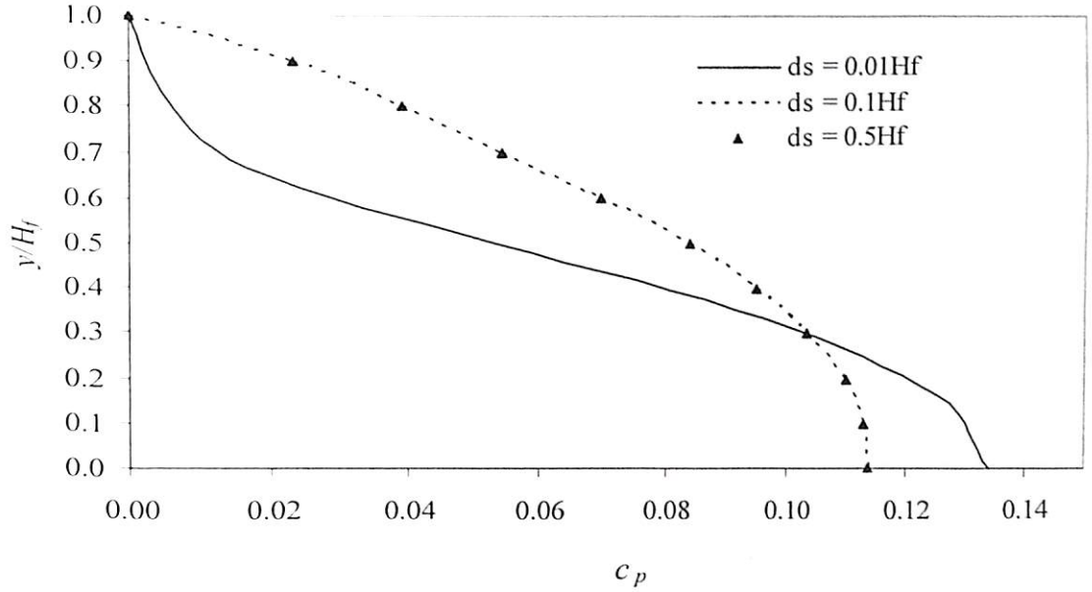

Fig. 4.116 Effect of sediment layer thickness on hydrodynamic pressure distribution along dam-reservoir interface due to seismic excitation at t = 2.94 seconds

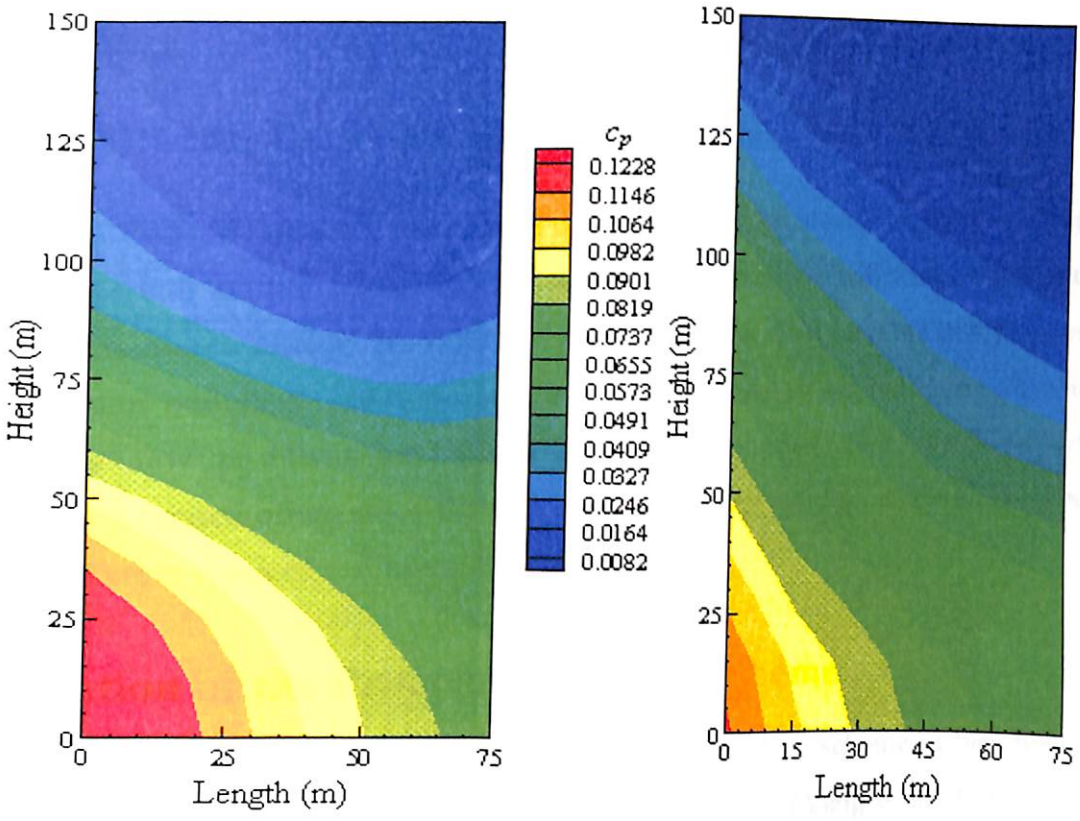

(i) $d_s = 0.01H_f$ (ii) $d_s = 0.1H_f$

Fig. 4.117 Pressure contour due to seismic excitation at $t = 2.94$ seconds

PART - III

4.3 ANALYSIS OF DAM-RESERVOIR COUPLED SYSTEM

In this section, the two dimensional analysis of a dam exposed to infinite reservoir having an absorptive reservoir bottom is carried out considering dam-reservoir interaction and degradation effects due to ageing. In order to examine the feasibility and accuracy of the proposed truncation boundary condition and the iterative scheme for the dam-reservoir coupled systems, few problems are solved using the computer code developed. A parametric study is carried out to study the dynamic response of the dam-reservoir coupled system under different types of excitation frequencies.

4.3.1 Validation of the Proposed Iterative Scheme

To examine the feasibility and accuracy of the proposed iterative scheme, a benchmark problem has been solved and compared with existing literature (Yang et al. 1996). The geometry and material properties of the coupled system considered in the present case are same as considered by Yang et al. (1996) and are as follows. Structure: height (H_d) = 120m, width at top and base = 90m, mass density (ρ_d) = 23.6 kN/m^3, Poisson's ratio (ν) = 0.2, modulus of elasticity (E_d) = 2.76 × 10^7 kN/m^2, Fluid: depth (H_f) = 120m; acoustic speed (c) = 1439 m/sec, mass density (ρ_f) = 9.97 kN/m^3. The fluid and the structural domain are discretized with four and eight noded elements respectively. A typical finite element discretization for the fluid-structure system is shown in Fig. 4.118. The response of the fluid-structure system subjected to ramp acceleration is studied truncating the fluid-domain at a distance of $L = 0.5H_f$. In the present analysis, the structure and fluid domain are discretized by 6 × 8 (i.e., $N_h = 6$ and $N_v = 8$) and 8 ×16 (i.e., $N_h = 8$ and $N_v = 16$) respectively (not shown in Fig. 4.118). The results adopting present algorithm are superimposed with the results obtained by Yang et al. (1996). Fig.4.119 shows the horizontal displacement at the top of the structure due to ramp acceleration with reflection coefficient of 1.0. The comparison of the results shows the accuracy of the developed iterative scheme.

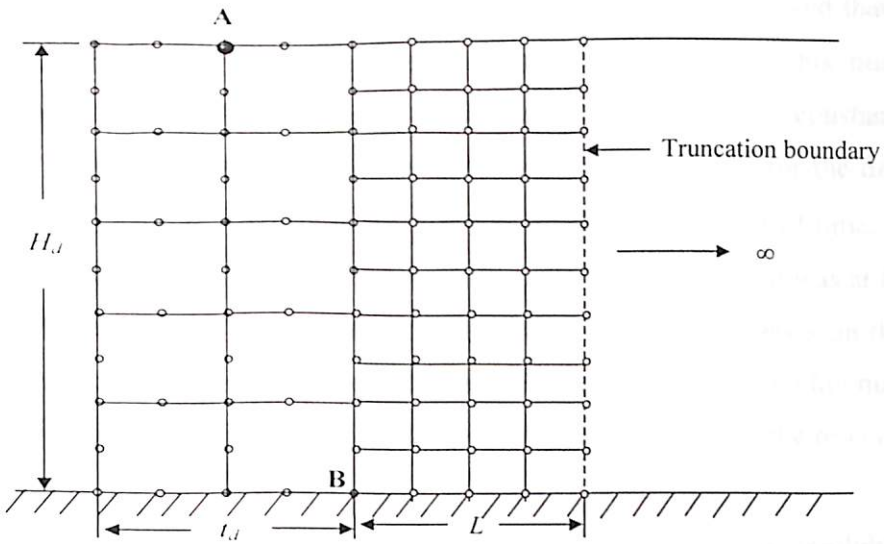

Fig. 4.118 Finite element mesh of a fluid-structure system

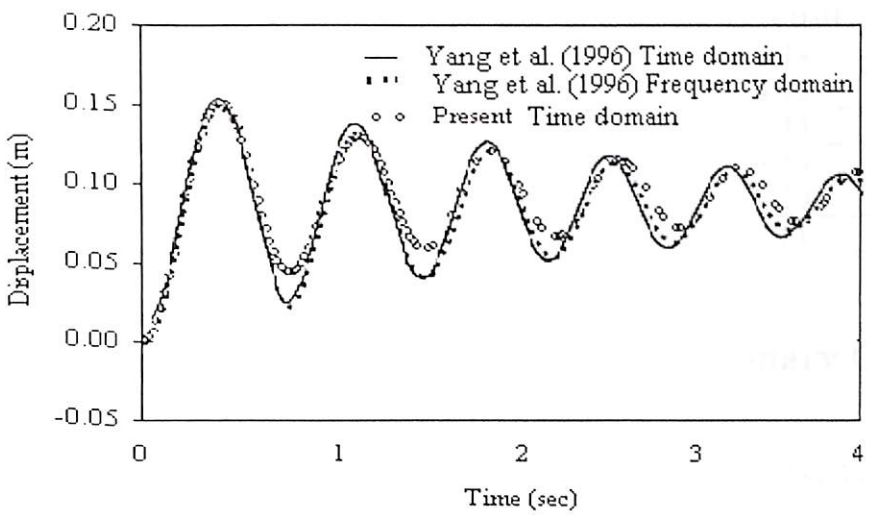

Fig. 4.119 Horizontal displacement at top of the structure due to ramp acceleration

4.3.2 Effectiveness of the Developed Iterative Scheme

To study the effectiveness of the present iterative scheme, the dam with the same geometrical and material parameters as in Section 4.1.1 are considered. The range of number of iterations for different modulus of elasticity of the dam and reflection coefficient is shown in Table 4.10. This iteration process is carried out for two different pre-assigned tolerance values, ε'' (eq. 3.120) as 0.001 and 0.01. It is observed that very few numbers of iterations are sufficient to obtain a desired convergence in results. The number of iterations is not constant for the analysis of the dam at each time step. The range of

variations at different time steps is given in Table 4.10. It is observed that the number of iterations required at the initial stage is comparatively more. This number gradually reduces to a lower value after a few time steps and becomes almost constant. For example, the number of iterations required for a tolerance value of 0.001 for the dam having E_d = 3.15×10^7 kN/m^2 and $\alpha = 0.5$ are from 4-18 for different instant of time. This means the iteration number reduces to 4 after a few time steps from 18, which was at the initial stage. It is observed from Table 4.10 that the number of iterations depends on the flexibility of the dam and reflection coefficient of the reservoir bottom. The iteration number increases for higher flexibility of the dam and reduces for higher rigidity of the reservoir bottom.

Table 4.10 Number of iterations for different modulus of elasticity of dam and reflection coefficient of the reservoir bottom

Modulus of Elasticity (kN/m^2)	α	**No. of Iterations for** $\varepsilon'' = 0.001$	**No. of Iterations for** $\varepsilon'' = 0.01$
3.15×10^6	1.0	5-19	4-14
	0.5	8-20	4-15
3.15×10^7	1.0	3-18	3-13
	0.5	4-18	3-13
3.15×10^8	1.0	3-12	2-10
	0.5	3-17	2-11

4.3.3 Effectiveness of the Proposed Far-Boundary Condition for Dam-Reservoir System

To evaluate the effectiveness of the proposed far-boundary condition for the coupled dam-reservoir system, a typical finite element discretization of the dam-reservoir system is considered as shown in Fig. 4.120. A simplified geometry of the Koyna dam having the same material properties as described in Section 4.1.1 is considered. The depth of the water is considered to be equal to the height of the dam. The acoustic wave speed in water and the mass density of water are considered to be 1438.7m/sec and 999.8 kg/m^3 respectively. The reflection coefficient, α is taken as 0.5. The ground excitation of the dam is considered as sinusoidal $a_g = a.\sin(\omega t)$, where the magnitude of a is chosen as unity, i.e., 1.0 m/sec^2. The value of ω is considered as 8.2475 rad/sec, which is the half of the fundamental frequency of the dam having an elastic modulus (E_d) of 3.15×10^7 kN/m^2. The two systems are solved separately and the interaction effects are incorporated through the iterative scheme proposed in the present analysis. In view of lack of analytical

procedure for a dam-reservoir coupled system, the effectiveness of the proposed TBC is established by analyzing its convergence characteristics. Therefore, the results are compared with those obtained by placing the proposed truncation boundary at a sufficiently large distance away from the dam (i.e., at $L = 3.0H_f$) for which Sommerfeld condition and the present condition produce identical results. In the present case, the dam is discretized using a discretization of $N_v = 5$ and $N_h = 3$, that has been found to give convergent results in Tables 4.1.

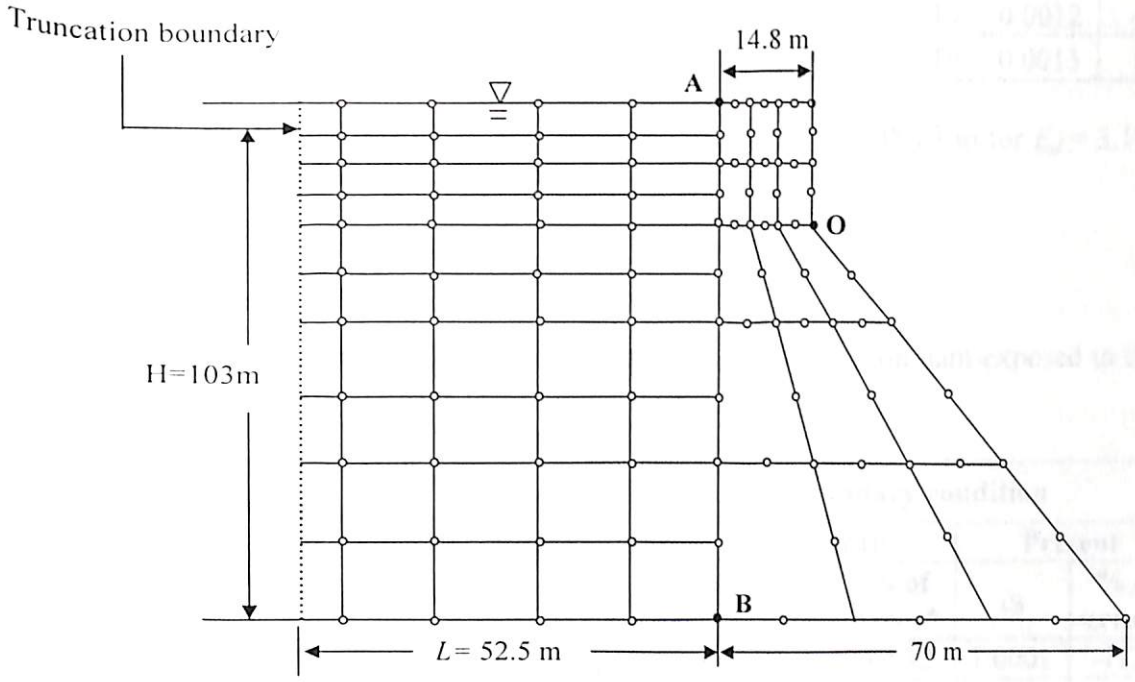

Fig. 4.120 Finite element mesh of dam-reservoir system

The horizontal crest displacements of the dam (u_x) and the hydrodynamic pressure coefficient at the base of the upstream face of the dam, ($c_b = p_b/\rho_f aH_f$) are tabulated in Tables 4.11 and 4.12 respectively for different elastic properties of the dam material. Here, p_b is the hydrodynamic pressure at the bottom of the dam-reservoir interface, ρ_f is the density of water, g is the gravitational acceleration and H_f is the depth of the reservoir. The values tabulated are at a time instant, $t = 0.75T$, when the amplitude of sinusoidal loading is maximum.

Table 4.11 Comparison of horizontal crest displacement of dam exposed to infinite reservoir for different truncation boundary conditions

E_d (kN/m^2)	L/H_f	Mesh size ($N_v \times N_h$)	Truncation boundary condition					
			Sommerfeld		Sharan 1992		Present	
			u_x (m)	% of error*	u_x (m)	% of error*	u_x (m)	% of error*
3.15×10^6	0.2	10×2	0.1080	-35.50	0.1501	-10.35	0.1515	-9.51
	0.5	10×5	0.1464	-12.57	0.1576	-5.88	0.1661	-0.83
3.15×10^7	0.2	10×2	0.0216	-30.31	0.0280	-9.67	0.0300	-3.22
	0.5	10×5	0.0289	-6.69	0.0283	-8.70	0.0306	-1.37
3.15×10^8	0.2	10×2	0.0014	11.31	0.0011	-15.19	0.0012	-4.33
	0.5	10×5	0.0014	10.42	0.0012	-4.19	0.0013	0.68

* Compared with the values of u_x = 0.1675 m, 0.031 m and 0.0013 m for $E_d = 3.15\times10^6$, 3.15×10^7 and 3.15×10^8 kN/m^2 respectively

Table 4.12 Comparison of hydrodynamic pressure coefficient on dam exposed to infinite reservoir for different truncation boundary conditions

E_d (kN/m^2)	L/H_f	Mesh size ($N_v \times N_h$)	Truncation boundary condition					
			Sommerfeld		Sharan		Present	
			c_b	% of error*	c_b	% of error*	c_b	% of error*
3.15×10^6	0.2	10 × 2	1.0307	-8.92	0.9356	-17.32	1.0001	-11.62
	0.5	10 × 5	1.0882	-3.84	0.9838	-13.06	1.1124	-1.70
3.15×10^7	0.2	10 × 2	0.8019	-33.17	0.8759	-27.00	0.9215	-23.20
	0.5	10 × 5	1.3334	11.13	0.9448	-21.26	1.1819	-1.50
3.15×10^8	0.2	10 × 2	1.0955	29.75	0.7204	-14.67	0.7598	-10.00
	0.5	10 × 5	1.0006	18.51	0.7276	-13.82	0.8542	1.17

* Compared with the values of c_b = 1.1316, 1.1999 and 0.8443 for $E_d = 3.15\times10^6$, 3.15×10^7 and 3.15×10^8 kN/m^2 respectively

Large crest displacements are obtained for the case when the dam is considered extremely flexible and the dam shows small deformations when the rigidity of the dam is increased (Table 4.11). The hydrodynamic response of the coupled system due to harmonic excitation is dependent on the natural frequencies of coupled dam-reservoir system. The dependence of development of hydrodynamic pressure coefficients at the dam base on the flexibility of the dam (Table 4.12) cannot be generalized from the present

analysis. This is because the effect of dam-reservoir interaction is to alter the fundamental properties of the dam-reservoir coupled system. The fundamental frequencies (ω_d) of the dam having elastic moduli 3.15×10^6 kN/m^2, 3.15×10^7 kN/m^2 and 3.15×10^8 kN/m^2 are 5.216 rad/sec, 16.495 rad/sec and 52.16 rad/sec respectively. Hence, the frequency ratio (ω_d/ω) for the three cases are 0.632, 2.0 and 6.324. Since the reservoir depth and acoustic velocity of water is kept constant for all the cases analyzed, the fundamental frequency of the reservoir is constant for all the cases. It is observed from the Table 4.12, that the pressure coefficients increase as the frequency ratio (ω_d/ω) approaches 2.0, and tends to reduce with an increase in frequency ratio ($\omega_d/\omega = 6.324$). The tabulated results show that a length of the reservoir, $L = 0.5H_f$ can be used considering present truncation boundary condition to obtain the hydrodynamic response of a dam-reservoir with negligible error. The results indicate that the proposed far-boundary condition is more effective as the flexibility of the structure reduces.

To evaluate the effectiveness of the developed truncation boundary condition (TBC) with the incorporation of Short Time Fourier Transform (STFT) in the proposed algorithm for dam-reservoir interaction, the Koyna dam-reservoir system is considered with the same geometrical and material properties as in Section 4.3.3. The dynamic magnifications of strength and stiffness parameters due to rapid application of seismic strains are not considered. Due to lack of classical solution, the response of the coupled dam-reservoir system is compared with those obtained at $L = 3.0H_f$. The crest displacement of the dam and the hydrodynamic pressure coefficient (c_b) at the bottom of the upstream face of the dam due to the horizontal component of Koyna earthquake are presented herein. It is evident from Figs. 4.121 and 4.122 that at $L = 0.5H_f$, the algorithms using STFT gives crest displacements and pressure coefficients without much loss in accuracy.

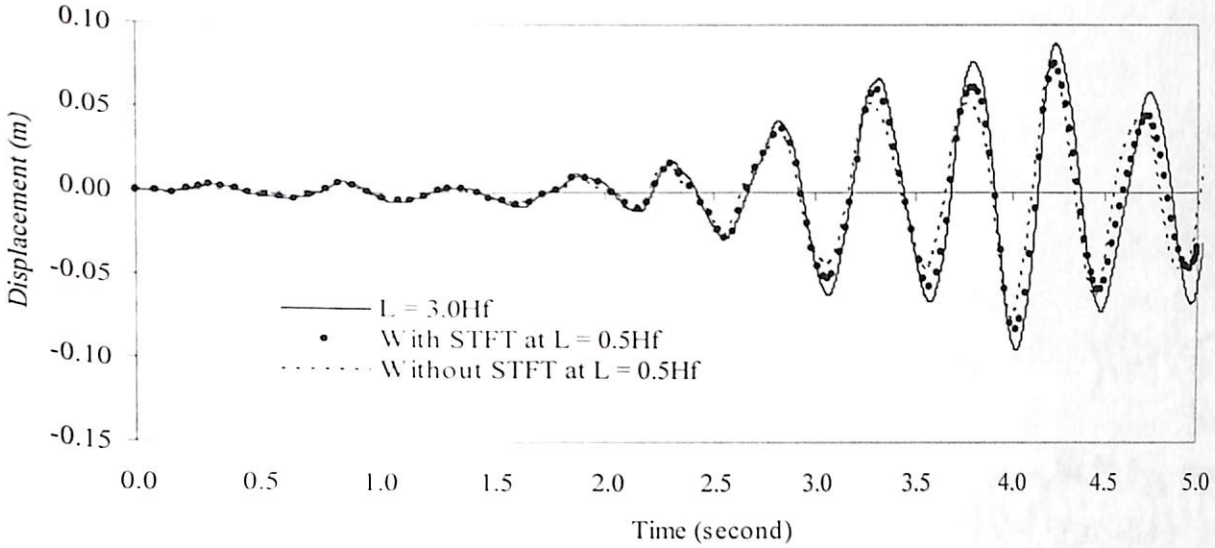

Fig. 4.121 Crest displacement of Koyna dam due to Koyna earthquake

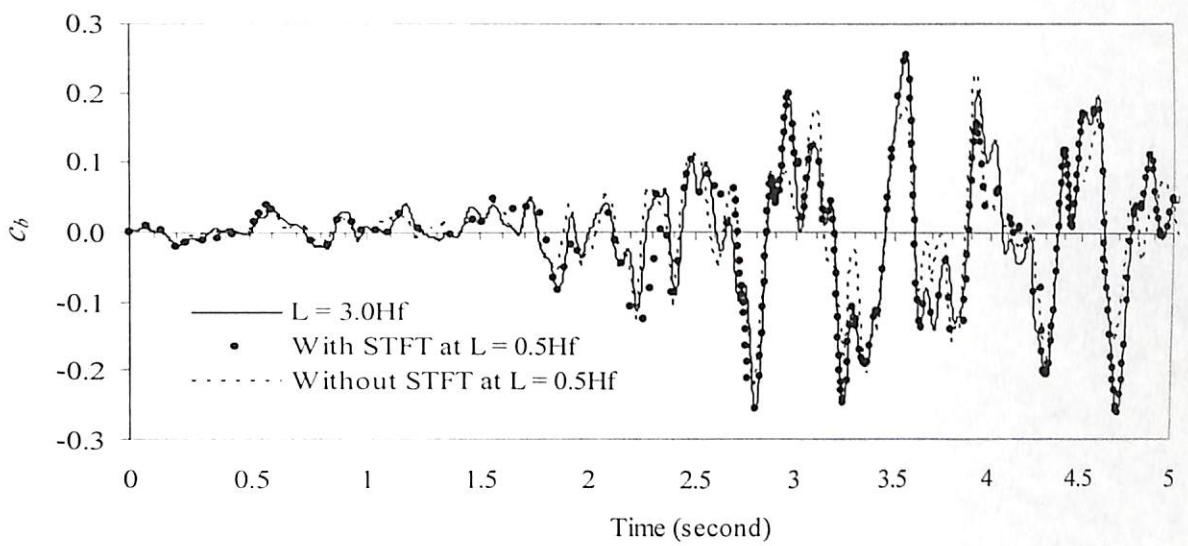

Fig. 4.122 Hydrodynamic pressure at the bottom of Koyna dam due to Koyna earthquake

4.3.4 Analysis of Dam-Reservoir System without Degradation

A two-dimensional linear elastic dynamic analysis is carried out to study the effect of reservoir bottom absorption in the evaluation of hydrodynamic pressure in the reservoir in the presence of an elastic dam with vertical upstream face under horizontal ground excitation. Degradation of the elastic dam due to ageing is not considered in this section.

4.3.4.1 Effect of Reservoir Bottom Absorption

A parametric study is carried out to study the effect of reservoir bottom absorption on the hydrodynamic response of the structure subjected to different types of excitation. A typical two-dimensional model of a concrete gravity dam monolith with vertical upstream face is considered as in Fig. 4.120. The material properties of the concrete dam are same as considered in Section 4.1.1. Here, the dynamic magnifications of strength and stiffness parameters of concrete due to rapid application of seismic strains are not considered. The acoustic wave speed (c) is 1438.7 m/sec, mass density of water (ρ_f) is 999.8 N/m^3. The fluid-structure system is excited under different types of acceleration: (i) ramp, (ii) sinusoidal with different excitation frequencies and (iii) seismic. The graphical results plotted in Figs. 4.123 and 4.124 show that the reservoir bottom absorption has negligible effect on the displacement and hydrodynamic pressure due to the application of ramp acceleration. It is also evident from the literature (Hatami 1997 & Chuhan et al. 2001) that reservoir bottom absorption effect is frequency dependent and not pronounced for low excitation frequencies.

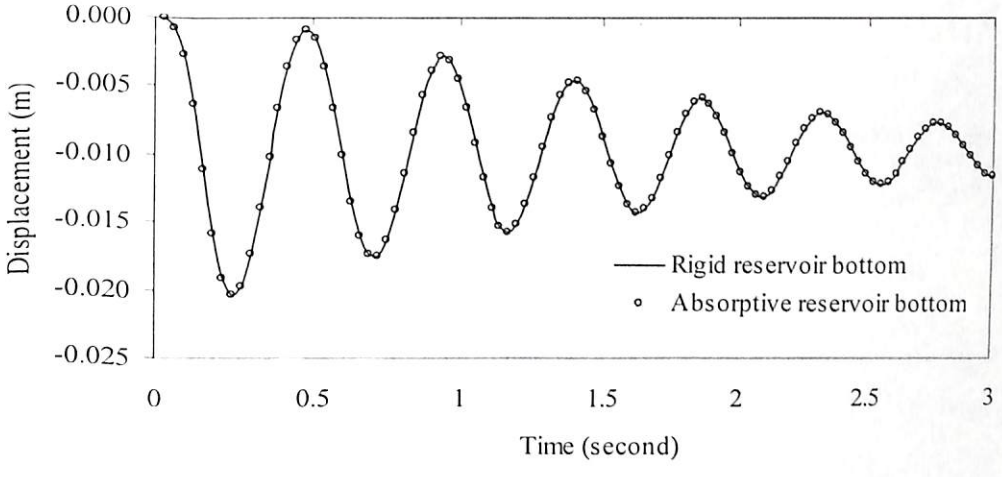

Fig. 4.123 Displacement at top of the dam due to ramp acceleration

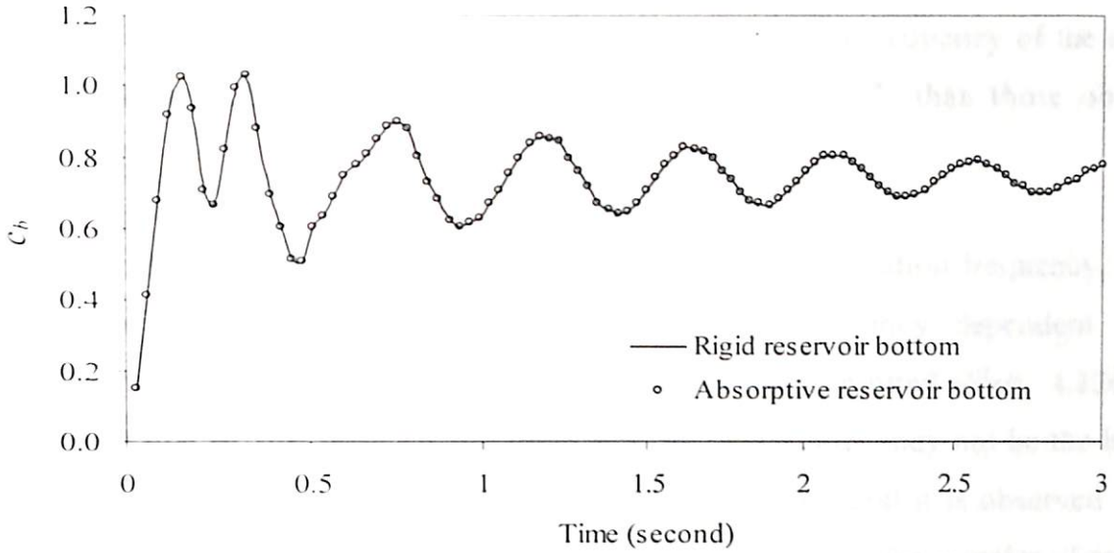

Fig. 4.124 Hydrodynamic pressure coefficient at the bottom of the dam due to ramp acceleration

To study the effect of the absorptive reservoir bottom due to sinusoidal excitation on coupled dam-reservoir system, the same geometry and material of the dam-reservoir system as in the previous case is considered. The dam-reservoir system is subjected to sinusoidal excitation frequencies (i) equal to the resonant frequency of the dam, ω = 16.495 rad/sec, (ii) lower than the resonant frequency of the reservoir, ω = 0.877 rad/sec (at Tc/H_f = 100), (iii) equal to the resonant frequency of the reservoir, ω = 36.897 rad/sec (at Tc/H_f = 4) and (iv) higher than the resonant frequency of the reservoir, ω = 87.763 rad/sec (at Tc/H_f = 1). The peak ground acceleration in this case is considered as 1.0 m/sec^2.

The displacements and hydrodynamic pressure coefficients at an excitation frequency equal to ω = 16.495 rad/sec are plotted in Figs. 4.125 and 4.126. It is seen that the reduction in crest displacement and hydrodynamic pressure coefficient due to absorptive effect of the reservoir bottom is more pronounced than that for ramp acceleration. At Tc/H_f = 100, when the excitation frequency (ω = 0.877 rad/sec) is very much smaller than the resonant frequency of the reservoir, the crest displacements and the hydrodynamic pressure coefficients (c_b) obtained show that the effect of reservoir bottom absorption is negligible (Fig. 4.127 and 4.128). The effect of reservoir bottom absorption on the dam-reservoir coupled system excited at the resonant frequency of the reservoir (Tc/H_f = 4) is to significantly reduce the crest displacements of the dam and hydrodynamic

pressure coefficients (c_b) at the base of the dam (Figs. 4.129 and 4.130). Also, at $Tc/H_f = 1$, when the excitation frequency is greater than the fundamental frequency of the reservoir, the reservoir bottom effect is significant (Fig.4.131 and 4.132) than those obtained at $Tc/H_f < 4$.

It is interesting to note that with an increase in the excitation frequency, the crest displacements of the dam reduce, which is due to frequency dependent damping mechanism at the reservoir bed. The pressure coefficients plotted (Figs. 4.126, 4.128, 4.130 and 4.132) are at the base of the dam and the magnitudes may not be the highest at the base for different excitation frequencies. However, in general it is observed from the results that the effect of reservoir bottom is significant for higher frequencies of excitation.

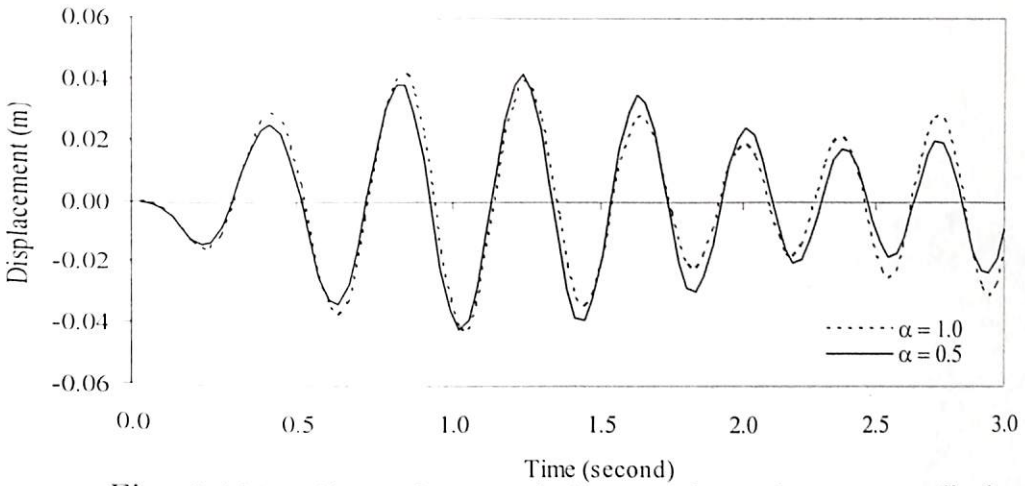

Fig. 4.125 Effect of reservoir bottom absorption on crest displacement of the dam due to sinusoidal excitation (ω = 16.495 rad/sec)

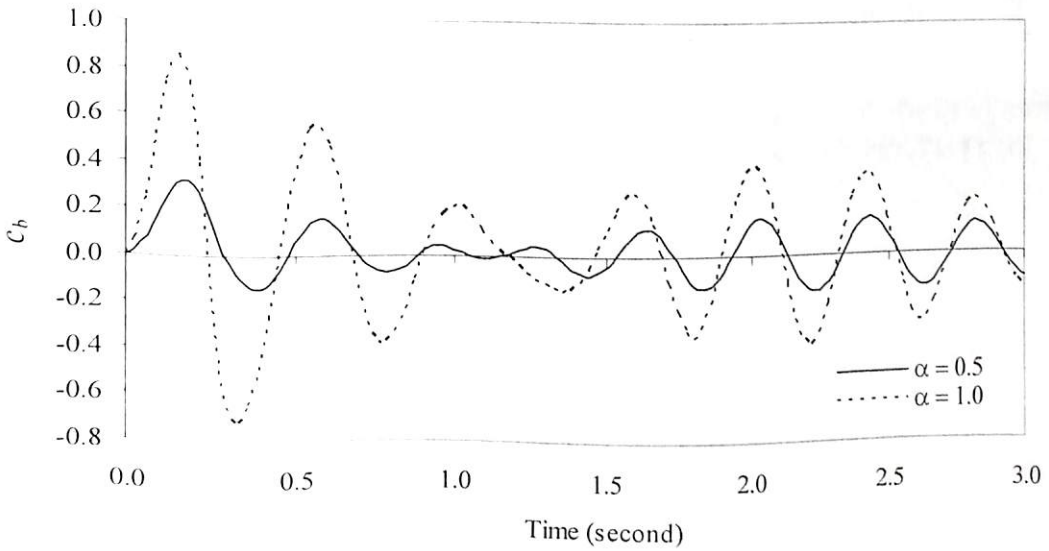

Fig. 4.126 Effect of reservoir bottom absorption on hydrodynamic pressure coefficient due to sinusoidal excitation (ω = 16.495 rad/sec)

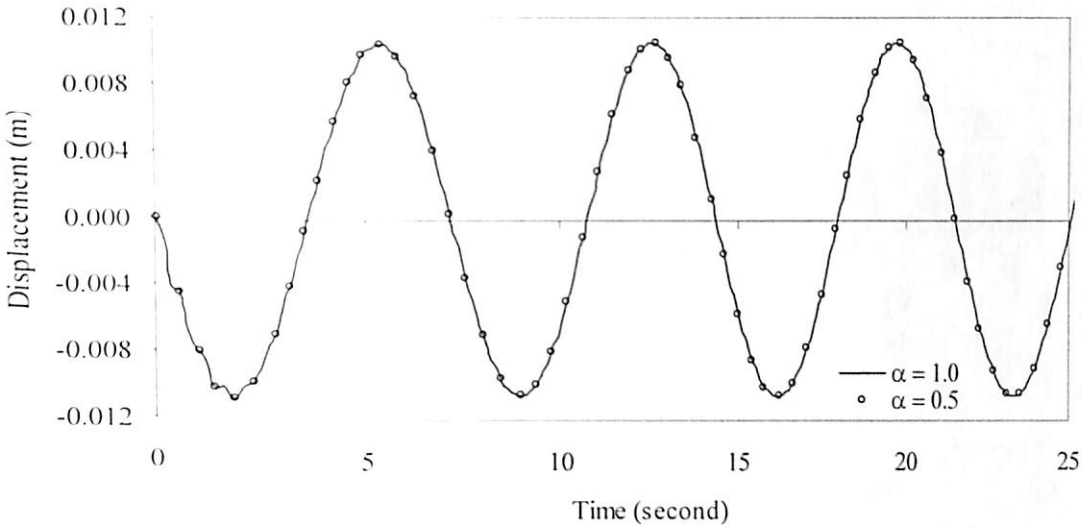

Fig. 4.127 Effect of reservoir bottom absorption on crest displacement of dam due to sinusoidal excitation (ω = 0.877 rad/sec)

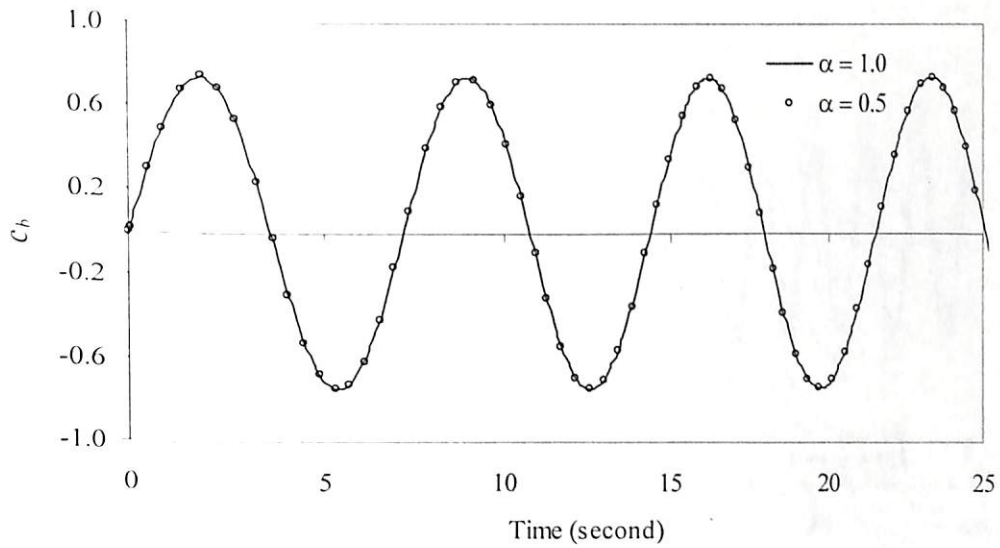

Fig. 4.128 Effect of reservoir bottom absorption on hydrodynamic pressure coefficient due to sinusoidal excitation (ω = 0.877 rad/sec)

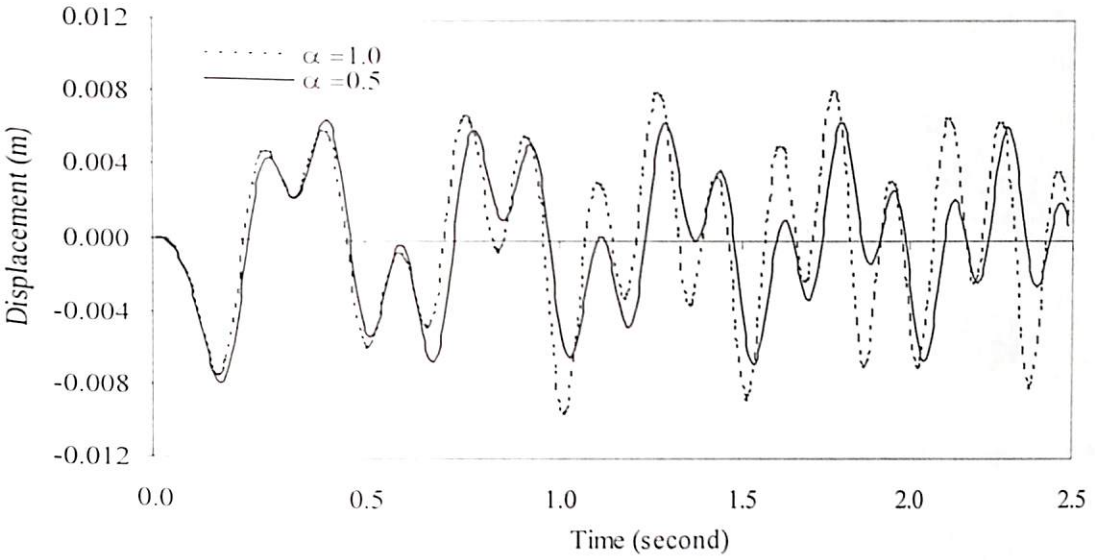

Fig. 4.129 Effect of reservoir bottom absorption on crest displacement of dam due to sinusoidal excitation (ω = 36.897 rad/sec)

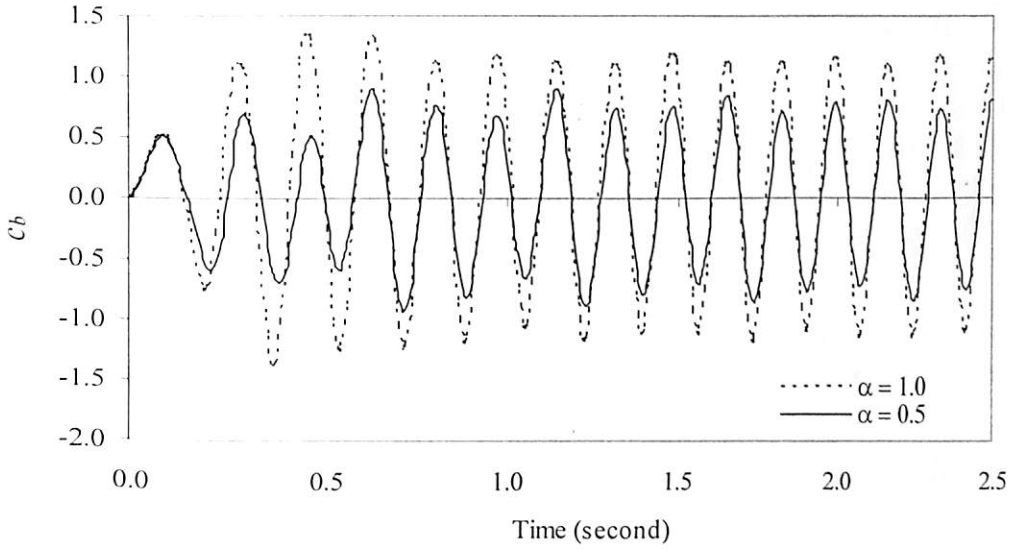

Fig. 4.130 Effect of reservoir bottom absorption on hydrodynamic pressure coefficient due to sinusoidal excitation (ω = 36.897 rad/sec)

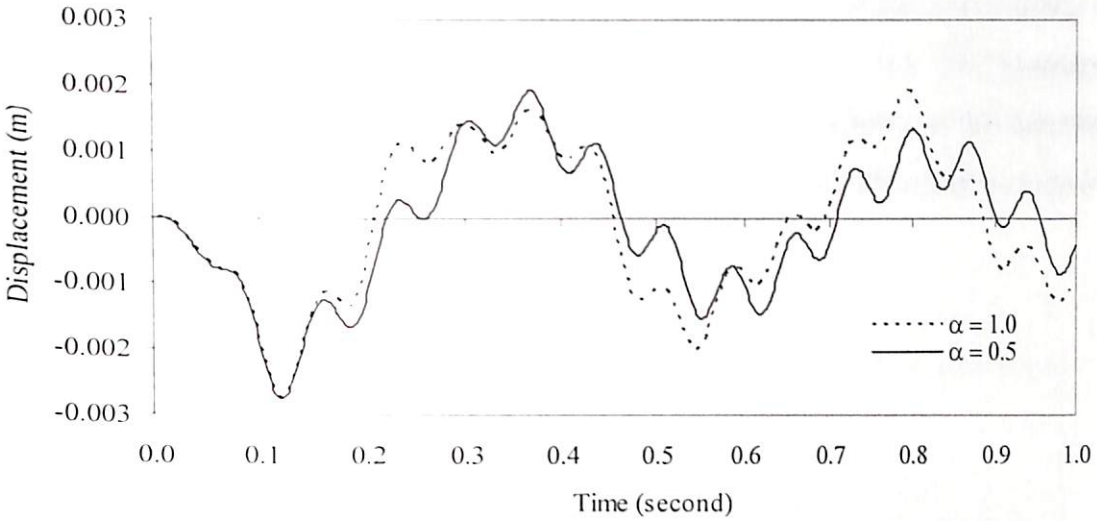

Fig. 4.131 Effect of reservoir bottom absorption on crest displacement of dam due to sinusoidal excitation (ω = 87.763 rad/sec)

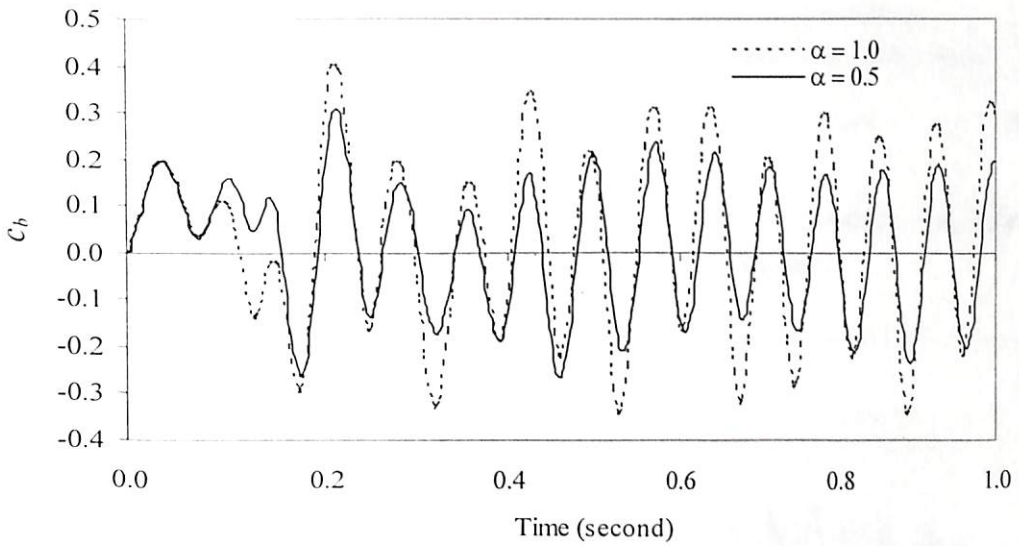

Fig. 4.132 Effect of reservoir bottom absorption on hydrodynamic pressure coefficient due to sinusoidal excitation (ω = 87.763 rad/sec)

The random vibration caused by an earthquake generally consists of many frequencies. Hence, it is important to evaluate the effectiveness of the proposed algorithm for seismic analysis of dam-reservoir system in time domain. To observe the effect of the reservoir bottom absorption due to seismic excitation, the dam with the same material and geometrical properties as above is considered. The variation of normalized crest displacement due to Koyna earthquake (Fig. 4.5) is plotted to observe the effect of absorption at the reservoir bottom. It is observed from Fig. 4.133 and 4.134 that the crest

displacement and hydrodynamic pressure coefficient (c_b) is reduced considerably due to absorptive reservoir bottom with reflection coefficient of α = 0.5. The hydrodynamic pressure at the upstream face of the dam depends on the acceleration of the dam-reservoir interface. The acceleration of the flexible dam thus affects the hydrodynamic response due to seismic excitation.

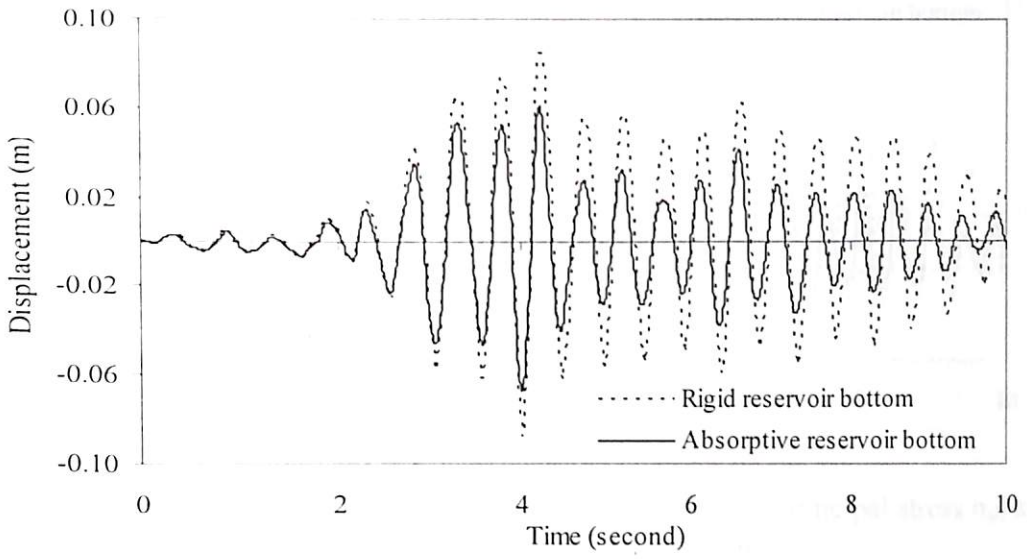

Fig.4.133 Effect of reservoir bottom absorption on crest displacement of the dam due to Koyna earthquake

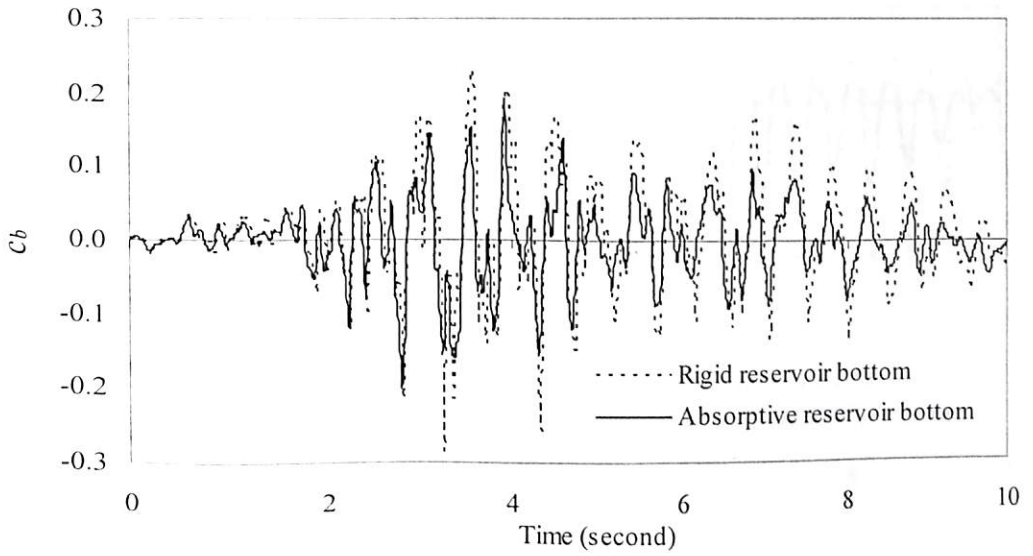

Fig. 4.134 Effect of reservoir bottom absorption on hydrodynamic pressure coefficient at point B due to Koyna earthquake

The stresses at any node are evaluated as described in Section 3.2.7. The principal stresses σ_{p1} (maximum tensile and minimum compressive) and σ_{p2} (maximum compressive and minimum tensile) at point B and O (Fig. 4.120) are plotted in Figs. 4.135

- 4.136 and 4.137 - 4.138 respectively. It is observed from these graphs that the principal stresses in the dam reduce significantly in the presence of the absorptive reservoir bottom. It is interesting to note that the magnitudes of stresses at the point O are higher than the stresses at point B because of development of stress concentration.

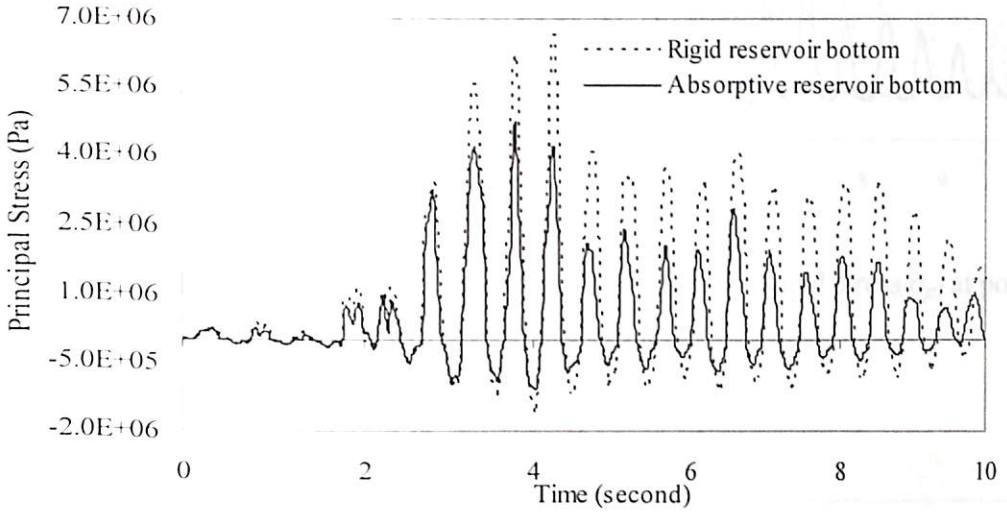

Fig. 4.135 Effect of reflection coefficient on principal stress σ_{p1} at point B of the dam due to Koyna earthquake

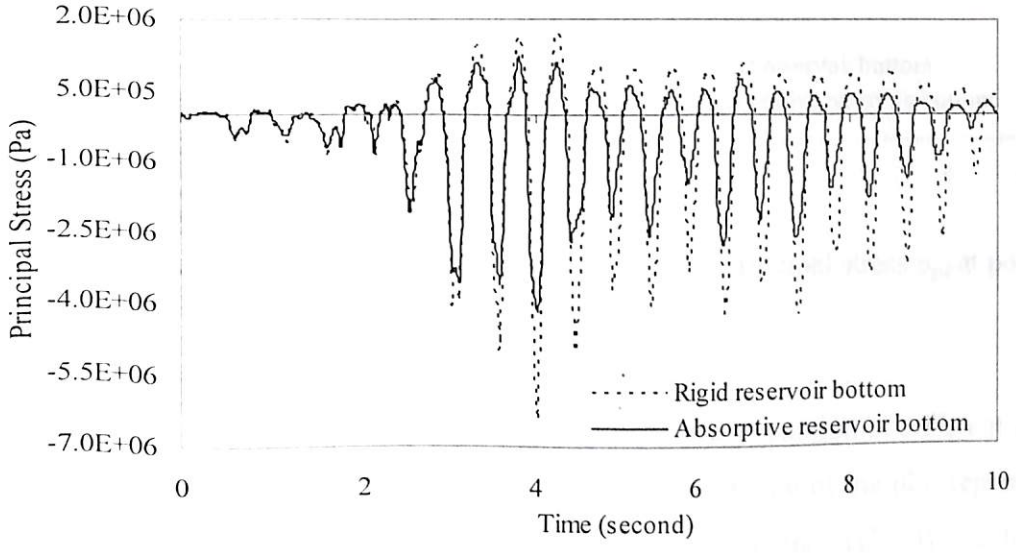

Fig. 4.136 Effect of reflection coefficient on principal stress σ_{p2} at point B of the dam due to Koyna earthquake

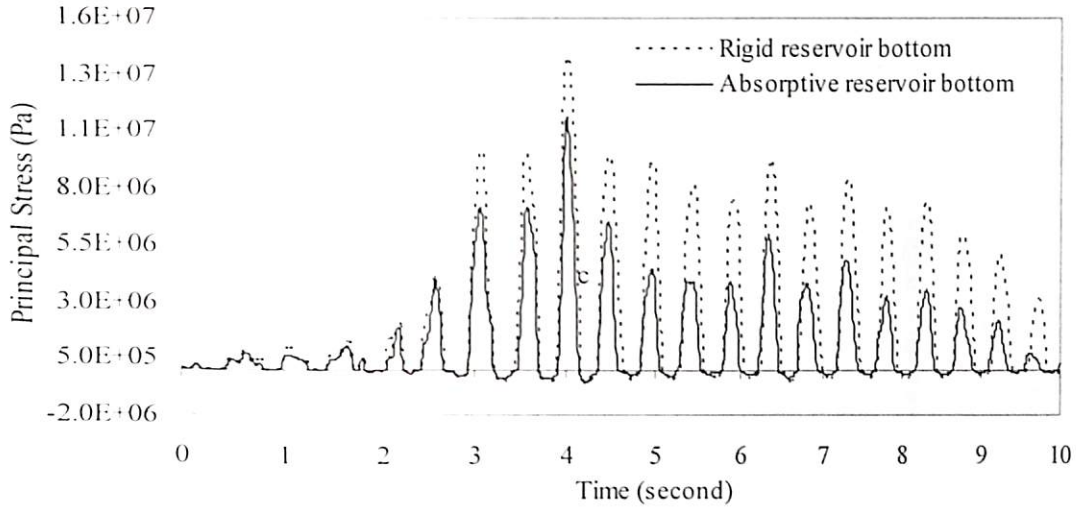

Fig. 4.137 Effect of reflection coefficient on principal stress σ_{p1} at point O of the dam due to Koyna earthquake

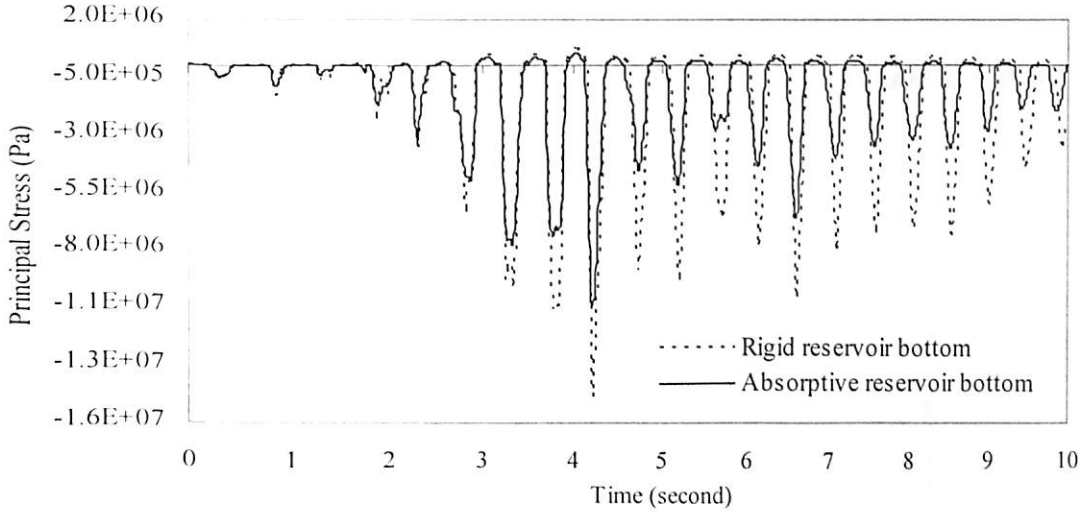

Fig. 4.138 Effect of reflection coefficient on principal stress σ_{p2} at point O of the dam due to Koyna earthquake

The velocity vectors in the reservoir due to seismic excitation at different instants of time are plotted in Figs. 4.139 to 4.142. The height and width of the plot represent the reservoir height and length respectively. The lengths of the velocity vectors are proportional to the magnitude of the velocity. Figs. 4.139 and 4.140 show the velocity vectors for rigid reservoir bottom (α =1.0) and Figs. 4.141 - 4.142 for absorptive reservoir bottom (α = 0. 5). The magnitudes and directions of the velocity vectors in these figures show the effect of reservoir bottom absorption at different instants of time.

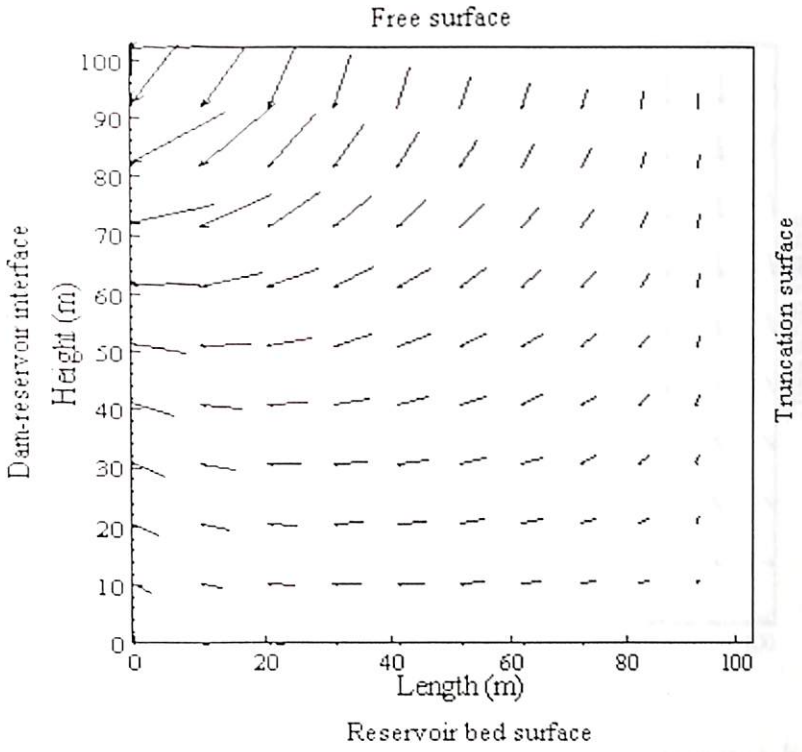

Fig. 4.139 Velocity vector in the reservoir with rigid bottom at 3.25 sec

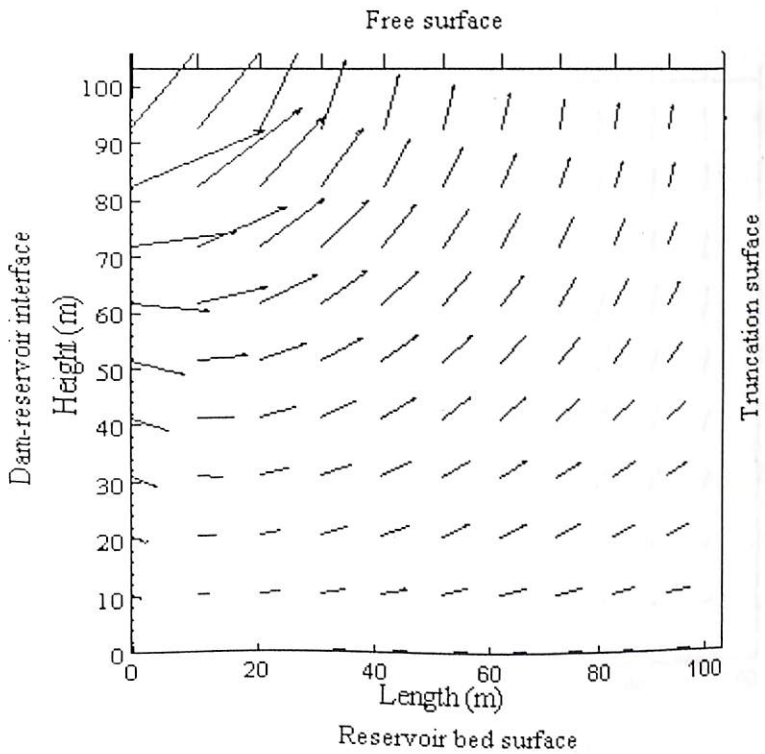

Fig. 4.140 Velocity vector in the reservoir with rigid bottom at 3.91 sec

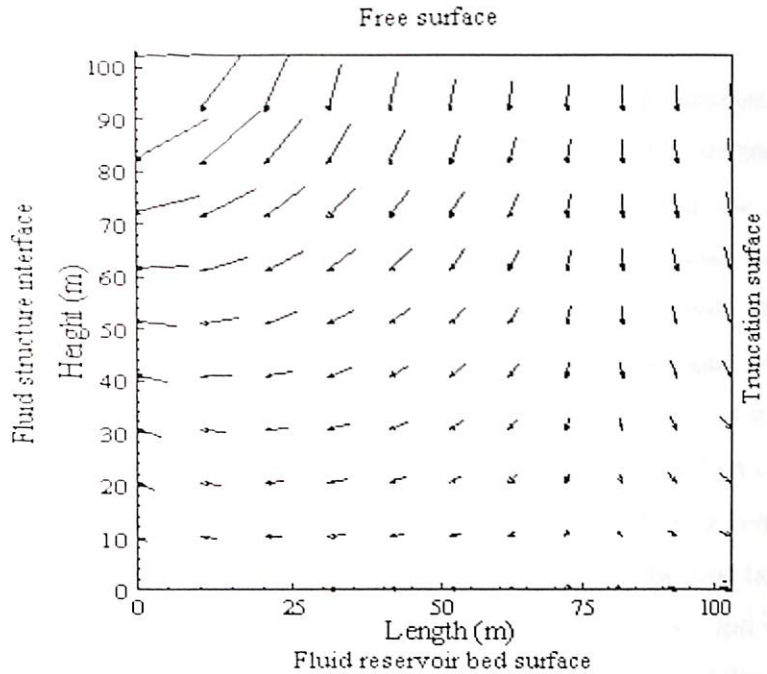

Fig. 4.141 Velocity vector in the reservoir with absorptive bottom at 3.25 sec

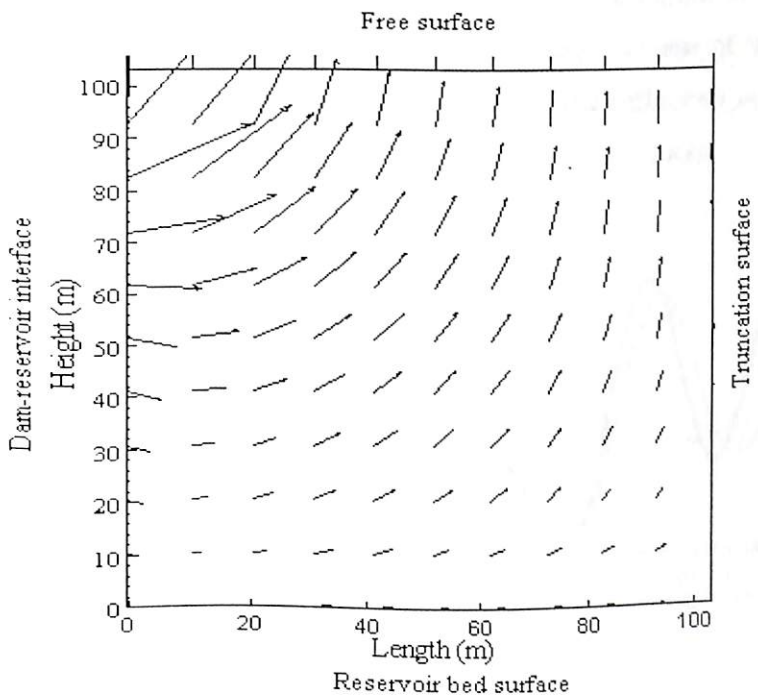

Fig. 4.142 Velocity vector in the reservoir with absorptive bottom at 3.91 sec

4.3.4.2 Effect of Sediment Layer on Dam Response

To study the effect of sediment layers at the reservoir bottom, the dam-reservoir system as in Section 4.3.4.1 is considered with same material properties. The sediment is assumed to have a density (ρ_s) of 2 kN/m^3, and velocity of wave propagation in the sediment material (c_s) as 2200 m/sec and elastic modulus as 4.5×10^9 N/m^2. It is seen from the graphical results presented in Section 4.3.4.1 that the effect of reservoir bottom absorption is more pronounced in the case of excitation frequency near the resonant frequency (36.897 rad/sec in this case) of the reservoir. Therefore, in the present investigation a harmonic excitation of $\omega = 36.897$ rad/sec has been considered to study the effect of sediment layers on the hydrodynamic response of the dam-reservoir system. Here, a layer of sediment of thickness d_s overlying a rigid foundation rock is considered as the first layer. The depth of the second layer is considered to be very large to represent infinite rigid strata. The elastic modulus of the second layer E_{s2} is adopted as 5 times the elastic modulus of the first layer, E_{s1}. The density of the second layer is considered to be 3.6 kN/m^3. It is observed from Fig. 4.143 that the crest displacements are affected by the increasing depth of the sediment layer. A significant reduction in the hydrodynamic pressure coefficient at the bottom of the dam-reservoir interface (Fig. 4.144) is observed with the increase of sediment layer thickness. An increase in sediment layer thickness reduces the reflection coefficient; and hence the hydrodynamic response of the dam-reservoir system is reduced.

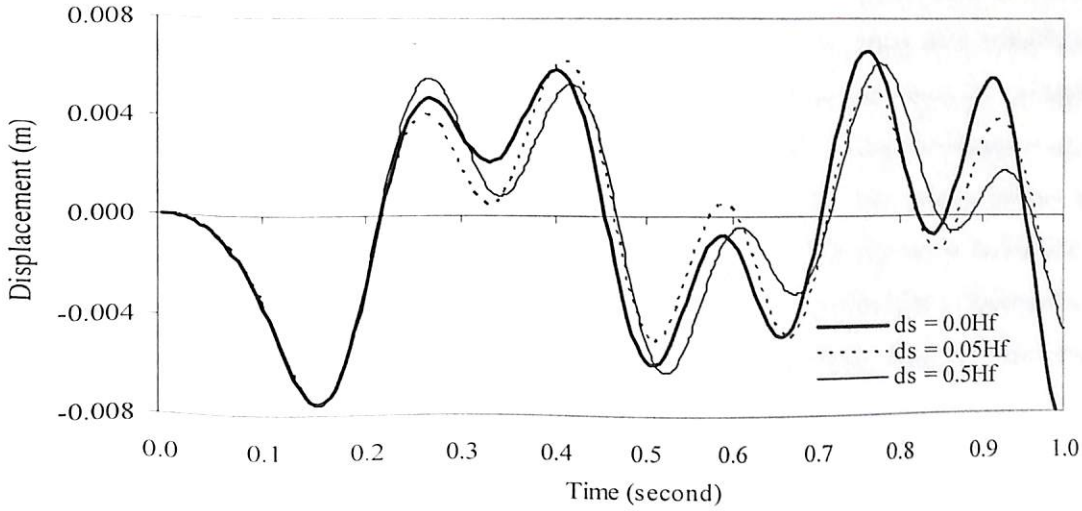

Fig. 4.143 Effect of sediment layer on crest displacement of the dam due to sinusoidal excitation ($\omega = 36.897$ rad/sec)

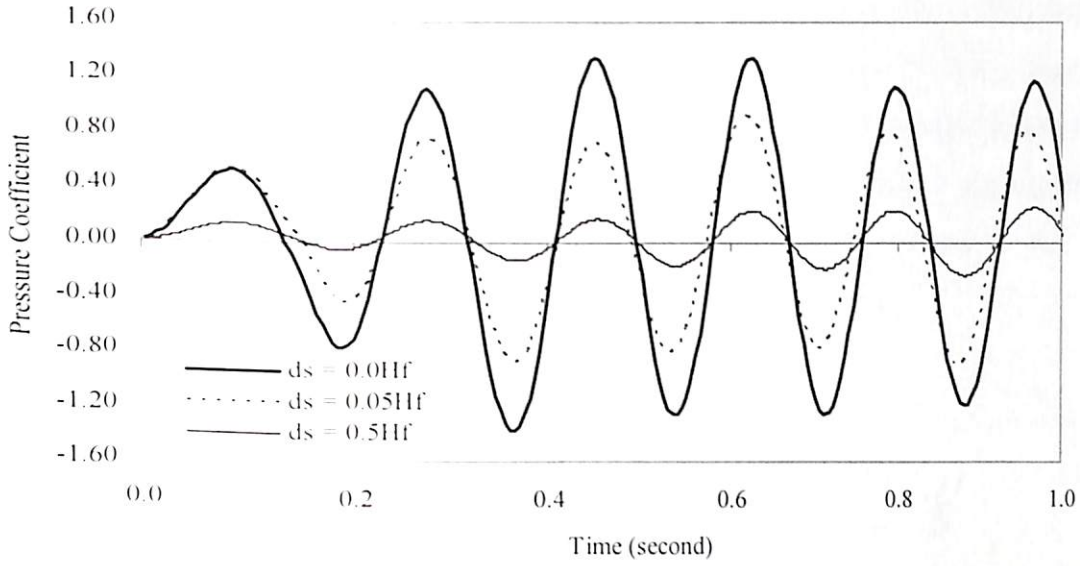

Fig. 4.144 Effect of sediment layer on pressure coefficient at the bottom of the dam-reservoir interface due to sinusoidal excitation (ω = 36.897 rad/sec)

4.3.5 Analysis of Dam-Reservoir System with Degradation

The effect of the dam-reservoir interaction is to modify the dynamic behavior of the dam. A concrete dam is generally designed for a life of 100 years or more. The design and seismic analysis of the dam is generally done considering the 28 days characteristic strength of concrete. However, as these structures age, incidences of degradation due to environmental factors may threaten their durability and seismic performance. It is evident from the literature reviewed that no established assessment methods exist to effectively predict the dynamic behavior of ageing dams. Techniques for repair and retrofitting are still in the early stage of research. A methodology that may be used to determine if retrofitting measures should be taken is not available. Effective implementation of repair strategy requires knowledge of degradation mechanism and the performance of the degraded structure. The proposed methodology of prediction of dynamic behavior of an ageing dam can be used as a basis for selecting an appropriate period for continued service or for determining need of repair when subjected to seismic loading and extreme environmental conditions.

4.3.5.1 Dam with Rigid Reservoir Bottom

A typical section of Koyna dam having the same geometrical and material parameters as in Section 4.3.3 is considered for the analysis. The crest displacements of the Koyna dam

under Koyna earthquake (Fig. 4.5) considering the effect of dam–reservoir interaction are plotted in Fig.4.145. It is observed that the effect of dam-reservoir interaction is to increase the crest displacements. Fig. 4.146 shows the principal stresses (maximum tensile and minimum compressive), σ_{pl} at the neck of the dam (point O) without any degradation considering dam-reservoir interaction effect. The graphical results plotted in Fig. 4.146 show that the magnitude of stress increases when the reservoir is full.

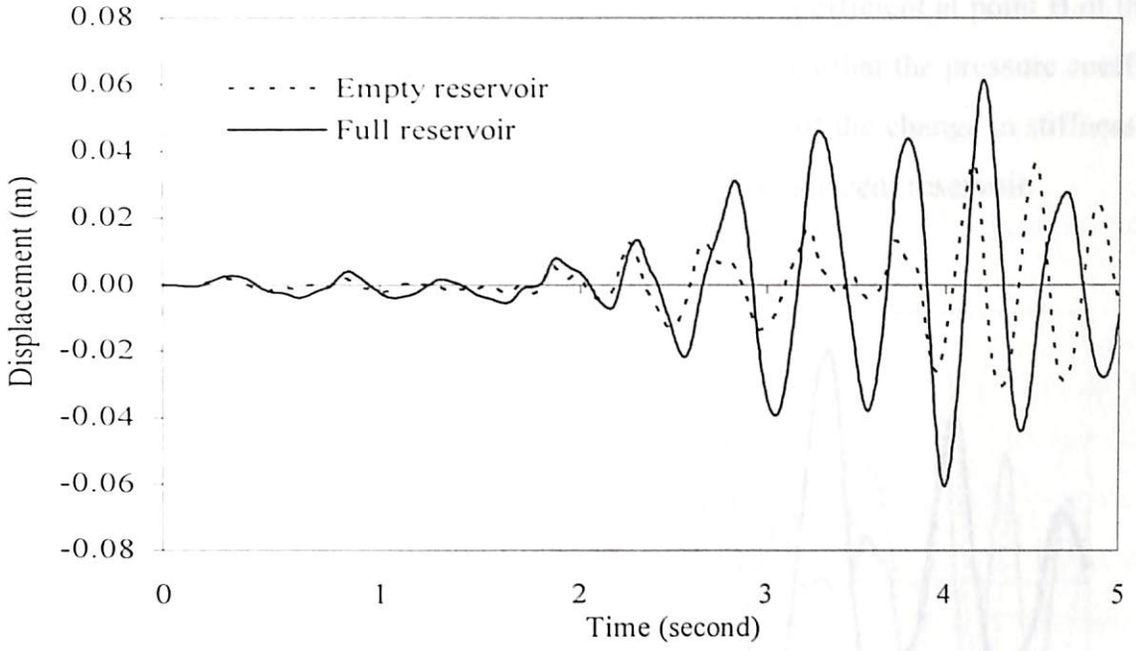

Fig. 4.145 Effect of reservoir water on crest displacements of dam due to Koyna earthquake (without degradation)

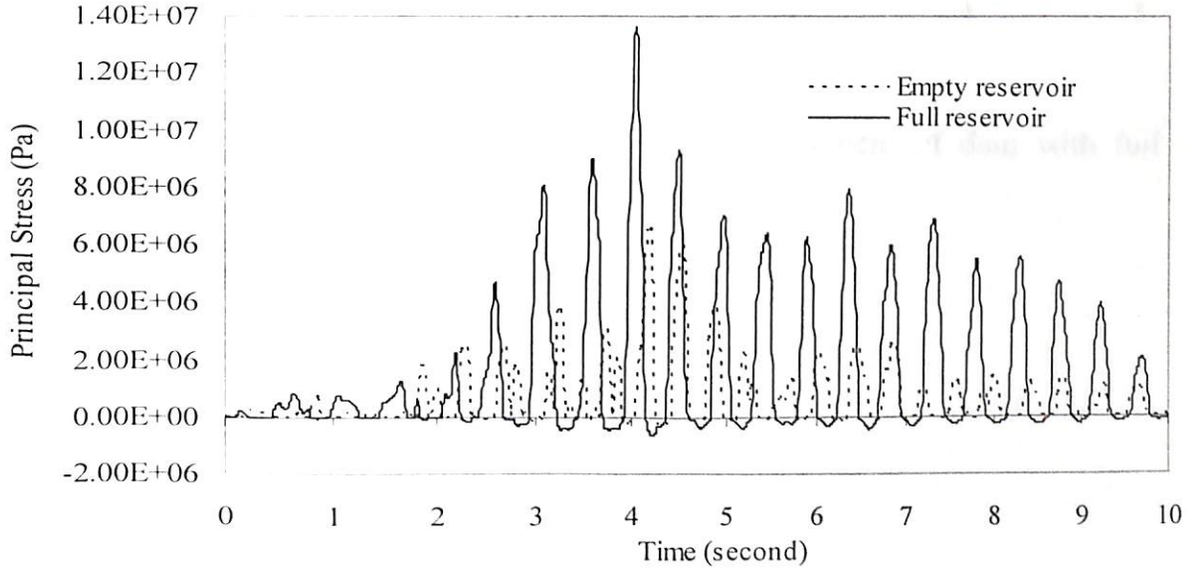

Fig. 4.146 Effect of reservoir water on principal stress σ_{pl} at point O of dam due to Koyna earthquake

The ageing effect of the dam under seismic excitation considering dam-reservoir interaction is studied. The crest displacements of the dam at 1, 25 and 75 years are presented for isotropic degradation under horizontal component of Koyna earthquake in Fig. 4.147. The percentages of degradation considering hygro-chemo-mechanical degradation with a design life of 100 years and a_s = 0.57 (eq. 3.29) at 1, 25 and 75 years are 0.0, 19.1 and 46.6 respectively. It is observed from the graphical results in Fig 4.147 that the coupled dam-reservoir system exhibits an increased displacement trend for higher percentage of degradation. While comparing the pressure coefficient at point B of the dam due to Koyna earthquake as seen in Fig. 4.148, it is observed that the pressure coefficients are affected by the degradation of the dam. This is because of the change in stiffness of the dam structure that alters the acceleration of the dam in the adjacent reservoir.

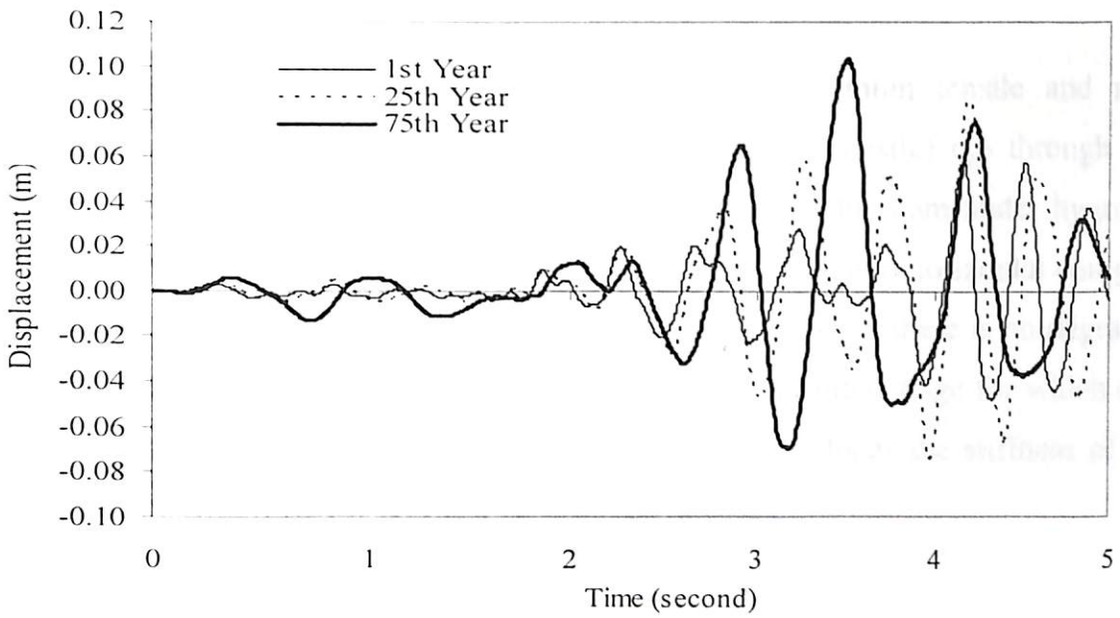

Fig. 4.147 Ageing effect on crest displacement of dam with full reservoir water due to Koyna earthquake

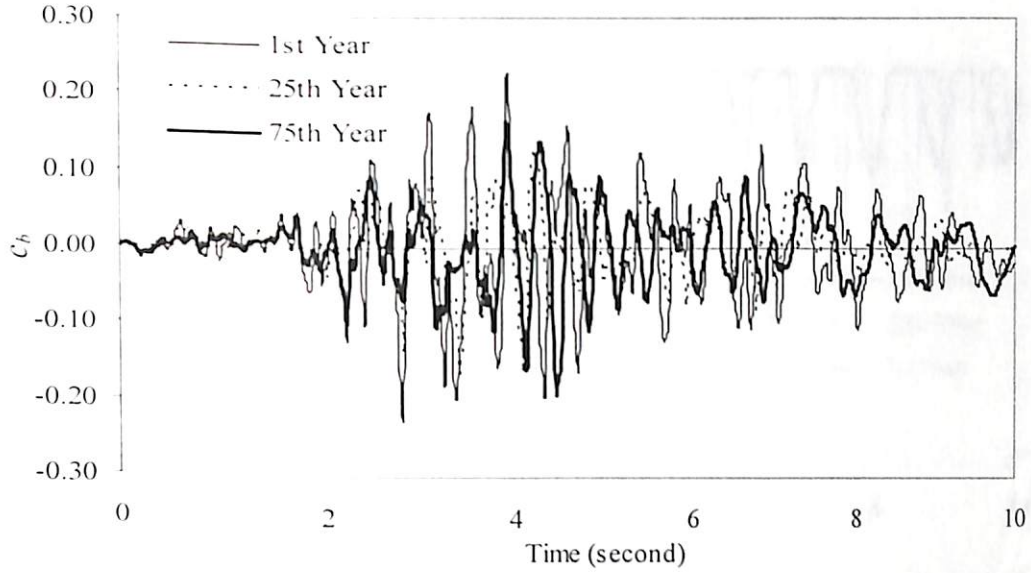

Fig. 4.148 Ageing effect of dam on pressure coefficient at point B due to Koyna earthquake

The development of principal stresses, σ_{p1} (maximum tensile and minimum compressive) and (maximum compressive and minimum tensile) σ_{p2} through different ages has been plotted in Fig. 4.149 and 4.150 considering the dam under hygro-chemo-mechanical (HCM) degradation. The stresses are obtained due to horizontal component of Koyna earthquake. It is noticed that the stresses are more when there is no degradation in the dam. This is because of higher stiffness of the dam at initial stage for which energy is not dissipated through damage. Increase in degradation reduces the stiffness of the dam and allows energy dissipation leading to reduced stresses.

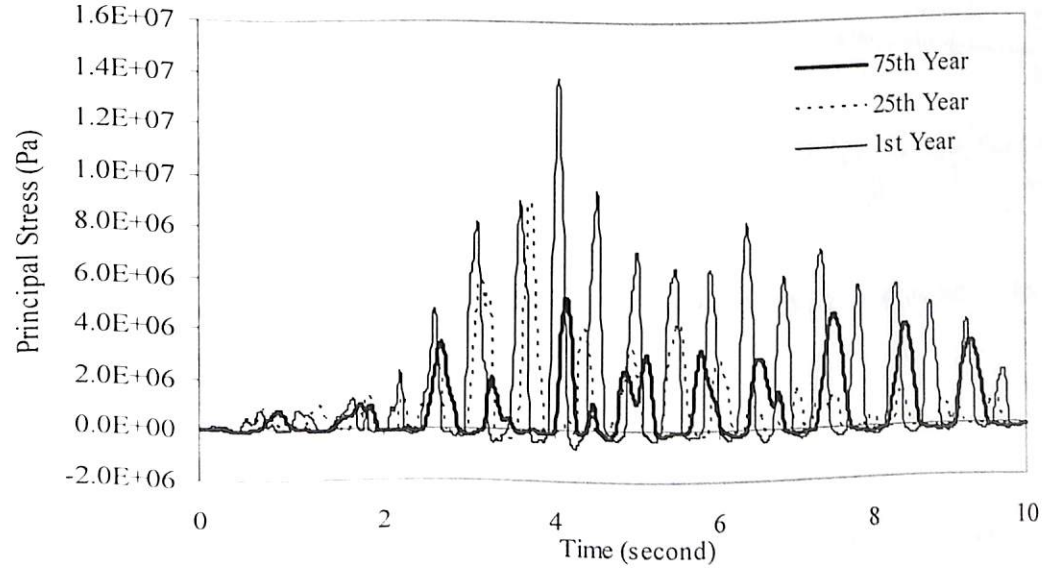

Fig. 4.149 Effect of ageing on principal stress (σ_{p1}) at point O due to Koyna earthquake

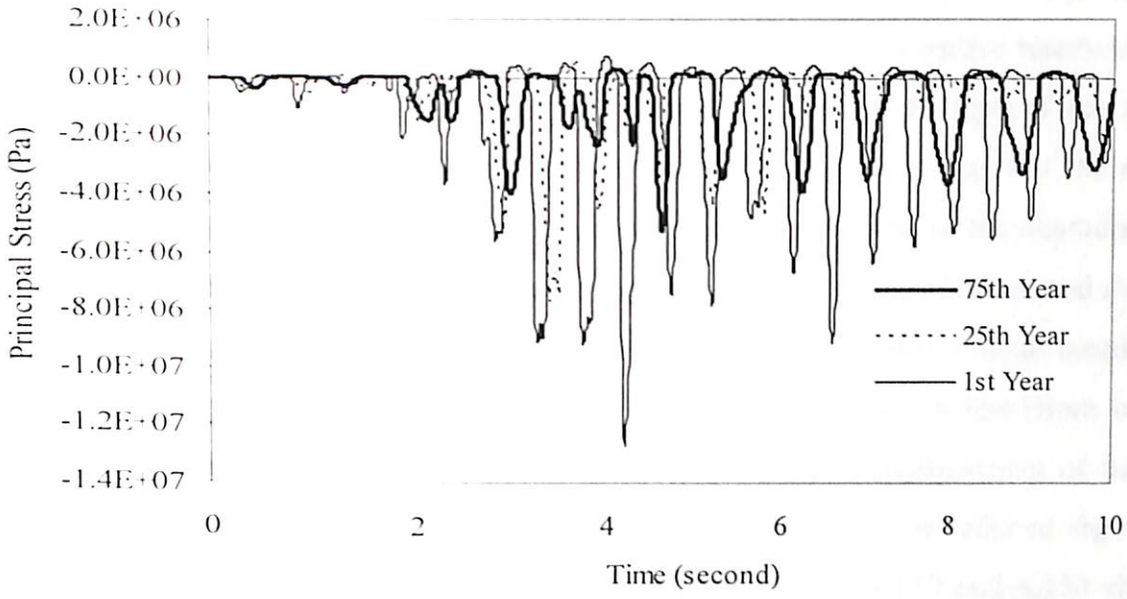

Fig. 4.150 Effect of ageing on principal stress (σ_{p2}) at point O due to Koyna earthquake

The variation in principal stress (σ_{p1}) are obtained due to seismic excitation and plotted in Fig. 4.151 to observe the variation of stresses for design life of 50 years and 100 years. Thus, if the design life of the dam and the environmental factors are known, the structural response at a certain age can be determined to evaluate its safety.

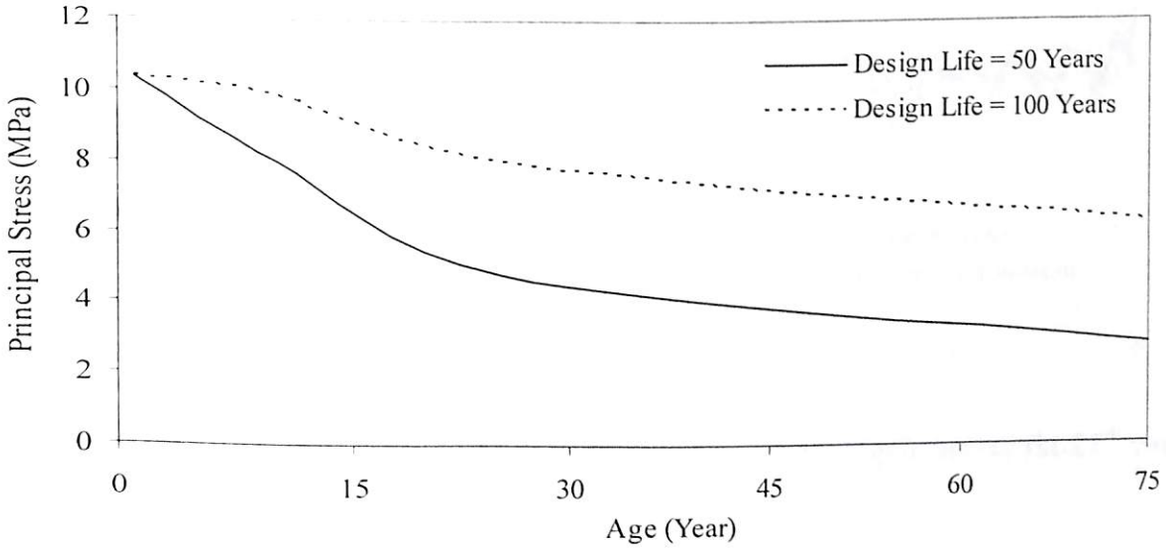

Fig. 4.151 Effect of design life on principal stress (σ_{p1}) at point O due to Koyna earthquake

4.3.5.2 Dam with Absorptive Reservoir Bottom

The presence of sediments at the bottom of the reservoir will make the reservoir bed absorptive. Analysis of the Koyna dam with the same material parameters as in Section

4.3.5.1 is carried out considering the reservoir bottom absorption. The reflection coefficient in the present study is considered to be 0.5 for the absorptive reservoir bottom at all ages. The reflection coefficient will remain constant at all ages if the reservoir sediment is flushed out at regular intervals to maintain a constant depth of the sediment layer. The analysis is carried out to determine the seismic response of the degraded Koyna dam (Fig. 4.120) in the 25th and 75th year with absorptive reservoir bottom and the results are plotted in graphical forms (Figs. 4.152 - 4.159). The degradation indices considering a design life of 100 years at the 25th and 75th year are 0.191 and 0.466 (from eq. 3.36) respectively. It was observed from Fig. 4.133 that, the crest displacement of the newly constructed (i.e., at the 1st year) dam due to Koyna earthquake is reduced significantly when an absorptive reservoir bottom is considered. But Figs. 4.152 and 4.153 show that though the crest displacement increases with an increase in age, the significance of absorption at the reservoir bed reduces comparatively.

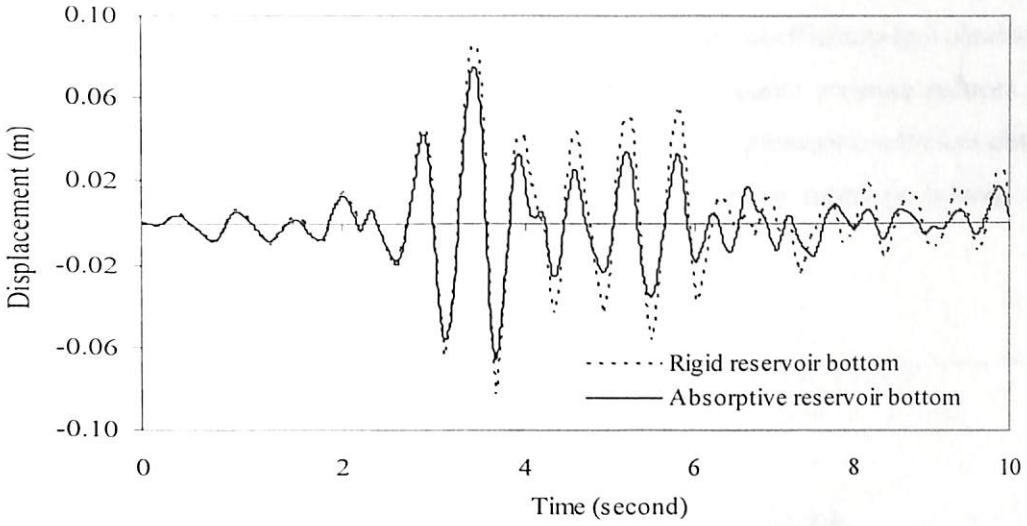

Fig. 4.152 Effect of absorptive reservoir bottom on crest displacement (at 25th year)

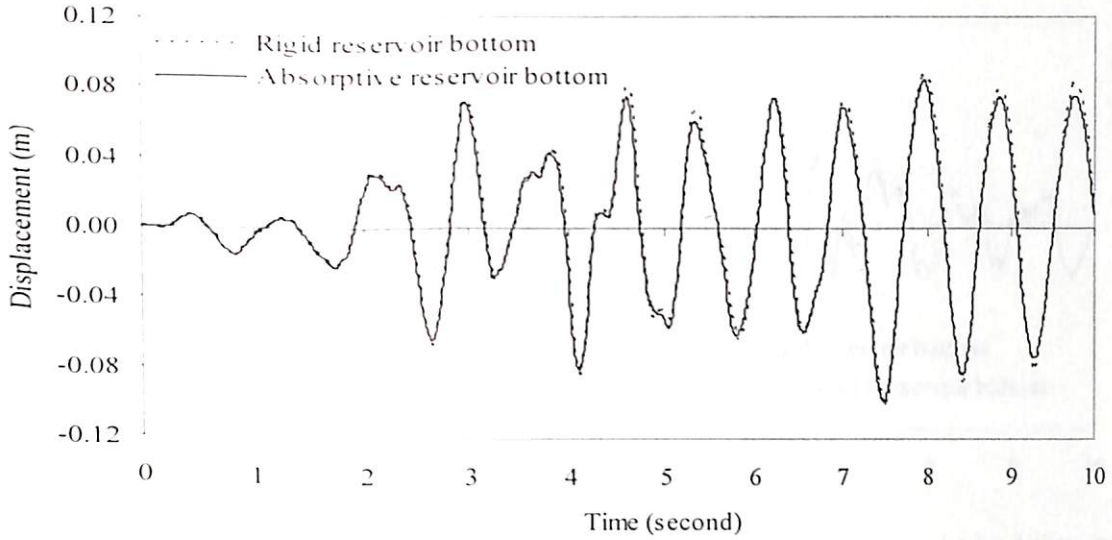

Fig. 4.153 Effect of absorptive reservoir bottom on crest displacement (at 75th year)

The hydrodynamic pressures developed at the bottom of the dam-reservoir interface (c_b) due to seismic excitation in the 25th and 75th year are plotted in Figs. 4.154 and 4.155 respectively. While comparing with the pressure coefficients (c_b) obtained in the first year (Fig. 4.134), it was observed that the hydrodynamic pressure reduces with an increase in the degradation of the dam. The hydrodynamic pressure coefficient obtained at different ages show that the significance of the absorptive reservoir bottom is more pronounced at an early age.

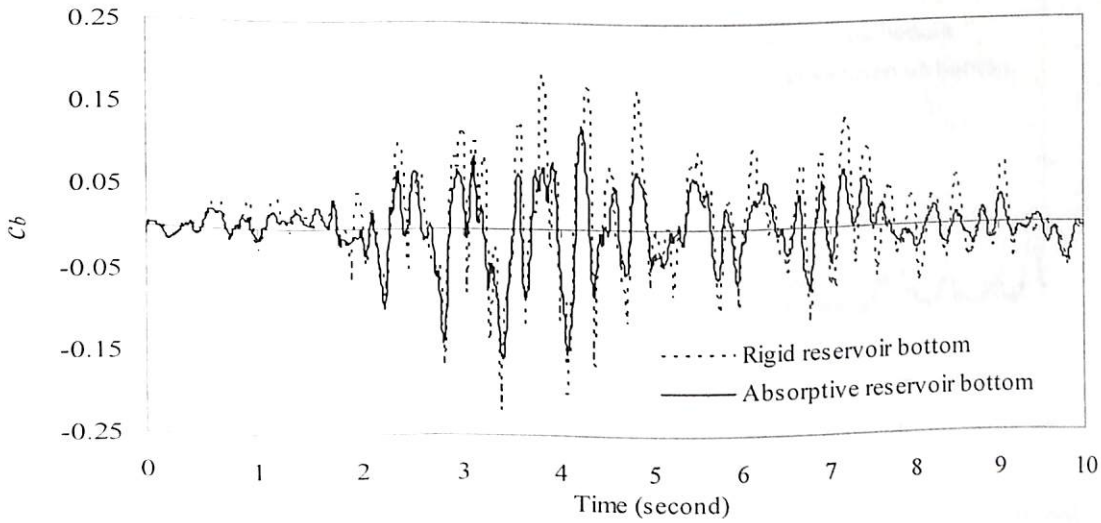

Fig. 4.154 Effect of absorptive reservoir bottom on hydrodynamic pressure (at 25th year)

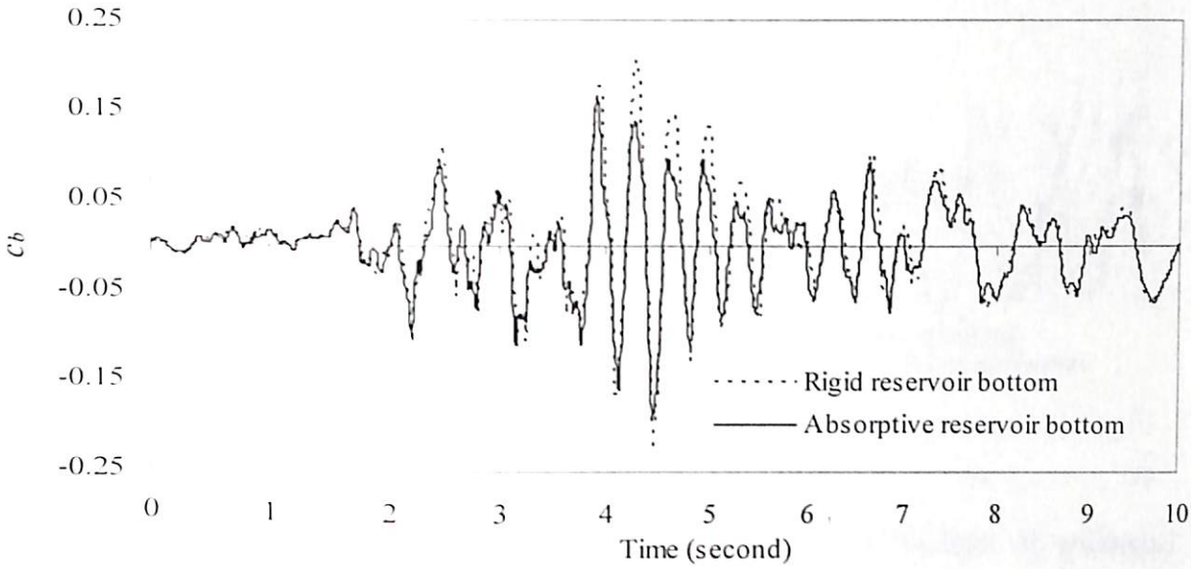

Fig. 4.155 Effect of absorptive reservoir bottom on hydrodynamic pressure (at 75th year)

The principal stresses (maximum tensile and minimum compressive), σ_{pl} at points B and O of the degraded dam due to seismic excitation at 25th and 75th year are plotted in Figs. 4.156 – 4.159. On comparing with the stresses obtained at points B and O in the first year (Figs. 4.135 and 4.137), it is observed that the stresses reduce significantly due to the effect of degradation. However, as the age of the dam becomes more, (Figs. 4.156 and 4.157) the difference in stresses by considering the reservoir bottom absorption is not much.

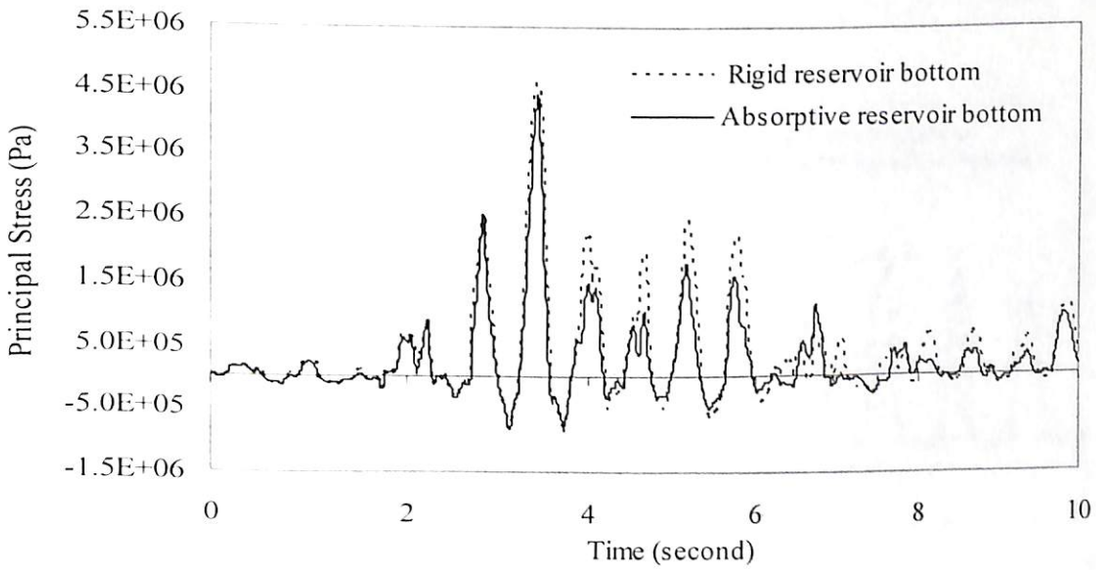

Fig. 4.156 Effect of absorptive reservoir bottom on principal stress σ_{pl} at point B at 25th year

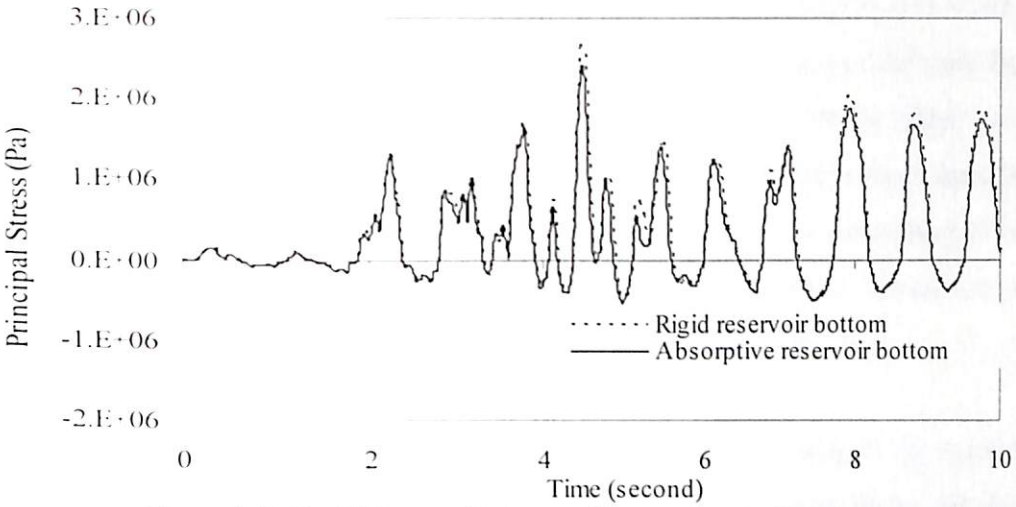

Fig. 4.157 Effect of absorptive reservoir bottom on principal stress σ_{p1} at point B at 75th year

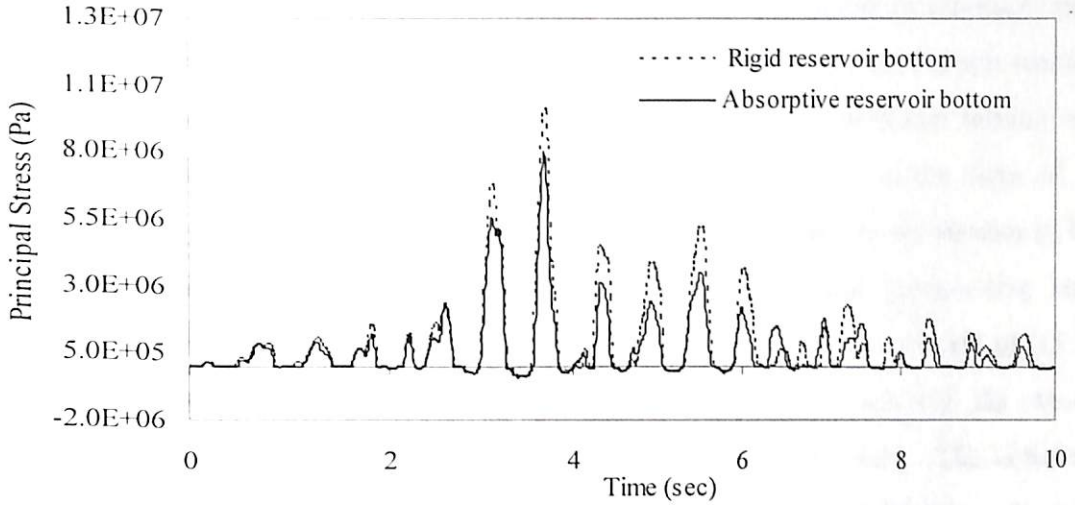

Fig. 4.158 Effect of absorptive reservoir bottom on principal stress σ_{p1} at point O at 25th year

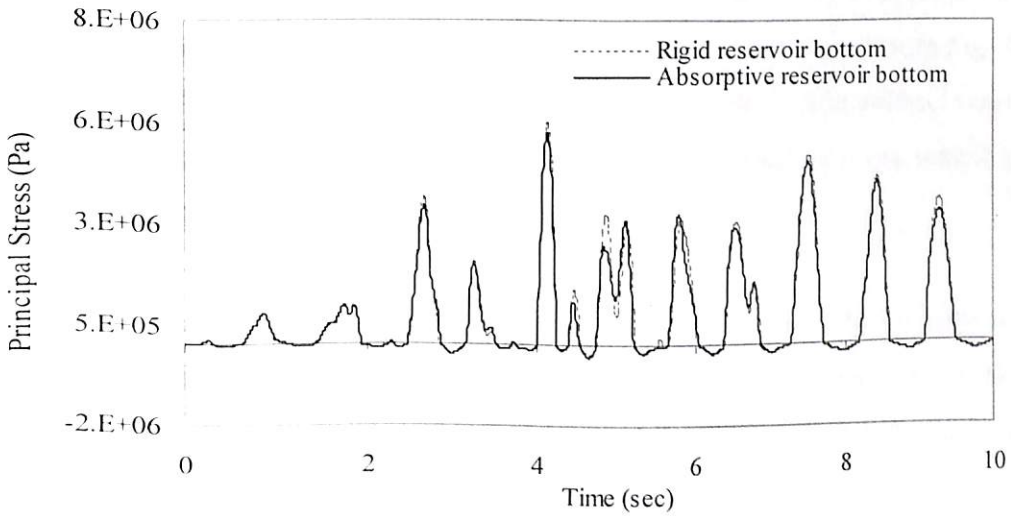

Fig. 4.159 Effect of absorptive reservoir bottom on principal stress σ_{p1} at point O at 75th year

As observed in the crest displacements and pressure coefficients, it is noted that the effect of absorptive reservoir bottom is significant at the initial ages of the dam. However, this effect is negligible when the age of dam becomes high, i.e., for the higher percentage of degradation. This implies that the effect of degradation with age is more than the effect of reservoir bottom absorption and cannot be neglected. It is also interesting to note that the principal stresses, σ_{p1} at neck (i.e., at point O) are more than that in base (i.e., at point B) due to the development of stress concentration at the neck of the dam.

To design earthquake resistant dams or to evaluate the safety of the existing dams during earthquakes, it is necessary to know the stress distribution inside the dam body considering dam-reservoir interaction effects. It is easy to find out the most vulnerable zones from the stress contours, where the developed stresses exceed the allowable stresses of the material during an earthquake. The principal stresses, σ_{p1} (maximum tensile and minimum compressive) and σ_{p2} (maximum compressive and minimum tensile) at two different time instants are plotted at different ages of the dam in the form of stress contours (Figs. 4.160 to 4.163). The legends adjacent to the figures are stresses in Pascal (Pa). The positive and negative stresses indicate tensile and compressive stresses respectively. These stresses are obtained considering a reflection coefficient of 0.5 at the reservoir bed. It is observed from Fig.4.160 (i) that at t = 2.0 seconds, the maximum tensile stresses are concentrated near the upstream face of the dam. The compressive stresses are highest near the neck of the dam (point O). On comparing Fig. 4.15 and Fig. 4.160, it is noted that due to the effect of the dam-reservoir interaction, the nature of stresses are altered at different locations of the dam body. At t = 4.28 seconds, where the principal stresses at point O reaches its peak (Fig. 4.137), it is observed from Fig. 4.161(i) that the magnitude of the stresses are increased. As in the case of dam without considering the effect of reservoir (Fig.4.16), the stresses along the vertical face are tensile and the highest compressive stresses are concentrated around point O.

At the 75th year, the stresses in the degraded dam due to the effect of dam-reservoir interaction, considering a reflection coefficient of 0.5 at the reservoir bed are plotted in Figs. 4.162 to 4.163. On comparing the stresses in Fig. 4.162 with the stresses plotted at the 75th year without the effect of the reservoir in Fig. 4.18 at 2.0 seconds, it is seen that the stress distribution pattern are altered. The magnitude of stresses is reduced when the effect of degraded dam-reservoir interaction with absorptive reservoir bottom is

considered. On considering the effect of dam-reservoir interaction and absorptive reservoir bottom, (Fig.4.162 (i)) the tensile stresses are concentrated along the upstream face of the dam. Maximum compressive stress occurs at point O of the dam, (Fig.4.162 (ii)), the magnitude of which is much less than the magnitude of maximum tensile stress occurring at the same point in the absence of the reservoir.

At t = 4.28 seconds, unlike the stress distribution pattern in the case of empty dam (Fig.4.19), it is observed from Fig. 4.163 that the compressive stresses are concentrated around point O and the maximum tensile stresses are along the vertical upstream face of the dam, which is much higher than stresses in the other parts of the dam body. On comparing the stress contours (Fig.4.19 and Fig.4.163), it is noted that the effect of dam reservoir interaction is to cause compressive stress concentration near the heel of the dam.

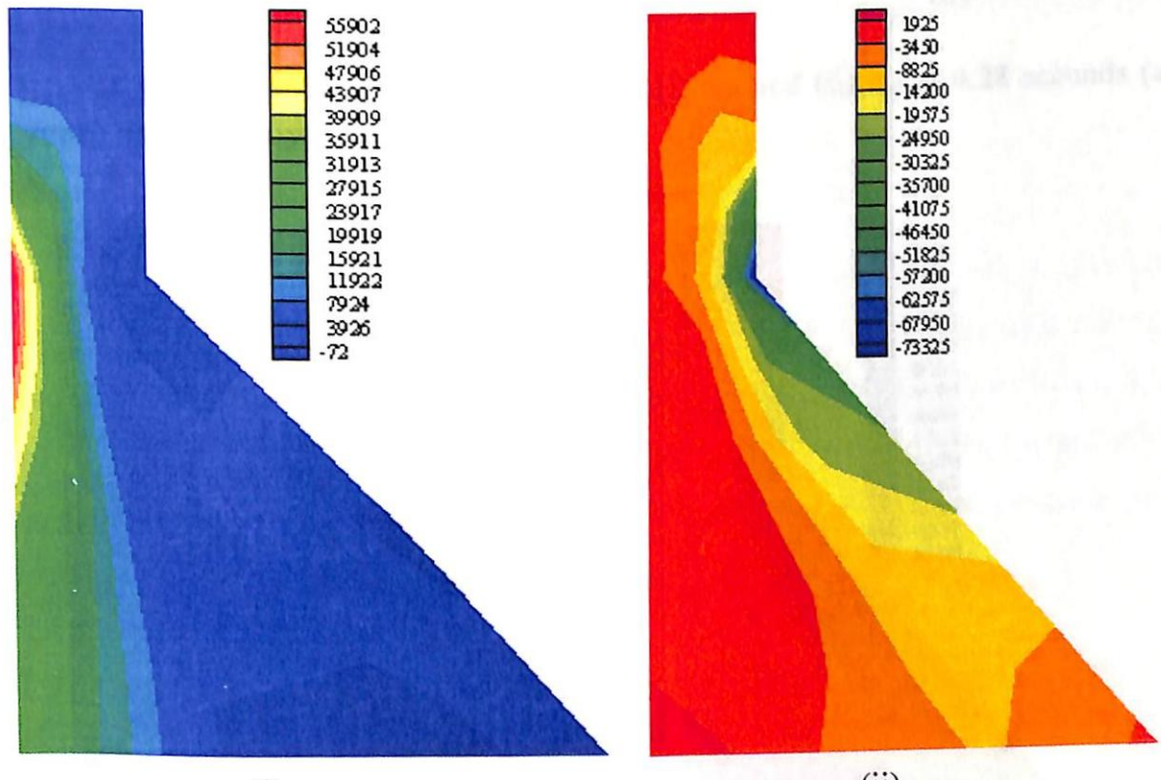

(i) (ii)

Fig. 4.160 Contour for principal stress (i) σ_{p1} and (ii) σ_{p2} at 2.0 seconds (at 1st year) due to Koyna earthquake

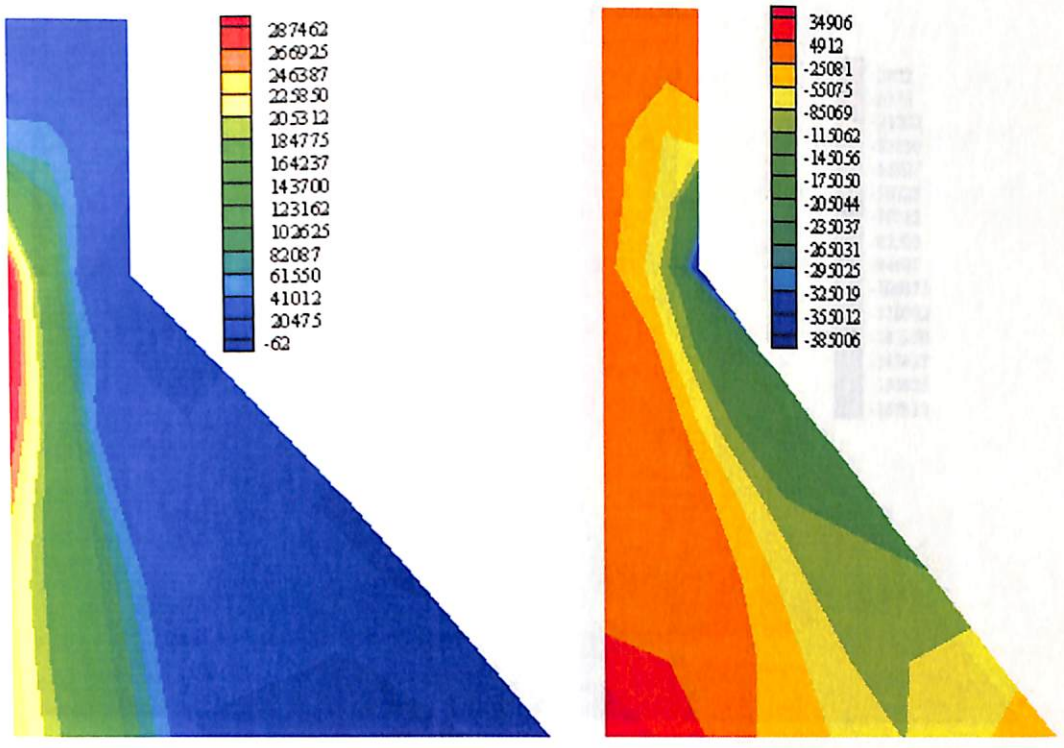

(i) (ii)

Fig. 4.161 Contour for principal stress (i) σ_{p1} and (ii) σ_{p2} at 4.28 seconds (at 1st year) due to Koyna earthquake

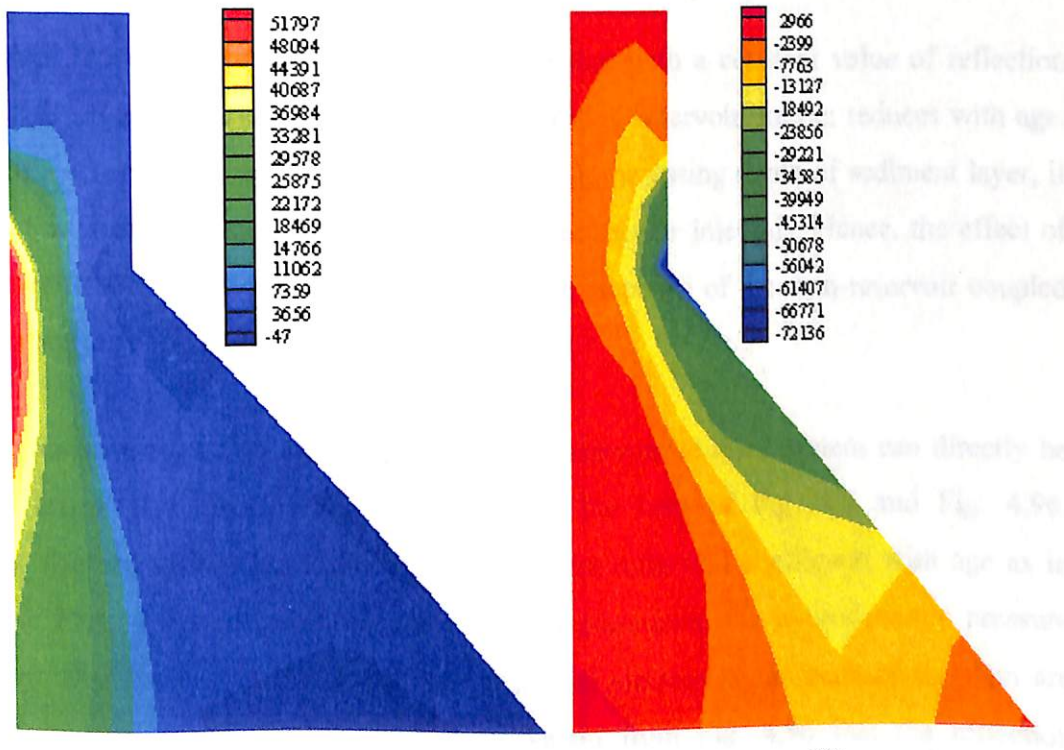

(i) (ii)

Fig. 4.162 Contour for principal stress (i) σ_{p1} and (ii) σ_{p2} at 2.0 seconds (at 75th year) due to Koyna earthquake

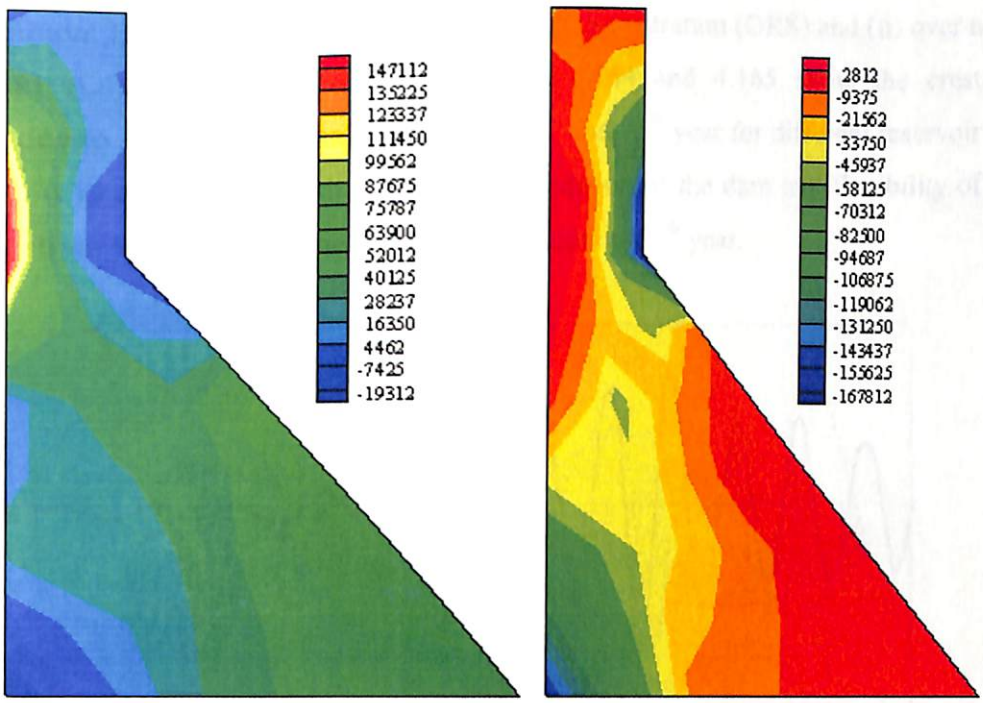

Fig. 4.163 Contour for principal stress (i) σ_{p1} and (ii) σ_{p2} at 4.28 seconds (at 75th year) due to Koyna earthquake

4.3.5.3 Dam with Varying Depth of Sediment Layer

It is observed from the results presented above that with a constant value of reflection coefficient the significance of the effect of absorptive reservoir bottom reduces with age. The value of reflection coefficient will reduce with increasing depth of sediment layer, if the sediment is not flushed out of the reservoir at regular intervals. Hence, the effect of increasing depth of sediment layer on the seismic response of the dam-reservoir coupled system is important to study.

The response of the aged concrete dam-reservoir coupled system can directly be determined from the proposed algorithm with the help of Fig. 4.3 and Fig. 4.96. Considering the variation in degradation index and reflection coefficient with age as in Fig. 4.3 and Fig. 4.96 respectively, the crest displacement, the hydrodynamic pressure coefficient at the base and the maximum principal stresses at the neck of the dam are evaluated due to Koyna earthquake. It is evident from Fig. 4.96 that the reflection coefficients are also affected by the elastic modulus of the layer over which the sediment lies. Generally, a concrete gravity dam is constructed on sound bedrock (U.S. Army Corps of Engineers 1995). Therefore, while evaluating the seismic response of Koyna dam (Fig.

4.120), the sediment layer is considered to be (i) over a rigid stratum (ORS) and (ii) over a flexible stratum (OFS) as in Section 4.2.9. Figs. 4.164 and 4.165 show the crest displacements due to Koyna earthquake obtained at 1st and 75th year for different reservoir bed conditions. It is observed that the effect of degradation of the dam and flexibility of the underlying strata is to increase the crest displacements at 75th year.

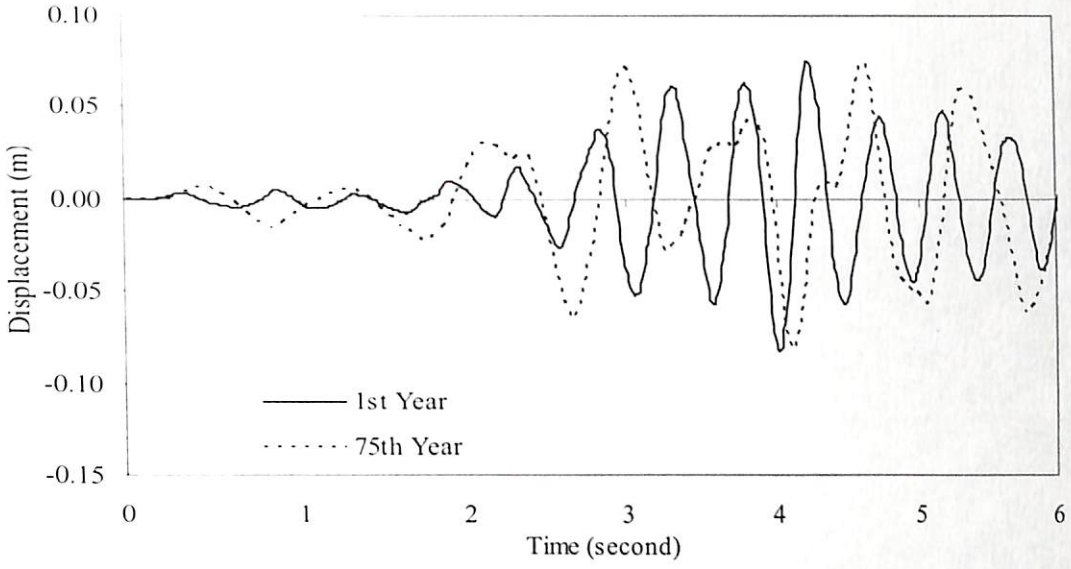

Fig. 4.164 Crest displacement due to Koyna earthquake considering sediment layer on rigid stratum

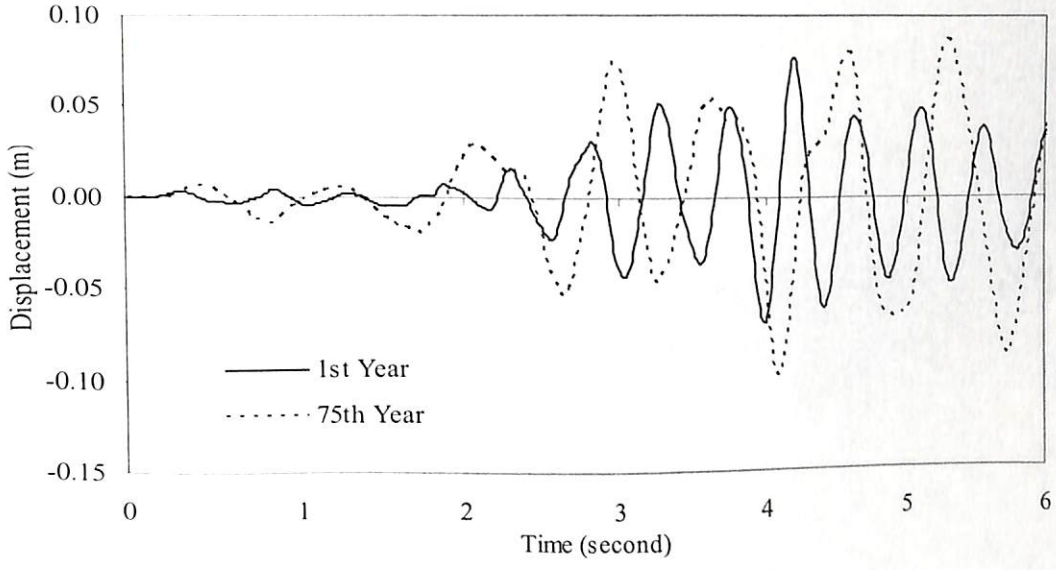

Fig. 4.165 Crest displacement due to Koyna earthquake considering sediment layer on flexible stratum

The hydrodynamic pressure coefficients at the bottom of the dam-reservoir interface at the 1st and 75th year are plotted for different reservoir bed conditions in Figs. 4.166 and 4.167. It is observed from the graphical results that the reduction in hydrodynamic pressure is more significant when the sediments layer is deposited over a rigid stratum (Fig. 4.166) than for the case when the sediment is deposited over a flexible stratum (Fig. 4.167).

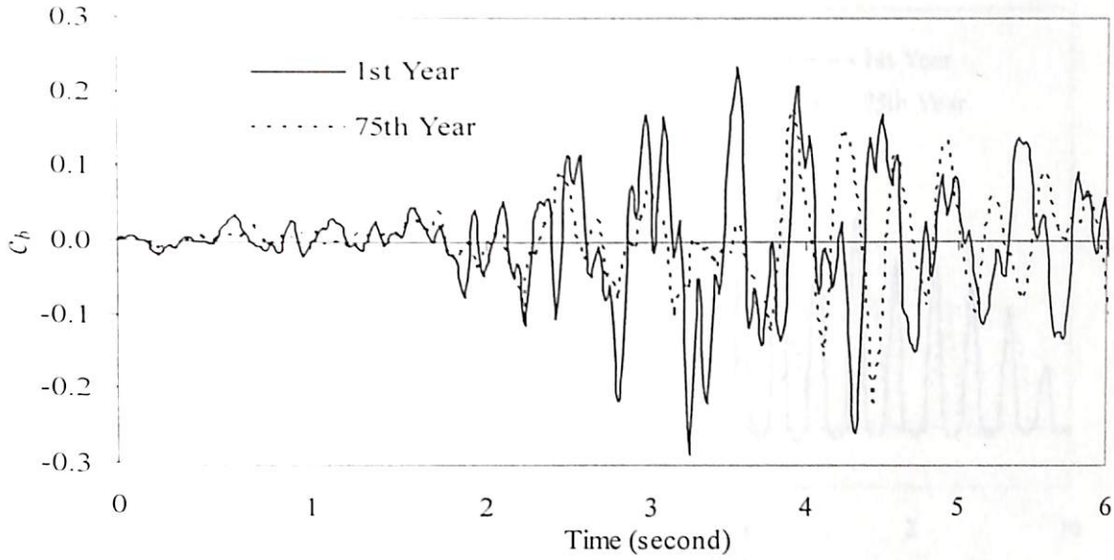

Fig. 4.166 Hydrodynamic pressure coefficient at the bottom of the dam-reservoir interface due to Koyna earthquake, considering sediment layer lying over rigid stratum

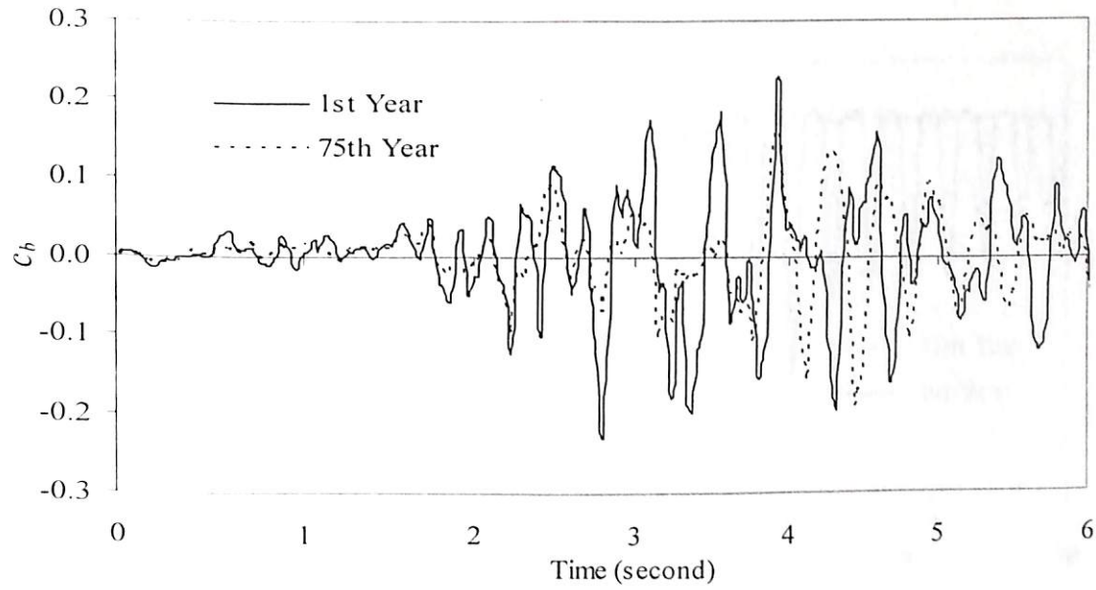

Fig. 4.167 Hydrodynamic pressure coefficient at the bottom of the dam-reservoir interface due to Koyna earthquake, considering sediment layer lying over flexible stratum

The principal stress, σ_{p1} (maximum tensile and minimum compressive) and σ_{p2} (maximum compressive and minimum tensile) at the neck of the dam (at point O of the dam in Fig. 4.120) at 1st and 75th year are plotted in Figs. 4.168 to 4.171. It is observed that the principal stresses at the neck of the dam are influenced by the rigidity of the stratum over which the sediment layer is deposited.

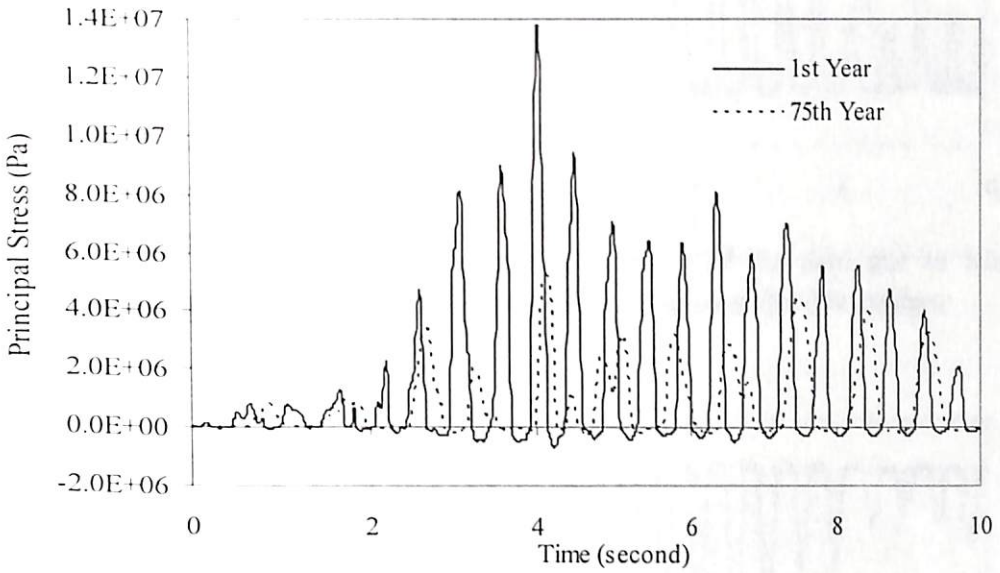

Fig. 4.168 Principal stress σ_{p1} at point O of the dam due to Koyna earthquake considering sediment layer lying over rigid stratum

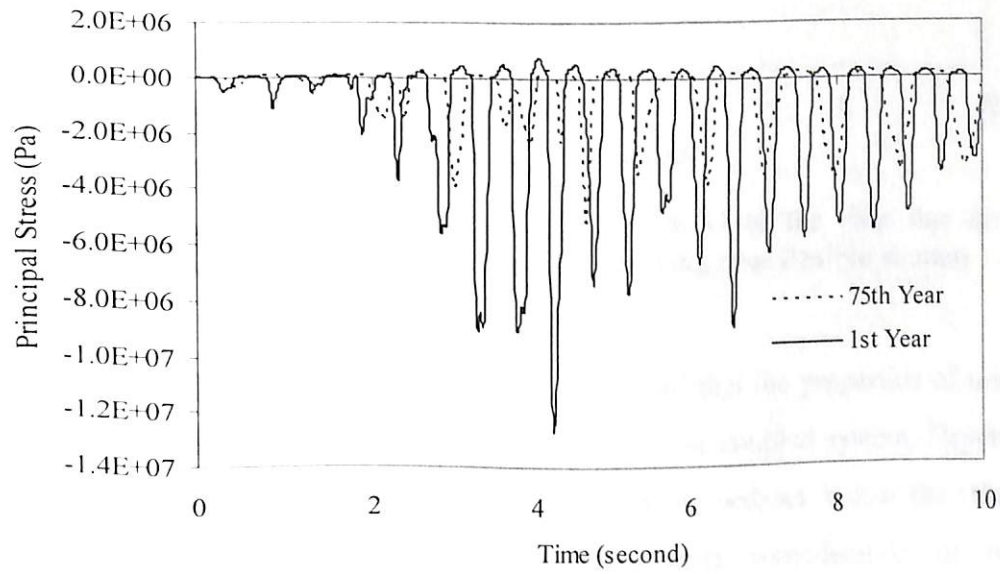

Fig. 4.169 Principal stress σ_{p2} at point O of the dam due to Koyna earthquake considering sediment layer lying over rigid stratum

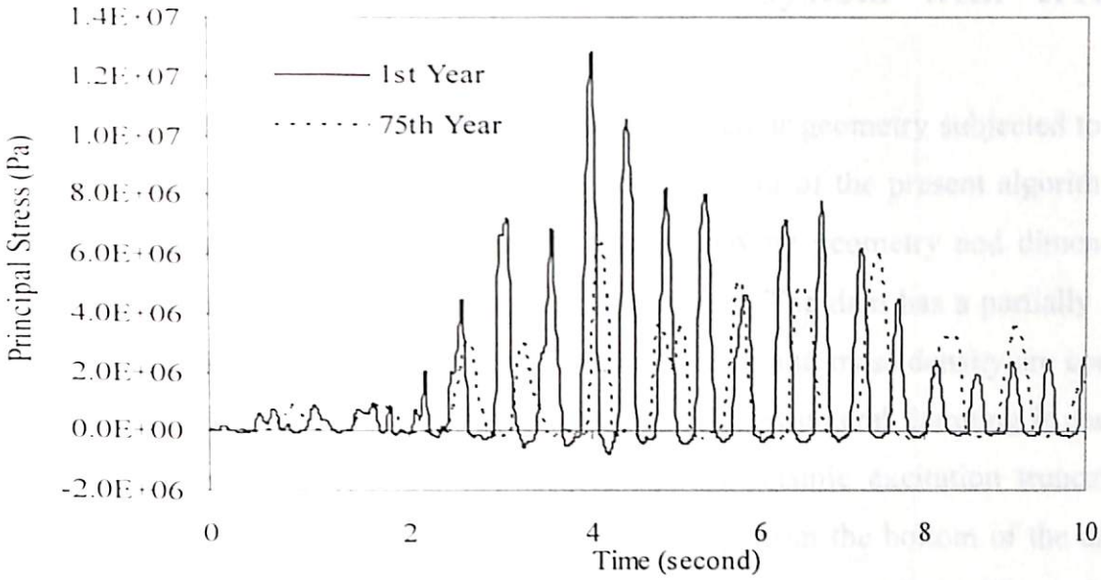

Fig. 4.170 Principal stress σ_{p1} at point O of the dam due to Koyna earthquake considering sediment layer lying over flexible stratum

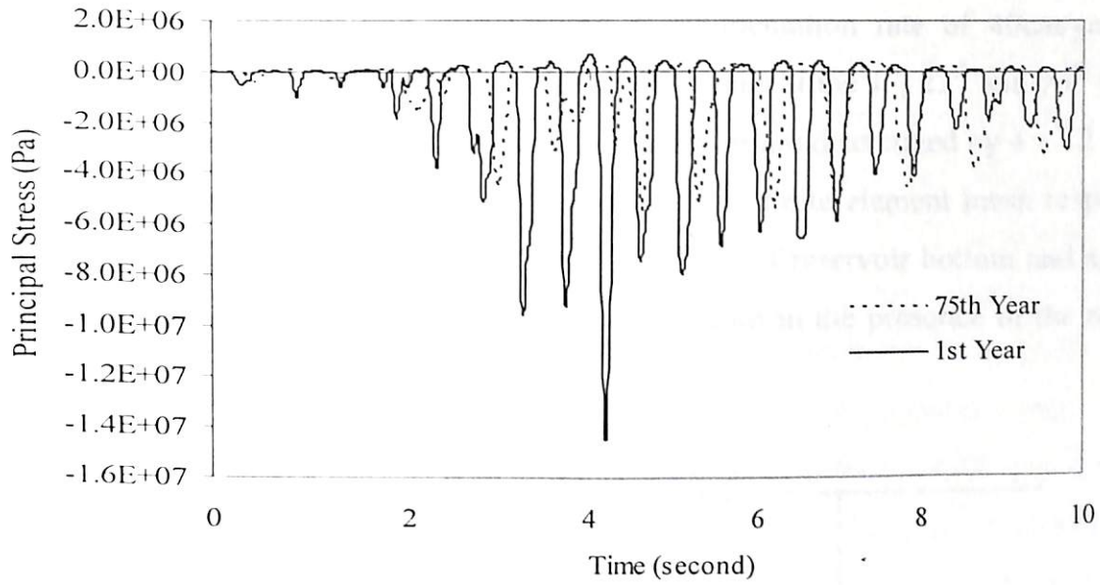

Fig. 4.171 Principal stress σ_{p2} at point O of the dam due to Koyna earthquake considering sediment layer lying over flexible stratum

It is evident from the graphical results presented that the properties of underlying layers influence the seismic response of the dam-reservoir coupled system. Depending on the actual site conditions and material parameters of the bedrock below the reservoir, a seismic analysis of an existing dam may necessitate consideration of reflection coefficients at the bottom of the reservoir that vary with depth of sediment layer and age.

4.3.6 Response of a Dam-Reservoir System with Irregular Geometry

The analysis of a dam-reservoir system having an irregular geometry subjected to seismic excitation is the main motivation behind the development of the present algorithm using finite element technique. A dam-reservoir system having geometry and dimensions as shown in Fig. 4.172 is adopted for the seismic analysis. The dam has a partially inclined upstream face. The modulus of elasticity, Poisson's ratio and mass density are considered as 31500 MPa, 0.235 and 2415.816 kg/m^3 respectively. Structural damping is considered as 3%. The dam-reservoir system is analyzed under seismic excitation truncating the infinite reservoir at a distance of 120m (i.e., at $L = H_f$) from the bottom of the dam. The Koyna earthquake (Fig.4.5) is adopted for the present seismic analysis. The analyses are carried out to determine the seismic response of degraded dam in the 1st and 75th year with different reflection coefficients at the respective ages. The reflection coefficients at the reservoir bottom are determined considering a sedimentation rate of 40cm/year. The degradation indices considering a design life of 100 years at the 1st, 25th and 75th year are 0.0, 0.191 and 0.466 respectively. The dam and reservoir are discretized by 4 × 12 (i.e., N_h = 4 and N_v = 12) and 8 × 24 (i.e., N_h = 8 and N_v = 24) finite element mesh respectively (Fig. 4.173). The significance of considering the effect of reservoir bottom and ageing is evaluated by comparing the seismic response of the dam in the presence of the reservoir with rigid bottom.

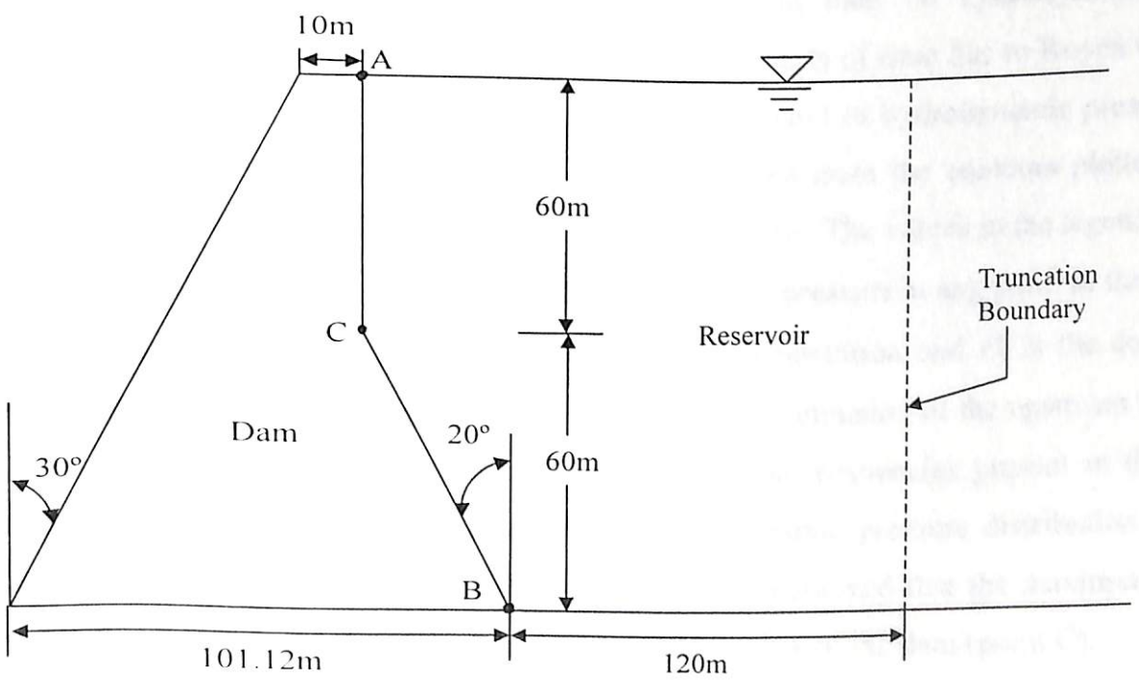

Fig. 4.172 Geometry of a dam-reservoir system with partially inclined upstream face

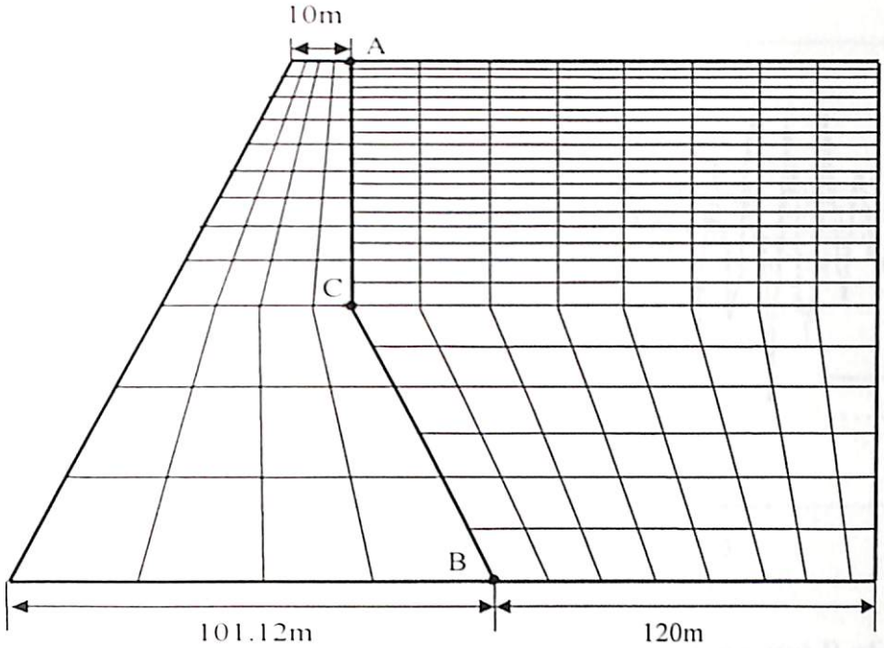

Fig. 4.173 Finite element mesh of the partially inclined dam-reservoir system

The coupled response of the partially inclined elastic dam-reservoir system considering rigid reservoir bottom is studied under earthquake excitation and compared with the case of rigid dam. Fig. 4.174 shows the effect of flexibility of the dam on hydrodynamic pressure developed at the bottom of the dam i.e., at point B (Fig.4.172). It is observed that flexibility of the dam changes the fundamental properties of the dam-reservoir system and hence peaks in pressure coefficients at the bottom of the dam are obtained at different instants of time. The effect of flexibility of the dam on hydrodynamic pressure distributions along its upstream face at different instants of time due to Koyna earthquake are observed in Fig. 4.175 and 4.176. The development of hydrodynamic pressure in the reservoir considering a flexible dam is further noted from the contours plotted in Figs. 4.177 and 4.178 at t = 2.0 and 4.2 seconds respectively. The values in the legend represent the pressure coefficients ($c_p = p/\rho_f g H_f$). Here p is the pressure at any point in the reservoir, ρ_f is the density of water, g is the gravitational acceleration and H_f is the depth of the reservoir. It is noted from the results that the partial inclination of the upstream face of the dam, coupling of the dam-reservoir system and the frequencies present in the seismic excitation affects the development of the hydrodynamic pressure distribution along the dam-reservoir interface. Therefore, it can not be generalized that the maximum pressure occurs at the bottom of the dam (point B) or at the neck of the dam (point C).

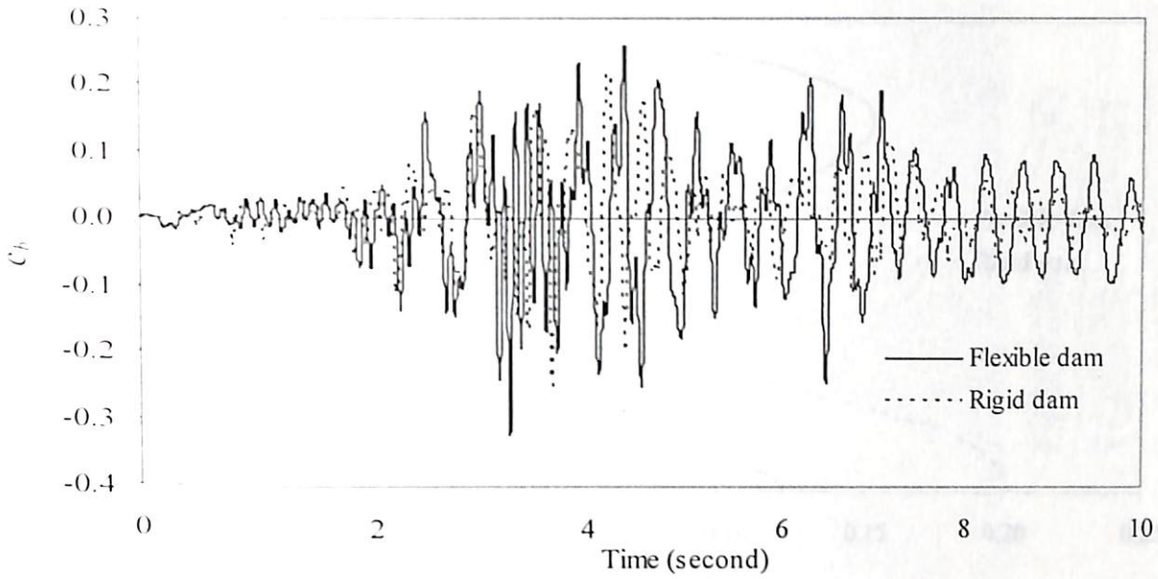

Fig. 4.174 Hydrodynamic pressure coefficient at point B of the dam subjected to Koyna earthquake

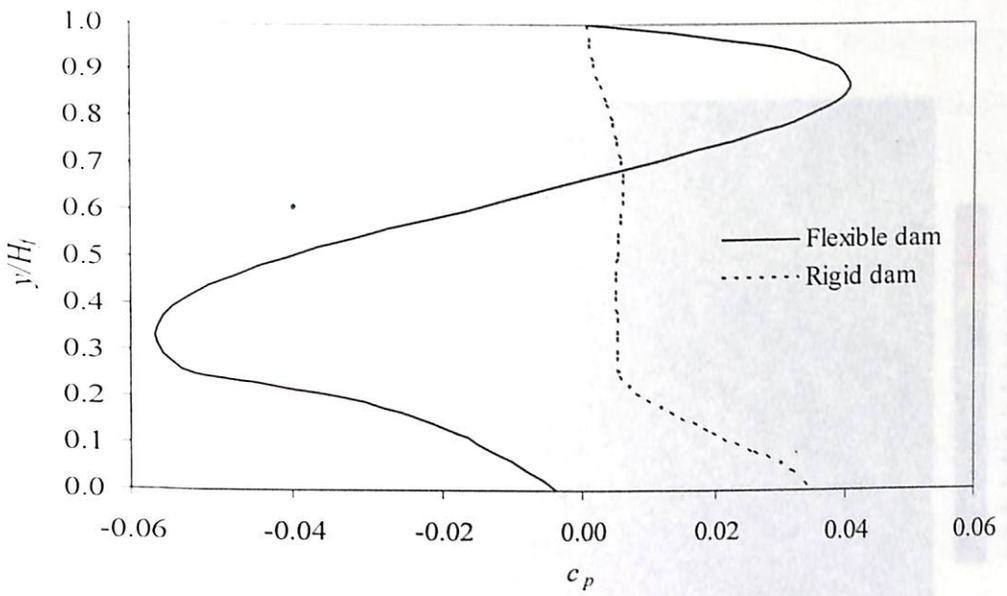

Fig. 4.175 Hydrodynamic pressure distribution along the upstream face of dam (t = 2.0 sec)

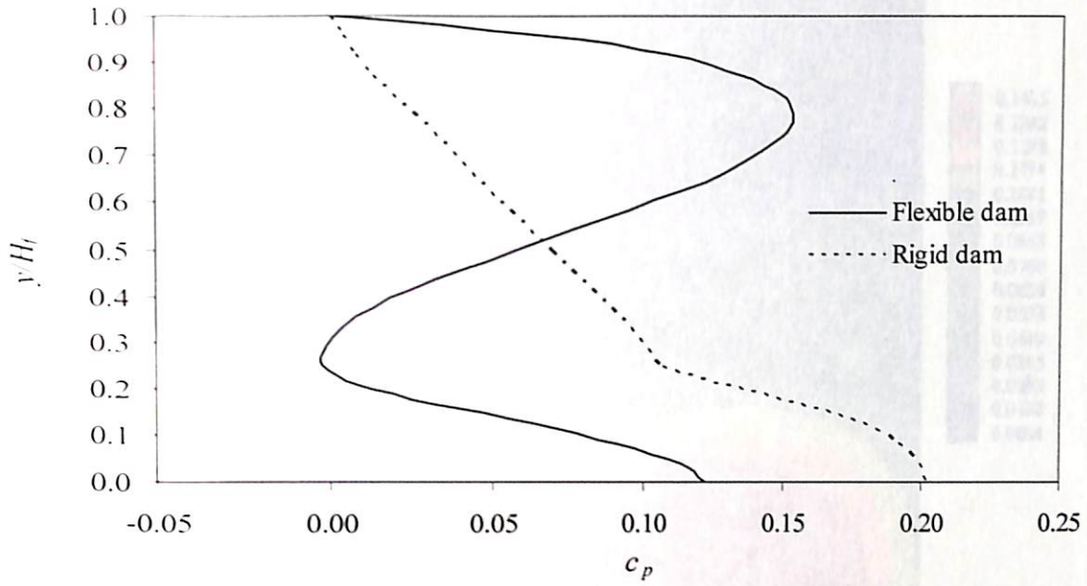

Fig. 4.176 Hydrodynamic pressure distribution along the upstream face of dam (t = 4.2 sec)

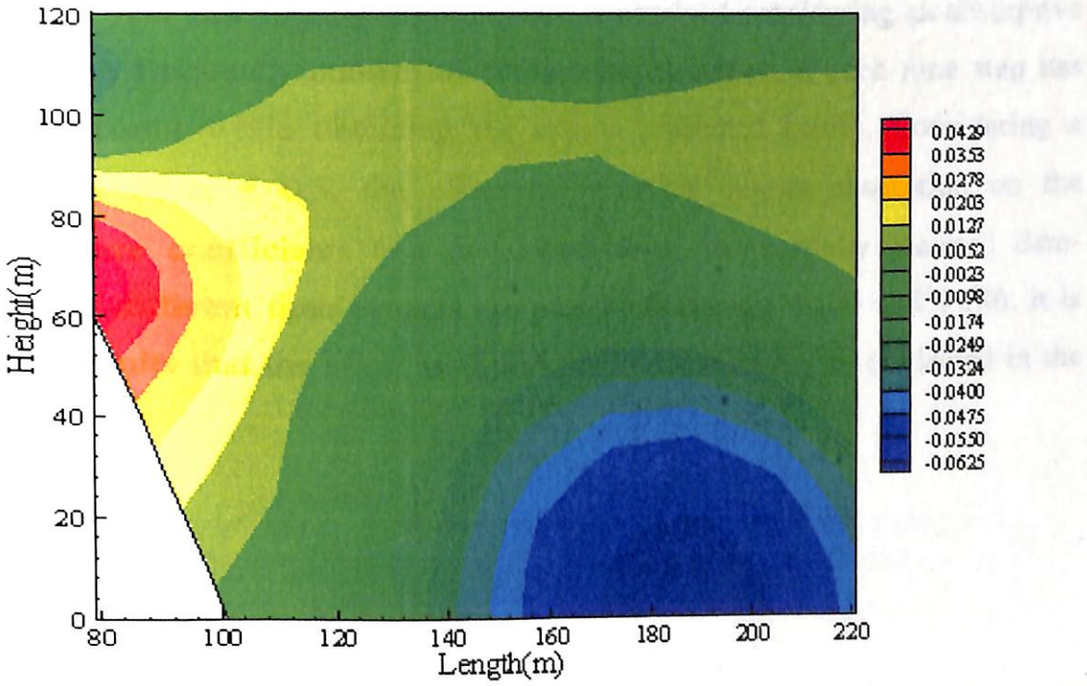

Fig. 4.177 Pressure contour due to rigid reservoir bottom at 2.0 sec

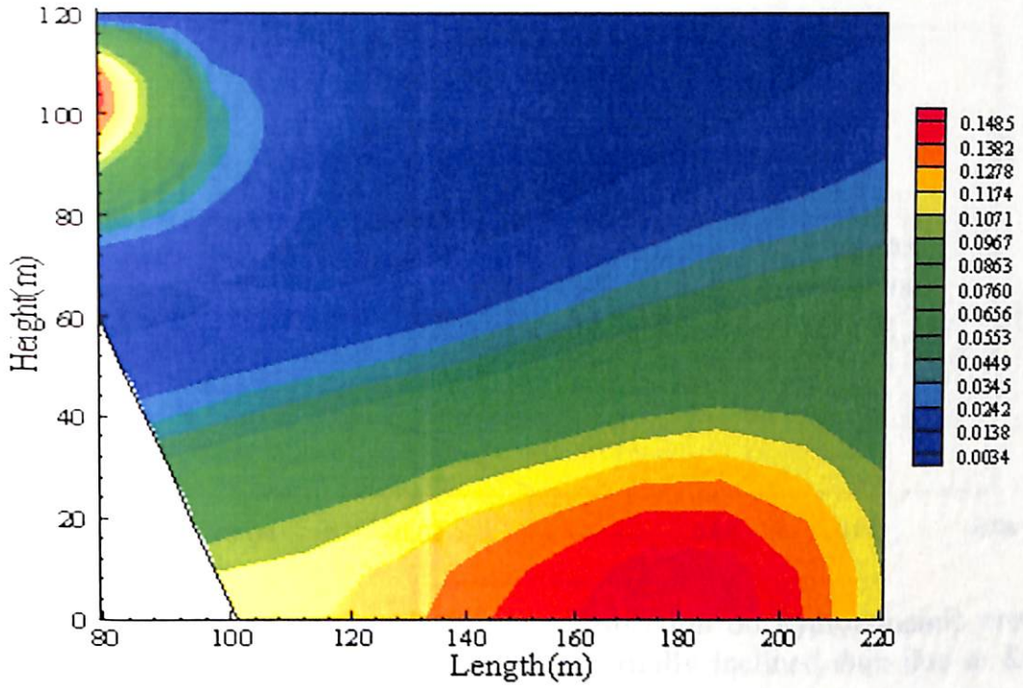

Fig. 4.178 Pressure contour due to rigid reservoir bottom at 4.2 sec

The hydrodynamic pressure coefficients along the dam-reservoir interface (Fig.4.172) in the 1st year due to Koyna earthquake is obtained considering an absorptive reservoir bottom. The frequency content of earthquake excitation at each time step has been taking into account while obtaining the results presented herein. Considering a reflection coefficient of $\alpha = 0.5$, the effect of reservoir bottom absorption on the hydrodynamic pressure coefficients (c_p) developed along the partially inclined dam-reservoir interface at different time instants are presented in Figs. 4.179 and 4.180. It is observed from the results that the effect is significant and should not be neglected in the analysis.

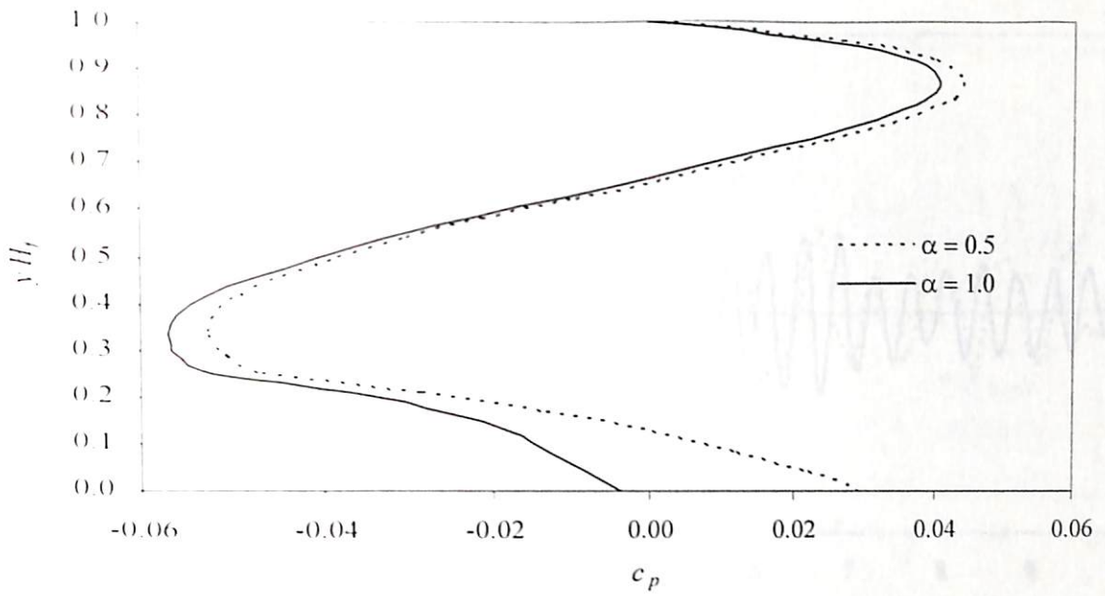

Fig. 4.179 Effect of reservoir bottom absorption on hydrodynamic pressure distribution along the upstream face of partially inclined dam due to Koyna earthquake at t = 2.0 sec

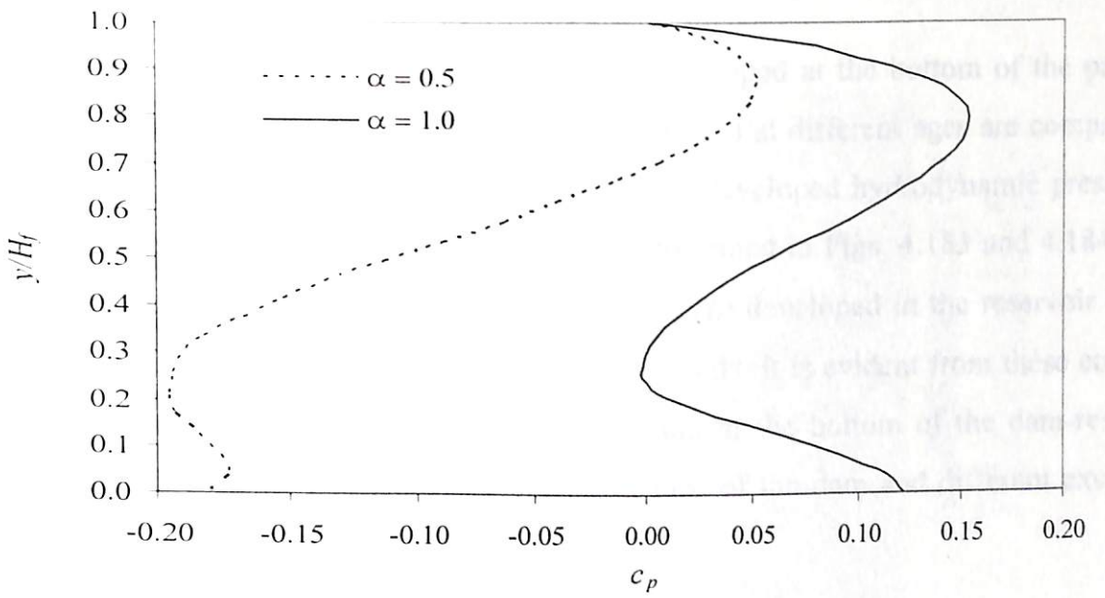

Fig. 4.180 Effect of reservoir bottom absorption on hydrodynamic pressure distribution along the upstream face of partially inclined dam due to Koyna earthquake at t = 4.2 sec

The seismic response of the dam-reservoir system is further studied considering degradation of concrete with age. The reflection coefficients at a particular age are determined considering a sedimentation rate of 40 cm/year over a layer of rigid rock. The crest displacements, pressure coefficients of the partially inclined dam at different ages are presented in Fig. 4.181 - 4.182. It is observed from Fig. 4.181 that the crest displacements are of very high magnitudes in the 75th year.

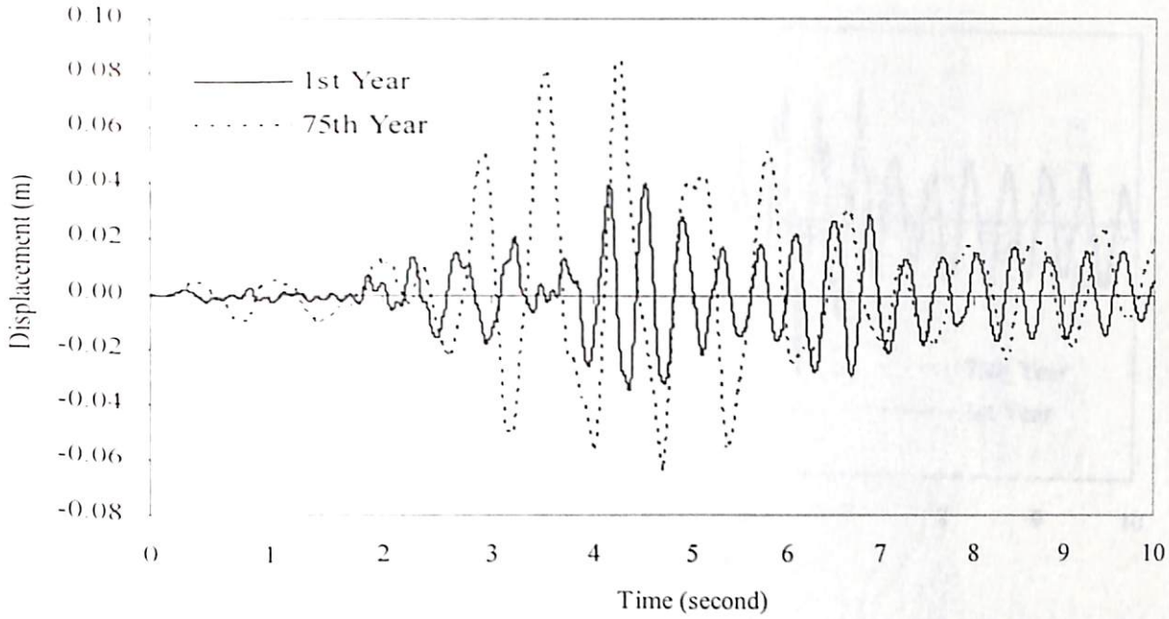

Fig. 4.181 Effect of ageing on horizontal crest displacement of the dam subjected to Koyna earthquake

The hydrodynamic pressure coefficients developed at the bottom of the partially inclined dam-reservoir interface (point B of Fig. 4.172) at different ages are compared in Fig. 4.182. It is observed that the magnitude of the developed hydrodynamic pressure is different at different age. The pressure contours presented in Figs. 4.183 and 4.184 show the hydrodynamic pressure coefficients ($c_p = p/\rho_f gH_f$) developed in the reservoir due to Koyna earthquake at $t = 2.025$ seconds and 4.2 seconds. It is evident from these contours that the highest pressure coefficients may not occur at the bottom of the dam-reservoir interface (point B) due to the inclined upstream face of the dam and different excitation frequencies present in the seismic excitation.

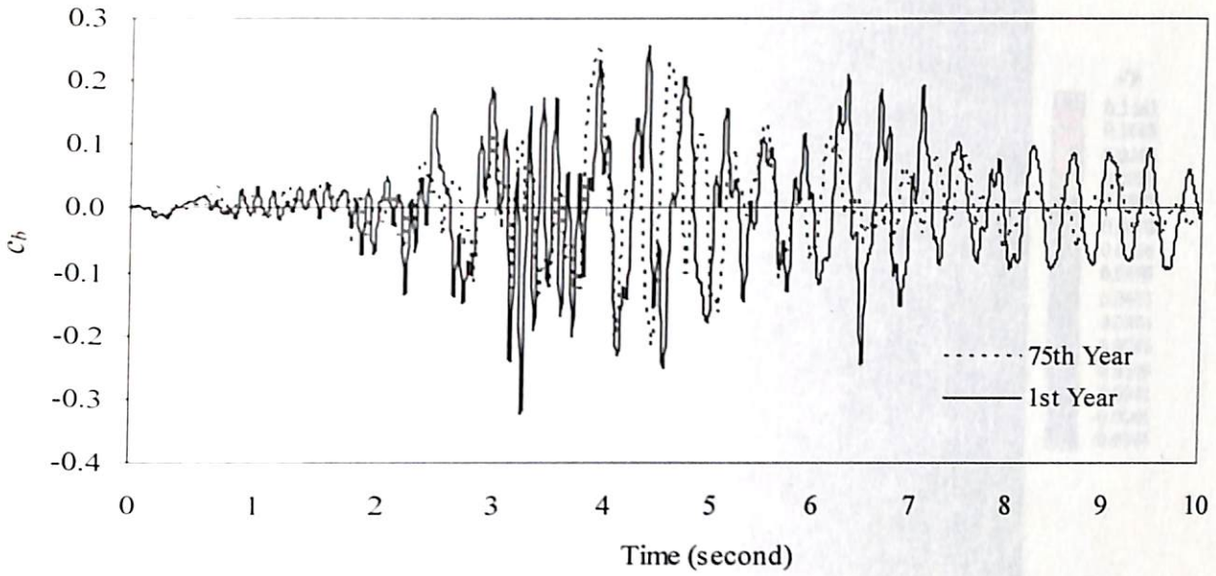

Fig. 4.182 Effect of ageing on pressure coefficients at point B of the dam due to Koyna earthquake

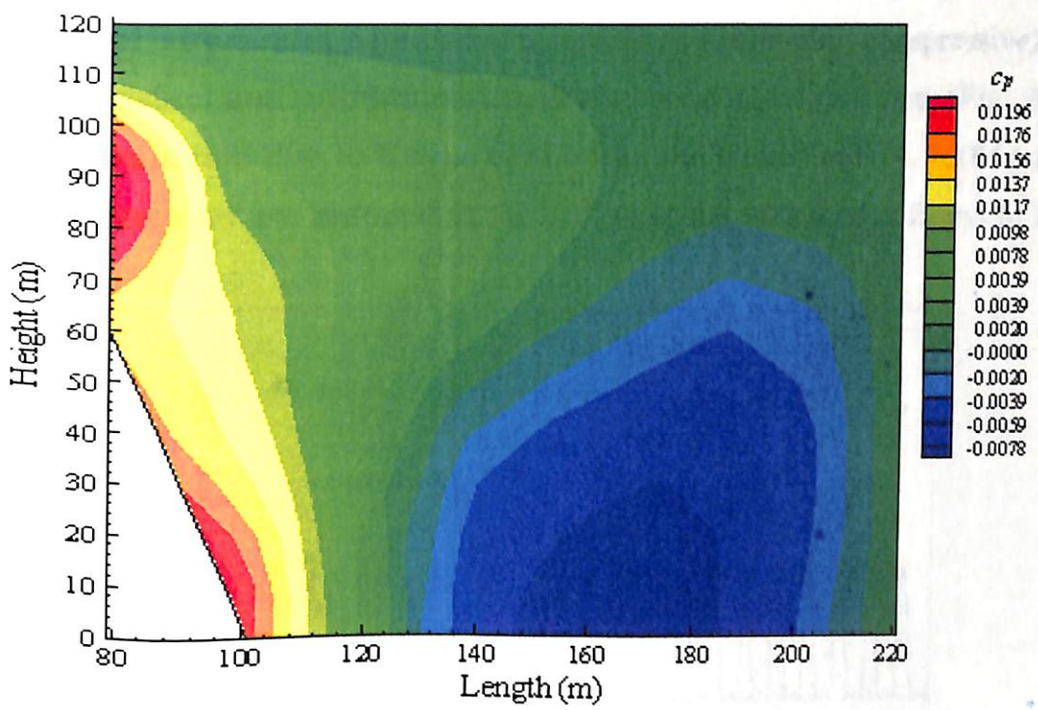

Fig. 4.183 Pressure contour in the reservoir due to Koyna earthquake in the 75th year at t = 2.025 sec

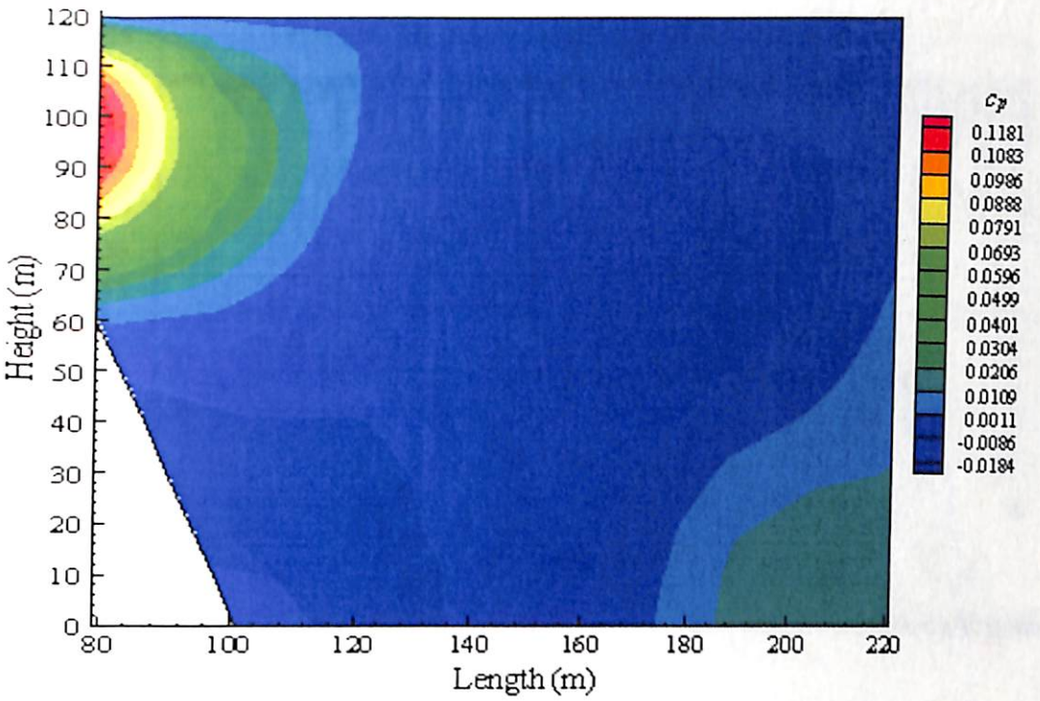

Fig. 4.184 Pressure contour in the reservoir due to Koyna earthquake in the 75th year at t = 4.2 sec

The principal stresses σ_{p1} (maximum tensile and minimum compressive) and σ_{p2} (maximum compressive and minimum tensile) at point C of the dam (Fig. 4.172) at different ages are evaluated due to Koyna earthquake and plotted in Figs. 4.185 and 4.186. It is observed that stresses are reduced at the 75th year due to loss of stiffness of the dam.

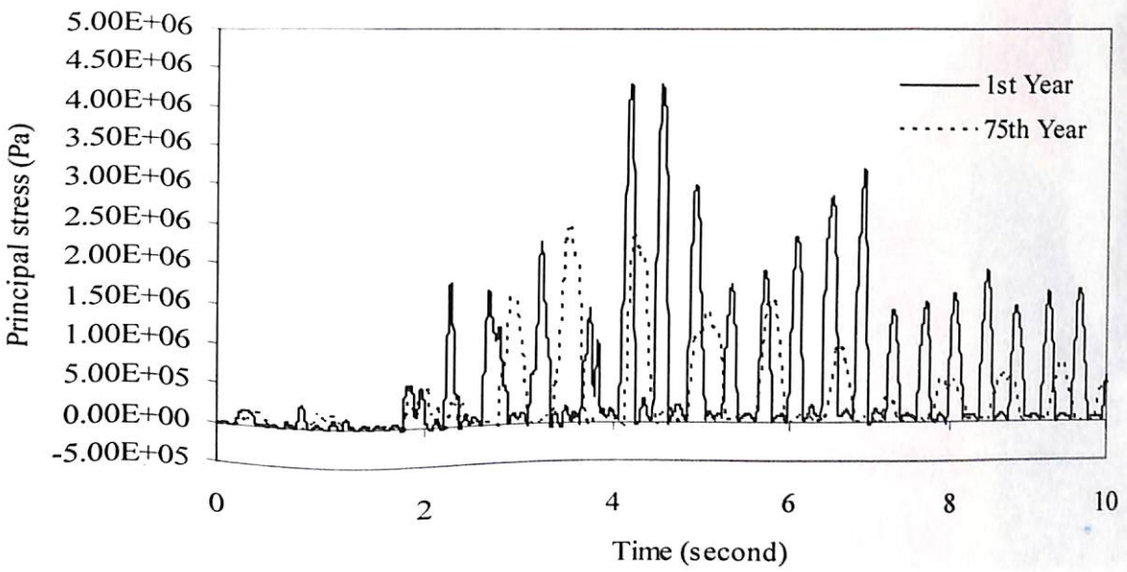

Fig. 4.185 Principal stress σ_{p1} at point C of the dam due to Koyna earthquake

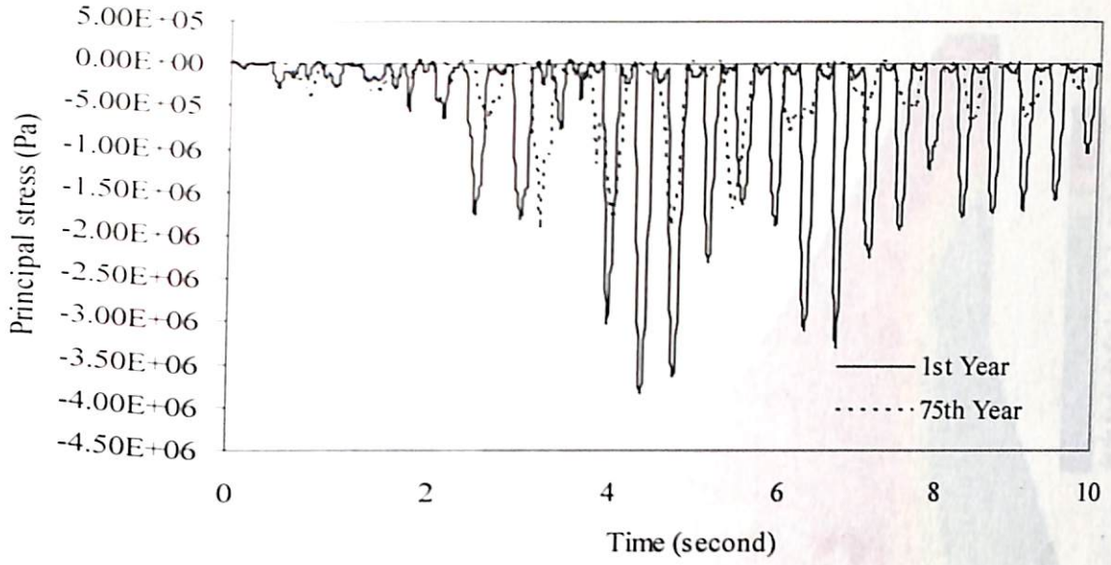

Fig. 4.186 Principal stress σ_{p2} at point C of the dam due to Koyna earthquake

The stress contours at different time instants are plotted in Figs. 4.187 and 4.188, which shows the stresses developed in the dam body at the 75th year. The figures in legend represent the stresses in Pa. It is observed from these figures that the region near the point C of the dam is most vulnerable as high magnitudes of compressive stresses are developed.

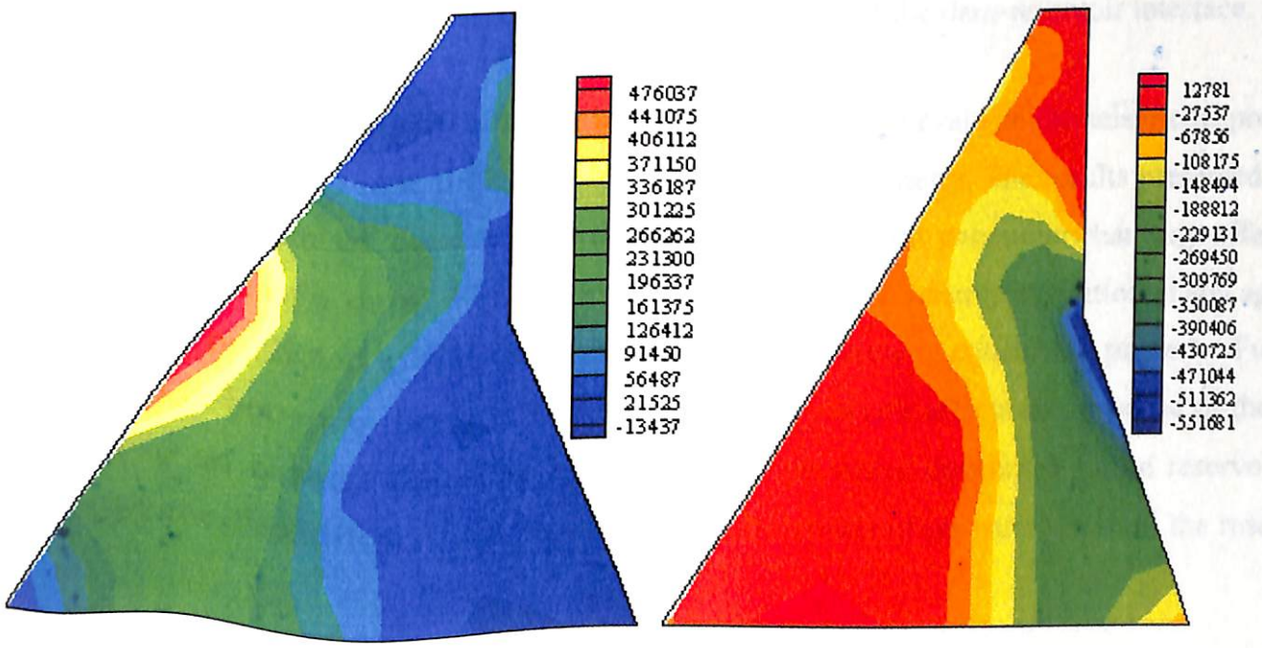

(i) σ_{p1} (ii) σ_{p2}

Fig. 4.187 Principal stress contour (i) σ_{p1} and (ii) σ_{p2} in dam due to Koyna earthquake at $t = 2.0$ sec

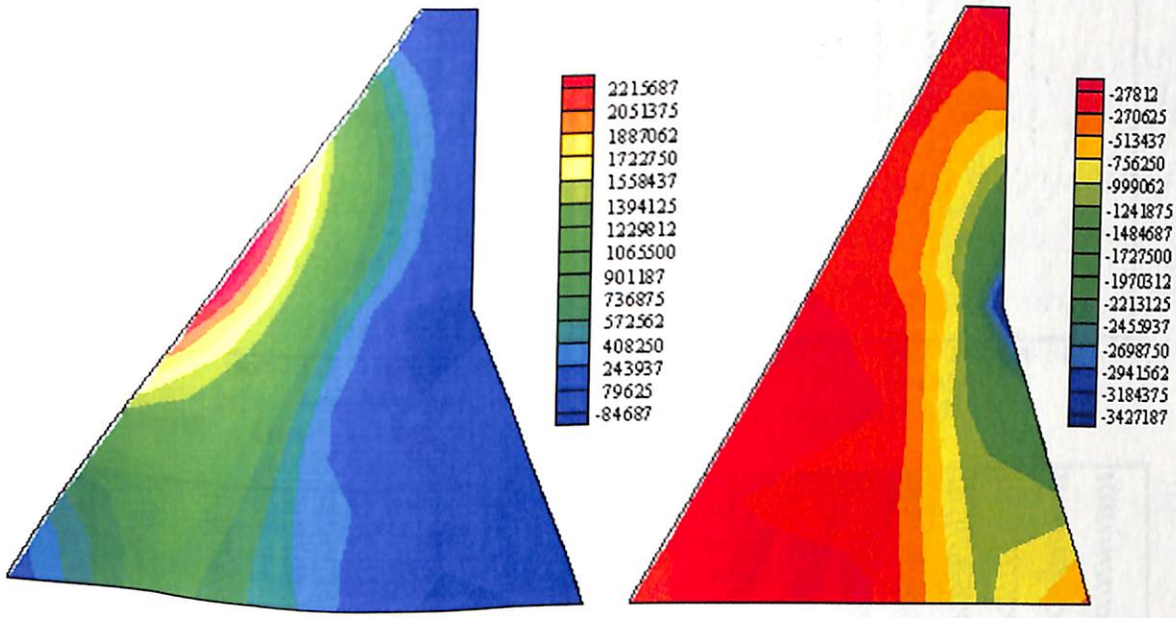

(i) σ_{p1} (ii) σ_{p2}

Fig. 4.188 Principal stress contour (i) σ_{p1} and (ii) σ_{p2} in dam due to Koyna earthquake at t = 4.2 sec

The velocities of fluid particles in the reservoir at different instants of time are plotted in the form of velocity vectors in Fig. 4.189. The lengths of the vectors represent the magnitudes of the velocities. It is interesting to observe that the velocities of the fluid particles in the reservoir are affected by the geometry of the dam-reservoir interface.

The proposed algorithm can efficiently be used to evaluate the seismic response of a concrete dam at any age that may have a complex geometry. The results presented show that the degradation of concrete with age is an important parameter that may affect the seismic response of a dam. The behavior of a dam due to seismic excitation at any age can be accurately predicted if the degradation of the concrete is considered properly. Further, the interaction between the dam and the adjacent reservoir affects the response of the dam subjected to an earthquake. The hydrodynamic pressures developed in the reservoir are affected by the flexibility of the dam and the absorption of pressure waves at the reservoir bottom.

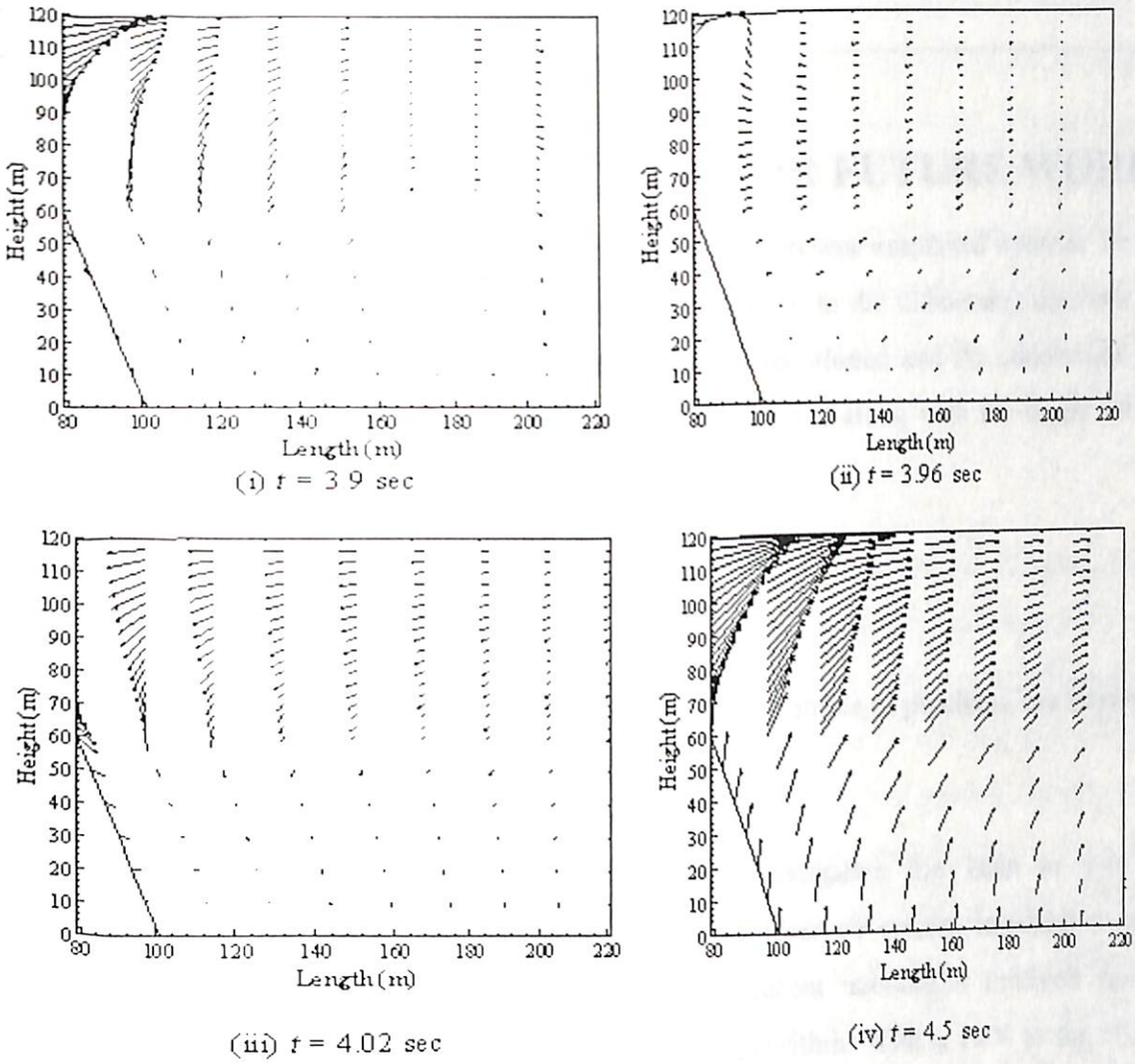

Fig. 4.189 Velocity vectors in the reservoir due to Koyna earthquake

CHAPTER 5

CONCLUSIONS AND SCOPE FOR FUTURE WORK

The conclusions drawn based on the findings of the present numerical exercise for the dynamic analysis of aged concrete gravity dam adjacent to the unbounded reservoir are summarised in this chapter. The major findings are mentioned and the conclusions are drawn accordingly. The limitations of the present scheme along with the scope for the future research of the present problem are also spelt out.

5.1 CONCLUSIONS

Based on the numerical experiments, carried out on a number of problems, the important findings and conclusions drawn are summarised below.

The primary objective of the present investigation has been to gain an understanding of the behaviour of the coupled dam-reservoir system, in which an aged concrete dam like structure interacts with the adjacent unbounded reservoir having sediments at its bed, through a stable numerical algorithm. With a view to the above, software DAACDRS (Dynamic Analysis of Aged Concrete Dam Reservoir System) is developed, in which, a general time domain analysis for the coupled dam-reservoir system is carried out, considering fluid-structure interaction effects. The analysis is carried out considering water to be linearly compressible, inviscid and of small amplitude of motion. Provision is made in the program to take into account the geometrical non-linearity of the dam. The deflection & stress field in the dam and the velocity & pressure developed in the reservoir, under the action of external loading, can be readily computed using the developed software. The skyline algorithm is used to reduce the computational time and the storage space. A post processor module for obtaining the pressure contours, velocity vectors, stress contours based on the analysis data is also supplemented with the DAACDRS.

As mentioned earlier, the two domains *viz.*, the reservoir and the dam are analysed independently and are interconnected together through the common interface adopting an efficient iterative scheme. The governing equation for water is expressed in

terms of the pressure variable and is discretized by the finite element method. The advantage of using pressure based formulation is that it significantly reduces the degrees of freedom and thereby reduces computational time and storage space. Also, additional precautions such as incorporation of penalty parameter to take care of the irrotationality conditions are not required unlike in displacement based formulation. Another advantage of this approach is that the pressure field obtained from the analysis of the reservoir domain may be directly transferred to the dam at the dam-reservoir interface to evaluate the forces unlike other methods, where pressure has to be calculated from velocity or displacement or their potential.

The dam-reservoir interaction effects are achieved in an iterative manner, where the equilibrium conditions along the common interface of the dam and the reservoir are satisfied. The developed iterative scheme is simple and straightforward in implementation and produces effective results. The two fields are solved individually and the interaction effects are enforced at the interface of the coupled system. The pressure in the reservoir domain and the displacement in the dam are converged simultaneously till a desired level of convergence is achieved. It is observed that only a few numbers of iterations are sufficient to obtain reasonable convergent results. The number of iteration depends on the flexibility of the dam. This number is being increased as dam becomes more flexible. The major advantages of the iterative scheme are: (*a*) The resulting matrices remain symmetric as the systems are dealt with separately. (*b*) The size of matrices required to be inverted is comparatively smaller as the two systems are solved in a decoupled manner. (*c*) The matrices involved in the solution of the system equations are decomposed into triangular forms at the beginning of the iteration, and thereby only two forward-eliminations and back-substitutions are required at each iteration step. Thus, the time required to obtain the coupled response for a particular time instant is minimised.

The developed numerical procedure can account for the concrete degradation process and can predict the seismic behavior of the dam at any age depending on the design life of the dam considering coupled dam-reservoir interaction effects. The response of the aged concrete dam to static and dynamic load is determined by incorporating a degradation index in the constitutive matrix of the dam. The estimation of the degradation index is based on the value of porosity of concrete that increases with the

adverse environmental conditions and continuous state of submergence. In the present work, the degradation index is determined from experimental results in published literature. It is a known fact that concrete gains strength with age. Therefore, in the present formulation, the elastic modulus of concrete at any age considers the inherent strength gain as well as degradation due to extreme environmental conditions. This may be beneficial to assess the safety of existing dams during its lifetime. A time dependent isotropic degradation index is evaluated based on hygro-chemo-mechanical effect for aged dams. The numerical results show that the crest displacement of the dam becomes more and the magnitude of the stress in the dam body becomes less with the increasing age of the dam.

The effect of geometrical non-linearity is negligible for the kind of problems considered in the present investigation. The material degradation of the concrete dam may alter the behaviour of the adjacent reservoir domain significantly. There is a common belief that in case of rigid dam, the magnitude of the hydrodynamic pressure becomes high. But this is not always true. The magnitude of the hydrodynamic pressure may increase significantly for the elastic dam as well. Moreover, if the resonance between the two systems occurs, the developed hydrodynamic pressure may increase manifold. Hence, the dam, exposed to unbounded reservoir are to be analysed, paying due considerations to these aspects.

In the finite element analysis of the reservoir, problems arise mainly because of the large extent of the reservoir domain. A simple but effective far-boundary condition is developed at the truncation surface to overcome this problem. The truncation boundary condition is obtained from the derivation of the exact solution that can be used for determining hydrodynamic pressure at the upstream face of a rigid dam. The present far-boundary condition has the following advantages: (*i*) Implementation of the developed far-boundary condition in the finite element program is quite simple; (*ii*) The symmetrical forms of the matrices remain unchanged; (*iii*) It includes the reservoir bottom absorption effects due to the presence of sediments; (*iv*) It is applicable to the dam-reservoir systems of arbitrary geometries with the only limitation that beyond a certain distance from the dam, the reservoir is assumed to have a constant depth. The results using the developed far-boundary condition have proved its effectiveness. It is observed from the results that the proposed far-boundary condition produces accurate

results for all ranges of excitation frequencies. The results show that the unbounded reservoir domain may be truncated even at a relatively smaller distance away from the dam, resulting in great computational advantages, using present far-boundary condition. The convergence of the finite element results is attained at a very short distance away from the dam-reservoir interface (i.e., with 0.02 to 0.2 times the reservoir depth) for all excitation frequencies for the case when the upstream face of the dam is vertical. However, for the irregular geometry, the convergence would depend on magnitudes of inclination of the upstream face of the dam, reservoir bed, reflection coefficient and excitation frequencies. Since the truncation boundary condition is developed from the case when the dam face is vertical and the reservoir bed profile is horizontal, an increase in percentages of error is observed for higher inclinations of dam face and reservoir bed.

It is important that the boundary conditions at the reservoir bottom and truncation surface being frequency dependent should properly be incorporated in the time domain analysis. A unique method is incorporated in the present algorithm to account for the frequency content of earthquake excitation so that the damping parameters at the reservoir bottom and truncation surface can be estimated accurately. The non-stationary earthquake signal is divided into small time segments and the FFT of each time segment is obtained to ascertain the frequencies that exist in it. The dominant frequency at every time step is extracted and is used as an input in the seismic analysis. The effectiveness of the developed far-boundary condition has been increased with the incorporation of Short Time Fourier Transform for the analysis of dam-reservoir system under seismic excitation. The proposed time-frequency hybrid method is advantageous as the frequency dependent responses of the dam-reservoir system can be obtained in a time domain procedure. The implementation of this technique is simple as the time domain procedure remains the same and the algorithm can be modified to account for the dominant frequencies at every time step. As the procedure is in time domain and can efficiently account for different excitation frequencies the transformation of frequency dependent dynamic stiffness matrix as used in various time-frequency hybrid methods can be avoided.

The effect of the reservoir bottom absorption due to sediment deposited over the years is incorporated in the analysis procedure. The developed algorithm can effectively account for the reservoir bottom absorption under seismic excitation. The hydrodynamic

response of the degraded dam-reservoir system under seismic excitation may be determined for (i) constant sediment depth (sediment flushed out at regular intervals) and (ii) varying sediment depth (accumulating with age). It is observed that for a constant reflection coefficient, the significance of the absorptive effect of the reservoir bottom on the hydrodynamic pressure and on the degraded structural responses reduces with age. However, with increasing depth of sediment layer and degradation, the significance of absorptive reservoir bottom depends on the properties of the strata lying below the sediment layer. It is observed from the present study that the properties of the strata lying below the sediment layer, accumulating depth of sediment and degradation of the dam with age are important parameters in the dynamic analysis of the aging dam and may not be neglected.

The effect of reservoir bottom absorption is found to be small for lower values of excitation frequencies. But this effect may not be neglected if the excitation frequency becomes equal or more than the fundamental frequency of the reservoir. Further, the effect of gravity waves is found to be considerable for the lower values of excitation frequencies.

The study also reveals that the depth of sediment layer does not have much effect on the reflection coefficient for lower excitation frequency. But for an increasing excitation frequency it is observed that an increase in depth of sediment layer would reduce the reflection coefficient considerably. Therefore, if the frequency content of an earthquake excitation is high, it would necessitate incorporating the effect of frequency dependent reflection coefficient in the analysis procedure.

It is observed from the pressure contour diagrams for different configurations of the dam-reservoir systems that the magnitude of the hydrodynamic pressure decreases, when the dam-reservoir interface becomes inclined. The hydrodynamic pressure increases with the increase of the reservoir bed slope in upward direction and decreases with the increase of the reservoir bed slope in downward direction.

In general, the displacement of the dam increases with the increase of the age. But, sometimes, the displacement may decrease with the increase of dam age. This may be because of the resonance of the coupled system due to external excitation.

The stress contours of the dam give a clear picture of the critical zones, where the maximum stress may develop. It is possible from the developed algorithm to identify the hot spots, where the tensile and compressive stresses exceed the allowable tensile and compressive strength of a given material of the dam. Such analyses are essential for the safe design of dams or to monitor the health of the existing dams.

5.2 OUTCOME OF THE PRESENT WORK

The present work is an investigation of the dynamic response of an ageing concrete gravity dam coupled with the unbounded reservoir. The major contributions of present work are:

- A degradation model is developed for the dynamic analysis of aging concrete gravity dam. This analytical model can effectively account for the gain and loss in concrete strength due to various environmental factors with age.
- The hydrodynamic pressure developed at the upstream face of the dam is affected by the layered sediment deposited at the reservoir bottom. A numerical model is presented to evaluate the reflection coefficient at the reservoir bottom depending on (i) the thickness of the sediment layer that may increase with deposition of sediment with age and (ii) material parameter of the sediment and the underlying rock strata.
- A non-reflecting boundary condition is developed which can be used in a finite element model of the infinite reservoir, at a relatively short distance from the upstream face of the dam. The robustness of this boundary condition is tested at various frequencies of excitation. The comparison of results with published literature demonstrated the efficiency and novelty of the proposed boundary condition for the all range of excitations.
- The developed frequency dependent truncation boundary and the absorptive boundary at the reservoir bed has been made efficient under seismic excitation using Short Time Fourier Transform (STFT) which extracts the frequencies of the earthquake signal at each time step.
- The dynamic response of the ageing dam-reservoir coupled system under earthquake excitation can effectively be evaluated using the developed iterative

scheme. The stresses in the dam body, the velocity and pressure in the reservoir can be determined with a desirable level of accuracy at any time using the developed algorithm.

5.3 SCOPE FOR FUTURE WORK

An effective solution scheme is developed to analyze the dynamic behavior of an ageing concrete gravity dam interacting with the unbounded reservoir. There are certain other aspects that may be considered for further research:

- The degradation of concrete strength with age may induce formation of cracks. A study of crack formation and propagation may be carried out to predict the nonlinear behaviour of the dam. Inclusion of the material non-linearity in both isotropic and anisotropic materials may be the subject of further research.
- The present model does not account for thermal stresses due to hydration of concrete which may affect ageing of the dam.
- In the present work an isotropic degradation index is evaluated, which is considered to be same at every point of the dam. The present work may be extended to predict the orthotropic degradation index based on the plane of weakness such as the lift joint surface. Moreover, a dam being a massive concrete structure, the extent of porosity may not be same throughout the body of the dam. This may necessitate having different degradation index in the dam depending on its distance from the water surface.
- In the present work, the dynamic magnifications of strength and stiffness parameters of concrete due to rapid application of seismic strains are not considered, which may be another scope of research.
- The present problem may be extended to 3-dimensional form with the proper inclusion of radiation boundary condition for the unbounded reservoir.
- The present analysis is limited to the small fluid displacement. For the case of large fluid displacement, the non-linear convective term of the Navier Stokes equation, which is excluded in the present formulation, may play an important

role. Hence, a study may be useful considering the effect of non-linear convective term.

- The present problem may be extended to study the effect of foundation flexibility of dam considering soil-structure interaction to obtain more precise behaviour of the coupled system. More accurate behaviour may be obtained if coupled effect of the foundation-dam-reservoir interaction is considered.
- Based on the proposed method of predicting dynamic behavior of ageing concrete gravity dam, an earthquake vulnerability study can be carried out.

BIBLIOGRAPHY

Ahmadi, M.T. and Khoshrang, G. (1992) "Sefidrud dam's dynamic response to the large near-field earthquake of June 1990", *Dam Engineering*, 3, 85-113.

Andrade, W.P., Tomaz, R.J. Biitencourt, R.M. and Guerra, E. (1981) "A mix design for mass concrete", *Proceedings of Brazilian Concrete Institute*.

Antes, H. (1985) "A boundary element procedure for transient wave propagation in two dimensional isotropic elastic media", *International Journal of Finite Element Analysis and Design*, 1, 313-322.

Antes, H. and von Estorff, O. (1987) "Analysis of absorption effects on dynamic response of dam reservoir systems by boundary element methods", *Earthquake Engineering and Structural Dynamics*, 15, 1023-1036.

Antoniadis, I. and Kanarachos, A. (1988) "Decoupling procedures for fluid-structure interaction problems", *Computer Methods in Applied Mechanics and Engineering*, 70, 1-25.

Atkin, P.W. (1994) *Physical Chemistry*, 5th Edition, Oxford University Press, Oxford, U.K.

Au-Yang, M.K. and Galford, J.E. (1982) "Fluid-structure interaction - a survey with emphasis on its application to nuclear steam system design", *Nuclear Engineering and Design*, 70, 387-399.

Avilés, J. and Sesma, F.J.S. (1986) "Hydrodynamic pressures on dams with non-vertical upstream face", *Journal of Engineering Mechanics, ASCE*, 112(10),1054-1061.

Azmi, M., Paultre, P. (2002) "Three-dimensional analysis of concrete dams including contraction joint non-linearity", *Engineering Structures*, 24, 757-771.

Bangert, F., Grasberger, S., Kuhl, D., Meschke G. (2003) "Environmentally induced deterioration of concrete: physical motivation and numerical modelling", *Engineering Fracture Mechanics*, 70, 891–910.

Barlow, J. (1976) "Optimal stress locations in finite element method", *International Journal for Numerical Methods in Engineering*, 10, 243-751.

Batta, V. and Pekau, O.A. (1996) "Application of boundary element analysis for multiple cracking in conrete gravity dams", *Earthquake Engineering and Structural Dynamics*, 25, 15-30.

Bazant, Z.P. (1994) "Creep and thermal effects in concrete structures: a conceptus of some new developments", *Computational modelling of Concrete Structures, International Conf. EURO-C*, H. Mang, N. Bicanic and R. de Borst. eds., Pineridge Press, Swansea, Wales, 461-480.

Bazant, Z.P., Hauggaard, A.B., Baweja, S. and Ulm, F.J. (1997) "Microprestress-solidification theory for concrete creep. I: Aging and drying effects", *Journal of Engineering Mechanics, ASCE*, 123(11), 1188-1194.

Bazant, Z.P. and Xiang, Y. (1997) "Crack growth and lifetime of concrete under long time loading", *Journal of Engineering Mechanics, ASCE*, 123(4), 350-358.

Beer, G. and Meek, J.L. (1981) "The coupling of the boundary and finite element methods for infinite domain problems in elastoplasticity", *Boundary Element Methods*, Berlin, Springer , 575-591.

Bermúdez A, Durán R, Muschietti MA, Rodríguez R, Solomin J. (1995) "Finite element vibration analysis of fluid-solid systems without spurious modes", *SIAM Journal of Numerical Analysis*, 32, 1280-1295.

Bettess, P. (1977) "Infinite Elements", *International Journal for Numerical Methods in Engineering*, 11(1), 53-64.

Bhattacharjee, S.S. and Léger, P. (1994) "Application of NLFM models to predict cracking in concrete gravity dams", *Journal of Structural Engineering, ASCE*, 120(12), 1255-1271.

Bittencourt, R.M., Fontoura, J.T.F., Andrade, W.P. and Monteiro, P.J.M (2001) "Mass concrete mixtures based on fineness modulus and geometrical gradation", *Journal of Materials in Civil Engineering, ASCE*, 13(1), 33-40.

Bouaanani, N., Paultre, P. and Proulx, J. (2002) "Two-dimensional modelling of ice cover effects for the dynamic analysis of concrete gravity dams", *Earthquake Engineering and Structural Dynamics*, 31, 2083-2102.

Bouaanani, N., Paultre, P. and Proulx, J. (2003) "A closed-form formulation for earthquake-induced hydrodynamic pressure on gravity dams", *Journal of Sound and Vibration*, 261, 573-582.

Bougacha, S. and Tassoulas, J. L. (1991a) "Effect of sediment material on the response of concrete gravity dams", *Earthquake Engineering and Structural Dynamics*, 20(9), 849-858.

Bougacha, S. and Tassoulas, J.L. (1991b) "Seismic response of gravity dams. I. Modelling of sediments", *Journal of Engineering Mechanics, ASCE*, 117(8), 1826-1838.

Bougacha, S. and Tassoulas, J.L. (1991c) "Seismic response of gravity dams. II. Effects of sediments", *Journal of Engineering Mechanics, ASCE*, 117(8), 1839-1850.

Boussinesq, H. (1885) "Applications des potentiels al'etude de l'equilibre et du mouvement des solids elastique", Paris, Gauthier-Villars.

Bracewell, R.N. (1986) "The Fourier transform and its application", 2nd edition, McGraw-Hill, New York.

Brebbia, C.A. and Georgious, P. (1979) "Combination of boundary and finite elements for elastostatics", *Applied Mathematical Modelling*, 3,121-220.

Bustamante, I.J. and Flores, A. (1966) "Water pressure on dams subjected to earthquakes", *Journal of Engineering Mechanics Division, Proceedings of ASCE*, Oct, 15-127.

Bycroft, G.N. (1980) "Soil-foundations interaction and differential ground motion", *Earthquake Engineering and Structural Dynamics*, 8, 397-404.

Bycroft, G.N. and Mork, P.N. (1987) "Seismic response of dam with soil-structure interaction" *Journal of Engineering Mechanics, ASCE*, 113(9), 1420-1428.

Byfors, J. (1980) "Plain concrete at early ages", *Research Report F3:80*, Swedish Cement and Concrete Research Institute, Stockholm, Sweden.

Cervera. M., Oliver, J. and Faria, R. (1995) "Seismic evaluation of concrete dams via continuum damage models", *Earthquake Engineering and Structural Dynamics,* 24(9), 1225-1245.

Cervera, M., Oliver, J. and Prato, T. (1999a) "Thermo-Chemo-Mechanical Model for Concrete. I: Hydration and Aging", *Journal of Engineering Mechanics, ASCE*, 125, 1018 -1027.

Cervera, M., Oliver, J. and Prato, T. (1999b) "Thermo-Chemo-Mechanical Model for Concrete. II: Damage and Creep", *Journal of Engineering Mechanics, ASCE*, 125, 1028- 1039.

Cervera, M., Oliver, J. and Prato, T. (2000a) "Simulation of construction of RCC dams I: Temperature and aging", *Journal of Structural Engineering, ASCE*, 126(9), 1053-1061.

Cervera, M., Oliver, J. and Prato, T. (2000b) "Simulation of construction of RCC dams. II: Stress and Damage" *Journal of Structural Engineering, ASCE*, 126(9), 1062-1069.

Cetin, M. and Mengi, Y. (2003) "Transmitting boundary conditions suitable for analysis of dam-reservoir interaction and wave load problems", *Applied Mathematical modelling*, 27, 451- 470.

Chakrabarti, P. and Chopra, A.K. (1973) "Earthquake analysis of gravity dams including hydrodynamic interaction", *Earthquake Engineering and Structural Dynamics*, 2, 143-160.

Chandrashaker, R. and Humar, J.L. (1993) "Fluid-foundation interaction in the seismic response of gravity dams", *Earthquake Engineering and Structural Dynamics*, 22, 1067-1084.

Chavez, J.W. and Fenves, G.L. (1995) "Earthquake analysis of concrete gravity dams including base sliding", *Earthquake Engineering and Structural Dynamics*, 24, 673-686.

Chen, H.C. and Taylor, R.L. (1990) "Vibration analysis of fluid solid systems using a finite element displacement formulation", *International Journal for Numerical Methods in Engineering*, 29, 683-698.

Chopra, A.K. (1967) "Hydrodynamic pressures on dams during earthquakes", *Journal of Engineering Mechanics, ASCE*, 93, 205-223.

Chopra, A.K. (1968) "Earthquake behavior of reservoir-dam systems", *Journal of Engineering Mechanics Division, ASCE*, 93,1475-1500.

Chopra, A.K. and Chakrabarti, P. (1972) "The earthquake experience at Koyna dam and stresses in concrete gravity dams", *Earthquake Engineering and Structural Dynamics*, 1,151-164.

Chopra, A.K. (1975) "An examination of standard earthquake design forces for concrete gravity dams", *Proceedings of International Symposium*, Swansea, UK, Sept. 8-11.

Chopra, A.K., Chakrabarti, P. and Gupta, S. (1980) "Earthquake response and concrete gravity dams including hydrodynamic interaction effects", *Report No. UCB/EERC-80/01, Earthquake Engineering Research Center*, University of Berkley, California.

Chopra, A.K. and Chakrabarti, P. (1981) "Earthquake analysis of concrete gravity dams including dam-water-foundation rock interaction", *Earthquake Engineering and Structural Dynamics*, 9, 363-383.

Chopra, A.K. (1998) Dynamics of Structures, *Prentice Hall of India Pvt. Ltd., New Delhi*, ISBN-81-203-1043-8, 155-185.

Chuhan, Z., Xinfeng, C. and Guanglun W. (1999) "A coupling method of FE-BE-IE-IBE for nonlinear layered soil-structure interactions", *Earthquake Engineering and Structural Dynamics*, 28, 421-441.

Chuhan, Z., Chengda, Y. and Guanglun, W. (2001) "Numerical simulation of reservoir sediment and effects on hydrodynamic response of arch dams", *Earthquake Engineering and Structural Dynamics*, 30, 1817-1837.

Chwang, A.T. (1978) "Hydrodynamic pressure on sloping dams during earthquakes. Part - 2. Exact theory", *Journal of Fluid Mechanics*, 87, 343-348.

Chwang, A.T. and Housner, G.W. (1978) "Hydrodynamic pressure on sloping dams during earthquakes. Part-1. Momentum method ", *Journal of Fluid Mechanics*, 87, 335-341.

Clough, R.W. and Chang, C.H. (1981) "Seismic cavitation of gravity dam reservoirs", *Numerical Methods for Coupled Problems, Proceedings of International Conference held at University College, Swansea,* 7th-11th September, Pineridge Press, Swansea, U.K., 185-196.

Clough, R.W. and Chang, C.H. (1984) "Seismic cavitation effects on gravity dam reservoirs", *Numerical Methods in Coupled Systems*, (Lewis, R. W., Bettess, P., and Hinton, E., Eds.), Wiley, Chichester, U.K., 571-598.

Cole, D.L., Kosloff, D.D. and Minster, J.B. (1978) "A numerical boundary integral equation method for elastodynamics", *International Bulletin of Seismological Soceity of America,* 68, 1331-1357.

Combescure, A. Gibert, R.J., Jeanpierre, F., Hoffmann, A. and Livolant, M. (1980) "Fluid structure interaction: A general method used in CEASEMT computer programs", *Computers and Structures*, 12, 471-474.

Cook, R.D., Malkus, D.S. and Plesha, M.E. (1989) "Concepts and Applications of Finite Element Analysis",3rd Edition, John Wiley & Sons (ASIA) Pte Ltd, Singapore.

Copen, M.D., Lindholm, E.A. and Tarbox, G.S. (1977) Design of concrete dams. Handbook of Dam Engineering, Nostrand Reinhold; 385-465.

Coussy, O. (1995) Mechanics of porous continua. *John Wiley & Sons,* Chichester, England.

Daniell, W.E., Mir, R.A., Simic, M.S. and Taylor, C.A. (1995) Seismic behavior of concrete gravity dams", *10th European Conference on Earthquake Engineering,* 28th Aug. – 2nd Sep., 1994, Vienna, Austria, A.A. Balkema, Rotterdam, 1951-1955.

Darbre, G.R. and Wolf, J.P. (1988) "Criterion of stability and implementation issues of hybrid frequency time-domain procedure for nonlinear dynamic analysis", *Earthquake Engineering and Structural Dynamics*, 16, 569-581.

Darbre, G.R. (1993) "Nonlinear reservoir-dam interaction by way of the hybrid frequency time procedure", *Proceedings of the 2nd European Conference in Structural Dynamics, EURODYN'93*, Trondhiem, Norway, A.A. Balkema, Rotterdam.

Darbre, G.R. (1998) "Phenomenological two-parameter model for dynamic dam-reservoir interaction", *Journal of Earthquake Engineering*, 2(4), 513-524.

Dasgupta, G. and Chopra, A.K. (1979) "Dynamic stiffness matrices for viscoelastic half planes", *Journal of Engineering Mechanics, ASCE*, 105(EM5), 729-745.

Dasgupta, G. (1982) "A finite element formulation for unbounded homogeneous continua", *Journal of Applied Mechanics, ASME*, 49,136-140.

de Araújo, J.M. and Awruch, A.M. (1998) "Probabilistic finite element analysis of concrete gravity dams", *Advances in Engineering Software*, 29(2), 97 –104.

de Borst R. (1987) "Smeared cracking, plasticity, creep and thermal loading – a unified approach", *Computer Methods in Applied Mechanics and Engineering*, 62, 89-110.

Deb, S.K. and Borsaikia A.C. (2006) "Design of mass concrete mix for gravity dam based on fineness modulus and geometrical gradation", *Indian Concrete Journal*, 80(1), 52-56.

Domínguez, J., Medina, F. and Maeso O. (1993) "Dynamic analysis in dam-soil-reservoir systems", *Boundary Elements in Dynamics*, Computational Mechanics Publications, Southampton, 607-647.

Domínguez, J., Gallego, R. and Japón, B.R. (1997) "Effects of porous sediments on seismic response of concrete gravity dams", *Journal of Engineering Mechanics, ASCE*, 123(4), 302-311.

Donlon, W.P. (1989) "Experimental investigation of nonlinear seismic response of concrete gravity dams", *Earthquake Engineering Research Laboratory. Report No. 89-01*. California Institute of Technology, Pasadena.

El-Aidi, B. and Hall, J.F. (1989) "Nonlinear earthquake response of concrete gravity dams", *Earthquake Engineering and Structural Dynamics*, 187, 837-865.

Engquist, B. and Majda, A. (1977) "Absorbing boundary conditions for the numerical simulation of waves", *Mathematics of Computation*, 31(139), 629-651.

Engquist, B. and Majda, A. (1979) "Radiation boundary conditions for acoustic and elastic wave calculations", *Communications on Pure and Applied Mathematics*, 32, 313-357.

Everstine, G.C. (1981) "A symmetric potential formulation for fluid-structure interaction", *Journal of Sound and Vibration*, 79, 157-160.

Fahjan, Y.M., Borekci, O.S. and Erdik, M. (2003) "Earthquake-induced hydrodynamic pressures on 3D rigid dam-reservoir system using DRBEM and a radiation matrix", *International Journal for Numerical Methods in Engineering*, 56(10), 1511-1532.

Feltrin,G., Wepf, D. and Bachmann, H. (1990) " Seismic cracking of concrete dams", *Dam Engineering*, 1, 279-289.

Feltrin, G., Galli, M. and Bachmann, H. (1992) "Influence of cracking on concrete gravity dams", *10th World Conference on Earthquake Engineering*, AA Balkema, Rotterdam, Brookefield, 4627-4632.

Feng, Y.Q. and Quevat, J.P. (1990) "Three-dimensional non-linear fluid-structure interaction problems: formulation by the finite and infinite element method", *International Journal for Numerical Methods in Engineering*, 30, 1115-1128.

Fenves, G. and Chopra, A.K. (1983) "Effects of reservoir bottom absorption effects in earthquake response of concrete gravity dams", *Earthquake Engineering and Structural Dynamics*, 11(3), 803-829.

Fenves, G. and Chopra, A.K. (1984) "Earthquake analysis and response of concrete gravity dams", *Report No.UCB/EERC-84/10, Earthquake Engineering Research Center, University of California, Berkley, California.*

Fenves, G. and Chopra, A.K. (1985) "Reservoir bottom absorption effects in earthquake response of concrete gravity dams", *Journal of Structural Engineering, ASCE*, 111(3), 545-562.

Fenves, G.L. and Chopra, A.K. (1987) "Simplified analysis of concrete gravity dams", *Journal of Structural Engineering, ASCE*, 113(8), 1688-1708.

Fenves, G. and Vargas-Loli, L.M. (1988) "Nonlinear dynamic analysis of fluid-structure systems", *Journal of Engineering Mechanics, ASCE*, 114, 219-240.

Fenves, G.L., Mojtahedi, S., and Reimer, R.B. (1989) "ADAP-88: A computer program for nonlinear earthquake analysis of concrete arch dams", *Report No. UCB/EERC-89/12, Earthquake Engineering Research Center,* University of California, Berkeley, CA 1989.

Fenves, G.L., Mojtahedi, S. and Reimer, R.B. (1992) "Effect of contraction joints on earthquake response of an arch dam", *Journal of Structural Engineering, ASCE*, 118(4), 1992, 1039-1055.

Fok, K.L., Hall, J.F. and Chopra, A.K. (1986) "EACD-3D, A computer program for three-dimensional earthquake analysis of concrete dams", *Earthquake Engineering Research Center, Report No. UCB/EERC-86/09, University of California, Berkeley*, July.

Gabor, D. (1946) "Theory of communication", *Journal of Institute of Electrical Engineering*, 93(3), 429-457.

Galli, M., Feltrin, G. and Bachmann, H. (1992) "Application of non-linear fracture mechanics to the seismic assessment of concrete gravity dams", *FRAMCOS-2 Conference*, July 25-28, 1992 Zurich, Switzerland.

Galli, M., Feltrin, G. and Bachmann, H., (1994) "The non-linear behavior of concrete gravity dams under severe earthquake excitation". *10th European Conference on Earthquake Engineering*, AA Balkema, Rotterdam, Brookefield.

Ghaemian, M and Ghobarah, A. (1999) "Nonlinear seismic response of concrete gravity dams with dam-reservoir interaction", *Engineering Structures*, 21, 306-315.

Ghanaat, Y. (1993) "GDAP, Graphics-based Dam Analysis Program", US Army Corps of Engineers, Waterways Experiment Station, Vicksburg, Mississippi.

Ghanaat, Y., Hall, R.L. and Redpath, B.B.(2000) "Measurement and computation of dynamic response of arch dams including interaction effects", *Journal of Seismology and Earthquake Engineering*, 2(3), www.iiees.ac.ir/English/Publication/jsee/jsee4_5.html

Ghrib, F. and Tinawi, R. (1995a) "Nonlinear behavior of concrete gravity dams using damage mechanics", *Journal of Engineering Mechanics, ASCE*, 121(4), 513-527.

Ghrib, F, Tinawi, R. (1995b) "An application of damage mechanics for seismic analysis of concrete gravity dams", *Earthquake Engineering and Structural Dynamics*, 24(2), 157-173.

Gill, S. (1951) "A process for the step-by-step integration of differential equations in an automatic digital computing machine", *Proceedings of the Cambridge Philosophical Society*, 47, 96-108.

Givoli, D. (2004) "High-order local non-reflecting boundary conditions: a review", *Wave Motion*, 39, 319-326.

Guan, F., Moore, I.D. and Lin, G. (1994) "Transient response of reservoir-dam-soil systems to earthquakes", *International Journal for Numerical & Analytical Methods in Geomechanics*, 18, 863-880.

Guan, F. and Moore, I.D. (1997) "New techniques for modelling reservoir-dam and foundation-dam interaction", *Soil Dynamics and Earthquake Engineering*, 16, 285-293.

Guanglun, W., Pekau, O.A, Chuhan, Z. and Shaomin, W. (2000) "Seismic fracture analysis of concrete gravity dams based on nonlinear fracture mechanics", *Engineering Fracture Mechanics*, 65(1), 67-87.

Haigh, S.K., Teymur B., Madabhushi S.P.G. and Newland, D.E. (2002) "Applications of wavelet analysis to the investigation of the dynamic behaviour of geotechnical structures", *Soil Dynamics and Earthquake Engineering*, 22 ,995–1005.

Hall, J.F. and Chopra, A.K. (1982) "Two-dimensional dynamic analysis of concrete gravity and embankment dams including hydrodynamic effects", *Earthquake Engineering and Structural* Dynamics, 10, 305-332.

Hall, J.F. and Chopra, A.K. (1983) "Dynamic analysis of arch dams including hydrodynamic effects", *Journal of Engineering Mechanics, ASCE*, 109, 149-167.

Hamdi, M.A. and Ousset, Y. and Verchery, G. (1978) "A displacement method for the analysis of vibrations of coupled fluid-structure systems", *International Journal for Numerical Methods in Engineering*,13, 139-150.

Hanna, Y.G. and Humar, J.L. (1982) "Boundary element analysis of fluid domain", *Journal of Engineering Mechanics, ASCE*, 108, 436-450.

Harris, D.W., Snorteland, N., Dohen, T. and Travers, F. (2000) "Shaking Table 2-D models of a Concrete Gravity Dam", *Earthquake Engineering and Structural Dynamics*, 29, 769-787.

Hatami, K. (1997) "Effect of reservoir bottom on earthquake response of concrete dams", *Soil Dynamics and Earthquake Engineering*, 16, 407-415.

Hinton, E. and Campbell, J.S. (1974) "Local and global smoothing of discontinuous finite element function using a least square method", *International Journal for Numerical Methods in Engineering*, 8, 461-480.

Horii, H. and Chen, S.C. (2000) "Computational fracture analysis of concrete gravity dams by crack-embedded elements – toward and engineering evaluation of seismic safety" *Engineering Fracture Mechanics*, 70, 1029-1045.

Hubert, F.X., Burlion, N. and Shao, J.F. (2001) "Consequences of dessication on mechanical damage of concrete", *Fracture Mechanics of Concrete Structures*, 1, 223-230.

Humar, J.L. and Jablonski, A.M. (1988) "Boundary element reservoir model for seismic analysis of gravity dam", *Earthquake Engineering and Structural Dynamics*, 16, 1129-1156.

Hung, T.K. and Wang, M.H. (1987) "Nonlinear hydrodynamic pressure on rigid dam motion", *Journal of Engineering Mechanics, ASCE*, 113, 482-499.

Ingraffea, A.R. and Saouma, V.E. (1985) "Numerical modelling of discrete crack propagation in reinforced and plain concrete", *Fracture Mechanics of Concrete:*

Structural Application and Numerical Calculation, Martinus NijHoff, The Hague, The Netherlands, 171-225.

Israil, A.S.M. and Banerjee, P.K. (1990) "Two-dimensional transient wave propagation problems by time domain BEM", *International Journal of Solids and Structures*, 26(8), 851-864.

IS 1893: 1984 (Reaffirmed 1998) Criteria for earthquake resistant design of structures, *Bureau of Indian Standards*, New Delhi, India, 39-46.

Karabalis, D.L. and Beskos, D.E. (1985) "Dynamic response of three-dimensional flexible foundations by time domain BEM and FEM", *Soil Dynamics and Earthquake* Engineering, 24(2), 91-101.

Khalili, N., Valliappan, S., Tabatabaie, Y.J. and Yazdchi, M. (1997) "ID infinite element for dynamic problems in saturated porous media", *Communications in Numerical Methods in Engineering* ,13, 727-738.

Kim, D.K. and Yun, C.B. (2000) "Time-domain soil-structure interaction analysis in two-dimensional medium based on analytical frequency dependent infinite elements", *International Journal for Numerical Methods in Engineering,* 47, 1241-1261.

Kotsubo, S. (1960) "Dynamic water pressure on dams during earthquake", *2nd World Conference on Earthquake Engineering*, 799- 814.

Krajcinovic, D. (1989) "Damage mechanics", *Mechanics of Materials*, 8, 117-197.

Küçükarslan, S. (2003) "Dam-reservoir interaction including the reservoir bottom effects in time domain", *16th ASCE Engineering Mechanics Conference, July 16-18, 2003, University of Washington, Seattle.*

Küçükarslan, S. (2005) "An exact truncation boundary condition for incompressible–unbounded infinite fluid domains", *Applied Mathematics and Computation*, 163(1), 61–69.

Kuhl, D, Bangert, F, Meschke, G. (2004) "Coupled chemo-mechanical deterioration of cementitious materials. Part I: Modeling", *International Journal of Solids and Structures*, 41, 15 - 40.

Kuo, J. (1982) "Joint Opening Nonlinear Mechanism: Interface Smeared Crack Model", *EERC Report No. 82/10*, University of California, Berkeley, California.

Léger, P. and Katsouli, M. (1989) "Seismic stability of concrete gravity dams", *Earthquake Engineering and Structural Dynamics*; 18, 889-902.

Lemaître, J. and Chaboche, J.L. (1989) "Aspect phénoménologique de la rupture par endommagement", *Journal de mécanique appliquée*, Paris, France, 23, 317-367.

Leurer, K.C. (1997) "Attenuation in fine-grained marine sediments: Extension of the Biot-Stoll model by the "effective grain model" (EGM)", *Geophysics*, 62(5), 1465–1479.

Li, X., Romo, M.P. and Avilés, L.J. (1996) "Finite element analysis of dam-reservoir systems using an exact far-boundary condition", *Computers and Structures*, 60, 751-762.

Lindvall, A. (2001) "Environmental actions and response: Reinforced concrete structures exposed in road and marine environments", *Licentiate of Engineering Thesis*, Chalmers University of Technology, Göteborg, Sweden.

Liou, G.S. and Huang, P.H. (1994) "Effect of flexibility on impedance functions for circular foundation", *Journal of Engineering Mechanics, ASCE*, 120, 1429-1446.

Liu, W.K. and Cheng, H.G. (1985) "A Method of Computation Fluid-Structure Interaction", *Computers and Structures*, 20, 311-320.

Lotfi, V. (1986) "Analysis of response of dams to earthquakes", *Geotechnical Engineering Report, GR86-2*, Department of Civil Engineering, University of Texas, Austin, Texas.

Lotfi, V. (2004a) "Seismic analysis of concrete dams using the pseudo-symmetric technique", *Dam Engineering*, XIII (2), 119-145.

Lotfi, V. (2004b) "Frequency domain analysis of concrete gravity dams by decoupled modal approach", *Dam Engineering*, XV (2), 141-165.

Lotfi, V., Roesset, J.M. and Tassoulas, J.L. (1987) "A technique for the analysis of the response of dams to earthquakes", *Earthquake Engineering and Structural Dynamics*, 115, 463-490.

Luco, J.E. and Mita, A. (1987) "Response of a circular foundation on a uniform halfspace to elastic waves", *Earthquake Engineering and Structural Dynamics*, 5, 105-118.

Lysmer, J. and Kuhlemeyer, R.L. (1969) "Finite dynamic model for infinite media", *Journal of Engineering Mechanics, ASCE*, 95(EM4), 859-877.

Maity, D. (1998) "Dynamic response of structures interacting with fluid of infinite extent using finite element technique", *Doctoral Thesis*, IIT Kharagpur.

Maity, D. and Bhattacharya, S.K. (1999) "Time domain analysis of infinite reservoir by finite element method using a novel far-boundary condition", *International Journal of Finite Element Analysis and Design*, 32, 85-96.

Maity, D. and Bhattacharyya, S.K. (2002) "Influence of Upstream Profile of Dam and Reservoir Bed on the Development of Hydrodynamic Pressure", *Journal of the Institution of Engineers, India*. 82,197-200.

Maity, D. and Bhattacharya, S.K. (2003) "A parametric study on fluid–structure interaction problems", *Journal of Sound and Vibration*, 263(4), 917-935.

Maity, D. and Bhattacharyya, S.K. (2003) "Dynamic analysis of dam-reservoir system using a novel far-boundary condition", *Advances in Vibration Engineering*, 2(4), 362-378.

Maity, D. (2004) "Coupled hydrodynamic response of dam-reservoir systems", *Journal of the Institution of Engineers*, 85, 213-220.

Maity, D. (2005) "A novel far-boundary condition for the finite element analysis of infinite reservoir", *Applied Mathematics and Computation*, 170(2), 1314-1328.

Maity, D. and Tripathi, R.R. (2005) "Damage assessment of structures from changes in natural frequencies using genetic algorithm", *Structural Engineering and Mechanics, An International Journal*, 19(1), 21-42.

Mansur, W.J. (1983) "A time stepping technique to solve the wave propagation problems using boundary element method", *Doctoral Thesis*, Southampton University, England.

Mathews, J.H. (2001) Numerical Methods for Mathematics, Science and Engineering, *Prentice-Hall of India*, New Delhi, 257-314.

Mazars, J. and Pijaudier-Cabot, G. (1989), "Continuum Damage Theory – Application to Concrete", *Journal of Engineering Mechanics, ASCE*, 115(2),345-365.

Mazzotti, C., Savoia, M. and Tralli, A. (2001) "Isotropic damage model for nonlinear creep behaviour of concrete in compression", *Fracture Mechanics of Concrete Structures*, 1, 255-262.

Medrano, S.A., Obernhuber, P. and Zenz, G. (1995) "Reservoir-dam-soil interaction: a comparative study", *Soil Dynamics and Earthquake Engineering VII*, C.A. Brebbia, Wessex Institute of Technology, United Kingdom & A.S. CAKMAK, Princeton University, USA.

Meschke, G. and Grasberger, S. (2003) "Numerical modeling of coupled hygromechanical degradation of cementitious materials", *Journal of Engineering Mechanics, ASCE*, 129(4), 1 -10.

Mlakar, P.F. (1987) "Nonlinear response of concrete gravity dams to strong earthquake induced ground motion", *Computers and Structures*, 26(1/2), 165- 173.

Modi, P.N. and Seth, S.M. (1989) *Hydraulic and Fluid Mechanics*, 9th Edition, Standard Book House, New Delhi, India.

Morin, P.B., Léger, P. and Tinawi, R. (2002) "Seismic behaviour of post-tensioned gravity dams: Shake table experiments and numerical simulations", *Journal of Structural Engineering, ASCE*, 128(2), 140-152.

Morand, H. and Ohayon, R. (1979) "Substructure variational analysis of the vibrations of coupled fluid-structure systems finite element results", *International Journal of Numerical Methods in Engineering*, 14, 741-755.

Müller, W.C. (1981) "Simplified analysis of linear fluid-structure interaction", *International Journal for Numerical Methods in Engineering*, 17, 113-121.

Nagarajaiah, S. and Varadarajan, N. (2005) "Short time Fourier transform algorithm for wind response control of buildings with variable stiffness TMD", *Engineering Structures*, 27, 431-441.

Nath, B. (1969) "Hydrodynamic pressure on high dams due to vertical earthquake motions", *Proceedings of Institution of Civil Engineers*, 42, March, 413-421.

National Research Council (1990) "Earthquake input", *Earthquake Engineering for Concrete Dams: Design, Performance and Research Needs*, National Academy Press, ISBN-0-309-04336-0, Washington, D.C., 16-19.

Neville, A.M. and Brooks, J.J. (1987) "Elasticity and creep", *Concrete Technology*, Pearson Education (Singapore) Pte. Ltd., 4th Indian Reprint, 209-234.

Niu, Y.Z., Tu, C.L., Liang, R.Y. and Zhang, S.W. (1995) "Modeling of thermo-chemical damage of early-age concrete", *Journal of Structural Engineering, ASCE*, 121(4), 717-726.

Niwa, A. and Clough, R.W. (1980) "Shaking table research on concrete dam models", *Report No.UCB/EERC-80/05*, Earthquake Engineering Research Center, University of California, Berkeley.

Niwa, Y., Fukui, T., Kato, S. and Fujuiki, K. (1980) "An application of the integral equation method to two-dimensional elastodynamics", *Theoretical and Applied Mechanics*, Tokyo, University of Tokyo Press, 28, 281-290.

Niwa, A. and Clough R.W. (1982) "Nonlinear seismic response of arch dams", *Earthquake Engineering and Structural Dynamics*, 10, 267-281.

Norman, C.D. and Anderson, F.A. (1985) "Reanalysis of cracking in large concrete dams in the U.S. Army Corps of Engineers", *Proc. 15th Int. Conference on Large Dams, Question 57, Lausanne, Switzerland.*

Oberti, G. and Castoldi, A. (1980) "The use of models in assessing the behaviour of concrete dams", *Dams and Earthquake*, Institution of Civil Engineers, London, England.

Okamoto, S. and Takahashi, T. (1960) "On behavior of an arch dam during earthquakes", *Proceedings of 2nd World Conference on Earthquake Engineering*, II, 1401-1412.

Oliver, J., Cervera, M., Oller, S. and Lubliner, J., (1990) "Isotropic damage models and smeared crack", *Computer Aided Analysis and Design of Concrete Structures*, Pineridge Press, Swansea England, 945-957.

Olson, L.G. and Bathe, K.J. (1983) "A study of displacement-based fluid finite elements for calculating frequencies of fluid and fluid-structure systems", *Nuclear Engineering and Design*, 76, 137-151.

Olson, L.G. and Bathe, K.J. (1985a) "An infinite element for analysis of transient fluid-structure interactions", *Engineering Computations*, 2, 319-330.

Olson, L.G. and Bathe, K.J. (1985b) "Analysis of fluid-structure interactions. A direct symmetric coupled formulation based on the fluid velocity potential", *Computers and Structures*, 21, 21-32.

Oskouei, A.V. and Dumanoglu, A.A. (2001) "Nonlinear dynamic response of concrete gravity dams: cavitation effect", *Soil Dynamics and Earthquake Engineering*, 21, 99-112.

Pal, N. (1974) "Seismic cracking of concrete dams", *Journal of Structural Division ASCE*, 102, 1827-1844.

Paul, D.K., Zienkiewicz, O.C. and Hinton, E. (1981) "Transient dynamic analysis of reservoir-dam interaction using staggered solution schemes", *Numerical Methods for Coupled Problems, Proceedings of International Conference held at University College, Swansea, 7th-11th September*, Pineridge Press, Swansea, U.K., 321-331.

Pekau, O.A., Chuhan, Z. and Lingmin, F. (1991) "Seismic fracture analysis of concrete gravity dams", *Earthquake Engineering and Structural Dynamics*, 20, 335-354.

Pinsky, P.M. and Abboud, N.N. (1989) "Two mixed variational principles for exterior fluid-structure interaction problems", *Computers and Structures*, 33, 621-635.

Proulx, J. and Paultre, P. (1997) "Experimental and numerical investigation of dam–reservoir–foundation interaction for a large gravity dam", *Canadian Journal of Civil Engineering*, 24 (1), 90-105.

Ralston, A. and Wilf, H.S. (1965) Mathematical Models for Digital Computers, Wiley, New York.

Rao, R.V. and Rao, N.S.V. (1998) "Time-domain analysis of flexible foundations using Lancoz vectors", *Journal of Geotechnical and Geoenvironmental Engineering*, 124(9), 830-839.

Rashed, A.A. and Iwan, B.B.(1984) "Hydrodynamic pressure of short length gravity dams", *Journal of Engineering Mechanics, ASCE*, 110(9), 1264-1283.

Rots, J.G. (1991) "Smeared and discrete representation of localized fracture", *International Journal of Fracture*, 51, 45-59.

Safak, E. (2006) "Time-domain representation of frequency-dependent foundation impedance functions", *Soil Dynamics and Earthquake Engineering*, 26, 65–70.

Sain, T. and Chandra Kishen, J.M. (2003) "Residual life assessment of concrete structures", *Proceedings of Structural Engineering Convention, 2003, An International Meet, IIT Kharagpur, India, Ed. Bhattacharyya S.K.*, 161-169.

Saini, S.S. (1978) "Modelling of hydrodynamic effects on dams using finite elements", *Journal of Institution of Engineers* (India), 59(I3), 204-210.

Saini, S.S., Bettess, P., Zienkiewicz, O.C. (1978) "Coupled hydrodynamic response of concrete gravity dams using finite and infinite elements", *Earthquake Engineering and Structural Dynamics*, 6, 363-374.

Saini, S.S. and Garg, S.S. (1997) "Finite element analysis of gravity dams using substructure technique", *Journal of Institute of Engineers* (India), 78(May), 21-26.

Sandberg, G. and Göransson, P. (1988) "A symmetric finite element formulation for acoustic fluid-structure interaction analysis", *Journal of Sound and Vibration*, 123(3), 507-515.

Sandberg, G. (1995) "A new strategy for solving fluid-structure problems", *International Journal for Numerical Methods in Engineering*, 38, 357-370.

Selby, A. and Severn, R.T. (1972) "An experimental assessment of the added mass of plates vibrating in water", *International Journal of Earthquake Engineering and Structural Dynamics*, 1(2), 189-200.

Sharan, S.K. (1985a) "Finite element modelling of infinite reservoirs", *Journal of Engineering Mechanics, ASCE*, 111, 1457-1469.

Sharan, S.K. (1985b) "Finite element analysis of unbounded and incompressible fluid domains", *International Journal of Numerical Methods in Engineering*, 21, 1659-1669.

Sharan, S.K., Gladwell, G.M.L. (1985) "A general method for the dynamic response analysis of fluid-structure systems", *Computers and Structures*, 21(5), 937-943.

Sharan, S.K. (1986) "Modelling of radiation damping in fluids by finite elements", *International Journal of Numerical Methods in Engineering*, 23, 945-958.

Sharan, S.K. (1987a) "Time domain analysis of infinite fluid vibration", *International Journal of Numerical Methods in Engineering*, 24, 945-958.

Sharan, S.K. (1987b) "A non-reflecting boundary in fluid-structure interaction", *Computers and Structures*; 26, 841-846.

Sharan, S.K. (1992) "Efficient finite element analysis of hydrodynamic pressure on dams", *Computers and Structures*; 42, 713-723.

Shetty, M.S. (1998) Concrete Technology. *S. Chand & Company,* Ramnagar, New Delhi.

Simo, J. and Ju, J. (1987) "Strain and stress-based continuum damage models – I. Formulation", *International Journal of Solids and Structures*, 23(7), 821-840.

Singh, R.K., Kant, T. and Kakodkar, A. (1991) "Coupled shell-fluid interaction problems with degenerate shell and three-dimensional fluid elements", *Computers and Structures*, 38, 515-528.

Skrikerud, P. and Bachmann, H. (1986) "Discrete crack modelling for dynamically loaded, Unreinforced concrete structures", *Earthquake Engineering and Structural Dynamics*, 14, 297-315.

Sommerfeld, A. (1949) "Partial Differential Equations in Physics", Academic Press, New York, N. Y.

Spyrakos, C.C., Beskos, C.C. (1986) "Dynamic response of flexible strip foundation by boundary and finite elements", *Soil Dynamics and Earthquake Engineering*, 5(2), 84-96.

Steffens, A., Li, K. and Coussy, O. (2003) "Ageing approach to water effect on alkali–silica reaction degradation of structures", *Journal of Engineering Mechanics, ASCE*, 129(1), 50-59.

Tan, H. and Chopra, A.K. (1995) "Earthquake analysis of arch dams including dam-water-foundation rock interaction", *Earthquake Engineering and Structural Dynamics*; 24, 1453-1474.

Tekie, P.B. and Ellingwood, B.R. (2003) "Seismic fragility assessment of concrete gravity dams", *Earthquake Engineering & Structural Dynamics*, 32(14), 2221-2240.

Thompson, L.L. and Pinsky, P.M. (1996a) "A space-time finite element method for structural acoustics in infinite domains. Part 1: Formulation, stability and convergence", *Computer Methods in Applied Mechanics and Engineering*, 132, 195-227.

Thompson, L.L. and Pinsky, P.M. (1996b) "A space-time finite element method for structural acoustics in infinite domains. Part 2: Exact time-dependent non-reflecting boundary conditions", *Computer Methods in Applied Mechanics and Engineering*, 132, 229-258.

Tinawi, R., Léger, P., Leclere, M. and Cipolla, G. (2000) "Seismic safety of gravity dams: from shake table experiments to numerical analyses", *Journal of Structural Engineering, ASCE*, 126(4), 518-529.

Touhei, T. and Ohmachi, T. (1993) "A FE-BE method for dynamic analysis of dam-foundation-reservoir systems in the time domain", *Earthquake Engineering and Structural Dynamics*, 22, 195-209.

Tsai, C.S. and Lee, G.C. (1987) "Arch dam-fluid interactions: by FEM-BEM and substructure concept", *International Journal of Numerical Methods in Engineering*, 24, 2367-2388.

Tsai, C.S. and Lee, G.C. (1989) "Hydrodynamic pressure on gravity dams subjected to ground motion", *Journal of Engineering Mechanics, ASCE*, 115, 598-617.

Tsai, C.S. and Lee, G.C. (1990) "Method for transient analysis of three-dimensional dam-reservoir interactions", *Journal of Engineering Mechanics, ASCE*, 116, 2151-2172.

Tsai, C.S., Lee, G.C. and Ketter, R.L. (1990) "A semi-analytical method for time-domain analysis of dam-reservoir interactions", *International Journal for Numerical Methods in Engineering*, 29, 913-933.

Tsai, C.S. and Lee, G.C. (1991) "Time-domain analysis of dam-reservoir system. II: substructure method", *Journal of Engineering Mechanics, ASCE*, 117, 2007-2026.

Tsai, C.S. (1992) "Semi-analytical solution for hydrodynamic pressures on dams with arbitrary upstream face considering water compressibility", *Computers and Structures*, 42, 497-502.

Tu, C.L. and Niu, N.Z. (1988) "Thermomechanical test of Dongjiang arch dam concrete", *Technical Report, Research Center of Structure and Materials*, Mid-South Design Institute for Hydroelectric Projects, Changsa, Hunan, China.

Ulm, F.J. and Coussy O. (1995) "Modelling of thermochemomechanical couplings of concrete at early ages", *Journal of Engineering Mechanics, ASCE*, 121(7), 785-794.

U.S. Bureau of Reclamation: Arch Dams. In Concrete Dams. Design Standards No.2 Denver: U.S. Department of the Interior 1965.

U.S. Bureau of Reclamation: Gravity Dams. In Concrete Dams. Design Standards No.2 Denver: U.S. Department of the Interior 1966.

U.S. Bureau of Reclamation (1976) Design of gravity dams, *Design manual for concrete gravity dams*, Denver.

U.S. Army Corps of Engineers (1977) The evaluation of dam safety. *Proceedings of Engineering Foundation Conference*, Pacific Grove, California, Nov- Dec.

U.S. Army Corps of Engineers (1995) Engineering and Design - Gravity Dam Design, CECW-ED Publication, EM 1110-2-2200, www.usace.army.mil/usace-docs/eng-manuals/em1110-2-2200/toc.htm

Vaish, A.K. and Chopra, A.K. (1974) "Earthquake finite element analysis of structure-foundation systems", *Journal of Engineering Mechanics Div, ASCE*, EM6, 1101-1116.

Valliappan, S. and Zhao, C. (1992) "Dynamic response of concrete gravity dams including dam-water-foundation interaction", *International Journal for Numerical and Analytical Methods in Geomechanics*, 16, 79-99.

Vargas-Loli, L.M. and Fenves, G.L. (1989) "Effects of concrete cracking on the earthquake response of gravity dams", *Earthquake Engineering and Structural Dynamics*, 18, 575-592.

Vitharana, N., Bell, G., Jensen, J. and Sinha, J. (2002) "Seismic assessment of Wyangala concrete gravity dam and intake towers", *ANCOLD Conference on Dams*, www.ghd.com.au/papers/Dams/ancoldwyangala.pdf

von Estorff, O. and Prabucki, M.J. (1990) "Dynamic response in time domain by coupled boundary and finite elements", *Computational Mechanics*, 6, 35-46.

von Estorff, O. (1991) "Dynamic response of elastic blocks by time domain BEM and FEM", *Computers and Structures*, 38(3), 289-300.

von Estorff, O. and Antes, H. (1991) "On FEM-BEM coupling for fluid structure interaction analyses in the time domain", *International Journal for Numerical Methods in Engineering*, 31, 1151-1168.

von Estorff, O. and Firuziann, M. (2000) "Coupled BEM/FEM approach for nonlinear soil/structure interaction", *Engineering Analysis with Boundary Elements*, 24,715-725.

von Kármán, T. (1933) "Discussion of water pressures on dams during earthquakes", *Transactions of ASCE*, 98, 434-436.

Washa, G.W., Saemann, J.C. and Cramer, S.M. (1989) "Fifty year properties of concrete made in 1937", *ACI Materials Journal*, 86(4), 367-371.

Weber, B. (1994) "Rational Transmitting boundaries for time domain analysis of dam-reservoir interaction", *Doctoral Thesis*, Swiss Federal Institute of Technology Zurich, http://e-collection.ethbib.ethz.ch/ecol-pool/diss/

Wepf, D.H., Wolf, J.P. and Bachmann, H. (1988) "Hydrodynamic-stiffness matrix based on boundary elements for time domain dam-reservoir-soil analysis", *Earthquake Engineering and Structural Dynamics*, 16, 417-432.

Werner, P. and Sundquist, K. (1949) "On hydrodynamic earthquake effects", *Transactions of American Geophysical Union*, 30(5), 636-657.

Westergaard, H.M. (1933) "Water pressure on dams during earthquakes" *Transactions of ASCE*, 98, 418-472.

White, W., Valliappan, S. and Lee, I.K. (1977) "Unified boundary for finite dynamic models", *Journal of Engineering Mechanics, ASCE*, 103(5), 949-964.

Wilson, E.L. (1969) "A method of analysis for the evaluation of foundation-structure interaction", *Proceedings of 4th World Conference on Earthquake Engineering*, Santiago, Chile.

Wolf, J.P. (1985) Dynamic soil-structure interaction, Prentice Hall: Englewood Cliffs, NJ.

Wolf, J.P. (1988) Soil-structure-interaction in time domain, Prentice Hall: Englewood Cliffs, NJ.

Wolf, J.P. and Song, C. (1994) "Dynamic stiffness matrix of unbounded soil by finite element multi-cell cloning" *Earthquake Engineering and Structural Dynamics*, 23, 233-250.

Yang, R., Tsai C.S. and Lee, G.C. (1990) "Far field modelling in 3D dam-reservoir interaction analysis", *Journal of Engineering Mechanics, ASCE*, 116 (10), 2151-2172.

Yang, R., Tsai, C.S. and Lee, G.C. (1993) "Explicit time-domain transmitting boundary for dam-reservoir interaction analysis", *International Journal of Numerical Methods in Engineering*, 36, 1789-1804.

Yang, R., Tsai, C.S. and Lee, G.C (1996) "Procedure for time domain seismic analysis of concrete gravity dams", *Journal of Engineering Mechanics, ASCE*, 122(2), 116-122.

Yann, J., Zhang, C. and Jin, F. (2004) "A coupling procedure of FE and SBFE for soil-structure interaction in the time domain", *Earthquake Engineering and Structural Dynamics*, 59(11), 1453-1471.

Yazdchi, M., Khalili, N. and Valliappan, S. (1999) "Dynamic soil–structure interaction analysis via coupled finite-element–boundary-element method", *Soil Dynamics and Earthquake Engineering*, 18, 499–517.

Yerli, H.R., Temel, B. and Kiral, E. (1998) "Transient infinite elements for 2D soil-structure interaction analysis", *Journal of Geotechnical and Geoenvironmental Engineering*, October, 976 -988.

Zangar, C.N. (1952) "Hydrodynamic pressures on dams due to horizontal earthquakes engineering", *Monograph No.11, Bureau of Reclamation.*

Zhang, X., Wegner, J.L. and Haddow, J.B. (1999) "Three-dimensional dynamic analysis in time-domain", *Earthquake Engineering and Structural Dynamics*, 28, 1501-1524.

Zhao, C. and Valliappan, S. (1992) "A numerical model for wave scattering problems in infinite media due to P- and SV- wave incidences", *International Journal for Numerical Methods in Engineering*, 33, 1661-1682.

Zhao, C., Valliappan, S. and Wang, Y.C. (1992) "Mechanism of solid-water interaction problems during earthquakes", *Computers and Structures*, 43(3), 397-409.

Zienkiewicz, O.C. (1964) "Hydrodynamic pressures due to earthquakes", *Water Power*, Sept, 382-388.

Zienkiewicz, O.C. and Newton, R.E. (1969) "Coupled vibration of a structure submerged in a compressible Fluid", *Proceedings of International Symposium on Finite Element Techniques, Stuttgart.*

Zienkiewicz, O.C., Kelly, D.W. and Bettess, P. (1977) "The coupling of finite element and boundary solution procedures", *International Journal for Numerical Methods in Engineering*, 11, 276-355.

Zienkiewicz, O.C. and Bettess, P. (1978) "Dynamic fluid-structure interaction", *Numerical modelling of the coupled problem.* Chap 5, Numerical Methods in Offshore Engineering. Wiley, Chichester.

Zienkiewicz, O.C., Hinton, E., Bicanic, N. and Fejzo, P. (1981) "Computational Models for the Transient Dynamic Analysis of Concrete Dams", *Dams and Earthquake, Institute of Civil Engineers*, Thomas Telford Limited, London, 171-178

Zienkiewicz, O.C., Paul, D.K. and Hinton, E. (1983) "Cavitation in fluid-structure response with particular reference to dams under earthquake loading", *Earthquake Engineering and Structural Dynamics*, 11, 463-481.

Zienkiewicz, O.C. and Taylor, R.L. (1991) The Finite Element Method, Vol.2, Solid and Fluid Mechanics, Dynamics and Nonlinearity, McGraw-Hill Book Co. U.K.

Zienkiewicz, O.C. and Taylor, R.L. (2000) The Finite Element Method, 5th Edition, Butterworth-Heinemann, Oxford, U.K.

LIST OF PUBLICATIONS RELATED TO PRESENT WORK

In Journals:

1. Gogoi, I. and Maity, D. (2005) "Seismic safety of aged concrete gravity dams considering fluid-structure interaction", *Journal of Earthquake Engineering*, 9(5), 637- 656.
2. Gogoi, I. and Maity, D. (2005) "A review on idealization and modelling of concrete gravity dam considering soil-structure-fluid interaction", *Dam Engineering*, XVI(2), 117-152.
3. Gogoi, I. and Maity, D. (2005) "Seismic performance of aged concrete gravity dams", The Institution of Engineers (India), *Journal of Civil Engineering Division*, 85, 241-246. (This paper has been awarded for "The Union Ministry of Water Resources, Department of Irrigation Prize")
4. Gogoi, I. and Maity, D. (2005) "A non-reflecting boundary condition for the finite element modeling of infinite reservoir with layered sediment", *Advances in Water Resources*, In press.
5. Gogoi, I. and Maity, D. "Effect of sediment layers on development of hydrodynamic pressure of elastic dams", *Computers and Structures* (Submitted after review)
6. Gogoi, I. and Maity, D. "Influence of sediment layers on dynamic behavior of aged concrete dams", *Journal of Engineering Mechanics, ASCE* (Submitted after review)
7. Gogoi, I. and Maity, D. "Finite element analysis of a dam-reservoir system under seismic excitation using STFT", *Journal of Sound & Vibration* (Communicated).

In Conferences:

1. Gogoi, I. and Maity. D. (2006) "Seismic behavior of an ageing dam", International Congress on Computational Mechanics and Simulation (ICCMS 06), December 2006, Guwahati, India. Accepted.
2. Gogoi, I. and Maity. D. (2006) "Seismic behavior of an ageing concrete dam adjacent to sedimented reservoir", 8th U.S. National Conference on Earthquake Engineering, San Francisco, April 18-22. 2006. Paper No. 325.

3. Gogoi, I. and Maity, D. (2005) "Absorptive effect of sediment layers on hydrodynamic response of dams", XXXI International Association of Hydraulic Engineering and Research Congress IAHR, 2005 Seoul, Korea, 11th – 16th September.

4. Gujare, R. A., Gogoi, I. and Maity, D. (2005) "A Non-Reflecting Boundary Condition for the Finite Element Modeling of Infinite Reservoir With Layered Sediment", Proceedings of the International Conference in Environmental Fluid Mechanics. 3-5 March, Indian Institute of Technology Guwahati, India, pp. 221-228.

5. Gogoi, I. and Maity, D. (2005) "Monitoring Safety of a Concrete Gravity Dam", Safety Conference on Managing Safety: Challenges Ahead Organized by Safety and Quality Forum, The Institution of Engineers (India). 14-16 February 2005, New Delhi, India, Paper No. 18.

6. Gogoi, I., Phani, L. K., Sharma, V. and Maity, D. (2004) "A Closed-Form Formulation for Hydrodynamic Pressure on Gravity Dams Considering Reservoir Bottom Effects", CD-ROM Proceedings of the Third International Conference on Theoretical, Applied, Computational and Experimental Mechanics. 28-30 December, 2004. Indian Institute of Technology, Kharagpur, India, Paper No. 297.

7. Gogoi, I., and Maity, D. (2004) "Vulnerability of Aged Concrete Gravity Dams", 13th World Conference on Earthquake Engineering (13 WCEE) August 1-6, 2004 at. Vancouver, Canada, Paper No. 1839.

8. Gogoi, I., and Maity, D. (2004) "Importance of Seismic Resistant Concrete Gravity Dam in Seismic Prone Area Like North East India", Proceedings of the World Congress on Natural Disaster Mitigation, The Institution of Engineers (India) under the aegis of World Federation of Engineering Organizations, 19-22 February. New Delhi, India, Vol. 2, 149-158.

9. Gogoi, I. and Maity, D. (2002), "Trends in Dynamic Analysis of Concrete Gravity Dams", 18th National Convention of Civil Engineers, 9-10 November 2002. The Institute of Engineers (India), Assam State Center, India, 49-57.